UNIVERSITÉ DE MONTRÉAL

JOINT INVERSION OF THE MAGNETIC ANOMALY DUE TO A KIMBERLITE PIPE AND ITS ANALYTIC SIGNAL

JINFU CHEN

DÉPARTMENT DES GÉNIES CIVIL,

GÉOLOGIQUE ET DES MINES

ÉCOLE POLYTECHNIQUE DE MONTRÉAL

MÉMOIRE PRÉSENTÉ EN VUE DE L'OBTENTION

DU DIPLÔME DE MAÎTRISE ÈS SCIENCES APPLIQUÉES

(GÉNIE MINÉRAL)

JUIN 2009

© Jinfu Chen, 2009

Library and Archives Canada

Published Heritage Branch

395 Wellington Street
Ottawa ON K1A 0N4
Canada

Bibliothèque et Archives Canada

Direction du Patrimoine de l'édition

395, rue Wellington
Ottawa ON K1A 0N4
Canada

Your file Votre référence
ISBN: 978-0-494-53896-8
Our file Notre référence
ISBN: 978-0-494-53896-8

NOTICE:

The author has granted a non-exclusive license allowing Library and Archives Canada to reproduce, publish, archive, preserve, conserve, communicate to the public by telecommunication or on the Internet, loan, distribute and sell theses worldwide, for commercial or non-commercial purposes, in microform, paper, electronic and/or any other formats.

The author retains copyright ownership and moral rights in this thesis. Neither the thesis nor substantial extracts from it may be printed or otherwise reproduced without the author's permission.

AVIS:

L'auteur a accordé une licence non exclusive permettant à la Bibliothèque et Archives Canada de reproduire, publier, archiver, sauvegarder, conserver, transmettre au public par télécommunication ou par l'Internet, prêter, distribuer et vendre des thèses partout dans le monde, à des fins commerciales ou autres, sur support microforme, papier, électronique et/ou autres formats.

L'auteur conserve la propriété du droit d'auteur et des droits moraux qui protège cette thèse. Ni la thèse ni des extraits substantiels de celle-ci ne doivent être imprimés ou autrement reproduits sans son autorisation.

In compliance with the Canadian Privacy Act some supporting forms may have been removed from this thesis.

While these forms may be included in the document page count, their removal does not represent any loss of content from the thesis.

Conformément à la loi canadienne sur la protection de la vie privée, quelques formulaires secondaires ont été enlevés de cette thèse.

Bien que ces formulaires aient inclus dans la pagination, il n'y aura aucun contenu manquant.

Canada

UNIVERSITÉ DE MONTRÉAL

ÉCOLE POLYTECHNIQUE DE MONTRÉAL

Ce mémoire intitulé:

JOINT INVERSION OF THE MAGNETIC ANOMALY DUE TO A KIMBERLITE PIPE AND ITS ANALYTIC SIGNAL

présenté par: CHEN Jinfu

en vue de l'obtention du diplôme de : Maîtrise ès sciences appliquées

a été dûment accepté par le jury d'examen constitué de :

M. MARCOTTE Denis, Ph.D., président

M. CHOUTEAU Michel, Ph.D., membre et directeur de recherche

M. KEATING Pierre, Ph.D., membre et codirecteur de recherche

M. GIROUX Bernard, Ph.D., membre

Acknowledgements

Firstly, I would like to express my sincere gratitude to my directors, Mr. Michel Chouteau and Mr. Pierre Keating, for giving me the opportunity to do research as a graduate student, for their trust, patience, encouragement, constant guidance, and for their financial support during the period of my study here.

Mr. Michel Chouteau has always been there to help me out and answer my questions. His encouragement has benefited me greatly. Mr. Pierre Keating has always answered my questions by email at once without any hesitation, and he has often come to Polytechnique to give guidance face to face. I greatly appreciate the trust and confidence in me that they have shown. Their kindness, enthusiasm, patience, carefulness, intellect, insights and dedication to science is a great spiritual wealth to inspire me to work and study well in the future.

Secondly, I would like to express my appreciation to Mr. Denis Marcotte who took his time to check my thesis on the condition that he was very busy. And I would like to express my appreciation to others who assisted me time by time. Mr. Bernard Giroux, who was the professor of the course of seismic method, gave me a lot of helpings with a great of patience. I would like to express my appreciation to Mr. Bouchedda Abderrezak for his generous technical assistance in the period of my study. I would also like to thank Mr. Intissar Rachid for his helping me in the period of time of the course study.

Besides, I would also like to thank my group; this is an outstanding group. Here, I worked silently and diligently in a friendly atmosphere. Numerous beautiful recollections here will keep in my heart forever.

Résumé

Dans l'interprétation des anomalies magnétiques, la détermination de la force de rémanence magnétique et direction est très importante. Ce problème peut être résolu par deux manières. Premièrement, le signal analytique du champ magnétique qui, pour les 2D structures, est indépendant de l'induction et de la direction de magnétisation peut être employé. Cependant, pour les structures 3D sa forme n'est pas totalement indépendante des directions d'induction et de magnétisation. La deuxième méthode est fondée sur l'hypothèse que la magnétisation rémanente ne change pas de manière significative selon la direction de magnétisation. Néanmoins, dans beaucoup d'applications, la magnétisation rémanente est souvent forte et ne peut pas être négligée.

L'objectif principal de cette étude est de développer un algorithme pour l'inversion conjointe de l'anomalie magnétique due à un cylindre circulaire droit vertical sous une polarisation arbitraire et son signal analytique. L'avantage principal d'une inversion conjointe est que l'information de deux ensembles de données différents est employée pour réduire la non unicité inhérente à l'inversion. L'inversion conjointe proposée donne des résultats plus robustes et plus précis que les inversions séparées de ces deux ensembles de données. D'ailleurs, il est possible de déterminer la direction du vecteur de rémanence aussi bien que sa force.

Afin de mettre en application l'inversion conjointe de tout le champ magnétique et de son signal analytique, j'ai développé les dérivés analytiques des paramètres de corps. Ces dérivés sont employés pour calculer la matrice Jacobinne utilisée dans l'inversion. Une nouvelle formule pour le rapport entre la magnétisation rémanente et la magnétisation induite est également présentée. L'inversion analytique de signal donne de meilleurs résultats pour la géométrie que l'inversion totale du champ magnétique. Dans la situation où la magnétisation rémanente n'est pas connue,

l'inversion de signal analytique est le meilleur choix pour la géométrie du corps magnétique.

En conclusion, l'inversion conjointe du champ magnétique total et de son signal analytique a été mise en application avec succès. L'inversion conjointe a une meilleure précision et stabilité que l'inversion séparée de l'anomalie magnétique ou de son signal analytique. Premièrement, elle donne de meilleurs résultats pour l'inclination élevée. Deuxièmement, elle a la meilleure stabilité et précision quand les valeurs initiales de l'inversion sont loin des valeurs vraies. Troisièmement, elle a la meilleure stabilité et la précision en présence du bruit.

Abstract

In the interpretation of magnetic anomalies, the determination of the magnetic remanent magnetization strength and direction is very important. This problem can be solved by two ways. Firstly, the analytic signal of the magnetic field which, for 2D structures, is independent of the induction and the magnetization direction can be used. However, its shape is not totally independent of the induction and magnetization directions for 3D structures. The second method is based on the assumption that the remanent magnetization does not significantly alter the total magnetization direction. Nevertheless, in many applications, remanent magnetization is often strong and cannot be disregarded.

The major objective of this study is to develop an algorithm for the joint inversion of the magnetic anomaly due to a vertical right circular cylinder with arbitrary polarization and its analytic signal. The main advantage of a joint inversion is that the information from two different data sets is used to reduce the non-uniqueness inherent in the inversion. The proposed joint inversion gives more robust and accurate results than the separate inversions of these two data sets. Moreover, it is possible to determine the direction of the remanent magnetization vector as well as its strength.

In order to implement the joint inversion of the total magnetic field and its analytic signal, I have developed the analytic derivatives of the body parameters. These derivatives are used to compute the Jacobian matrix used in the inversion. A new formula for the relationship between the remanent magnetization and the induced magnetization is also introduced. The inversion of analytic signal gives better results of geometry than total magnetic field inversion. In the situation where the remanent magnetization is not known, the analytic signal is best choice to be inversed for the geometry of the magnetic body.

Finally, the joint inversion of total magnetic field and its analytic signal was implemented successfully. The joint inversion has better precision and stability than

the separate inversion of the magnetic anomaly or its analytic signal. Firstly, it performs better for high inclinations. Secondly, it has the best stability and precision when the initial values of the inversion are far from the true values. Thirdly, it has the best stability and the precision in the presence of noise.

Condensé en français

Dans l'interprétation des anomalies magnétiques, la détermination de la force magnétique de rémanence et la direction est très importante. Ce problème peut être résolu par deux manières. Premièrement, le signal analytique du champ magnétique qui, pour les 2D structures, est indépendant de l'induction et de la direction de magnétisation peut être employé. Cependant, sa forme n'est pas totalement indépendante des directions d'induction et de magnétisation pour les structures 3D. La deuxième méthode est fondée sur l'hypothèse que la magnétisation rémanente ne change pas de manière significative toute la direction de magnétisation. Néanmoins, dans beaucoup d'applications, la magnétisation rémanente est souvent forte et ne peut pas être négligée.

L'objectif principal de cette étude est de développer un algorithme pour l'inversion conjointe de l'anomalie magnétique due à un cylindre circulaire droit vertical avec la polarisation arbitraire et son signal analytique. L'avantage principal d'une inversion conjointe est que l'information de deux ensembles de données différents est employée pour réduire le non unicité inhérente à l'inversion. L'inversion conjointe proposée donne des résultats plus robustes et plus précis que les inversions séparées de ces deux ensembles de données. D'ailleurs, il est possible de déterminer la direction du vecteur de rémanence aussi bien que sa force.

Afin de mettre en application l'inversion conjointe de tout le champ magnétique et de son signal analytique, j'ai développé les dérivés analytiques des paramètres de corps. Ces dérivés sont employés pour calculer la matrice Jacobinne utilisée dans l'inversion.

Singh et Sabina (1978) ont dérivé l'expression analytique des anomalies dues au cylindre vertical droit ; ce travail a résolu le problème de la modélisation pour l'inversion des anomalies magnétiques dues au cylindre vertical droit. Mais pour l'inversion du signal analytique et l'inversion conjointe du champ magnétique total et

du signal analytique, nous devons non seulement résoudre le problème de la modélisation, mais calculer également la matrice Jacobinne. Le signal analytique est défini comme l'amplitude du gradient total. Ainsi dériver des expressions analytique de dérivé analytique x, le dérivé analytique y et le dérivé analytique z du champ magnétique total dus au cylindre vertical droit est la chose nécessaire pour mettre en application l'inversion analytique du signal et l'inversion conjointe du champ magnétique total et du signal analytique. Dans les expressions analytiques du champ magnétique, il y a deux intégrales elliptiques incomplètes et deux intégrales elliptiques complètes; elles sont les clés pour obtenir les dérivés du champ magnétique total. Premièrement, nous devons obtenir les expressions analytiques pour les dérivés des intégrales elliptiques complètes et des intégrales elliptiques incomplètes; Pierre Keating a recommandé les formules concernées dans l'emplacement mathématique concerné pour résoudre ce problème. Et puis, dans les expressions analytiques des dérivés des intégrales elliptiques complètes et des intégrales elliptiques incomplètes, il y a les intégrales standard de Legendre. Ces intégrales standard de Legendre sont très importantes pour obtenir l'algorithme. Le calcul de ces intégrales standard de Legendre est donné par Carlson (1979) suivre la méthode d'applications successives du théorème de duplication. Carlson et Notis (1981) donnent les pseudo code pour les algorithmes, Chemam (2006) a utilisé les algorithmes de Carlson à programmer avec Matlab et je les utilise dans les calculassions des dérivées des intégrales elliptiques complètes et des intégrales elliptiques incomplètes à compléter les calculassions des dérivées analytiques. En cours de calcul des dérivés analytique du champ magnétique total, je compare les dérivés analytiques avec dérivés numériques pour contrôler le calcul. La méthode de dériver numérique repose sur les différences finies.

Une nouvelle formule pour le rapport entre la magnétisation rémanente et la magnétisation induite est également présentée à améliorer les résultats de l'inversion magnétique. La méthode je utilise pour l'inversion magnétique est Lenvenberg-Marquardt.

Après compléter l'inversion magnétique, on a proposé avec succès l'inversion analytique de signal. L'inversion analytique de signal analytique donne des meilleurs résultats de la géométrie que l'inversion le champ magnétique totale. Dans la situation où la magnétisation rémanente n'est pas connue, le signal analytique est le meilleur choix à inverser pour la géométrie du corps magnétique. La méthode je utilise est Lenvenberg-Marquardt.

Finalement, l'inversion conjointe du champ magnétique total et son signal analytique ont été accomplis avec succès. La formulation de l'inversion conjointe a été donnée, y compris la formulation du poids et la normalisation des deux ensembles des données.

La stabilité a été montrée dans les résultats de l'inversion conjointe appliquée au modèle synthétique. Contrairement à toute l'inversion de champ magnétique et à l'inversion analytique de signal, l'inversion conjointe a donné les meilleurs résultats en termes de précision et stabilité. Premièrement, elle exécute mieux pour l'inclination élevée. Deuxièmement, elle a la meilleure stabilité et précision quand les valeurs initiales de l'inversion sont loin des valeurs vraies. Troisièmement, elle a la meilleure stabilité et la précision en présence du bruit.

Finalement, l'inversion conjointe du champ magnétique total et son signal analytique ont été mis en application réelle avec succès. L'inversion conjointe a une meilleure précision et stabilité que l'inversion séparée de l'anomalie magnétique ou de son signal analytique.

Table of contents

Acknowledgements iv

Résumé v

Abstract vii

Condensé en français ix

Table of contents xii

List of tables xvii

List of figures xix

List of abbreviations xxxiii

List of appendices xxxv

Chapter 1 Introduction 1

1.1 Introduction 1
1.2 Diamonds and kimberlites 1
1.3 Geophysical surveys for kimberlites 2
1.4 Problem 6
1.5 Main objectives 8
1.6 Methodology 8
1.6.1 The works which are implemented to complete the planned jobs 8
1.6.2 The contributions of my thesis 11
1.7 The plan of the work 12

Chapter 2 Background 14

2.1 Introduction 14
2.2 Major concepts 14
2.2.1 Magnetic methods 14
2.2.2 Geomagnetic field 15
2.2.3 Magnetization 16
2.2.4 Magnetic susceptibility 17
2.2.5 Induced magnetization 18
2.2.6 Remanent magnetization 20

2.3 The progress of magnetic method and the historical development concerned of magnetic method survey for kimberlites 22
2.3.1 The progress of magnetic method 22
2.3.1.1 Depth-to-source estimation techniques 22
2.3.1.1.1 Werner deconvolution 22
2.3.1.1.2 CompuDepth 23
2.3.1.1.3 Naudy method 23
2.3.1.1.4 Analytic signal 23
2.3.1.1.5 Euler deconvolution 24
2.3.1.1.6 Source parameter imaging (SPI) 24
2.3.1.2 Parametric inversion 24
2.3.2 The magnetic method used for survey of kimberlites 25
2.3.2.1 Detecting the kimberlites 25
2.3.2.2 Inversion for magnetic anomalies due to a kimberlite pipe 27

Chapter 3 Derivatives of the magnetic field 28

3.1 Introduction 28
3.2 Formulas of derivatives of the magnetic field 28
3.2.1 Introduction of the basic theory 28
3.2.2 The z derivative of the magnetic anomaly due to right circular cylinder 33
3.2.3 The x derivative of the magnetic anomaly due to right circular cylinder 37
3.2.4 The y derivative of the magnetic anomaly due to right circular cylinder 41
3.3 Finite difference derivatives 41
3.4 Comparison of the responses from two methods 42
3.4.1 Comparison of the responses for first model 42
3.4.2 Comparison of the responses for second model 49
3.4.3 Comparison of the responses for third model 55
3.4.4 Comparison of the responses for fourth model 62
3.5 Conclusion 68

Chapter 4 Inversion of the magnetic field 69

4.1 Introduction of the magnetic field inversion 69
4.2 The problem 70
4.3 The solutions 71
4.3.1 The relationship between the total magnetization intensity and the remanent magnetization. 71
4.3.2 The explicit derivatives to replace numerical derivatives in the calculation of the jacobian matrix. 72

4.4 Levenberg -marquardt method 72
4.4.1 Description of levenberg -marquardt method 72
4.4.2 Forward modeling 74
4.4.3 The calculation of the jacobian matrix 75
4.4.4 The evaluation of initial values 75
4.4.5 The inversion technique 76
4.6 The convergence 80
4.7 Tests for the magnetic inversion 80
4.7.1 Tests for the magnetic inversion in absence of remanent magnetization 80
4.7.1.1 The validation with models for the magnetic inversion in absence of remanent magnetization 80
4.7.1.2 Robustness of the magnetic inversion in absence of remanent magnetization to initial values 84
4.7.2 Tests for the magnetic inversion in presence of remanent magnetization 86
4.7.2.1 The validation with models for the magnetic inversion in presence of remanent magnetization 86
4.7.2.2 The robustness of the magnetic inversion in presence of remanent magnetization to initial values 93
4.7.3 Tests for addition of noise 94
4.8 Discussion and conclusions 97
4.8.1 Discussion 97
4.8.2 Conclusions 99
Chapter 5 Inversion of the analytic signal 100
5.1 Introduction of the analytic signal 100
5.2 Forward modeling 102
5.3 Method of inversion 102
5.3.1 Jacobian matrix 103
5.3.2 Convergence 103
5.3.3 Technique of the inversion 103
5.4 Tests 107
5.4.1 Tests for the analytic signal inversion with method-1 107
5.4.1.1 Tests for the analytic signal inversion in absence of remanent magnetization with method-1 107

5.4.1.2 Tests for the analytic signal inversion in presence of remanent magnetization with method-1 111
5.4.1.3 Conclusion 114
5.4.2 Tests for analytic signal inversion with method-2 114
5.4.2.1 Tests for the analytic signal inversion in absence of remanent magnetization with method-2 115
5.4.2.1.1 Validation with models for the analytic signal inversion in absence of remanent magnetization (Method-2) 115
5.4.2.1.2 The robustness of the analytic signal inversion in absence of remanent magnetization to the initial values (method-2) 118
5.4.2.2 Tests for the analytic signal inversion in presence of remanent magnetization with method-2 119
5.4.2.2.1 The validation with models for the analytic signal inversion in presence of remanent magnetization (method-2) 119
5.4.2.2.2 The robustness of the analytic signal inversion in presence of remanent magnetization to the initial values (method-2) 122
5.4.2.3 Tests for addition of noise 123
5.5 Conclusions 126
5.6 Discussion 126
Chapter 6 Joint inversion of the magnetic field and its analytic signal 129
6.1 Introduction of joint inversion 129
6.2 The model of the joint inversion 131
6.3 Forward modeling 131
6.4 Formulation of the joint inversion 132
6.5 Normalization 134
6.6 Weighting of the two sets of the data 134
6.7 The convergence 135
6.8 The technique of the joint inversion 135
6.9 Tests 139
6.9.1 Tests for joint inversion in absence of remanent magnetization 139
6.9.1.1 The validation with models for joint inversion of the magnetic field and its analytic signal in absence of remanent magnetization 139
6.9.1.2 The robustness of the joint inversion of the magnetic field and its analytic signal in absence of remanent magnetization to the initial values ... 144

6.9.2 Tests for joint inversion in presence of remanent magnetization 144
6.9.2.1 The validation with models for joint inversion of the magnetic field and its analytic signal in presence of remanent magnetization 145
6.9.2.2 The robustness of joint inversion of the magnetic field and its analytic signal in presence of remanent magnetization to the initial values 151
6.9.3 Test for robustness to noise of the joint inversion 153
6.10 Application to the real data 156
6.11 Conclusions and discussion 164
Chapter 7 Conclusions and discussion 167
7.1 Conclusions 167
7.2 Discussion 168
References 171
Appendices 182

List of tables

Table 2.1 Descriptions of different types of remanent magnetization (adopted from Shearer, 2005) 20

Table 4.1 Results of the tests with models without remanent magnetization 81
Table 4.2 Results of tests of sensibilities to the initial values without remanent magnetization 85
Table 4.3 Results of the tests with models with remanent magnetization 87
Table 4.4 Results of tests of sensibilities with initials values with remanent magnetization 93
Table 4.5 Model of the inversion with remanent magnetization with addition of noise 94
Table 4.6 Results of the inversion with remanent magnetization with addition of noise (2nT) 95

Table 5.1 Results for analytic signal inversion without remanent magnetization (Method-1) 107
Table 5.2 Results of analytic signal inversion with remanent magnetization (Method-1) 114
Table 5.3 Results of the analytic signal inversion without remanent magnetization (Method-2) 117
Table 5.4 Results of tests of sensibilities to the initial values without remanent magnetization 118
Table 5.5 Results of the analytic signal inversion with remanent magnetization (Method-2) 119
Table 5.6 Results of tests of sensibilities with initials values with remanent magnetization 123

Table 5.7 Model to be tested with addition of noise 123
Table 5.8 Results tested with addition of noise 124
Table 6.9 Results of the joint inversion without remanent magnetization 139
Table 6.10 Comparison of results of inversions without remanent magnetization ... 143
Table 6.11 Results of tests of sensibilities with initials values for joint inversion without remanent magnetization 144
Table 6.12 Results of joint inversion with remanent magnetization 145
Table 6.13 Comparison of the results from all studied inversions in the presence of remanent magnetization 150
Table 6.14 Results of tests of sensibilities with initials values for joint inversion with remanent magnetization 151
Table 6.15 Comparison of results tested by magnetic field inversion (FI), analytic signal inversion (ASI) and joint inversion with addition of noise (2nT/5nT) 153
Table 6.16 Inverted depths of magnetic data upward of Peddie Pipe 160
Table A.17 -Parameters of the models of the vertical cylinders with remanent magnetization (1) 182
Table A.18 -Parameters of the models of the vertical cylinders with remanent magnetization (2) 183
Table A.19 -Parameters of the models of the vertical cylinders with remanent magnetization (1) 183
Table A.20 -Parameters of the models of the vertical cylinders with remanent magnetization (2) 184
Table A.21 -Results of analytic signal inversions of the models (1) 184
Table A.22 -Results of analytic signal inversions of the models (2) 185
Table A.23 -Results of analytic signal inversions of the models (1) 185
Table A.24 -Results of analytic signal inversions of the models (2) 186

List of figures

Fig.1.1 Model of kimberlite pipe (after Hawthorne, 1975) 3

Fig.1.2 Polarity of the Earth's magnetic field as a function of geological time. The paleomagnetic record is less detailed than the sea-floor data. Through the Cambrian to the Permian the field was mostly reversed, Triassic through Cretaceous mostly normal, and about half and half in the recent Cenozoic. 6

Fig.2.1 The orientation of the main magnetic field can be described using inclination (I) and declination (D). Inclination is the angle between the magnetic field vector and the local horizontal plane of the Earth. Declination is the angle between the magnetic field projections to the Earth's surface and geographic north. 16

Fig.2.2 The relationship between total magnetization, induced magnetization and remanent magnetization. 17

Fig.2.3 Orientation of atoms and dipole moments before magnetization 19

Fig.2.4 Orientation of atoms and dipole moments in the external field 19

Fig.3.1 Semi-infinite cylinder of radius a and the coordinate system used. The total magnetic field is evaluated at point P above the cylinder. 29

Fig.3.2 Contour of the total magnetic field of first model 43

Fig.3.3 Profile at y =1175m of the total magnetic field of first model 43

Fig.3.4 Contours of the calculated vertical gradient and the numerical vertical gradient of the first model 44

Fig.3.5 Profiles at y =1175m of the calculated vertical gradient and numerical vertical gradient of first model 44

Fig.3.6 Contours of the calculated horizontal x gradient and numerical horizontal x gradient of first model 45
Fig.3.7 Profiles at y =1175m of the calculated horizontal x gradient and numerical horizontal x gradient of first model 45
Fig.3.8 Contours of the calculated horizontal y gradient and numerical horizontal y gradient of first model 46
Fig.3.9 Profiles at y =1175m of the calculated horizontal y gradient and numerical horizontal y gradient of first model 46
Fig.3.10 Contours of the calculated analytic signal and numerical analytic signal of first model 47
Fig.3.11 Profiles at y =1175m of the calculated analytic signal and numerical analytic signal of first model 47
Fig.3.12 Contour of the total magnetic field of second model 49
Fig.3.13 Profile at y =425m at the total magnetic field of second model 50
Fig.3.14 Contours of the calculated vertical derivative and numerical vertical derivative of second model 50
Fig.3.15 Profiles at y =425m of the calculated vertical derivative and numerical vertical derivative of second model 51
Fig.3.16 Contours of the calculated x derivative and numerical x derivative of second model 51
Fig.3.17 Profiles at y =425m of the calculated x derivative and numerical x derivative of second model 52
Fig.3.18 Contours of the calculated y derivative and numerical y derivative of second model 53
Fig.3.19 Profiles at y =425m of the calculated y derivative and numerical y derivative of second model 53

Fig.3.20 Contours of the calculated analytic signal and numerical analytic signal of second model 54
Fig.3.21 Profiles at y =425m of the calculated analytic signal and numerical analytic signal of second model 54
Fig.3.22 Contour of the total magnetic field of third model 56
Fig.3.23 Profile at y =800m of the total magnetic field of third model 57
Fig.3.24 Contours of the calculated vertical derivative and numerical vertical derivative of third model 58
Fig.3.25 Profiles at y =800m of the calculated vertical derivative and numerical vertical derivative of third model 58
Fig.3.26 Contours of the calculated x derivative and numerical x derivative of third model 59
Fig.3.27 Profiles at y =800m of the calculated x derivative and numerical x derivative of third model 59
Fig.3.28 Contours of the calculated y derivative and numerical y derivative of third model 60
Fig.3.29 Profiles at y =800m of the calculated y derivative and numerical y derivative of third model 60
Fig.3.30 Contours of the calculated analytic signal and numerical analytic signal of third model 61
Fig.3.31 Profiles at y =800m of the calculated analytic signal and numerical analytic signal of third model 61
Fig.3.32 Contour of total magnetic field of fourth model 62
Fig.3.33 Profile at y =425m of total magnetic field of forth model 63
Fig.3.34 Contours of calculated vertical derivative and numerical vertical derivative of forth model 64
Fig.3.35 Profiles at y =425m of calculated vertical derivative and numerical vertical derivative of forth model 64

Fig.3.36 Contours of calculated x derivative and numerical x derivative of forth model 65

Fig.3.37 Profiles at y =425m of calculated x derivative and numerical x derivative of forth model 65

Fig.3.38 Contours of calculated y derivative and numerical y derivative of forth model 66

Fig.3.39 Profiles at y =425m of calculated y derivative and numerical y derivative of forth model 66

Fig.3.40 Contours of calculated analytic signal and numerical analytic signal of forth model 67

Fig.3.41 Profiles of y =425m of calculated analytic signal and numerical analytic signal of forth model 67

Fig.4.1 Relationship between the induced magnetization intensity J_i and remanent magnetization intensity J_r 71

Fig.4.2 Model Defang2: Geomagnetic field intensity: 55278nT , inclination of geomagnetic field : 69^0, declination of geomagnetic field : 12^0, depth of the cylinder:50m, diameter of the model : 160, height: 200m, magnetic susceptibility:0.01 SI. 82

Fig.4.3 Model Defang5: Geomagnetic field intensity: 55278nT , inclination of geomagnetic field : 30^0, declination of geomagnetic field : 12^0, depth of the cylinder:50m, diameter of the model : 160, height: 200m,magnetic susceptibility:0.01 SI. 83

Fig.4.4 Model Atestm1: Geomagnetic field intensity: 57170nT , inclination of geomagnetic field : 74^0, declination of geomagnetic field : -12^0, depth of the cylinder:100m, diameter of the model : 160,height: 300m,magnetic susceptibility:0.01 SI. 84

Fig.4.5 Model Vjina111t6: Geomagnetic field intensity: 57170nT , inclination of geomagnetic field : 74^0, declination of geomagnetic field : -12^0, depth of the cylinder: 60m, diameter of the model : 160, height: 300m, magnetic susceptibility: 0.01 SI. Inclination of remanent magnetization: 1^0, declination of the remanent magnetization: 30^0, position of the center of the cylinder: (375,375), konigsberger ratio parameter Q: 5 88

Fig.4.6 Model AteR1: Geomagnetic field intensity: 57170nT , inclination of geomagnetic field : 74^0, declination of geomagnetic field : -12^0, depth of the cylinder:60m, diameter of the model : 200, height: 300m, magnetic susceptibility:0.01 SI. Inclination of remanent magnetization: 70^0, declination of the remanent magnetization: -30^0, position of the center of the cylinder: (500,500), konigsberger ratio parameter Q:5 89

Fig.4.7 Model Vjina111t21116: Geomagnetic field intensity: 57170nT , inclination of geomagnetic field : 74^0, declination of geomagnetic field : -12^0, depth of the cylinder:80m, diameter of the model : 300, height: 600m, magnetic susceptibility:0.01 SI. Inclination of remanent magnetization: 210^0, declination of the remanent magnetization: 30^0, position of the center of the cylinder: (1050,1050), konigsberger ratio parameter Q:5 90

Fig.4.8 Model Vjina111t215n1: Geomagnetic field intensity: 57170nT , inclination of geomagnetic field : 74^0, declination of geomagnetic field : -12^0, depth of the cylinder:80m, diameter of the model : 200, height: 300m, magnetic susceptibility:0.01 SI. Inclination of remanent magnetization: 250^0, declination of the remanent magnetization: -30^0, position of the center of the cylinder: (375,375), konigsberger ratio parameter Q:5 91

Fig.4.9 Model Geomtest3: Geomagnetic field intensity: 57170nT , inclination of geomagnetic field : 74^0, declination of geomagnetic field : -12^0, depth of the cylinder:150m, diameter of the model : 160, height: 200m,magnetic

susceptibility:0.01 SI. Inclination of remanent magnetization: 65^0, declination of the remanent magnetization: -15^0, position of the center of the cylinder: (375,375), konigsberger ratio parameter Q:2 92

Fig.4.10.1 Model Vjina111t3: Geomagnetic field intensity: 57170nT, inclination of geomagnetic field : 74^0, declination of geomagnetic field : -12^0, depth of the cylinder:60m, diameter of the model : 160, height: 300m, magnetic susceptibility:0.01 SI. Inclination of remanent magnetization: 30^0, declination of the remanent magnetization: 30^0, position of the center of the cylinder: (375,375), konigsberger ratio parameter Q:5 addition of random noise: 2nT 96

Fig.4.11.2 Model Vjina111t3, no addition of noise 97

Fig.5.1 Model Defang2: Geomagnetic field intensity: 55278nT, inclination of geomagnetic field : 69^0, declination of geomagnetic field : 12^0, depth of the cylinder:50m, diameter of the model : 160, height: 200m, magnetic susceptibility:0.01 SI. 108

Fig.5.2 Model Defang5: Geomagnetic field intensity: 55278nT, inclination of geomagnetic field : 30^0, declination of geomagnetic field : 12^0, depth of the cylinder:50m, diameter of the model : 160, height: 200m, magnetic susceptibility:0.01 SI. 109

Fig.5.3 Model Atestm1: Geomagnetic field intensity: 57170Nt, inclination of geomagnetic field : 74^0, declination of geomagnetic field : -12^0,depth of the cylinder:100m, diameter of the model :160, height: 300m,magnetic susceptibility:0.01 SI. 110

Fig.5.4 Model Vjina111t6: Geomagnetic field intensity: 57170nT, inclination of geomagnetic field : 74^0, declination of geomagnetic field : -12^0, depth of the cylinder:60m, diameter of the model : 160, height: 300m, magnetic

susceptibility:0.01 SI. Inclination of remanent magnetization: 1^0, declination of the remanent magnetization: 30^0, position of the center of the cylinder: (375,375), konigsberger ratio parameter Q:5 111

Fig.5.5 Model AteR1: Geomagnetic field intensity: 57170nT, inclination of geomagnetic field : 74^0, declination of geomagnetic field : -12^0, depth of the cylinder:60m, diameter of the model : 200, height: 300m, magnetic susceptibility:0.01 SI. Inclination of remanent magnetization: 70^0, declination of the remanent magnetization: -30^0, position of the center of the cylinder: (500,500), konigsberger ratio parameter Q:5 112

Fig.5.6 Model Vjina111t21116: Geomagnetic field intensity: 57170nT, inclination of geomagnetic field : 74^0, declination of geomagnetic field : -12^0, depth of the cylinder:80m, diameter of the model : 300, height: 600m, magnetic susceptibility:0.01 SI. Inclination of remanent magnetization: 210^0, declination of the remanent magnetization: 30^0, position of the center of the cylinder: (1050,1050), konigsberger ratio parameter Q:5 113

Fig.5.7 Results of inversion for model Defang2 with Method-2 115

Fig.5.8 Results of inversion for model Defang5 with Method-2 116

Fig.5.9 Results of inversion for model Atestm1 with Method-2 117

Fig.5.10 Results of inversion for model Vjina111t6 with Method-2 120

Fig.5.11 Results of inversion for model AteR1 with Method-2 121

Fig.5.12 Results of inversion for model Vjina111t21116 with Method-2 122

Fig.5.13.1 Model Vjina111t3: Geomagnetic field intensity: 57170nT, inclination of geomagnetic field : 74^0, declination of geomagnetic field : -12^0, depth of the cylinder:60m, diameter of the model : 160, height: 300m, magnetic susceptibility:0.01 SI. Inclination of remanent magnetization: 30^0, declination of the remanent magnetization: 30^0, position of the center of the

cylinder: (375,375) , konigsberger ratio parameter Q:5 addition of random noise: 2nT 124
Fig.5.14.2 Model Vjina111t3, without addition of the noise 125

Fig.6.1 Results of joint inversion for model Defang2 140
Fig.6.2 Results of joint inversion for model Defang5 141
Fig.6.3 Results of joint inversion for model Atestm1 142
Fig.6.4 Results of joint inversion of the model Vjina111t6 147
Fig.6.5 Results of joint inversion of the model AteR1 148
Fig.6.6 Results of joint inversion of the model Vjina111t21116 149
Fig.6.7 Results of joint inversion of the model Vjina111t3 with 2nT noise 155
Fig.6.8 Results of the magnetic inversion for data of Peddie Pipe 157
Fig.6.9 Results of the analytic signal inversion for data of Peddie Pipe 158
Fig.6.10 Results of the joint inversion for data of Peddie Pipe 159
Fig.6.11 Results of the magnetic inversion for data of Peddie Pipe (12m up continuation) 160
Fig.6.12 Results of the analytic signal inversion for data of Peddie Pipe (12m up continuation) 162
Fig.6.13 Results of the joint inversion for data of Peddie Pipe (12m up continuation) 163

Fig.C.1 Contour of the total magnetic field of first set of data Depth =80m 193
Fig.C.2 profile at y =1175m of the total magnetic field of first model Depth =80m 194
Fig.C.3 Contours of the analytic vertical derivative and the numerical vertical derivative of first model Depth =80m. 194
Fig.C.4 Profiles at y =1175m of the analytic vertical derivative and the numerical vertical derivative of first model Depth =80m 195

Fig.C.5 Contours of the analytic x derivative and the numerical x derivative of first model Depth =80m. 196
Fig.C.6 Profiles at y =1175m of the analytic x derivative and the numerical x derivative of first model Depth =80m 196
Fig.C.7 Contours of the analytic y derivative and the numerical y derivative of first model Depth =80m. 197
Fig.C.8 Profiles at y =1175m of the analytic y derivative and the numerical y derivative of first model Depth =80m 197
Fig.C.9 Contours of the analytic signal and numerical analytic signal of first model Depth =80m 198
Fig.C.10 Profiles at y =1175m of the analytic signal and numerical analytic signal of first model Depth =80m 198
Fig.C.11 Contour of the total magnetic field of first model Depth =100m. 200
Fig.C.12 Profile at y =1175m of the total magnetic field of first model Depth =100m 200
Fig.C.13 Contours of the analytic vertical derivative and numerical vertical derivative of first model Depth =100m 201
Fig.C.14 Profiles at y =1175m of the analytic vertical derivative and numerical vertical derivative of first model Depth =100m 201
Fig.C.15 Contours of the analytic x derivative and numerical x derivative of first model Depth =100m 202
Fig.C.16 Profiles at y =1175m of the analytic x derivative and numerical x derivative of first model Depth =100m 203
Fig.C.17 Contours of the analytic y derivative and numerical y derivative of first model Depth =100m 203
Fig.C.18 Profiles at y =1175m of the analytic y derivative and numerical y derivative of first model Depth =100m 204

Fig.C.19 Contours of the analytic signal and numerical analytic signal of first model Depth =100m 204
Fig.C.20 Profiles at y =1175m of the analytic signal and numerical analytic signal of first model Depth =100m 205

Fig.D.1 Contour of the total magnetic field of second model Radius=200m. 206
Fig.D.2 Profile at y =425m of the total magnetic field of second model Radius=200m 207
Fig.D.3 Contours of the analytic vertical derivative and numerical vertical derivative of second model Radius=200m. 207
Fig.D.4 Profiles at y =425m of the analytic vertical derivative and numerical vertical derivative of second model Radius=200m 208
Fig.D.5 Contours of the analytic x derivative and numerical x derivative of second model Radius=200m. 208
Fig.D.6 Profiles at y =425m of the analytic x derivative and numerical x derivative of second model Radius=200m 209
Fig.D.7 Contours of the analytic y derivative and numerical y derivative of second model Radius=200m. 209
Fig.D.8 Profiles at y =425m of the analytic y derivative and numerical y derivative of second model Radius=200m 210
Fig.D.9 Contours of the analytic signal and numerical analytical signal of second model Radius=200m 211
Fig.D.10 Profiles of y =425m of the analytic signal and numerical analytical signal of second model Radius=200m 211
Fig.D.11 Contour of the total magnetic field of second set of data Radius=300m. ... 212
Fig.D.12 Profile at y =425m of the total magnetic field of second model Radius=300m 213

Fig.D.13 Contours of the analytic vertical derivative and numerical vertical derivative of second model Radius=300m 213

Fig.D.14 Profiles at y =425m of the analytic vertical derivative and numerical vertical derivative of second model Radius=300m 214

Fig.D.15 Contours of the analytic x x derivative and numerical x derivative of second model Radius=300m. 214

Fig.D.16 Profiles of y =425m of the analytic x derivative and numerical x derivative of second model Radius=300m 215

Fig.D.17 Contours of the analytic y derivative and numerical y derivative of second model Radius=300m. 215

Fig.D.18 Profiles at y =425m of the analytic y derivative and numerical y derivative of second model Radius=300m 216

Fig.D.19 Contours of the analytic signal and numerical analytic signal of second model Radius=300m. 216

Fig.D.20 Profiles at y =425m of the analytic signal and numerical analytic signal of second model Radius=300m 217

Fig.E.1 Contour of the total magnetic field of third set of data, total inclination = 40° 218

Fig.E.2 Profile y =800m of the total magnetic field of third model total inclination = 40° 218

Fig.E.3 Contours of the analytic vertical derivative and numerical analytic vertical derivative of third model, total inclination = 40° 219

Fig.E.4 Profiles at y =800m of the analytic vertical derivative and numerical analytic vertical derivative of third model, total inclination = 40° 219

Fig.E.5 Contours of the analytic x derivative and numerical analytic x derivative of third model, total inclination = 40° 220

Fig.E.6 Profiles at y =800m of the analytic x derivative and numerical analytic x derivative of third set of data, total inclination = 40° 220

Fig.E.7 Contours of the analytic y derivative and numerical analytic y derivative of third model, total inclination = 40° 221

Fig.E.8 Profiles of y =800m of the analytic y derivative and numerical analytic y derivative of third model, total inclination = 40° 221

Fig.E.9 Contours of the analytic signal and numerical analytic signal of third model, total inclination = 40°. 222

Fig.E.10 Profiles of y =800m of the analytic signal and numerical analytic signal of third set of data, total inclination = 40°. 222

Fig.E.11 Contour of total magnetic field of third set of data, total inclination = 30° 223

Fig.E.12 Profile y =800m of total magnetic field of third model, total inclination = 30° 223

Fig.E.13 Contours of analytic vertical derivative and numerical vertical derivative of third model, total inclination = 30° 224

Fig.E.14 Profiles at y = 800m of analytic vertical derivative and numerical vertical derivative of third model, total inclination = 30° 224

Fig.E.15 Contours of analytic x derivative and numerical x derivative of third model, total inclination = 30°. 225

Fig.E.16 Profiles at y = 800m of analytic x derivative and numerical x derivative of third model, total inclination = 30° 225

Fig.E.17 Contours of analytic y derivative and numerical y derivative of third model, total inclination = 30° 226

Fig.E.18 Profiles at y = 800m of analytic y derivative and numerical y derivative of third model, Total inclination = 30° 226

Fig.E.19 Contours of analytic signal and numerical analytic signal of third model, total inclination $=30^{\circ}$ 227

Fig.E.20 Profiles at y = 800m of analytic signal and numerical analytic signal of third model, total inclination $=30^{\circ}$ 227

Fig.F.1 Contour of total magnetic field of forth model, Remanent inclination $=-30^{\circ}$ 229

Fig.F.2 Profile at y =425m of total magnetic field of forth set of data, remanent inclination = -30° 229

Fig.F.3 Contours of analytic vertical derivative and numerical vertical derivative of forth model, remanent inclination $=-30^{\circ}$ 230

Fig.F.4 Profiles at y =425m of analytic vertical derivative and numerical vertical derivative of forth model, remanent inclination = -30° 230

Fig.F.5 Contours of analytic x derivative and numerical x derivative of forth set of data. Remanent inclination $=-30^{\circ}$. 231

Fig.F.6 Profiles at y =425m of analytic x derivative and numerical x derivative of forth model, remanent inclination = -30° 231

Fig.F.7 Contours of analytic y derivative and numerical y derivative of forth model remanent inclination $=-30^{\circ}$ 232

Fig.F.8 Profiles at y =425m of analytic y derivative and numerical y derivative of forth model, remanent inclination = -30° 232

Fig.F.9 Contours of analytic signal and numerical analytic signal of forth model remanent inclination $=-30^{\circ}$. 233

Fig.F.10 Profiles at y =425m of analytic signal and numerical analytic signal of forth model remanent inclination = -30° 233

Fig.F.11 Contour of total magnetic field of forth model remanent inclination= -10° 234

Fig.F.12 Profile at y =425m of total magnetic field of forth model, remanent inclination= -10° 235

Fig.F.13 Contours of analytic vertical derivative and numerical vertical derivative of forth model, remanent inclination = -10° 235

Fig.F.14 Profiles at y =425m of analytic vertical derivative and numerical vertical derivative of forth model, remanent inclination = -10° 236

Fig.F.15 Contours of analytic x derivative and numerical x derivative of forth model, remanent inclination = -10° 236

Fig.F.16 Profiles at y =425m of analytic x derivative and numerical x derivative of forth model, remanent inclination = -10° 237

Fig.F.17 Contours of analytic y derivative and numerical y derivative of forth model, remanent inclination = -10° 237

Fig.F.18 Profiles at y =425m of analytic y derivative and numerical y derivative of forth model, remanent inclination = -10° 238

Fig.F.19 Contours of analytic signal and numerical analytic signal of forth model remanent inclination = -10° 238

Fig.F.20 Profiles at y =425m of analytic signal and numerical analytic signal of forth model, remanent inclination = -10° 239

List of abbreviations

TFA	Total magnetic field anomaly
TMF	Total magnetic field inversion
RMN	Remanent magnetization magnetic field inversion
ANSIG	Inversion of amplitude of analytic signal of the magnetic field intensity
ANSUGREM	Remanent magnetization inversion of analytic signal
J_i	Induced magnetization intensity
J_r	Remanent magnetization intensity
J_{tot}	Total magnetization intensity of magnetic field
I_m	Total inclination of the magnetic field
D_m	Total declination of the magnetic field
I	Induced inclination of the magnetic field
D	Induced declination of the magnetic field
Ir/Inr.	Remanent magnetization inclination of magnetic field
Dr/Der.	Remanent magnetization declination of magnetic field
Q	Koenigsberger ration or coefficient of koenigsberger
rms	Root mean squares error
Th. / *th*	Depth extension of the cylinder
Dep.	Depth of the cylinder
Dia.	Diameter of the cylinder
MSu.	Magnetic susceptibility
SI	International system

T_0	Earth magnetic field intensity
I_0	Inclination of the geomagnetic field
D_0	Declination of the geomagnetic field
DRM	Detrital remanent magnetization
3D	Three dimensions

List of appendices

Appendix A: List of the models and results of the analytic inversion 182

Appendix B: Analytic expressions of the *a* derivative of the anomaly due to a vertical right circular cylinder with arbitrary polarization 186

Appendix C: Sensibility of the results of calculations of the derivatives to the changes of depth 192

Appendix D: Sensibility of the results of calculations of derivatives to changes of radius 206

Appendix E: Sensibility of the results of calculations of the derivative to changes of the inclination 217

Appendix F: Sensibility of the results of calculations of derivatives to changes of remanent inclination 228

Chapter 1 Introduction

1.1 Introduction

This chapter presents the originality of my research, the problems met, the progress made and the work plan. The goal of inversion is to minimize the difference between the observations and the response of a synthetic model. The minimization is obtained by varying the parameters of the model and is usually done in the least-squares sense. For the inversion of magnetic data due to the vertical right circular cylinder with arbitrary polarization, a major problem is the presence of magnetic remanent magnetization. This is especially the case in diamond exploration as the magnetization of the many kimberlites pipes, which are a major source of diamonds, is dominated by remanent magnetization. Separation of the remanent magnetization is very important. The identification of magnetic remanent magnetization has generated a lot of interesting research but many problems still remain. The inversion of magnetic data in the presence of remanent magnetization is unstable; specifically the remanent magnetization direction and intensity are poorly resolved. The 2D analytic signal of a 2D magnetic anomaly is independent of the inducing field direction and remanent magnetization direction; however the 3D analytic signal is not totally independent of the local geomagnetic field and remanent magnetization orientations. A joint inversion of the magnetic anomaly and its analytical signals should increase the stability of the inversion. In this respect, I developed a joint inversion scheme that makes use of the Levenberg- Marquardt method using the magnetic field anomaly and its analytical signal. To do this, I need to derive the analytic expressions for the magnetic anomaly and its derivatives, as well as for its analytic signal, formulate the joint inversion, and correctly normalize and weight the two sets of data. Finally, results of the inversion will be tested with synthetic data and real case.

1.2 Diamonds and kimberlites

Diamonds have inspired dreams of wealth and power throughout history; most of them were insignias of royalty. They have value not only as gems, but also because

their unusual physical properties are indispensable to industry. They are required in drilling, metal cutting, and polishing of extremely hard surfaces (Erlich and Hausel, 2002). Most modern diamond exploration programs are designed to search for conventional diamondiferous host rocks: the kimberlite and lamproite, or for placer deposits presumably derived from these rocks. Mitchell and Bergman (1991) report that the total volume of known kimberlite in the world is on the order of >5,000km^3; for lamproite, it is only<100km^3. Kimberlite is thus the most important source of diamonds in the world.

Kimberlite is a volatile-rich, potassic, ultrabasic igneous rock that is enriched in some incompatible consitituents (Sr, Zr, Hf, Nb, and rare earth elements) and some compatible lithophile constituents (Ni, Cr, and Co), along with alkalis. The mineralogy of kimberlites is variable and complex. They occur as dikes, sills, blows, and pipes. Mitchell (1986) provided the following definition for kimberlite: inequigranular alkalic peridotites containing rounded and corroded megacrysts of olivine, phlogopite, magnesian ilmenite and pyrope set in fine grained groundmass of second generation euhedral olivine and phlogopite together with primary and secondary serpentine, pervoskite, carbonate and spinels. The spinels range in composition from titaniferous magnesian chromite to magnesian ulvospinel-ulvospinel-magnetite. Accessory minerals include diopside, monticellite, rutile, and nickeliferous sulphides. Some kimberlites contain major modal amounts of monticellite. The typical model of kimberlite is the shape of a carrot (See Fig.1.1).

1.3 Geophysical surveys for kimberlites

The classical model of a pipe is that of a carrot-shaped conical geometry with steeply dipping walls and a diameter vanishing with increasing depth (Skinner, 1986). Geophysical exploration methods have been used in the search for hidden kimberlite at a number of locations around the world (Litinskii 1963a,b; Gerryts 1967; Burley and Greenwood 1972; Hausel, McCallum, and Woodzick 1979; Hausel, Glahn, and Woodzick 1981; Patterson and MacFadyen 1984).The contrasting physical properties

of the diamondiferous host rock (in particular kimberlite, lamproite, and minette) and the country rock commonly allow these rocks to be distinguished by ground or airborne

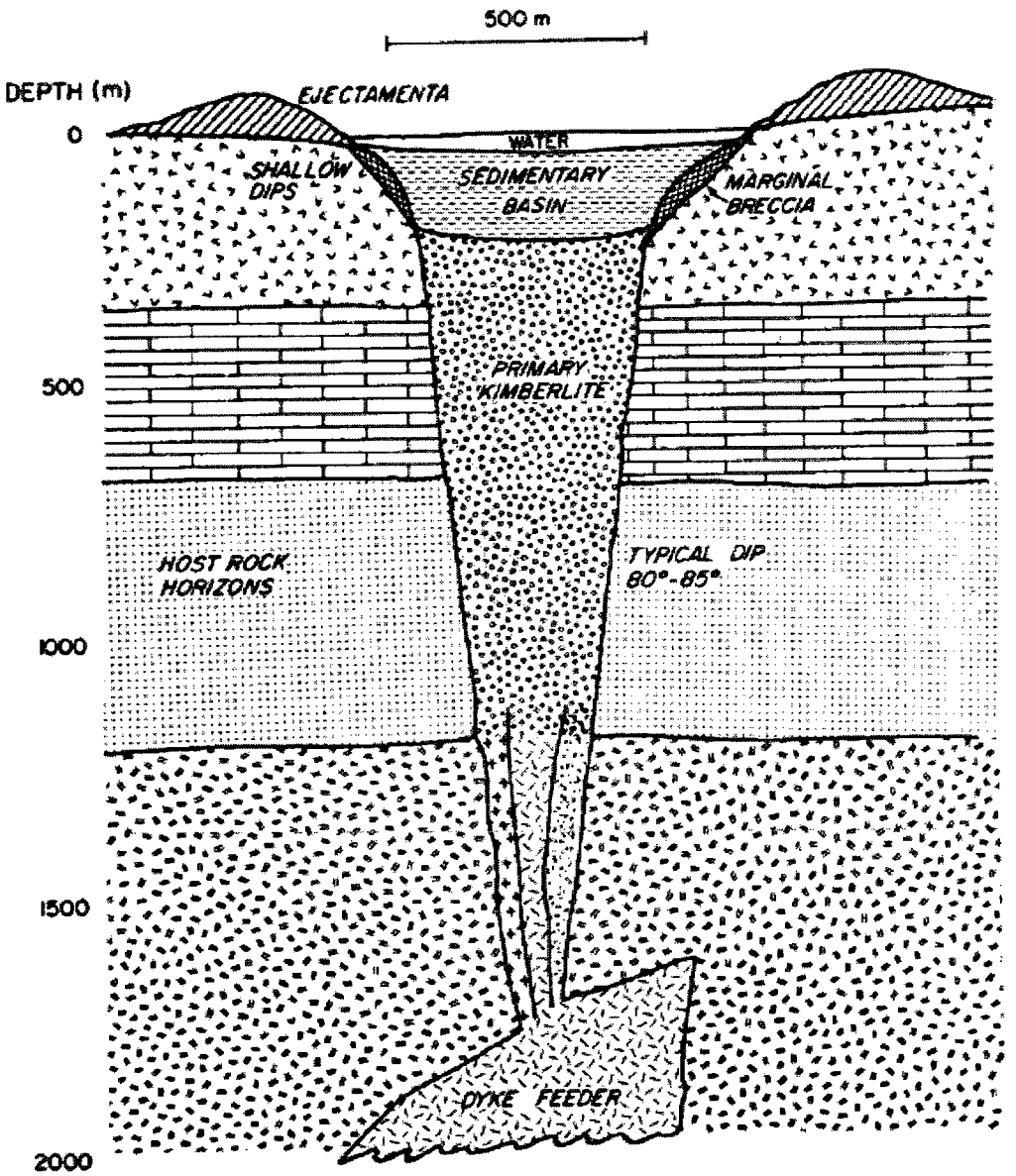

Fig.1.1 Model of kimberlite pipe (after Hawthorne, 1975)

exploration geophysical techniques. Very low frequency electromagnetic (VLF), conductivity, resistivity, seismic and gravity surveys have been used in the search for kimberlites for the direct and indirect indications of kimberlite pipes (Macnae 1995).

Among all those geophysical methods, the magnetic method is the most widely used as a primary search tool for detecting kimberlites. This is partly because magnetic airborne surveys are relatively simple and inexpensive compared to other geophysical methods. Airborne surveys can directly locate kimberlite pipes and define optimal targets for ground follow up surveys (Paulo et al., 2007). So both surface and airborne magnetic surveys have had good successes in detecting kimberlite (Bolivar and Brookins 1979, Macnae 1979, 1995, Nixon 1981, Jaques, Lewis, and Smith 1986, Coopersmith and Mitchell 1989, Atkinson 1989, and Sarma, Verma, and Satyanarayana 1999).

As for the causes of magnetic response, of course, the magnetic susceptibility is one of the main important causes. But I would like to underline the second main cause, the hard remanent magnetization. The natural remanent magnetization (NRM) is the phenomenon extensively studied by paleomagnetists whose interest lies in ancient magnetic fields; specifically their intensity and direction. There are a number of mechanisms that can cause NRM, of which the two important ones are: TRM or thermal remanent magnetization acquired by cooling from a high temperature, and CRM or chemical remanent magnetization when a magnetic mineral is formed by a chemical change at low temperature. The magnetic remanent magnetization vector is approximately oriented in the direction of the regional field at the time it was acquired. Commonly, the amplitude of hard remanent magnetization is larger than the amplitude of induced magnetism. The Koeningsberger ratio (Q) is defined as the ratio of the remanent to the induced response.

The magnetic response of kimberlites (Atkinson, 1989; Janse et al., 1989) has been mostly discussed in the geophysical exploration literature as if it was caused

solely by variations in magnetic susceptibility. Rock magnetism studies (Clark, 1983; Hargraves, 1989) and later discussions in this paper conclusively show that remanent magnetization may often be the main contributor to kimberlite magnetic responses. The direction and amplitude of the remanent magnetization may therefore be the most important property affecting many observed magnetic response.

A number of presentations at an airborne EM workshop held in Arizona in 1993 and subsequent discussions implied that about 20% to 50% of the Canadian kimberlites recently discovered in the North West Territories had a magnetic response of negative polarity (Smith et al., 1995; Paterson et al., 1993). In these cases, remanent magnetization is the dominant source of the observed anomaly, which causes that the location, sign and shape of a response to be quite different from that inferred from induced magnetisation alone.

It is reasonable to expect that the direction of remanent magnetization of a kimberlite has the same polarity as that of the Earth's field at the time of its emplacement. A compilation of the polarity over geological time is presented in the Fig.1.2.

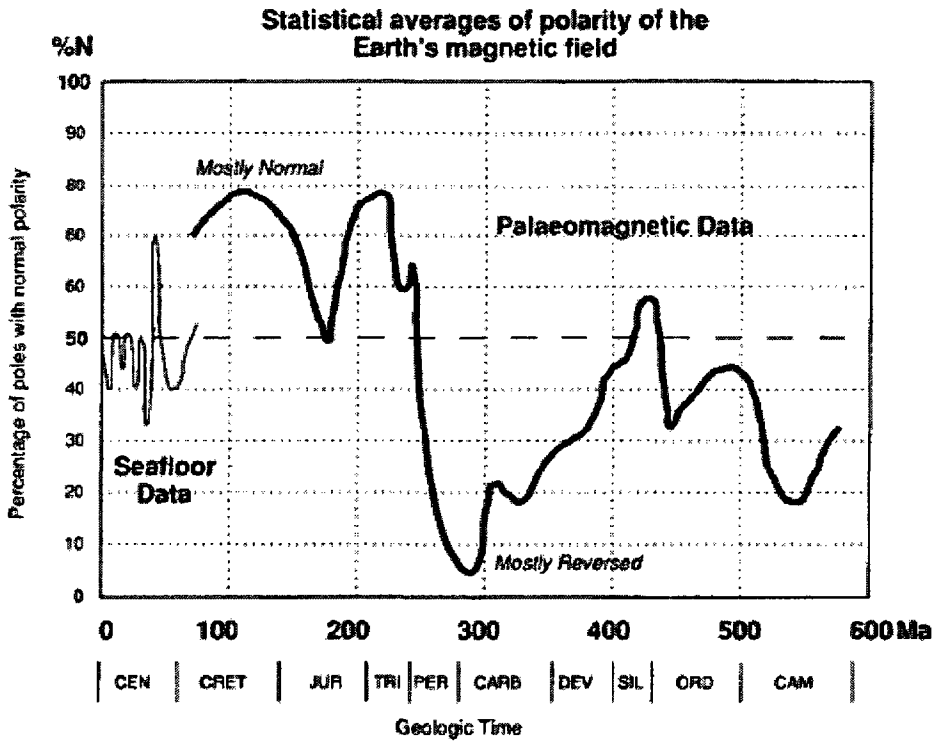

Fig.1.2 Polarity of the Earth's magnetic field as a function of geological time. The paleomagnetic record is less detailed than the sea-floor data. Through the Cambrian to the Permian the field was mostly reversed, Triassic through Cretaceous mostly normal, and about half and half in the recent Cenozoic.

Note that the Earth's field adapted from Macnae (1995) appears to be predominantly normal or predominantly reversed over extensive intervals for much of post-Cambrian geological time. At any specific location, independent of reversals, the direction of remanent magnetization is likely to be altered from that of the present Earth's field by continental drift (Macnae 1995). So, in the interpretation of the magnetic anomalies, the determination of the magnetic remanent magnetization strength and direction is very important.

1.4 Problem

Diamond exploration in Canada is accelerating. Since 1993, Ashton Mining has discovered 75 kimberlites in Canada, and is now focusing its attention in Quebec and

in northern Canada (Forrest, 2006). Diamond deposits in northern Canada are hosed in kimberlite intrusions within and adjacent to the Archean Slave Craton in the NWT and Nunavut Territories (Power, Belcourt, & Rockel, 2004). In most intrusive settings, there is a positive susceptibility contrast between the kimberlite and the surrounding rock. The best method to identify the signature of the kimberlite is magnetics. The magnetic signature of most kimberlite pipes is, at high magnetic latitudes, a circular anomaly; at lower magnetic latitudes, it becomes asymmetrical; and at the magnetic equator, the anomaly is mostly negative. The shape of the anomaly is also influenced by the presence of remanent magnetization (Keating & Sailhac, 2004).

Many of the kimberlites from the Northwest Territories in Canada have a reversed magnetization. In the interpretation of their magnetic anomalies, the determination and separation of the remanent magnetization is very important. Unfortunately, in many cases, it is difficult to determine from the magnetic data how much induced and remanent magnetization is present in the response. Thus, it would seem that remanent magnetization of minerals and rocks should be measured from orientated cores samples. However, these approaches are not always feasible and have limitations because of their cost and time consuming(E.Shearer, 2005). Two data based approaches have been developed: the first one was proposed by Nabighian (1972, 1974) who used the analytic signal concept to potential field data in two dimensions since the 2D analytic signal is independent of the induction and the magnetization direction. However, the shape of the 3D analytic signal as defined by Roest et al. (1992) is not (Xiong, 2006). The second method is based on the assumption that the remanent magnetization does not significantly alter the total magnetization direction. Li et al. (1996) for example, developed an algorithm, MAG3D, under this assumption. Nevertheless, in many applications, remanent magnetization is often strong and cannot be disregarded (Shearer, 2005).

Shearer utilizes the analytic signal to do a physical property inversion using the model of a cube (Shearer, 2005). The analytic signal introduced by Nabighian (1972,

1974), has many advantages. Firstly, for 2D structures, it is independent of remanent magnetization; secondly, it performs well at low magnetic latitudes (Keating & Sailhac, 2004). Many geophysicist use analytic signal to interpret the magnetic anomaly. But unfortunately, the 3D analytic signal is dependent on everything that total magnetic intensity itself may depend (Xiong, 2006), though the dependence is weak.

Chemam (2006) proposed a parametric and physical property inversion of magnetic data due to a vertical right cylinder with arbitrary polarization in the presence of the remanent magnetization. He utilized the analytic expression given by Singh and Sabina (Krishna Singh & Sabina, 1978) to compute the forward model, and he introduced the remanent magnetization into the inversion, and did the initial works for the separation the remanent magnetization from the total magnetization for anomalies due to the kimberlitic pipes. The stability and the precision of his inversion need to be improved; especially the inversion in the presence of the remanent magnetization sometimes is not stable and precise.

1.5 Main objectives

The goal of my research project is to improve the inversion of magnetic data due to a vertical right cylinder with arbitrary polarization, to improve the separation of the remanent magnetization vector from the total magnetization vector, to implement the analytical signal inversion, and to implement the joint inversion of magnetic field and its analytic signal. The joint inversion is expected to improve the stability of the inversion.

1.6 Methodology

1.6.1 The works which are implemented to complete the planned jobs

1. Derivatives of magnetic field

The following section deals with the derivation of the analytical expressions of the x derivatives, y derivatives and z derivatives of the magnetic field due to a right vertical cylinder and the comparison of the results from the analytical expressions of the derivatives to the results from the numerical derivatives.

Singh and Sabina (1978) derived the analytic expressions of the anomalies due to the right vertical cylinder; this resolved the problem of the forward modeling needed for the inversion of the magnetic anomalies due to the right vertical cylinder. But for the analytic signal inversion and the joint inversion of magnetic field and its analytic signal, we need not only to resolve the problem of forward modeling, but also to be able to calculate the partial derivatives of the Jacobian matrix.

The analytic signal is defined as the amplitude of total gradient. So deriving analytic expressions of the x, y and z derivatives of magnetic field due to the right vertical cylinder is the prerequisite to the implementation of the analytic signal inversion and the joint inversion of the magnetic field and its analytic signal. In the analytic expressions of the magnetic field, there are two incomplete elliptic integrals and two complete elliptic integrals; they are the key points to the computation of the derivatives of the magnetic field. Firstly, we need to get the analytic expressions for the derivatives of the complete elliptic integrals and the incomplete elliptic integrals. Secondly, in the analytic expressions for the derivatives of the complete elliptic integrals and the incomplete elliptic integrals, there are the Legendre's standard integrals which are expressed in terms of the so-called factors R_f, R_d. The factors R_f, R_d are essential and their calculation is given by Carlson (1979), using the method of successive applications of the duplication theorem. Carlson and Notis (1981) present the pseudo-code for the algorithms; Chemam (2006) programmed it in Matlab.

In the process of the calculation of the analytic derivatives of the magnetic field, I compare the analytic derivatives with the numerical derivatives to check the accuracy of the computations. The numerical derivatives are computed using differences.

2. Modeling and inversion

In this section, modeling and inversion algorithms will be implemented in order to determine the parameters about the geometry, such as the depth and the diameter of the targets and the physical parameters: the total magnetization and the remanent magnetization, inclination and declination and the strength of the remanent magnetization.

The inversion proceeds into three steps. The first step is to invert the magnetic data only. Magnetic have no inherent depth resolution (Li and Oldenburg, 1996). Generally speaking, the methodology to overcome this problem is to use in the inversion an appropriate weighting function that counteracts the depth decay of the data kernels. There is no distinct separable factor defining the decay in the kernel, therefore we resort to an empirical estimate. But it is not easy to realize it successfully. Singh and Sabina (1978) derived the analytic expressions of the anomalies due to the right vertical cylinder; this cylinder is semi-infinite. In the real situation, the cylinders of kimberlites are always finite in terms of their depth extension; this explains why the magnetic has the depth decay. So I will use the finite model to fit the surface data to overcome the decay of the magnetic field.

I will use the analytic expressions of Jacobian matrix to replace the numerical derivatives in order to improve the stability of the inversion and accuracy of the results. I will substitute a new relationship between the remanent magnetization and the induced magnetization to stabilize the inversion.

In first step, the direct problem, that is the forward modeling, is solved using the mathematical formulation given by Singh and Sabina (1978), for the magnetic

anomalies due to a right vertical cylinder. Chemam (2006) gives the expression as for the remanent magnetization. The Levenberg-Marquardt least-squares method will be used to solve the inverse problem.

The second step is to invert the analytic signal. The analytic expressions of the analytic signal of the magnetic field due to the right vertical cylinder will be derived to solve the problem of the forward modeling. And with the analytic expressions of the analytic signal of the magnetic field, the expressions of the Jacobian matrix for the analytic signal inversion are derived to implement the analytic signal inversion successfully. The Levenberg-Marquardt a square-least technique is used in the inversion.

The third step is the joint inversion of the magnetic field and its analytic signal. The formulation of the joint inversion will be given, including the weighting and normalization of the two sets of data.

3. Application of the techniques to the synthetic data and real data.

All the programming is done in Matlab. Potent, the software of Geophysical Software Solution will be used to generate the synthetic data for this study. To test the capability and the precision of the algorithms, each parameter of the parameter vector will be varied; these are the depth and diameter of the model cylinder, the inclination and the declination of the remanent magnetization.

The results of the magnetic field, analytic signal inversion and the joint inversion will be compared to determine the advantages and disadvantages of the three methods.

The algorithm will be applied to real data.

1.6.2 The contributions of my thesis

The contributions of this study are as follows:

1. Improvement of the magnetic field inversion by using analytic expressions for the Jacobian matrix and substitution of a new formula for the relationship between the remanent magnetization and the induced magnetization.

2. Derivation of the analytic derivatives of the mathematical expressions for the magnetic field due to right vertical cylinder given by Singh and Sabina (1978) to make the analytic signal inversion possible, and implementation of the analytic signal inversion successfully. The inversion of the analytic signal is very useful in the presence of remanent magnetization since the results of the analytic signal inversion are less dependent of the orientation of the remanent magnetization, which increased the precision of the inversion.

3. Implementation of the joint inversion of the magnetic field and its analytic signal inversion to increase stability and the precision of the results.

1.7 The plan of the work

The outline of the thesis is as follows:

Chapter 1.

The originality of the problem, the situation of the study of this domain: including the works done by others, the problem to be resolved. The outline of the research I planned to do, the description of the methods I selected to complete my research, the contribution of my works to improve in this domain and the plan of my work to be proceeded in the following chapters.

Chapter 2.

Introduction of the concepts related to the magnetic method and the search for kimberlites. The process of the development of the magnetic method and the techniques used to search for kimberlites will be reminded to clearly present the problem I am going to solve.

Chapter 3.

Derivation of the analytic expressions for x, y and z derivatives of the magnetic anomaly due to the right vertical cylinder, and as well as the analytic expression of the analytic signal of the magnetic anomaly due to right vertical cylinder, and the comparison of computations done with the analytic expressions to computations done by numerical techniques. The programming will be in Matlab. The parameters related to the geometry of the target, the properties of the total magnetic field and the remanent magnetization will be varied in order to determine the reliability and stability and the robustness of the algorithms.

Chapter 4.

The magnetic field inversion is implemented, with the Levenberg-Marquardt method; finite extension model will be used to overcome the problem of the decay of the magnetic field. The inversion scheme is tested using synthetic data generated by Potent.

Chapter5.

The inversion of analytic inversion is implemented, with the same Levenberg-Marquardt method. The algorithm of inversion is tested using the synthetic data generated by Potent.

Chapter 6.

The algorithm of joint inversion of the magnetic field and its analytic signal inversion is implemented. The normalization and the weighting of the two sets of data are used. The results of the joint inversion are tested by synthetic data and the algorithm will be applied to the real data. The results of the magnetic field, analytic signal inversion and the joint inversion are compared to determine the advantages and disadvantages of the three methods.

Chapter 7.

Conclusions and discussion.

Chapter 2 Background

2.1 Introduction

To understand well the development to be presented in this paper, I shall give a brief overview of the concepts pertaining to the magnetic method in relation to the topic of this thesis, and give an outline of the historical developments concerned with the contribution of the remanent magnetization and its extraction from the magnetic data.

2.2 Major concepts

2.2.1 Magnetic methods

The study of the earth's magnetism is the oldest branch of geophysics. It has been known for more than three centuries. The magnetic field has been studied almost continuously since Gilbert's time, but it was not until 1843 that Von Wrede first used variations in the field to locate deposits of magnetic ore. The magnetic method is a tool to underground with the study of map the distribution of magnetic materials underground using variations in the magnetic field (Telford et al, 1990).

Until the late 1940s, magnetic field measurements were mostly made from its vertical component. This limited measurements mainly to the land surface. After World War II the fluxgate magnetometer made airborne measurements possible. Later, came the proton-precession and optically pump alkali-vapor magnetometers, which measure the total magnetic field and are more accurate. Now digital recording and processing of magnetic data removes much of the tedious works involved in reducing measurements to magnetic maps. With the development of computer science, the interpretation algorithms now make modelling of the distributions of magnetization possible.

2.2.2 Geomagnetic field

As far as exploration geophysics is concerned, the geomagnetic field of the Earth is comprised of three parts: the main field, the external field, and the variations of the main field. The main field originates internally; its distribution could be mathematically represented by a series of spherical harmonics from globally derived observations to yield the International Geomagnetic Reference Field (IGRF) (Merrill et al., 1996). The highly varying external field is, under normal conditions, a small fraction of the geomagnetic field, less than one percent, and originates from external sources such as electric currents in ionized layers of the outer atmosphere. Lastly, variations in the main field are caused by localized magnetic anomalies in the crust (Telford et al., 1990). These magnetic anomalies are the targets for the exploration geophysicists.

The main magnetic field of the Earth at any point (T) is a vector quantity and can be described using three parameters: inclination, declination, and strength. The orientation of the main field can be described using the first two parameters, as depicted in Figure 2.1. Inclination is the angle between the magnetic field and the local horizontal surface plane of the earth. Declination is the angle between the magnetic field projections to the Earth's surface and geographic north.

The magnetic field vector could also be described using three components in a Cartesian coordinate system. x positive is north, z positive is down, and y positive is east.

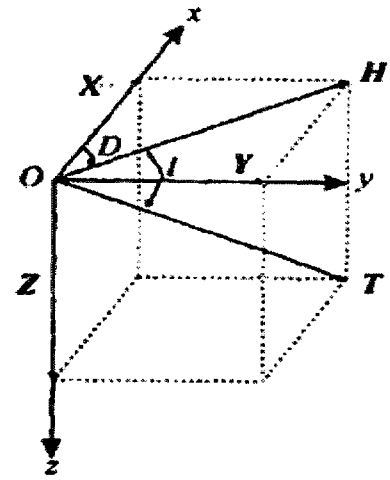

Fig.2.1 The orientation of the main magnetic field can be described using inclination (I) and declination (D). Inclination is the angle between the magnetic field vector and the local horizontal plane of the Earth. Declination is the angle between the magnetic field projections to the Earth's surface and geographic north.

X , Y , Z are respectively the three components, they have the relationship with T as follows:

$$X = H\cos D, Y = H\sin D, Z = H\tan I = T\sin I$$
$$T = \sqrt{H^2 + Z^2} = \sqrt{X^2 + Y^2 + Z^2}, H = T\cos I \quad (2.1)$$

The unit of T , X , Y , Z is Tesla (T) in SI system and gamma (γ) in cgs system.
1T=Wb/m², 1 γ=1nT = 10^{-9} T

2.2.3 Magnetization

The source distribution of the magnetic field can be described in terms of dipole density. The net volume density of magnetic dipole moments is magnetization; $\vec{J}$ Magnetization is a vector quantity defined as the sum of the individual dipole moments, $\vec{m}_i$ divided by a volume, V.

$$\vec{J} = \frac{1}{V}\sum_i \vec{m}_i \quad (2.2)$$

Magnetization is a function of location and varies from point to point (Blakely, 1996).

In a material, magnetization consists of two parts, induced magnetization, $\vec{J}_i$ and remanent magnetization, $\vec{J}_r$ (Figure 2.2)

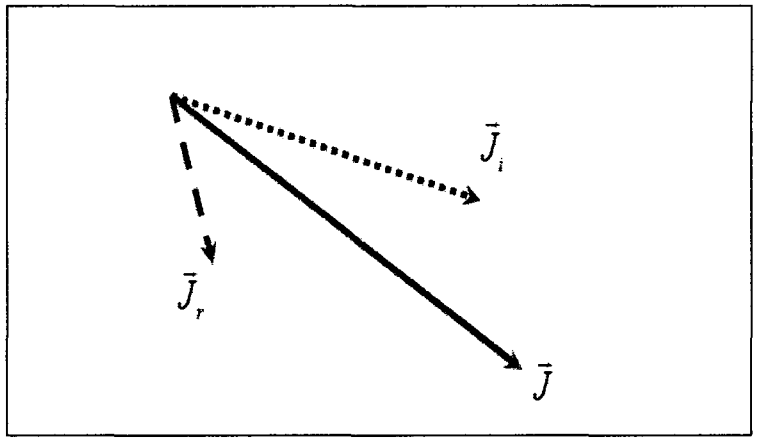

Fig.2.2 The relationship between total magnetization, induced magnetization and remanent magnetization.

$$\vec{J} = \vec{J}_i + \vec{J}_r \quad (2.3)$$

The unit of magnetization is the ampere/meter (A/m) in the SI system, while it is the gauss (G) in the cgs system, the relationship is that 1gauss=10^3 A/m.

2.2.4 Magnetic susceptibility

The degree to which a magnetic body is magnetized by induction is determined by its magnetic susceptibility. Susceptibility is the fundamental rock parameter in magnetic prospecting. The magnetic response of rocks and minerals is determined by the amounts and susceptibilities of magnetic materials in them (Telford, Geldart, and Sheriff, 1990).

Rocks that have a significant concentration of ferro and or ferri-magnetic minerals tend to have the highest susceptibilities. Consequently, basic and ultrabasic rocks have the highest susceptibility, acid igneous and metamorphic rocks have intermediate to low values, and sedimentary rocks have very small susceptibilities in general.

Table 2.1 Magnetic susceptibility values for common mineral and rock types. Taken from Sharma (1997)

Mineral or Rock Type		Magnetic Susceptibility ($\kappa \times 10^{-6}$ SI)
Granite (with magnetite)		20 – 40,000
Slates		0 – 1,200
Basalt		500 – 80,000
Oceanic basalts		300 – 36,000
Limestone (with magnetite)		10 – 25,000
Gneiss		0 – 3,000
Sandstone		35 – 950
Hematite (ore)		420 – 10,000
Magnetite (ore)		$7 \times 10^4 - 14 \times 10^6$
Magnetite (crystal)		150×10^6

Whole rock susceptibilities can vary considerably owing to a number of factors in addition to mineralogical composition. Susceptibilities depend upon the alignment and shape of the magnetic grains dispersed throughout the rock (Reynolds, 1997). Table 2.1 lists the magnetic susceptibility values for common minerals and rocks

2.2.5 Induced magnetization

Magnetization is a vector quantity defined as the sum of the individual dipole moments. Generally speaking; the atoms of the magnetisable material are disordered. We can say that, in this situation, the dipole moments in the magnetisable material are arranged randomly (Figure 2.3). So the net magnetic moment of the material is zero. The magnetisable body does not show the magnetism.

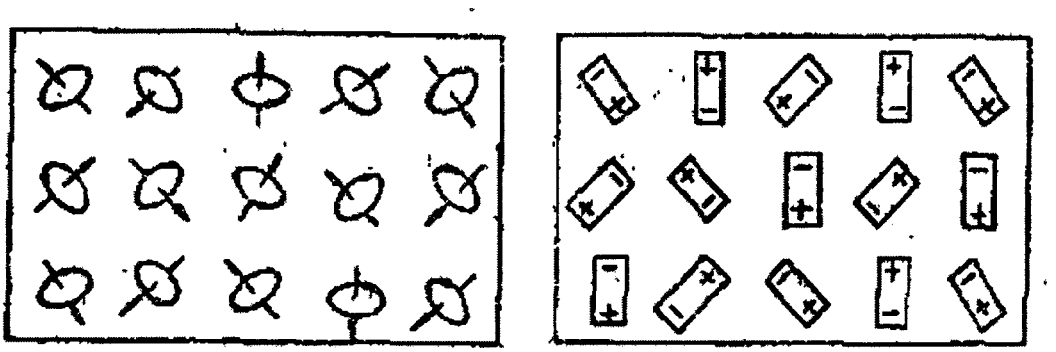

(a) Atoms and molecules before magnetization

(b) Dipole moments before magnetization

Fig.2.3 Orientation of atoms and dipole moments before magnetization

When the magnetisable body is placed in an external magnetic field, the molecules and atoms are reoriented orderly, so their spins line up, and the molecules dipole are too reoriented orderly (Figure 2.4), at this moment, the sum of the dipole moments is not zero, the material is magnetized (Huixiang et al., 1988).

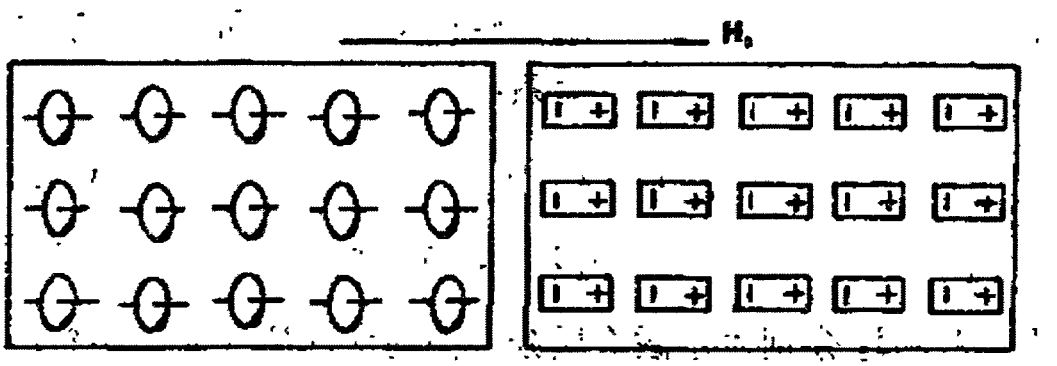

(a) The orientation of atoms in the external field

(b) The orientation of dipole moments in the external field

Fig.2.4 Orientation of atoms and dipole moments in the external field

2.2.6 Remanent magnetization

As discussed above, the induced magnetization is due to the reorientation of the atomic magnetic moments in the presence of the external field. The property of those rocks and minerals is paramagnetism. They have atomic moments to partially align parallel to the applied field, thereby to produce a net magnetization in the direction of the applied field in the presence of external field. There is, however, a class of magnetism of great importance to geomagnetic studies. Certain materials not only have atomic moments, but neighboring moments interact strongly with each other. Such materials are said to be ferromagnetic. The ferromagnetic materials have an ability to retain the magnetization in the absence of external magnetic fields. This permanent magnetization is called remanent magnetization, which we denote here by $\bar{J}_r$ (Blakely, 1996).

$\bar{J}_r$ is a function of volume, atomic, crystallographic, chemical makeup, and grain size of the magnetic minerals. Small magnetic grains support strong, stable remanent magnetizations. It is also affected by the geologic, tectonic, and thermal history of the mineral or rock (Blakely, 1996). The various processes by which rocks can acquire a remanent magnetization are detailed in the table 2.2 (Shearer, 2005).

Table 2.1 Descriptions of different types of remanent magnetization (adopted from Shearer, 2005)

Remanent Magnetization	Acronym	Rock Types	Description
Natural	NRM	All	Summation of all remanent magnetization components (primary and secondary).
Thermal	TRM	Igneous, Metamorphic	Primary remanent magnetization acquired during cooling from a temperature above the Curie temperature in the presence of an external magnetic field.
Viscous	VRM	All	Secondary remanent magnetization acquired over time, related to thermal agitation and causes decay of primary remanent magnetization.
Depositional	DRM	Sedimentary	Primary remanent magnetization acquired during deposition in the presence of an external field by the physical rotation of magnetic mineral particles. Usually occurs as grains settle out of water.
Post-depositional	PDRM	Sedimentary	Acquired during post-depositional retention of interstitial grains.
Chemical	CRM	All	Remanent magnetization acquired during growth of magnetic minerals in presence of an external field. Includes growth by nucleation or replacement.
Isothermal	IRM	All	Secondary remanent magnetization acquired over a short time at one temperature in a strong, external field.

There are two types of remanent magnetization. Primary remanent magnetizations are acquired by the cooling and solidification of an igneous rock from above the Curie temperature to normal surface temperature (TRM) or by detrital remanent magnetisation (DRM). Secondary remanent magnetisations, such as chemical, viscous or post-depositional remanent magnetisations, may be acquired later on in the rock's history.

It is very important to consider that not only may $\bar{J}_r$ exceed $\bar{J}_i$, but the direction of remanent magnetisation may be quite different from that of the ambient induced field at a location.

2.3 The progress of magnetic method and the historical development concerned of magnetic method survey for kimberlites

Here we recall the progress of magnetic method to outline the main advances and the problems of the magnetic exploration. Then we summarize the methods used in exploration of kimberlites.

2.3.1 The progress of magnetic method

2.3.1.1 Depth-to-source estimation techniques

As the initial method of interpretation of magnetic methods, the depth estimation has contributed a lot in obtaining the semi-quantitative representation of the source locations. These techniques estimate target parameters by looking at various attributes of an anomaly (curve matching, straight-slope, half-width, amplitude, horizontal extent between various characteristic points, etc) (Henderson and Zietz, 1948; Peters, 1949; Vacquier et al., 1951; Smellie, 1956; Hutchison, 1958; Grant and Martin, 1966; Koulomzine et al.,1970; Barongo, 1985). Trial-and-error methods were developed (Talwani, 1965), in which magnetic anomalies were calculated iteratively until a good fit with observed data was obtained. In the 1970s, automated depth analysis began to replace the graphical and trial and error techniques based on the 2D models. In the 1990s, 3D automated depth estimation appeared.

2.3.1.1.1 Werner deconvolution

Werner (1955) proposed a method for interpreting overlapping anomalies if they can be interpreted as attributable to thin sheets. Given that the causative bodies are two dimensional and have a polygonal cross section, it can be achieved by taking the horizontal derivative of the observed profile. This method was extended to 3D

multiple sources by Hansen (2002) by using deconvolution on the complex form of the analytic signal.

2.3.1.1.2 CompuDepth

O'Brien (1972) introduced CompuDepth, a frequency-domain technique, based on a spectral formulation of the analytic signal (Nabighian, 1972) that determines location and depth to 2D magnetic sources. Wang and Hansen (1990) extended this method to estimate the locations of the corners of 3D homogeneous polyhedral bodies.

2.3.1.1.3 Naudy method

Naudy (1971) provided a method that uses a matched filter calculating profile over a vertical dike or thin plate. The filter is applied to the observed and reduced-to-the-pole components. Shi (1991) replaced the observed and reduced-to-the-pole components by the horizontal and vertical components of the magnetic profile to improve Naudy's method.

2.3.1.1.4 Analytic signal

Nabighian (1972, 1974) introduced the concept of the analytic signal for magnetic interpretation and showed that its amplitude yields a bell-shaped function over each corner of a 2D body with polygonal cross section. For an isolated corner, the maximum of the bell shaped curve is located exactly over the corner, and the width of the curve at half its maximum amplitude equals twice the depth to the corner. In addition, the results are not affected by the remanent magnetization. Roest et al (1992) used the 3D analytic signal to obtain the positions of magnetic contacts and the depth of the rim of the circular feature beneath southern Lake Huron from gridded data. The absolute value of the 3D analytic signal is defined as the square root of the squared sum of the vertical and the two horizontal derivatives of the magnetic field; it is the norm of the gradient vector of the magnetic field.

2.3.1.1.5 Euler deconvolution

Thompson (1982) proposed a technique for analyzing magnetic profiles based on Euler's relation for homogeneous functions. This technique uses first order x, y and z derivatives to determine location and depth for various idealized targets (sphere, cylinder, thin dike, contact), each characterized by a specific structural index. Many improvements were made to this method. Reid et al (1990) extended this method to 3D situation. Mushayandebvu et al. (2001) introduced a second equation derived from Euler equation used in conjunction with the standard Euler equation to make the results more stable, which is called extended Euler deconvolution. It is extended to 3D by Nabighian and Hansen (2001) using generalized Hilbert transforms (Nabighian, 1984). Hansen and Suciu (2002) extended the single source Euler deconvolution technique to multiple sources to deal with the overlapping effects of nearby anomalies. Keating and Pilkington (2000) proposed applying Euler deconvolution to the amplitude of the analytic signal. Mushayandebvu et al (2004) presented a grid-based version of Euler deconvolution to extend Euler deconvolution to gridded data to allow for the first time the estimation of strikes, dips, and susceptibilities from gridded data using an automatic process.

2.3.1.1.6 Source parameter imaging (SPI)

Thurston and Smith (1997) and Thurston et al (1999, 2002) developed the source parameter imaging (SPI) technique, based on the complex analytic signal, to compute source parameter from line data or gridded magnetic data, which is referred to as the local wavenumber method. Solution grids using the SPI technique gives the edge locations, depths, dips and susceptibility contracts. It works best for isolated 2D sources.

2.3.1.2 Parametric inversion

Inversion is an automatic numerical procedure that constructs a model of subsurface geology from measured magnetic data and other information, with the

additional condition that input data are reproduced within a given error tolerance (Nabighian et al., 2005). The parametric inversion is a quantitative inversion technique for recovering the geometry of causative bodies that reproduce observed data. This method requires certain a priori information, such as a known magnetization direction.

2.3.2 The magnetic method used for survey of kimberlites

2.3.2.1 Detecting the kimberlites

In the early 1972', Burley and Greenwood (1972) found magnetic anomalies over all known kimberlites in Lesotho. Macnae (1979) pointed out that, although ground geophysical surveys of kimbelites have been described first, all the pipes were first detected by means of an airborne reconnaissance survey. Most kimberlites have a distinctive aeromagnetic signature, in general, a roughly circular anomaly. However, at ground level the anomaly is more complex and it can have internal highs or be elongated (Keating and Sailhac, 2004). Macnae (1979) gave an example of an aeromagnetic survey that was flown by Geoterrex Ltd., of Ottawa, Canada. Lines were flown 400m apart, at an average flight height of 120m. The magnetic response over two of the selected anomalies coincided with the results of EM anomalies obtained over the same targets. After Macnae (1979), Nixon (1981), Atkinson (1989) and Sarma and Verma (1996) proposed respectively that aeromagnetics or ground magnetics are almost invariably primary search tool used for detecting and delineating kimberlites. Nixon (1981) mentioned that discrete magnetic anomalies may occur within individual pipes. Atkinson (1989) states that the variable and complex nature of magnetic responses found over kimberlites is more likely to reflect the nature of the body itself than the differential weathering of the pipe as stated by some authors (Sarma and Verma, 1999). Macnae (1995) also reports examples of aeromagnetic anomalies from the Sheoak area of southern Australia which contain several kimberlite responses within a highly variable magnetic background. Sama et al (1999) used the ground magnetic vertical intensity contour map to map the Majhgawan

kimberlite pipe near Panna in central India successfully. They obtained the geologically reasonable 3D model satisfying the contour map.

Cowan et al (2000) review the techniques that can be used to screen kimberlite magnetic anomalies. Three-dimensional Euler deconvolution can be used to automatically locate circular anomalies (Paterson et al., 1991). This technique tends to generate a large number of false targets. Keating (1995) proposed a technique called matched filter that is based on first-order regression analysis between a window of the grided data and a typical target theoretical anomaly. Experience shows that the matched filter technique does not work well at very low magnetic latitudes and does not perform well in the presence of strong magnetic remanent magnetization (Keating and Sailhac, 2004). A new technique designed to overcome this problem was proposed by Keating (Keating and Sailhac, 2004). The new technique is based on a first order regression over a moving window, between the analytic signal of the observed magnetic field and the theoretical analytic signal of a magnetic vertical cylinder. Results where the correlation coefficient between the analytic signal and the theoretical analytic signal within a moving window are above a certain threshold are retained. Additional criteria can later be used to refine the target selection. Its advantage is that the shape of analytic signal is much less dependent on the direction of the magnetic field and remanent magnetization of the kimberlite than total magnetic field anomalies. Paulo et al (2007) proposed a new technique in Serra da Canastra which is located in the central portion of the Brazilian province in a low magnetic latitude region. This interpretation strategy was based on joint analysis of analytic signal and Euler deconvolution. A selected kimberlite target should typically have a roughly circular analytic signal anomaly coincident with a depth (1-200m) and structural (N=2) constrained Euler solution. It simultaneously meets two requirements: have a roughly circular analytic signal anomaly and be coincident with the constrained Euler equation. The proposed approach led to the recognition of previously known pipes and generation of new targets.

2.3.2.2 Inversion for magnetic anomalies due to a kimberlite pipe

Using the model of cylinder given by Singh and Sabina (1978), Cheman (2006) implemented a parametric inversion of the magnetic field due to a cylinder, using the mathematical expressions of the magnetic anomaly caused by a vertical right circular cylinder with arbitrary polarization. His first important contribution is the evaluation of the direction of the magnetization by the method of magnetic moment derived by integration of the field components. The evaluation of the direction of the magnetization is the essential prerequisite for implementation of the magnetic inversion. His second important contribution is the estimation of the initial values of the parameters of the model, such as the depth, the diameter from the amplitude ratio of the enhanced and the simple analytic signal (Hsu et al., 1996) and the coordinates of the center of the cylinder from the maximum or minimum of reduction to pole, or the maximum of the amplitude of analytic signal of the magnetic field reduced to the pole. His third important contribution is development of magnetic field inversion algorithm using the Levenberg-Marquardt square-least method, especially, an inversion of remanent magnetization has been implemented to estimate the remanent magnetization. But the stability and the precision of this inversion, especially for the inversion of the remanent magnetization, needs to be improved.

Chapter 3 Derivatives of the magnetic field

3.1 Introduction

In the preceding chapter, I presented a brief overview of the concepts pertaining to the magnetic method in relation to the topic of this thesis, and gave an outline of the historical developments related to remanent magnetization and its extraction from the magnetic data.

For the accurate inversion of magnetic data, remanent magnetization should be included. Remanent magnetization is the net magnetization present in a material in the absence of an external field. If present, it could lead to the erroneous interpretation of magnetic data. The analytic signal is the amplitude of the total gradient of the anomalous magnetic data. The analytic signal is weakly independent of the local geomagnetic field and the remanent magnetization, and therefore the joint inversion with the magnetic anomaly and its analytic signal is expected to increase the stability of the inversion. Here, I propose to do the joint inversion combining the magnetic anomaly and its analytic signal. Firstly, the analytic signal inversion will be implemented. The amplitude of the analytic signal is defined as the square root of the squared sum of the vertical and the two horizontal derivatives of the magnetic field. I therefore need to compute the vertical and the two horizontal derivatives of the magnetic field to construct the mathematical model for analytic signal inversion. I use the finite difference derivatives and I compare the results with those from the analytic derivatives to test the algorithms.

3.2 Formulas of derivatives of the magnetic field

3.2.1 Introduction of the basic theory

Singh and Sabina (1978) give a closed form solution for the total anomalous magnetic field due to a vertical right circular cylinder with arbitrary polarization under the assumption that the magnetization is uniform. Chemam (2006) used it to calculate the forward model needed for the inversion of the magnetic anomaly due to a vertical

cylinder with and without the remanent magnetization. The total magnetic anomaly due to the right circular cylinder is expressed as follows:

$$F = 2\pi a \cdot J_{tot}\left[(C-A)\cdot I(1,0;0) - (E-A)\cdot\frac{1}{r}I(1,1;-1) - BI(1,1;0)\right] \quad (3.1)$$

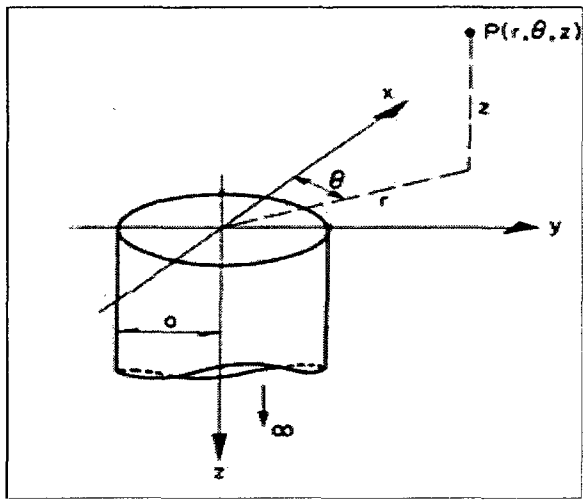

Fig.3.1 Semi-infinite cylinder of radius a and the coordinate system used. The total magnetic field is evaluated at point P above the cylinder.

$$C = nN$$
$$A = lL\cos^2\theta + (lM + mL)\sin\theta\cos\theta + mM\sin^2\theta$$
$$E = lL\sin^2\theta - (lM + mL)\sin\theta\cos\theta + mM\cos^2\theta$$
$$B = (lN + nL)\cos\theta + (mN + nM)\sin\theta$$
$$l = \cos I_0 \cos D_0$$
$$m = \cos I_0 \sin D_0$$
$$n = \sin I_0$$
$$L = \cos I_m \cos D_m$$
$$M = \cos I_m \sin D_m$$
$$N = \sin I_m$$

$$I(1,0;0)=\begin{cases}-\dfrac{k|z|}{4a\sqrt{ar}}F_0(k)-\dfrac{1}{2a}\Lambda_0(\beta,k)+\dfrac{1}{a}, & (a>r)\\ -\dfrac{k|z|}{4a^2}F_0(k)+\dfrac{1}{2a}, & (a=r)\\ -\dfrac{k|z|}{4a\sqrt{ar}}F_0(k)+\dfrac{1}{2a}\Lambda_0(\beta,k) & (a<r)\end{cases}$$

$$I(1,1;-1)=\begin{cases}\dfrac{|z|E_0(k)}{2k\sqrt{ar}}-\dfrac{k|z|}{4ar\sqrt{ar}}(a^2+r^2+\dfrac{z^2}{2})F_0(k)+\dfrac{a^2-r^2}{4ar}\Lambda_0(\beta,k)+\dfrac{r}{2a}, & (a>r)\\ \dfrac{|z|E_0(k)}{2ka}-\dfrac{k|z|}{4a^3}(2a^2+\dfrac{z^2}{2})F_0(k)+\dfrac{1}{2}, & (a=r)\\ \dfrac{|z|E_0(k)}{4k\sqrt{ar}}-\dfrac{k|z|}{4ar\sqrt{ar}}(a^2+r^2+\dfrac{z^2}{2})F_0(k)+\dfrac{r^2-a^2}{4ar}\Lambda_0(\beta,k)+\dfrac{a}{2r}, & (a<r)\end{cases}$$

$$I(1,1;0)=\frac{1}{k\sqrt{ar}}\left[\left(1-\frac{k^2}{2}\right)F_0(k)-E_0(k)\right]$$

With

$$F_0(k)=\frac{2}{\pi}K(k)$$

$$E_0(k)=\frac{2}{\pi}E(k)$$

$$k=\sqrt{\frac{4ar}{(a+r)^2+z^2}}$$

$$\beta=\arcsin(\sqrt{\frac{z^2}{(a-r)^2+z^2}})$$

(I_0,D_0) and (I_m,D_m) are the inclination and declination of the Earth's magnetic field and the total magnetic field intensity, a is the radius of the cylinder, z is the depth

of the top of the cylinder and J_{tot} is the total magnetic field intensity. $K(k)$ and $E(k)$ are two complete elliptic integrals:

$$K(k) = \int_0^{\pi/2} \frac{d\varphi}{\sqrt{1-k^2\sin^2\varphi}}$$
$$E(k) = \int_0^{\pi/2} \sqrt{1-k^2\sin^2\varphi}\,d\varphi$$

$\Lambda_0(\beta,k)$ is Lambda function:

$$\Lambda_0 = \frac{2}{\pi}\left[K(k)\cdot E(\beta,\sqrt{1-k^2}) + (E(k)-K(k))\cdot K(\beta,\sqrt{1-k^2})\right]$$

In the formula above, $K(\beta,\sqrt{1-k^2})$ and $E(\beta,\sqrt{1-k^2})$ are the incomplete elliptic integrals.

For the magnetic anomaly with the remanent magnetization, equation (3.1) is changed to equation (3.2):

$$F = 2\pi a\cdot J_i\left[(C-A)\cdot I(1,0;0) - (E-A)\cdot\frac{1}{r}I(1,1;-1) - BI(1,1;0)\right] \quad (3.2)$$

where:

$C = nN1$

$A = lL1\cdot\cos^2\theta + (lM1 + mL1)\sin\theta\cos\theta + mM1\sin^2\theta$

$E = lL1\cdot\sin^2\theta - (lM1 + mL1)\sin\theta\cos\theta + mM1\cos^2\theta$

$B = (lN1 + nL1)\cos\theta + (mN1 + nM1)\sin\theta$

with

$L1 = l + Q\cdot L$

$M1 = m + Q\cdot M$

$N1 = n + Q\cdot N$

$l = \cos I_0\cos D_0$

$m = \cos I_0\sin D_0$

$n = \sin I_0$

$L = \cos I_{rem}\cdot\cos D_{rem}$

$M = \cos I_{rem}\cdot\sin D_{rem}$

$N = \sin I_{rem}$

(I_0, D_0) and (I_{rem}, D_{rem}) are the inclination and declination of the Earth's magnetic field and the remanent magnetization, J_i is the inductive magnetic field intensity, Q is the Koenigsberger's ratio. To obtain the derivatives: $\frac{\partial F}{\partial x}, \frac{\partial F}{\partial y}, \frac{\partial F}{\partial z}$ needed for the calculation of the analytic signal, the key is to compute the derivatives of the functions

$$K(k) = \int_0^{\pi/2} \frac{d\varphi}{\sqrt{1-k^2 \sin^2 \varphi}},$$

$$E(k) = \int_0^{\pi/2} \sqrt{1-k^2 \sin^2 \varphi} d\varphi,$$

and the incomplete elliptic integrals: $K(\beta, \sqrt{1-k^2})$ and $E(\beta, \sqrt{1-k^2})$. In the site http://mathworld.wolfram.com/, the formulas for calculations of the derivatives for the complete and incomplete elliptic integrals can be found:

$$\frac{\partial E(k)}{\partial k} = \frac{E(k) - K(k)}{2k} \qquad (3.3)$$

$$\frac{\partial K(k)}{\partial k} = \frac{E(k) - (1-k)K(k)}{2(1-k)k} \qquad (3.4)$$

$$E(\beta, k) = \int_0^{\beta} \sqrt{1-k \sin^2 \varphi} d\varphi \qquad (3.5)$$

$$\frac{\partial E(\beta, k)}{\partial \beta} = \sqrt{1-k \sin^2 \beta} \qquad (3.6)$$

$$\frac{\partial E(\beta, k)}{\partial k} = \frac{E(\beta, k) - K(\beta, k)}{2k} \qquad (3.7)$$

$$K(\beta, k) = \int_0^{\beta} \frac{1}{\sqrt{1-k \sin^2 \varphi}} d\varphi \quad 0<k<1 \qquad (3.8)$$

$$\frac{\partial K(\beta,k)}{\partial \beta} = \frac{1}{\sqrt{1-k\sin^2\beta}} \qquad (3.9)$$

$$\frac{\partial K(\beta,k)}{\partial k} = \frac{E(\beta,k)}{2(1-k)k} - \frac{K(\beta,k)}{2k} - \frac{\sin(2\beta)}{4(1-k)\sqrt{1-k\sin^2\beta}} \qquad (3.10)$$

the two incomplete elliptic functions are transformed as follow:

$$K(\beta,k) = \sin\beta \times R_f(\cos^2\beta, 1-k^2\sin^2\beta, 1) \quad (3.11)$$

$$E(\beta,k) = \sin\beta \times R_f(\cos^2\beta, 1-k^2\sin^2\beta, 1) - \frac{1}{3}k^2\sin^2\beta \times R_d(\cos^2\beta, 1-k^2\sin^2\beta, 1) \qquad (3.12)$$

where

$$R_f(x',y',z') = \frac{1}{2}\int_0^\infty [(t+x')(t+y')(t+z')]^{-\frac{1}{2}} dt \quad (3.13)$$

$$R_d(x',y',z') = \frac{3}{2}\int_0^\infty (t+x')^{-\frac{1}{2}}(t+y')^{-\frac{1}{2}}(t+z')^{-\frac{3}{2}} dt \quad (3.14)$$

the calculation of R_f, R_d are given by Carlson (Carlson, 1979). So the calculations from equation from (3.3) to (3.10) have been resolved. This means that the calculations of the analytic method for the complete and incomplete elliptic integrals have been obtained, and the analytic expression for Lambda function has been derived.

3.2.2 The z derivative of the magnetic anomaly due to right circular cylinder

I have to split the full expression into parts because that the mathematic expressions are too long. The needed terms, together with the simplified notation are:

$$k^2 = \frac{4ar}{(a+r)^2 + z^2}, \quad (3.15)$$

$$dkz = \frac{\partial k}{\partial z} = \sqrt{\frac{(a+r)^2+z^2}{4ar}} \times \frac{-4arz}{\left[(a+r)^2+z^2\right]^2} \quad (3.16)$$

$$\sin^2\beta = \frac{z^2}{(a-r)^2+z^2}, \quad (3.17)$$

$$d\beta z = \frac{\partial\beta}{\partial z} = \sqrt{\frac{(a-r)^2+z^2}{(a-r)^2}} \times \sqrt{\frac{(a-r)^2+z^2}{z^2}} \times \frac{z(a-r)^2}{[(a-r)^2+z^2]^2} \quad (3.18)$$

$$dEz = \frac{\partial E(k)}{\partial z} = \frac{E(k)-K(k)}{2k^2} \times 2k \times dkz \quad (3.19)$$

$$dKz = \frac{\partial K(k)}{\partial z} = \frac{E(k)-(1-k^2)K(k)}{2(1-k^2)k^2} \times 2k \times dkz \quad (3.20)$$

$$dE\beta m\beta = \frac{\partial E(\beta,\sqrt{1-k^2})}{\partial\beta} = \sqrt{1-(1-k^2)\sin^2\beta} \quad (3.21)$$

$$dE\beta mm = \frac{\partial E(\beta,\sqrt{1-k^2})}{\partial(\sqrt{1-k^2})} = \frac{E(\beta,\sqrt{1-k^2})-K(\beta,\sqrt{1-k^2})}{2(\sqrt{1-k^2})^2} \times 2\sqrt{1-k^2} \quad (3.22)$$

$$dmz = \frac{\partial(\sqrt{1-k^2})}{\partial z} = \frac{-dkz}{\sqrt{1-k^2}} \quad (3.23)$$

$$dE\beta mz = \frac{\partial E(\beta,\sqrt{1-k^2})}{\partial z} = dE\beta m\beta \times d\beta z + dE\beta mm \times dmz \quad (3.24)$$

$$dK\beta m\beta = \frac{\partial K(\beta,\sqrt{1-k^2})}{\partial\beta} = \frac{1}{\sqrt{1-(1-k^2)\sin^2\beta}} \quad (3.25)$$

$$dK\beta mm = [\frac{E(\beta,\sqrt{1-k^2})}{2k^2(1-k^2)} - \frac{K(\beta,\sqrt{1-k^2})}{2(1-k^2)} - \frac{\sin(2\beta)}{4k^2\sqrt{1-(1-k^2)\sin^2\beta}}] \times (2\sqrt{1-k^2}) \quad (3.26)$$

$$dK\beta mz = dK\beta m\beta \times d\beta z + dK\beta mm \times dmz \quad (3.27)$$

$$dLamdaz = \frac{2}{\pi}\{[dKz \times E(\beta,\sqrt{1-k^2}) + K(k) \times dE\beta mz] + [(dEz - dKz) \times K(\beta,\sqrt{1-k^2}) + (E(k) - K(k)) \times dK\beta mz \quad (3.28)$$

$$DI100zu1 = \frac{-1}{2\pi\sqrt{ar}}[k \times K(k) + z \times dkz \times K(k) + z \times k \times dKz] \quad (3.29)$$

$$DI100zu2 = \frac{-1}{2a} \times dLamdaz \quad (3.30)$$

$$DI100zu = DI100zu1 + DI100zu2 \quad (3.31)$$

$$DI100zm = \frac{-1}{2\pi a^2}(dkz \times z \times K(k) + k \times K(k) + k \times z \times dKz) \quad (3.32)$$

$$DI100zd = DI100zu1 - DI100zu2 \quad (3.33)$$

$$DzEk = \frac{\partial(zE(k)/k)}{\partial z} = \frac{1}{k} \times E(k) + z \times E(k) \times (-\frac{dkz}{k^2}) + z \times \frac{1}{k} \times dEz \quad (3.34)$$

$$a2r2z = k(a^2 z + r^2 z + z^3/2)K(k) \quad (3.35)$$

$$\begin{aligned} Da2r2zz = {} & dkz \times (a^2 z + r^2 z + z^3/2) \times K(k) \\ & + k \times (a^2 + r^2 + 3z^2/2) \times K(k) \\ & + k \times (a^2 z + r^2 z + z^3/2) \times dKz \end{aligned} \quad (3.36)$$

$$a2z = k(2a^2 z + z^3/2)K(k) \quad (3.37)$$

$$Da2z = dkz \times (2a^2 z + z^3/2) \times K + k \times (2a^2 + 3z^2/2) \times K + k \times (2a^2 z + z^3/2) \times dKz \quad (3.38)$$

$$DI111zu1 = \frac{1}{\pi\sqrt{ar}} \times DzEk \quad (3.39)$$

$$DI111zu2 = \frac{-1}{2\pi ar\sqrt{ar}} \times Da2r2zz \quad (3.40)$$

$$DI111zu3 = \frac{a^2 - r^2}{4ar} \times dLamdaz \quad (3.41)$$

$$DI111zu = DI111zu1 + DI111zu2 + DI111zu3 \quad (3.42)$$

$$DI111zm1 = \frac{1}{\pi a} \times DzEk \quad (3.43)$$

$$DI111zm2 = \frac{-1}{2\pi a^3} \times Da2z \quad (3.44)$$

$$DI111zm = DI111zm1 + DI111zm2 \quad (3.45)$$

$$DI111zd = DI111zu1 + DI111zu2 - DI111zu3 \quad (3.46)$$

$$IrequaZ = \frac{1}{a}(1 - \frac{z}{\sqrt{z^2 + a^2}}) \quad (3.47)$$

$$DIrequaZz = \frac{-a}{(a^2 + z^2)\sqrt{a^2 + z^2}} \quad (3.48)$$

$$DI110z = \frac{2}{\pi\sqrt{ar}}[(-\frac{1}{k^2} \times dkz - \frac{dkz}{2}) \times K(k) + (\frac{1}{k} - \frac{k}{2}) \times dKz - \frac{dEz \times k - E \times dkz}{k^2}] \quad (3.49)$$

$(r = 0)$

$I_110dz = 0;$

$I_100dz = DIrequaZz;$

$I_11m1dz = I_100dz / 2;$

$(r \neq 0, a = r)$

$I_110dz = DI110z;$

$I_100dz = DI100zm;$

$I_11m1dz = DI111zm;$

$(r \neq 0, a > r)$

$I_110dz = DI110z;$

$I_100dz = DI100zu;$

$I_11m1dz = DI111zu;$

$(r \neq 0, a < r)$

$I_110dz = DI110z;$

$I_100dz = DI100zd;$

$I_11m1dz = DI111zd;$

$(r = 0)$

$$DF = \frac{\partial F}{\partial z} = 2\pi a J_{tot}[(C-A)I_100dz - (E-A)I_11m1dz - BI_110dz]$$

$(r \neq 0)$

$$DF = \frac{\partial F}{\partial z} = 2\pi a J_{tot}[(C-A)I_100dz - (E-A)I11m1dz/r - BI_110dz] \quad (3.50)$$

Here $r = \sqrt{x^2 + y^2}$.

3.2.3 The x derivative of the magnetic anomaly due to right circular cylinder

$$dkx = \frac{\partial k}{\partial x} = \frac{x\{4a[(a+r)^2 + z^2] - 8ar(a+r)\}}{2kr[(a+r)^2 + z^2]} \quad (3.51)$$

$$dEx = \frac{\partial E(k)}{\partial x} = \frac{E(k) - K(k)}{2k^2} \times (2k) \times dkx \quad (3.52)$$

$$dKx = \frac{\partial K(k)}{\partial x} = \frac{E(k) - (1-k^2)K(k)}{2k^2(1-k^2)} \times (2k) \times dkx \quad (3.53)$$

$$d\beta x = \frac{\partial \beta}{\partial x} = \frac{xz(a-r)}{|a-r|r[(a-r)^2 + z^2]} \quad (3.54)$$

$$dmx = \frac{\partial(\sqrt{1-k^2})}{\partial x} = \frac{1}{2\sqrt{1-k^2}} \times (-2k) \times dkx \quad (3.55)$$

$$dE\beta mx = dE\beta m\beta \times d\beta x + dE\beta mm \times dmx \quad (3.56)$$

$$dK\beta mx = dK\beta m\beta \times d\beta x + dK\beta mm \times dmx \quad (3.57)$$

$$dLamdax = \frac{2}{\pi}\{[dKx \times E(\beta, \sqrt{1-k^2}) + K(k) \times dE\beta mx] + (dEx - dKx) \times K(\beta, \sqrt{1-k^2})$$
$$+ [E(k) - K(k)] \times dK\beta mx$$

(3.58)

$$DI100L = \frac{-z}{4a\sqrt{ar}} \quad (3.59)$$

$$DI100xL = \frac{\partial(DI100L)}{\partial x} = \frac{zx}{8ar^2\sqrt{ar}} \quad (3.60)$$

$$DI100xu = DI100xL \times k \times (\frac{2}{\pi}K(k)) + DI100L \times dkx \times (\frac{2}{\pi}K(k)) + DI100L \times k \times (\frac{2}{\pi}dKx) - \frac{1}{2a} \times dLamdax \tag{3.61}$$

$$DI100xm = (-\frac{z}{2\pi a^2}) \times [dkx \times K(k) + k \times dKx] \tag{3.62}$$

$$DI100xd = DI100xL \times k \times (\frac{2}{\pi}K(k)) + DI100L \times dkx \times (\frac{2}{\pi}K(k)) + DI100L \times k \times (\frac{2}{\pi}dKx) + \frac{1}{2a} \times dLamdax \tag{3.63}$$

$$DI111xu1 = (\frac{-zx}{2\pi r^2\sqrt{ar}}) \times (\frac{1}{k}) \times E(k) + (\frac{z}{\pi\sqrt{ar}}) \times (\frac{-dkx}{k^2}) \times E(k) + (\frac{z}{\pi\sqrt{ar}}) \times (\frac{1}{k}) \times dEx \tag{3.64}$$

$$I111xu2 = \frac{-kz}{4ar\sqrt{ar}}(a^2 + r^2 + z^2/2)F_0(k)$$

$$\begin{aligned} DI111xu2 = \frac{\partial I111xu2}{\partial x} = {} & [(\frac{3zx}{8ar^3\sqrt{ar}}) \times (a^2 + r^2 + z^2/2) + (\frac{-zx}{2ar\sqrt{ar}})] \times k \times (\frac{2}{\pi}K(k)) \\ & + [(\frac{-kx}{4ar\sqrt{ar}}) \times (a^2 + r^2 + z^2/2) \times (\frac{2}{\pi}K(k))] \times dkx \times (\frac{2}{\pi}K(k)) \\ & + [(\frac{-kx}{4ar\sqrt{ar}}) \times (a^2 + r^2 + z^2/2) \times (\frac{2}{\pi}K(k))] \times k \times (\frac{2}{\pi}dKx) \end{aligned} \tag{3.65}$$

$$I111xu3 = \frac{a^2 - r^2}{4ar}\Lambda_0(\beta, k)$$

$$DI111xu3 = \frac{\partial I111xu3}{\partial x} = [\frac{-(a^2 + r^2)x}{4ar^3}] \times \Lambda_0(\beta, k) + \frac{a^2 - r^2}{4ar} \times dLamdax \tag{3.66}$$

$$DI111xu4 = \frac{x}{2ar} \tag{3.67}$$

$$DI111xu = DI111xu1 + DI111xu2 + DI111xu3 + DI111xu4 \quad (3.68)$$

$$DI111xm1 = \frac{z}{\pi a}[\frac{(-dkx)\times dEx}{k^2} + \frac{dEx}{k}] \quad (3.69)$$

$$DI111xm2 = [\frac{-z(2a^2 + z^2/2)}{2\pi a^3}]\times[dkx\times K(k) + k\times dKx] \quad (3.70)$$

$$DI111xm = DI111xm1 + DI111xm2 \quad (3.71)$$

$$DI111xd = DI111xu1 + DI111xu2 - DI111xu3 + [\frac{-ax}{2r^3}] \quad (3.72)$$

$$\begin{aligned} DI110x = {} & [(\frac{-x}{\pi r^2\sqrt{ar}})\times\frac{2-k^2}{2k}\times K(k) + \frac{2}{\pi\sqrt{ar}}\times(\frac{-(2+k^2)\times dkx}{2k^2})\times K(k) \\ & + \frac{2}{\pi\sqrt{ar}}\times\frac{2-k^2}{2k}\times dKx] - [(\frac{-x}{\pi r^2\sqrt{ar}})\times\frac{1}{k}\times E(k) \\ & + \frac{2}{\pi\sqrt{ar}}\times(\frac{-dkx}{k^2})\times E(k) + \frac{2}{\pi\sqrt{ar}}\times\frac{1}{k}\times dEx] \end{aligned}$$

(3.73)

In addition to the above, the derivatives of the coefficients, such as C, A, E and B need to be derived as follows:

$$d\sin x = \frac{\partial(\sin\theta)}{\partial x} = \frac{y^2}{r^3} \quad (3.74)$$

$$d\cos x = \frac{\partial(\cos\theta)}{\partial x} = -\frac{xy}{r^3} \quad (3.75)$$

$$d\sin 2x = \frac{\partial(\sin^2\theta)}{\partial x} = \frac{2xy^2}{r^4} \quad (3.76)$$

$$d\cos 2x = \frac{\partial(\cos^2\theta)}{\partial x} = -\frac{2xy^2}{r^4} \quad (3.77)$$

$$dscx = \frac{\partial(\sin\theta\cos\theta)}{\partial x} = \frac{y(y^2 - x^2)}{r^4} \quad (3.78)$$

$$dAx = lL(d\cos 2x) + (lM + mL)dscx + mM(d\sin 2x) \quad (3.79)$$

$$dCx = 0 \quad (3.80)$$

$$dEx = lL(d\sin 2x) - (lM + mL)dscx + mM(d\cos 2x) \quad (3.81)$$

$$dBx = (lN + nL)(d\cos x) + (mN + nM)(d\sin x) \quad (3.82)$$

$(r = 0)$

$DI100x = 0;$

$DI110x = 0;$

$DI111x / r = 0;$

$$DF = \frac{\partial F}{\partial X} = 0;$$

$r \neq 0, r = a$

$d110 = DI110x;$

$d100 = DI100xm;$

$d111 = DI111xm;$

$r \neq 0, r > a$

$d110 = DI110x;$

$d100 = DI100xu;$

$d111 = DI111xu;$

$r \neq 0, r < 0$

$d110 = DI110x;$

$d100 = DI100xd;$

$d111 = DI111xd;$

$DFt = 2\pi a J_{tot};$

$DF1 = (dCx - dAx) \times I(1,0;0) + (C - A) \times d100;$

$$DF2 = (dEx - dAx) \times (1/r) \times I(1,1;-1) + (E - A) \times [(-1) \times (x/r^3)] \times I(1,1;-1) + (E - A)/r \times d111$$

$DF3 = dBx \times I(1,1;0) + B \times d110$

$$DFx = DFt \times (DF1 - DF2 - DF3) \quad (3.83)$$

3.2.4 The y derivative of the magnetic anomaly due to right circular cylinder

Because of the symmetry of the x and y in the expressions, the y derivatives of the magnetic anomaly due to right circular cylinder is simply calculated by replacing x by y in the analytic expressions of the x derivatives, except that the y derivatives of the coefficients C, A, E and B are calculated as follows:

$$d\sin y = \frac{\partial(\sin\theta)}{\partial y} = -\frac{xy}{r^3} \qquad (3.84)$$

$$d\cos y = \frac{\partial(\cos\theta)}{\partial y} = \frac{x^2}{r^3} \qquad (3.85)$$

$$d\sin 2y = \frac{\partial(\sin^2\theta)}{\partial y} = -\frac{2x^2 y}{r^4} \qquad (3.86)$$

$$d\cos 2y = \frac{\partial(\cos^2\theta)}{\partial y} = \frac{2x^2 y}{r^4} \qquad (3.87)$$

$$dscy = \frac{\partial(\sin\theta\cos\theta)}{\partial y} = \frac{x(x^2 - y^2)}{r^4} \qquad (3.88)$$

Substituting the equations (3.84) to (3.88) for $\sin\theta, \cos\theta, \sin^2\theta, \cos^2\theta, \sin\theta\cos\theta$ in the expressions C, A, E, B, the y derivatives of the coefficients C, A, E, B are derived. And substituting them for that in the expressions of the x derivatives, and replace the x by y, the y derivatives are derived. And after x, y and z derivatives are derived, the analytic signal is derived as the formula below:

$$g = \|\nabla F\| = \sqrt{(\partial F/\partial x)^2 + (\partial F/\partial y)^2 + (\partial F/\partial z)^2} \qquad (3.89)$$

3.3 Finite difference derivatives

Derivatives can be calculated by using finite differences of the total magnetic field anomaly computed from the formulas of Singh and Sabina (1978). The vertical derivative of the magnetic field is obtained by computing the field at depth $z + \Delta z$ and $z - \Delta z$, dividing the difference by $2\Delta z$. The x and y derivatives are calculated in

the same way (Keating & Sailhac, 2004). We use $\Delta z = 0.01z$, but sometimes, we need to adjust the Δ to fit with calculated derivatives. The grid cell is $50 \times 50m$.

3.4 Comparison of the responses from two methods

In the following section, I compare both methods for calculating the derivatives for 4 different synthetic models. The first model, Emerson, is for a medium depth and big diameter cylinder, its inclination is more than 90° and less than 180° and its declination is less than 90°; the second model, Presenta77, is for a medium diameter and shallow source, and its inclination is high, its declination is less than zero; the third model, Dipolel, is for deeper source, and the diameter is smaller; the fourth model, Verm330, is for remanent magnetization.

3.4.1 Comparison of the responses for first model

The responses of the two methods are from first model, Emerson. $J_{tot} = 132nT$, $Total\ inclination = 152^\circ$, $Total\ declination = 64^\circ$, $Depth = 63m$, $Radius = 170m$. $Earth\ Field\ Inclination = 74^\circ$, $earth\ field\ declination = -12^\circ$.

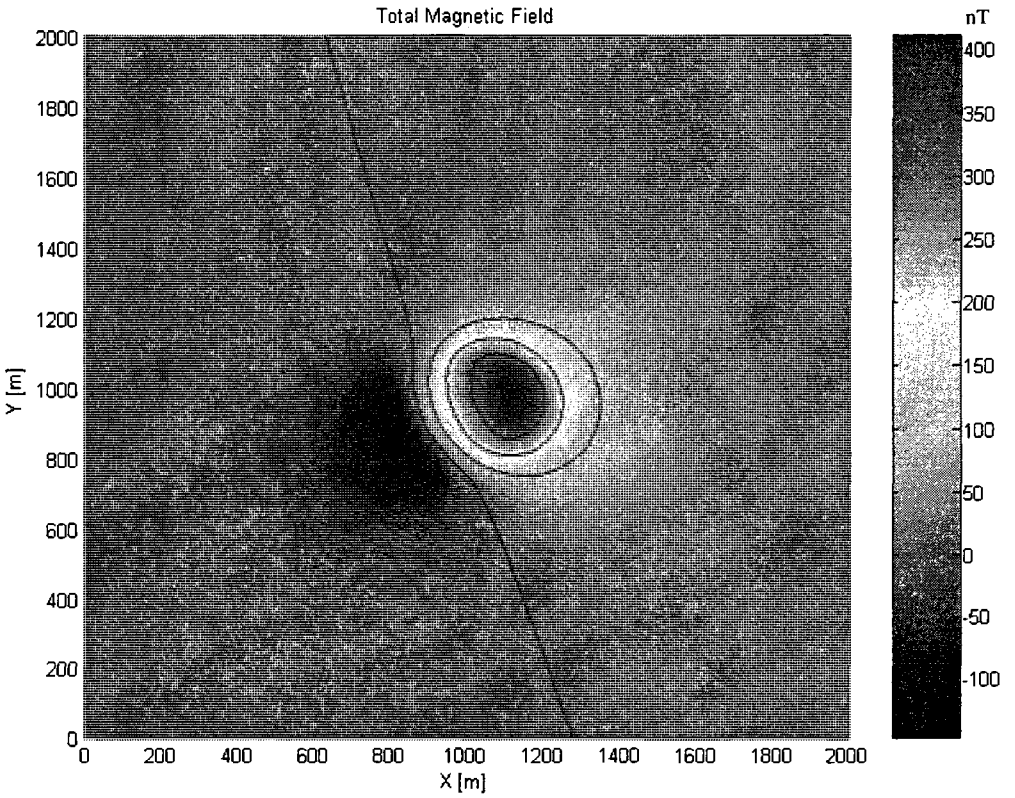

Fig.3.2 Contour of the total magnetic field of first model

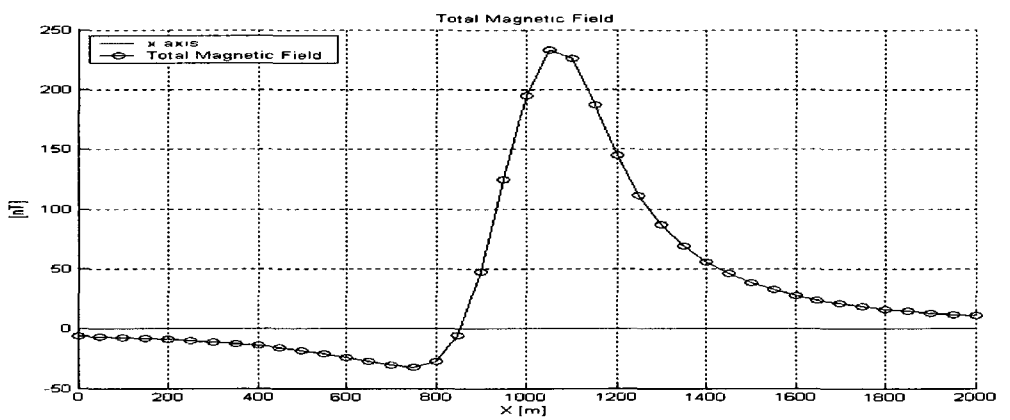

Fig.3.3 Profile at y =1175m of the total magnetic field of first model

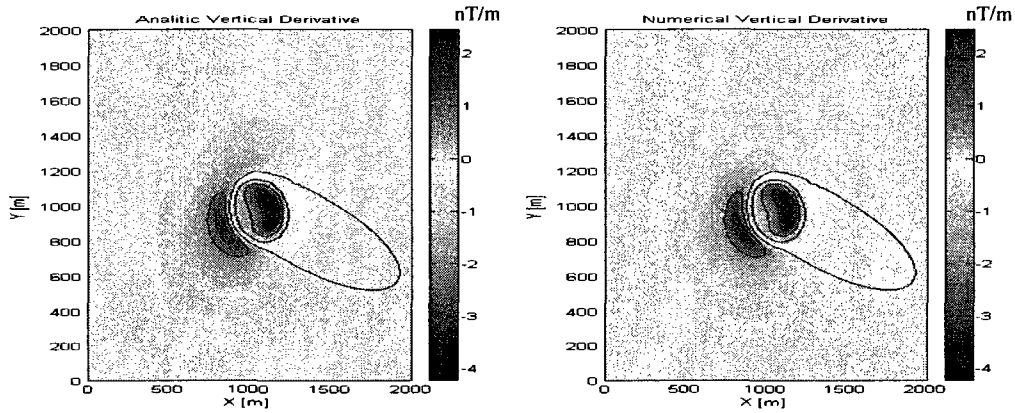

Fig.3.4 Contours of the calculated vertical gradient and the numerical vertical gradient of the first model

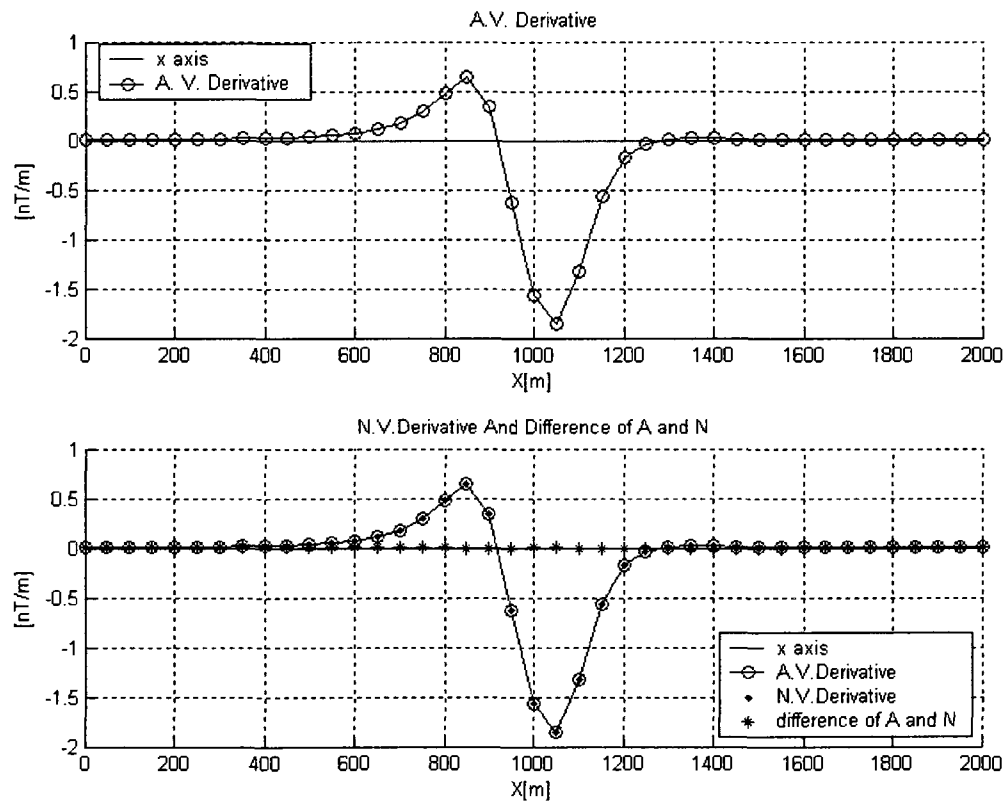

Fig.3.5 Profiles at y =1175m of the calculated vertical gradient and numerical vertical gradient of first model

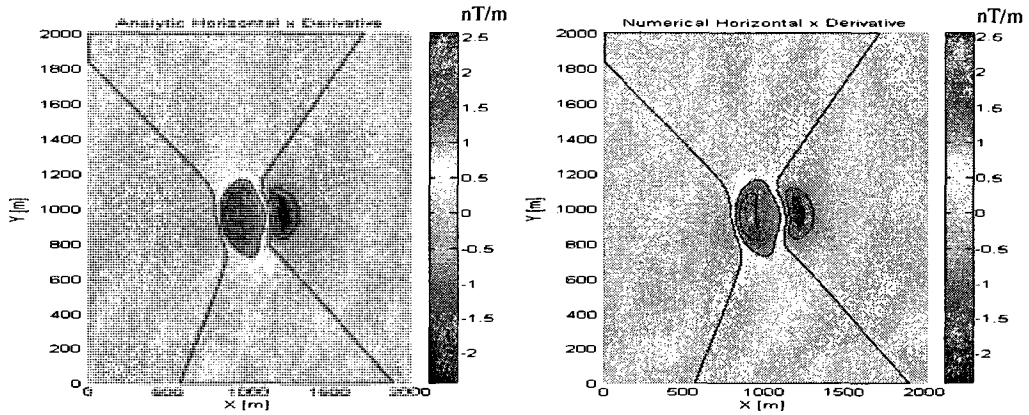

Fig.3.6 Contours of the calculated horizontal x gradient and numerical horizontal x gradient of first model

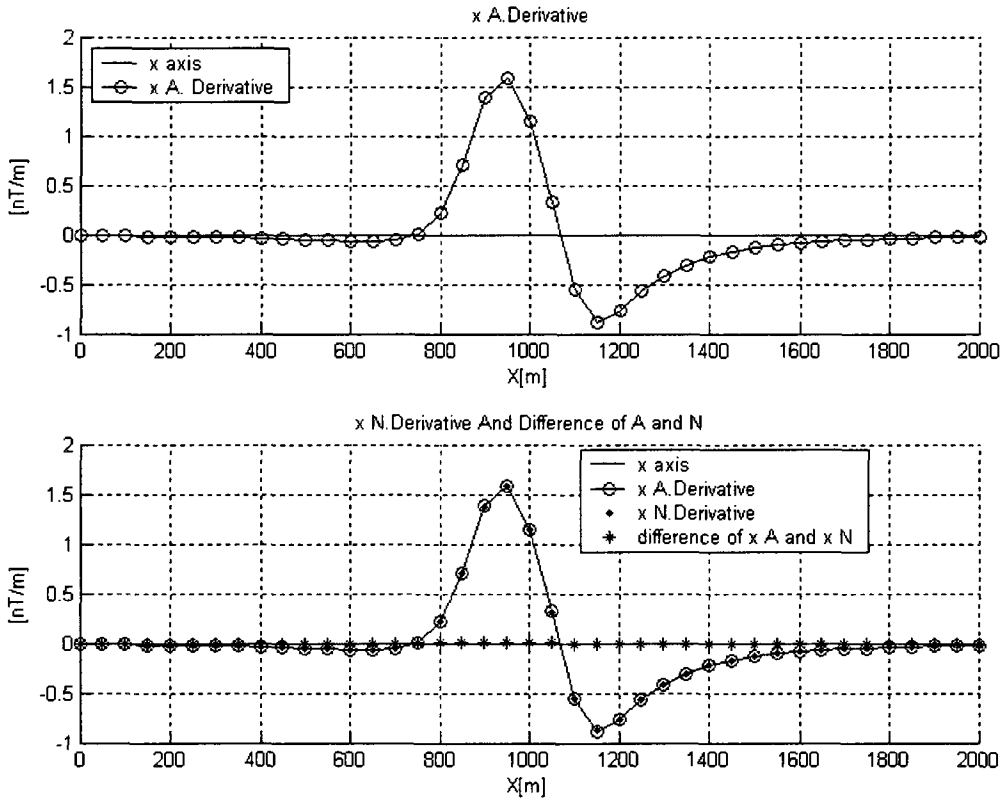

Fig.3.7 Profiles at $y = 1175$m of the calculated horizontal x gradient and numerical horizontal x gradient of first model

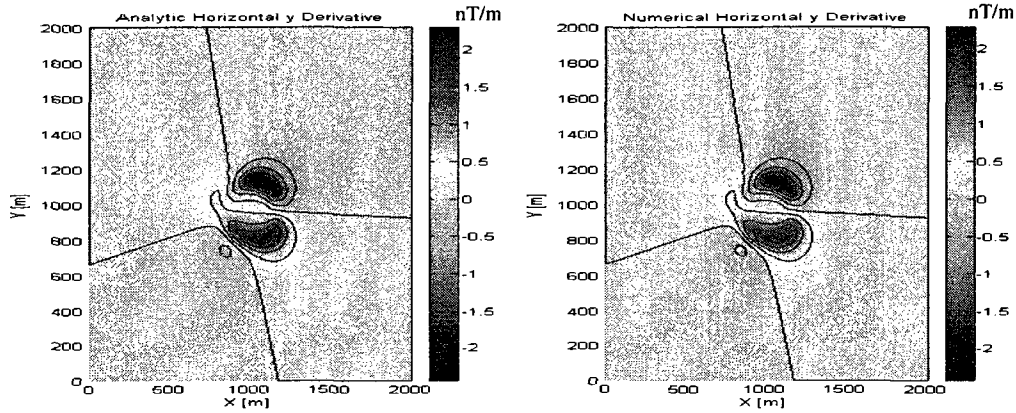

Fig.3.8 Contours of the calculated horizontal y gradient and numerical horizontal y gradient of first model

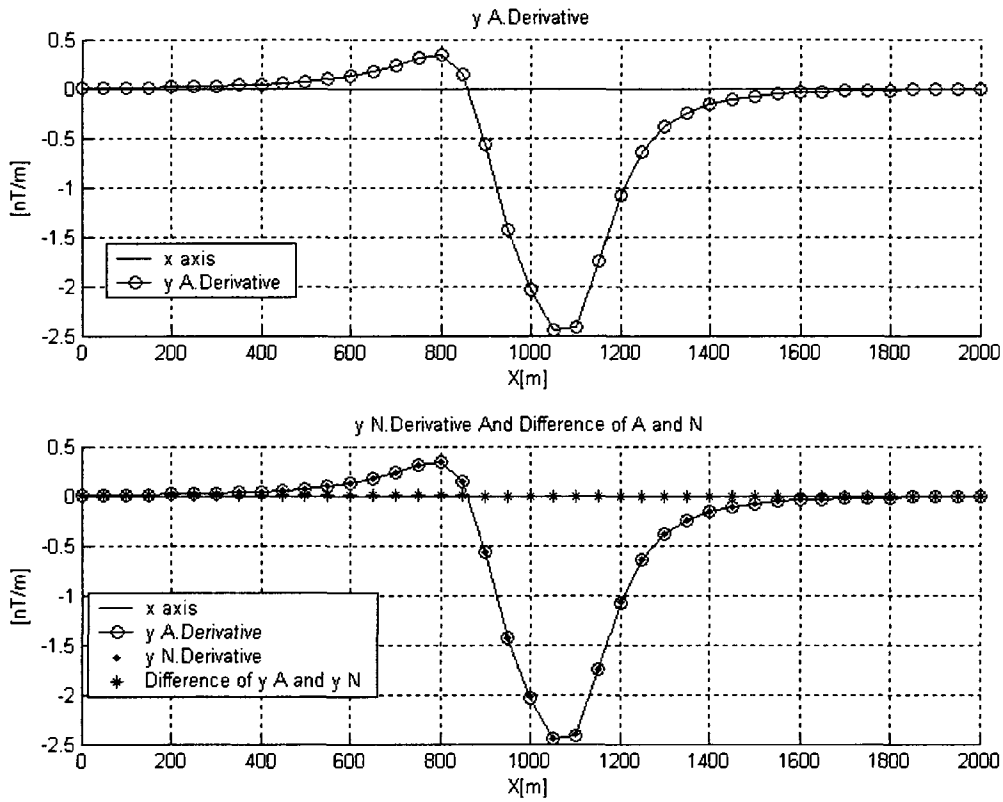

Fig.3.9 Profiles at y =1175m of the calculated horizontal y gradient and numerical horizontal y gradient of first model

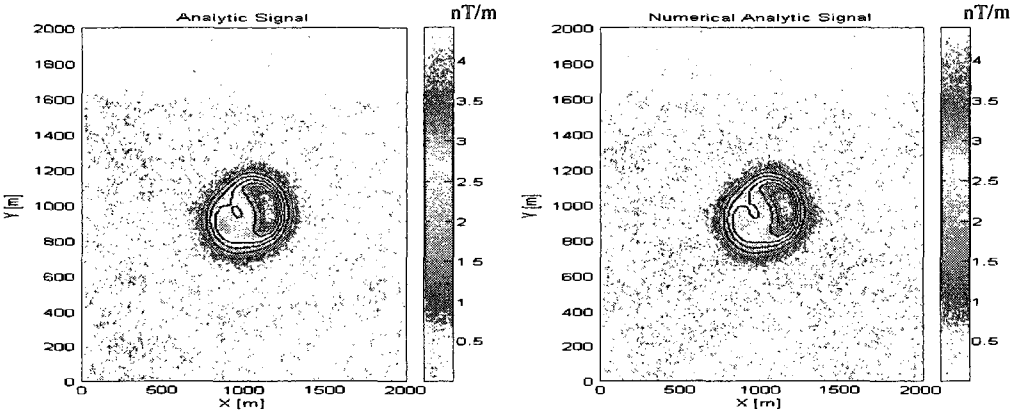

Fig.3.10 Contours of the calculated analytic signal and numerical analytic signal of first model

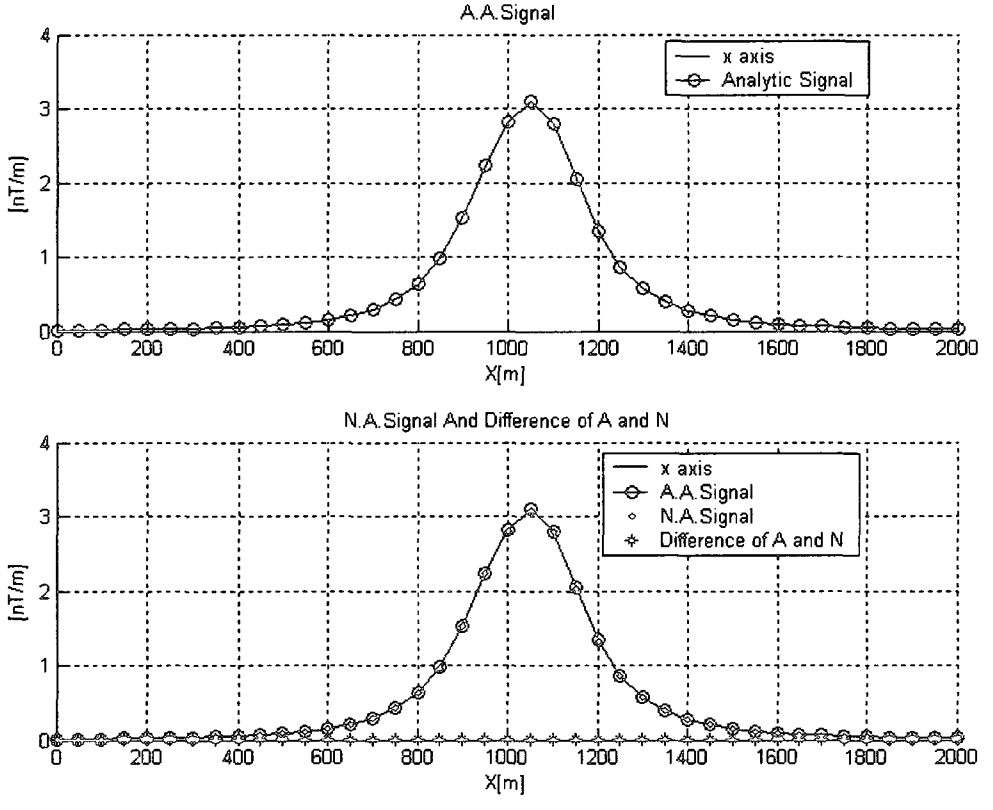

Fig.3.11 Profiles at $y = 1175$m of the calculated analytic signal and numerical analytic signal of first model

Fig.3.3. is the profile drawn at the position y=1175m. The top profile is for the analytic signal calculated by the analytic method, the bottom profile is for the comparison of the two methods, both profiles are on the same graph, and the difference between the results from two methods is presented. The two profiles are identical as their difference is always nearing zero (the difference is about 0.0001 to 0.0009). The shape of this profile agrees with its source position (y=1175m) on figure 1, the contour of the total magnetic field for the first data. Fig.3.4 presents the contours of the analytic vertical derivative and the numerical vertical derivative of the first model. The results from the analytic method and the numerical method are also identical. Fig.3.5 shows the profiles of the analytic vertical gradient and the numerical gradient of first model drawn at the position y=1175m. The two profiles are identical; the difference is always nearing zero. Fig.3.6 shows the contours of the analytic horizontal x gradient and numerical horizontal x gradient of first set of data. Fig.3.7 shows the profiles of the analytic horizontal x gradient and numerical horizontal x gradient of first model drawn at position y=1175m. The difference of results of two methods is nearing zero. Fig.3.8 shows the contours of the analytic horizontal y gradient and numerical horizontal y gradient of first data. Fig.3.9 is for the profiles of the analytic horizontal y gradient and numerical horizontal y gradient of first model drawn at the position y =1175m, the difference is zero. Fig.3.10 presents the contours of the analytic signal and numerical analytic signal of first model. The two figures are identical. Fig.3.11 shows the profiles of the analytic signal and numerical analytic signal of first model drawn at the position y=1175m. The two profiles are identical, their difference being nearing zero.

The robustness of the calculations of the derivatives to the changes of depth is illustrated in Appendix C. The derivatives of depth of 80m and 100m are illustrated in Appendix C. The results prove that the calculations of the derivatives have the robustness to the changes of the depth.

3.4.2 Comparison of the responses for second model

Next the algorithm is tested on the second model. The model consists of a cylinder with a depth to its top of 41m, the radius of 133m, the total inclination of 83°, the total declination of -38° $J_{tot} = 22nT$.

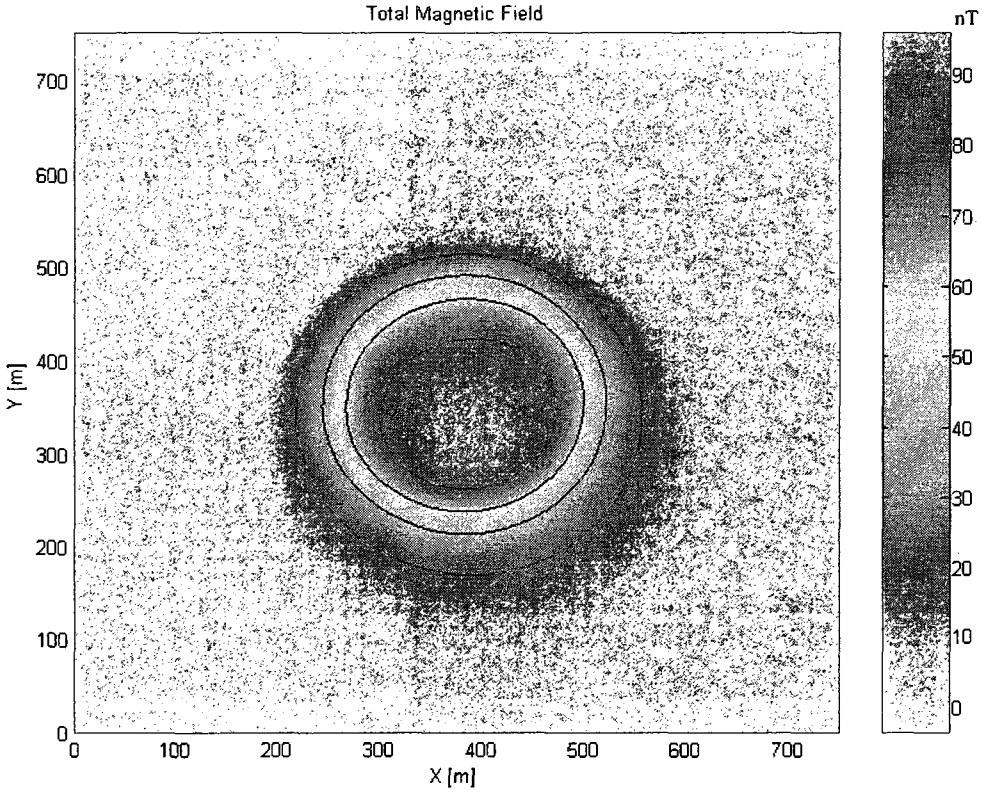

Fig.3.12 Contour of the total magnetic field of second model

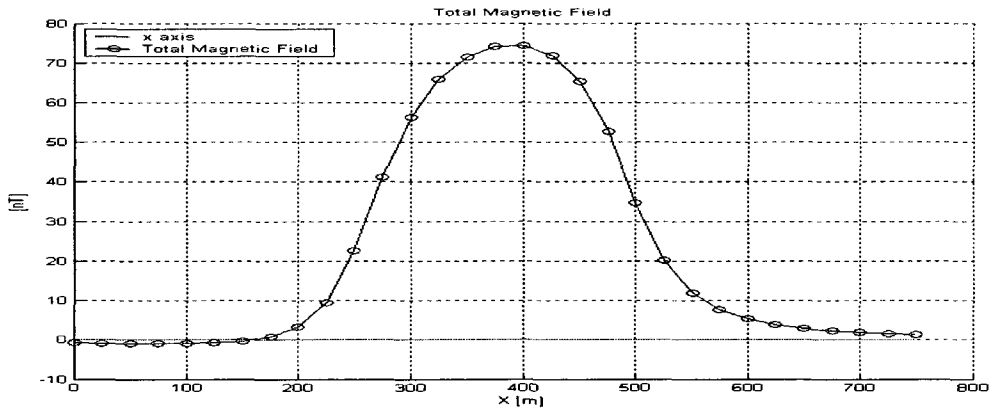

Fig.3.13 Profile at y =425m at the total magnetic field of second model

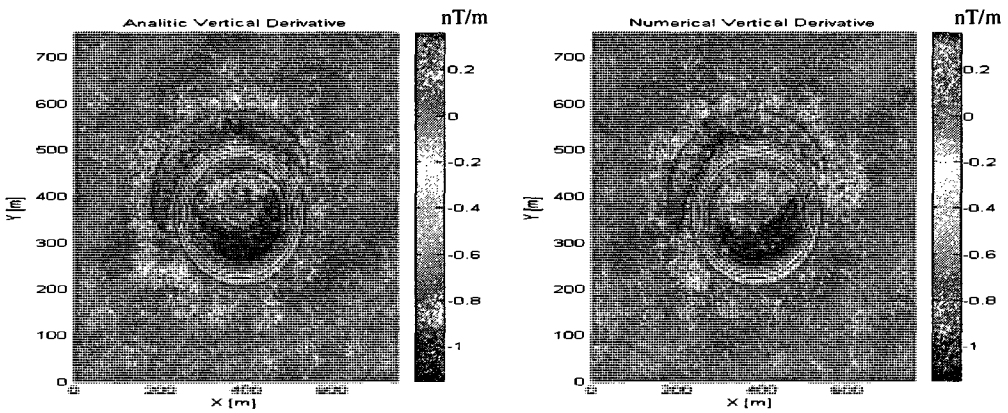

Fig.3.14 Contours of the calculated vertical derivative and numerical vertical derivative of second model

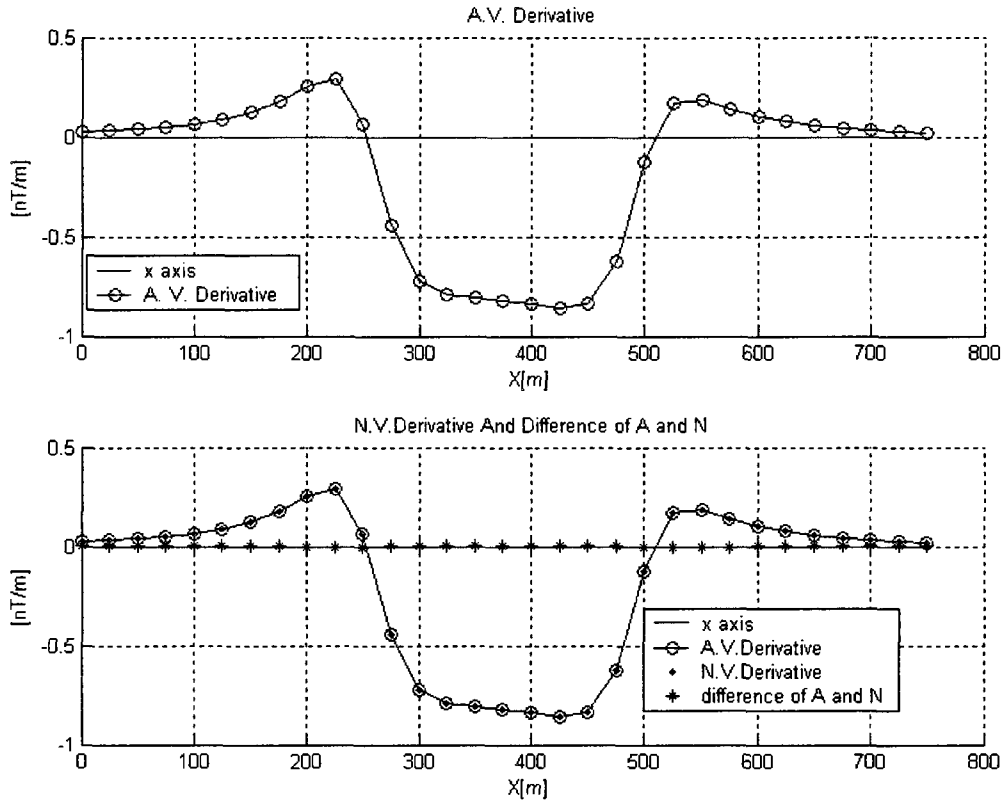

Fig.3.15 Profiles at y =425m of the calculated vertical derivative and numerical vertical derivative of second model

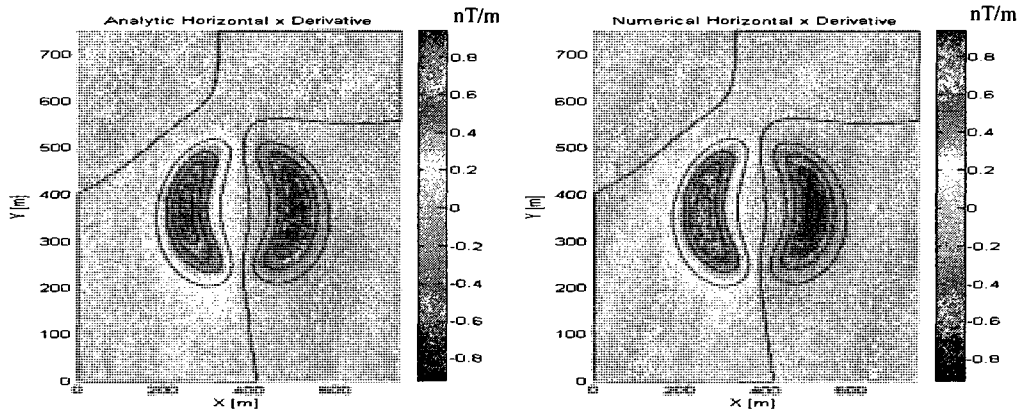

Fig.3.16 Contours of the calculated x derivative and numerical x derivative of second model

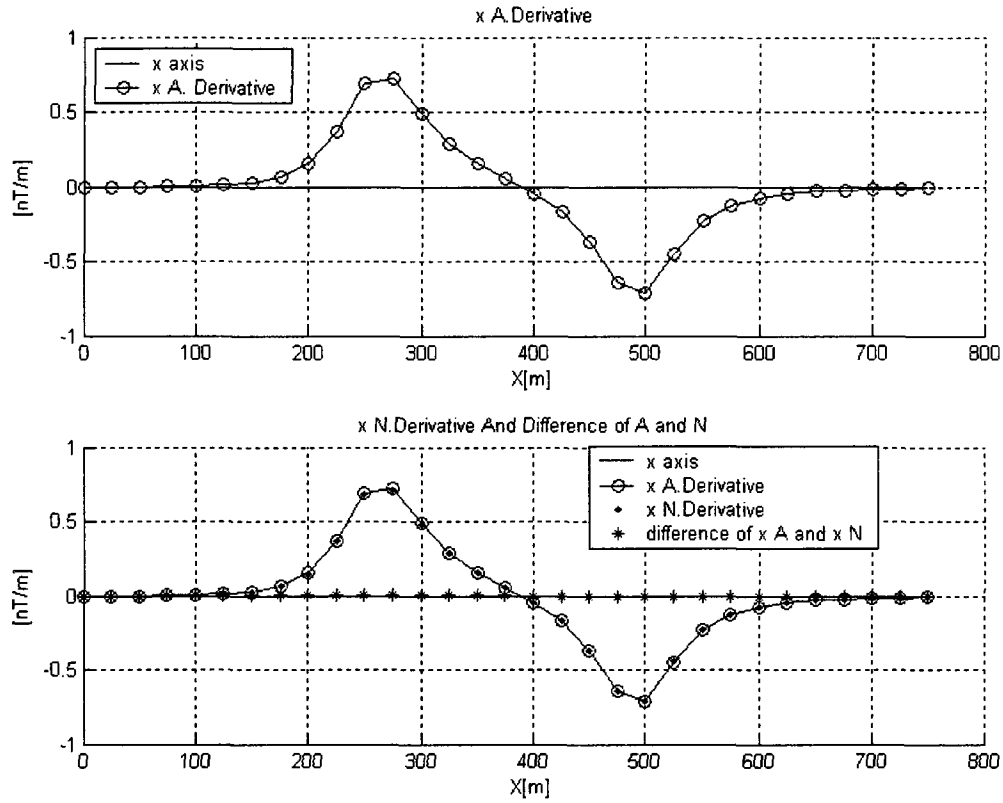

Fig.3.17 Profiles at y =425m of the calculated x derivative and numerical x derivative of second model

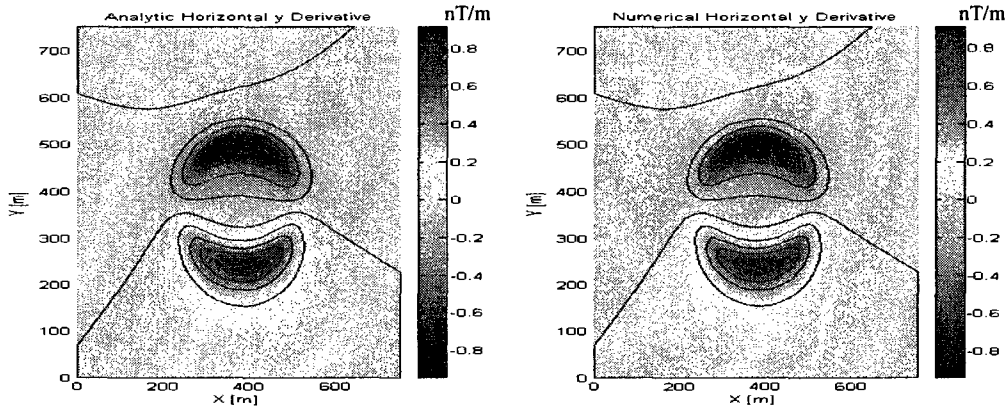

Fig.3.18 Contours of the calculated y derivative and numerical y derivative of second model

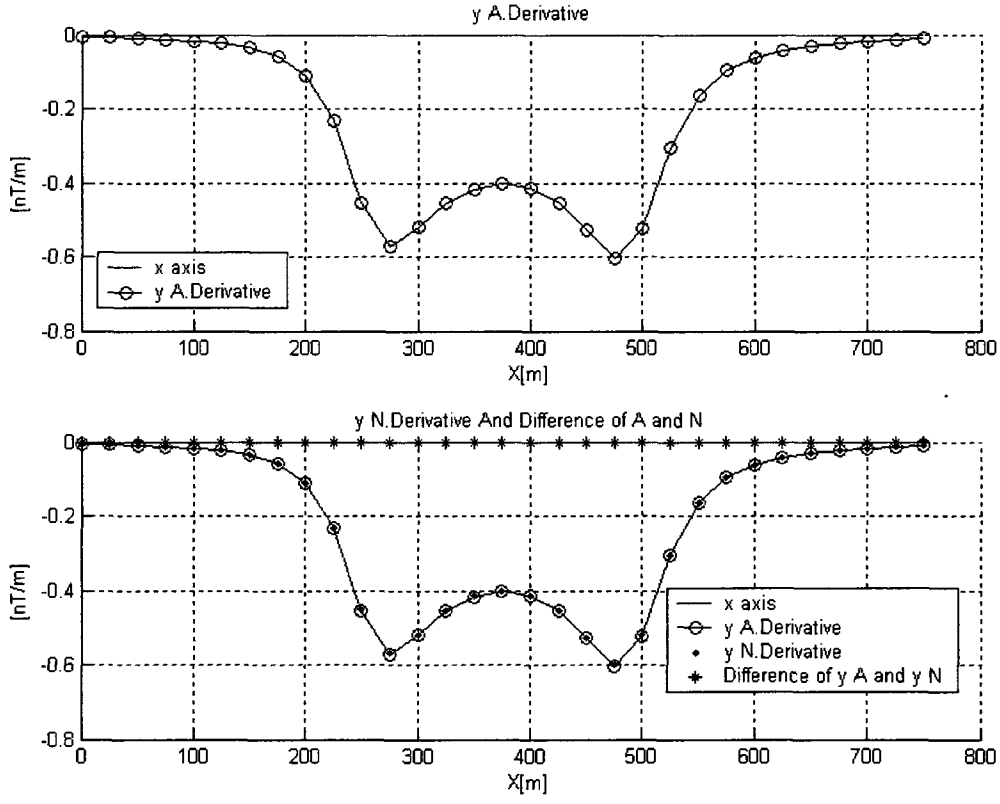

Fig.3.19 Profiles at y =425m of the calculated y derivative and numerical y derivative of second model

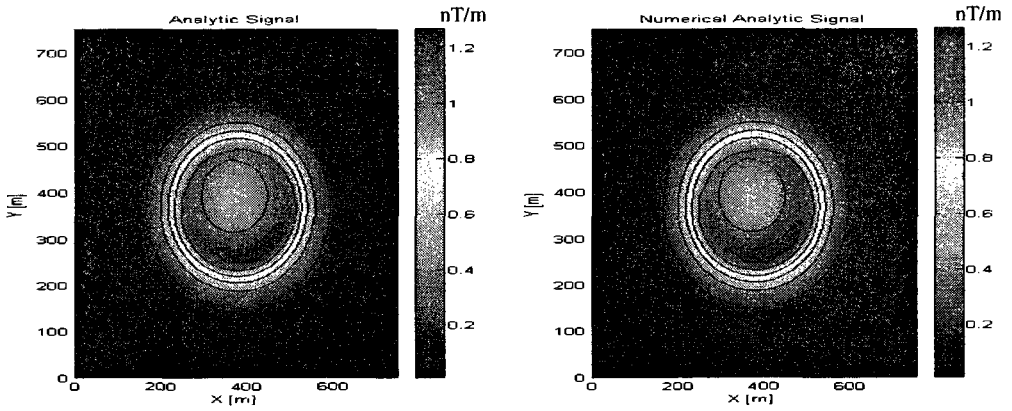

Fig.3.20 Contours of the calculated analytic signal and numerical analytic signal of second model

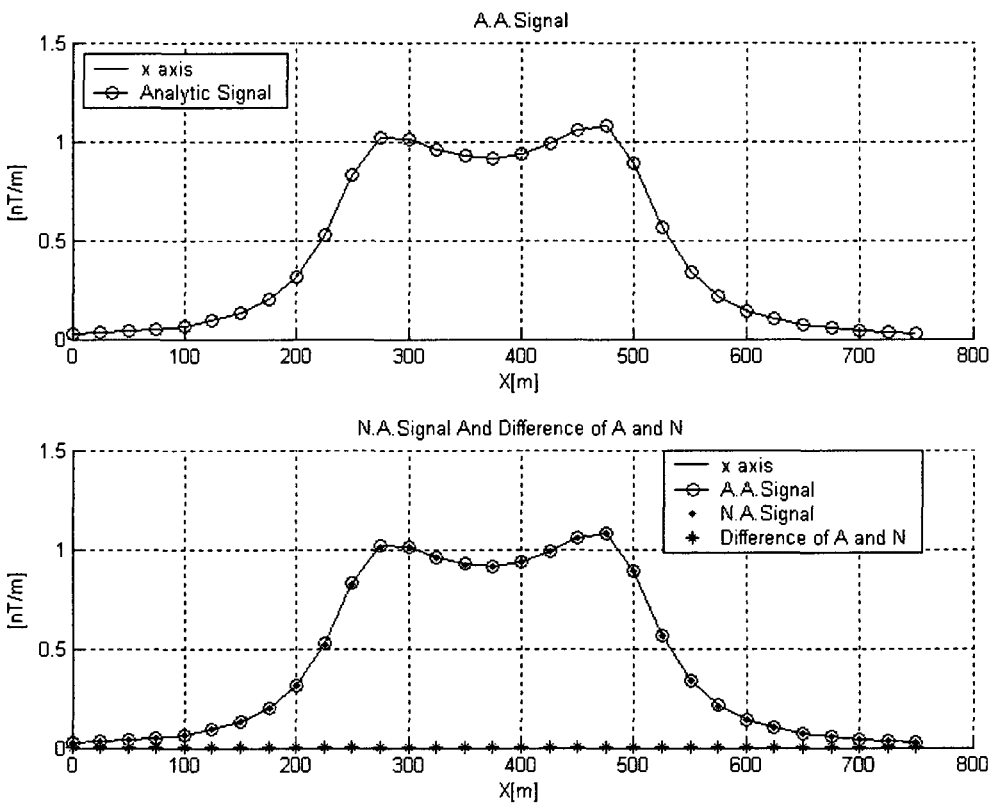

Fig.3.21 Profiles at y =425m of the calculated analytic signal and numerical analytic signal of second model

From Fig.3.12 to Fig.3.21 illustrate the second model; it can be seen that the results from two methods are identical. The robustness of the calculations of derivatives to changes of radius of cylinder is illustrated in Annex D. The derivatives of this model for the radius of 200m and of 300m are illustrated in Annex D. The results show that this algorithm of derivatives is robust to the changes of the radius of the cylinder.

3.4.3 Comparison of the responses for third model

We now compare the responses of the two methods for the third model. It consists of a cylinder with $J_{tot} = 3.33nT$, $Total\ inclination = 152^{\circ}$, $Total\ declination = -12^{\circ}$, $Depth = 99m$, $Radius = 80m$.

$Earth\ Field\ Inclination = 74^{\circ}$, $earth\ field\ declination = -12^{\circ}$.

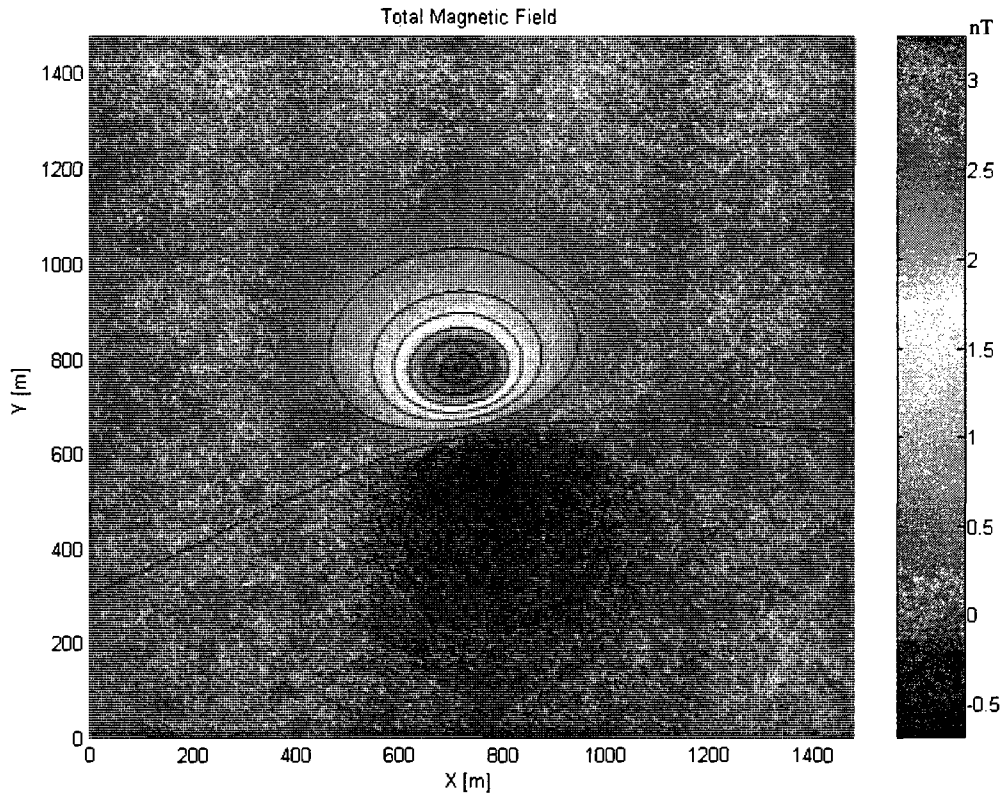

Fig.3.22 Contour of the total magnetic field of third model

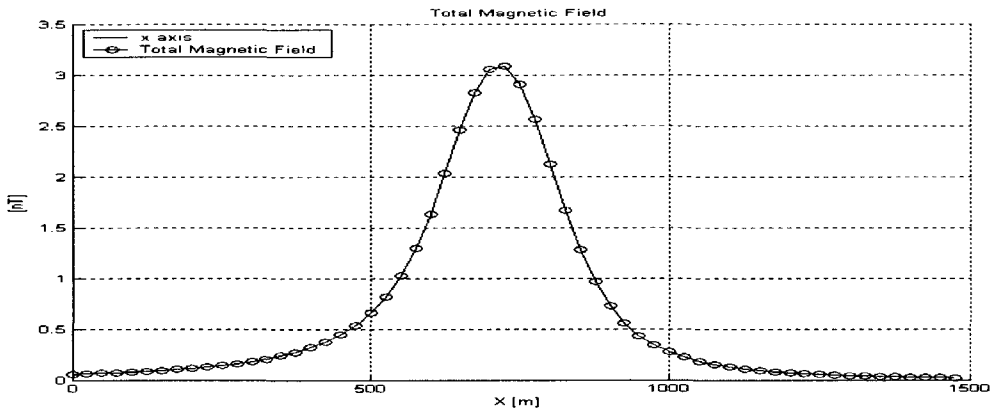

Fig.3.23 Profile at y =800m of the total magnetic field of third model

Figure 3.22 to 3.31 shows the contours and profiles of total magnetic field and gradients and analytic signal derived from the analytic method and numerical method. The results from the two methods are identical because of the difference of zero of two profiles.

The robustness of the calculations of the derivatives to changes of inclination is shown in Annex E. The results of the calculations of the derivatives of total inclination of 40° and of 30° are illustrated. It can be seen that the results from two methods are still identical with the change of the total inclination, even with a big change of total inclination from total inclination of 152° to 30°. That means this algorithm is very stable to the change of the total inclination.

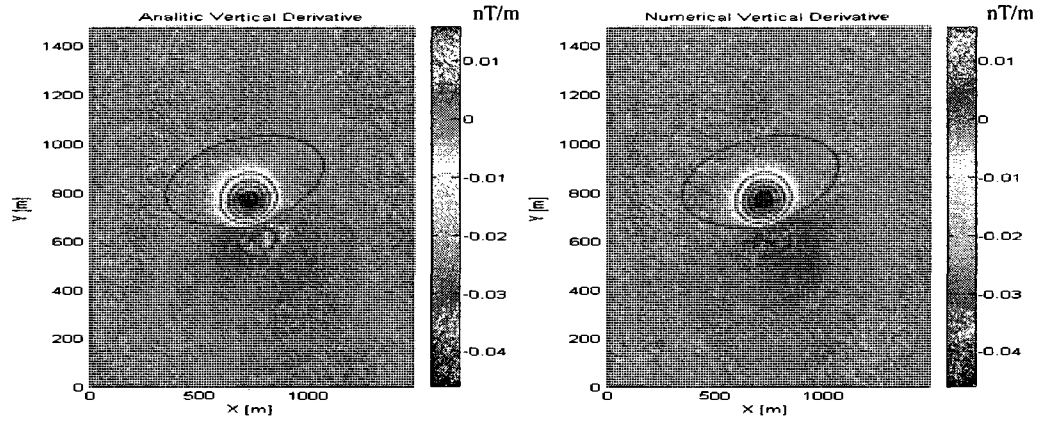

Fig.3.24 Contours of the calculated vertical derivative and numerical vertical derivative of third model

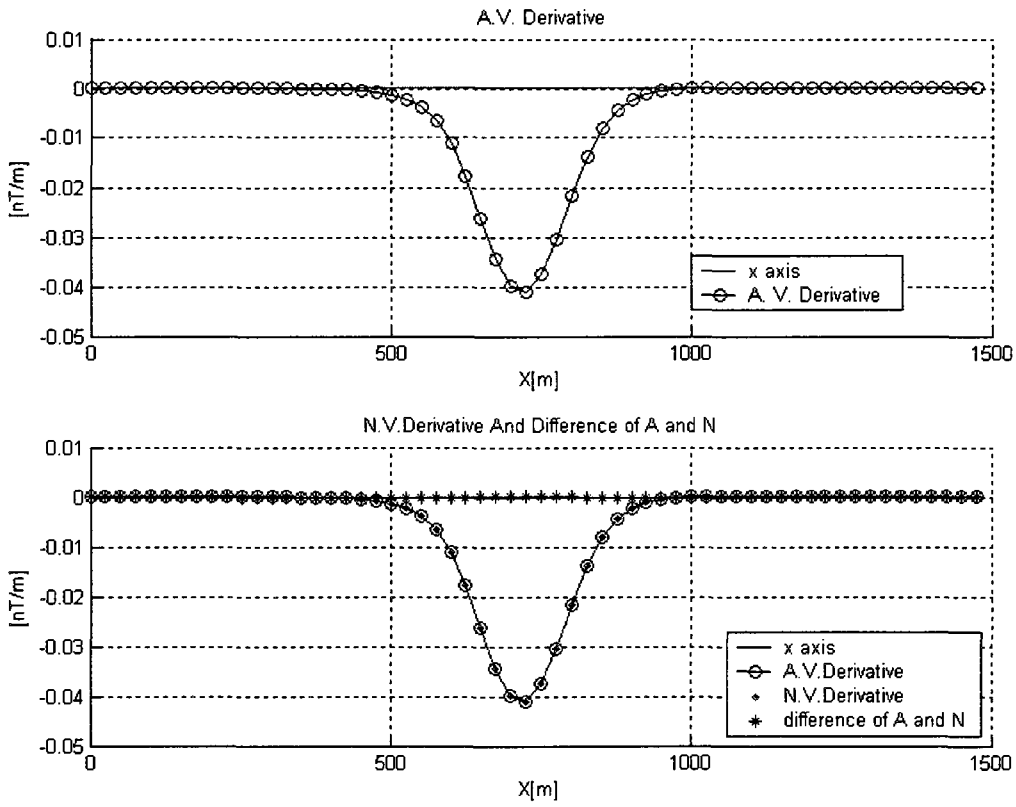

Fig.3.25 Profiles at y =800m of the calculated vertical derivative and numerical vertical derivative of third model

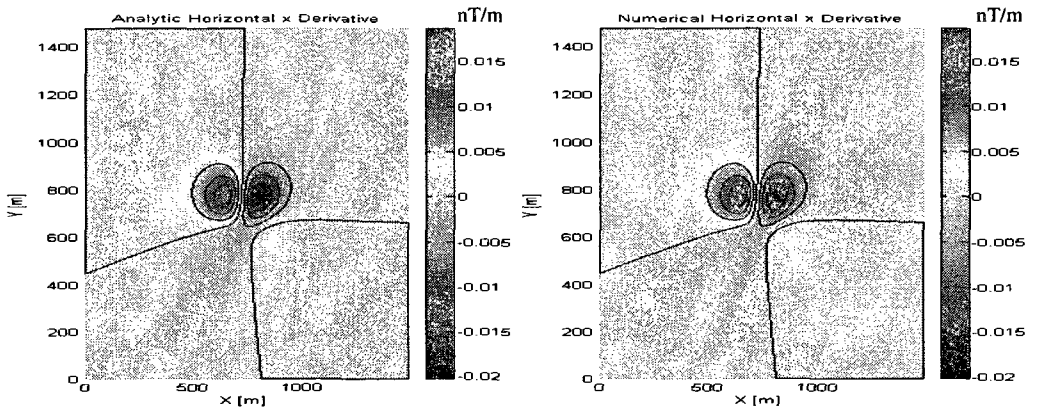

Fig.3.26 Contours of the calculated x derivative and numerical x derivative of third model

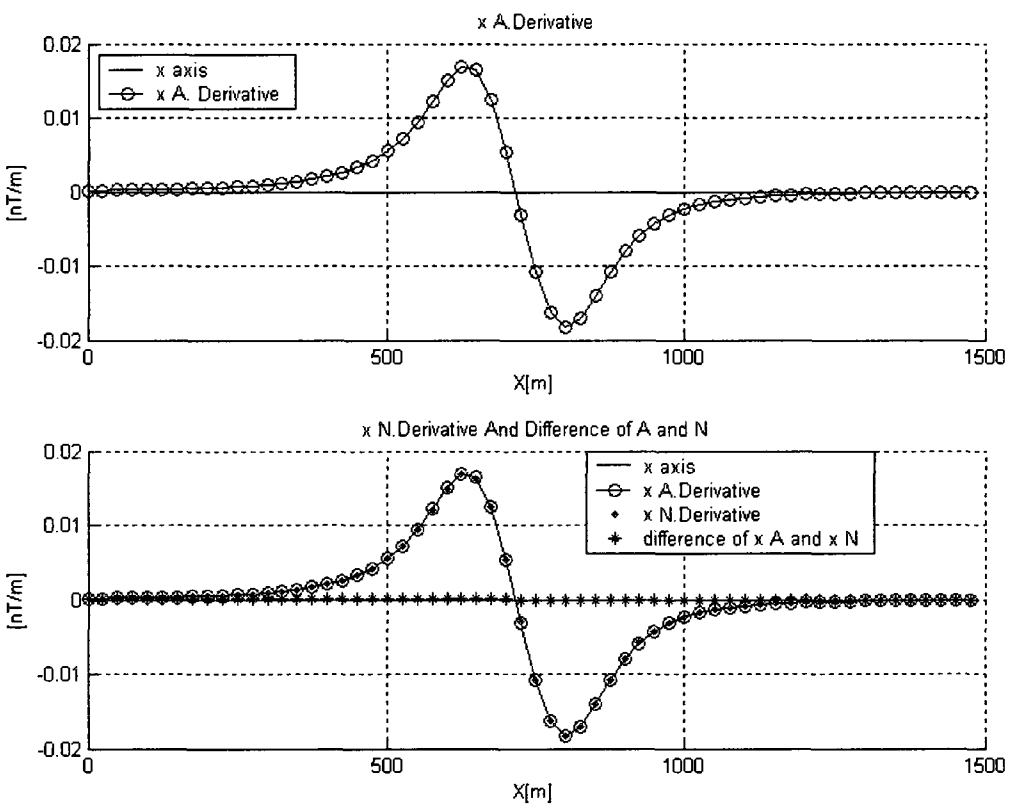

Fig.3.27 Profiles at y =800m of the calculated x derivative and numerical x derivative of third model

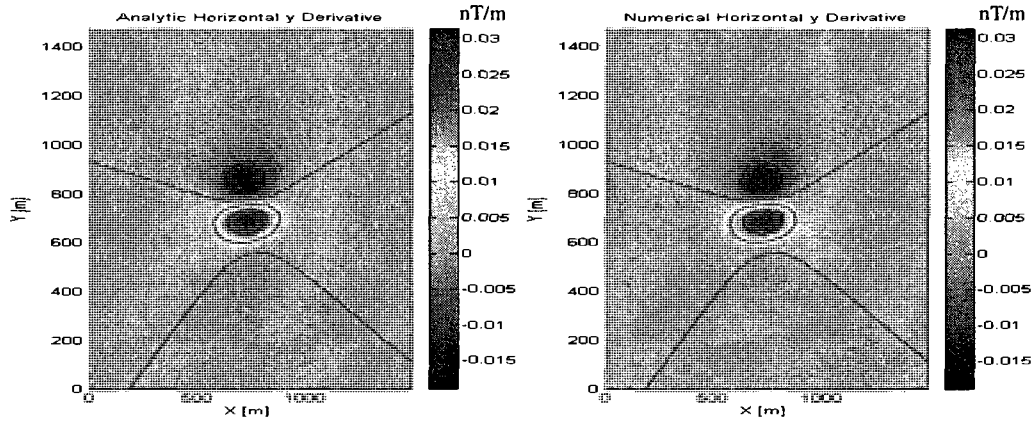

Fig.3.28 Contours of the calculated y derivative and numerical y derivative of third model

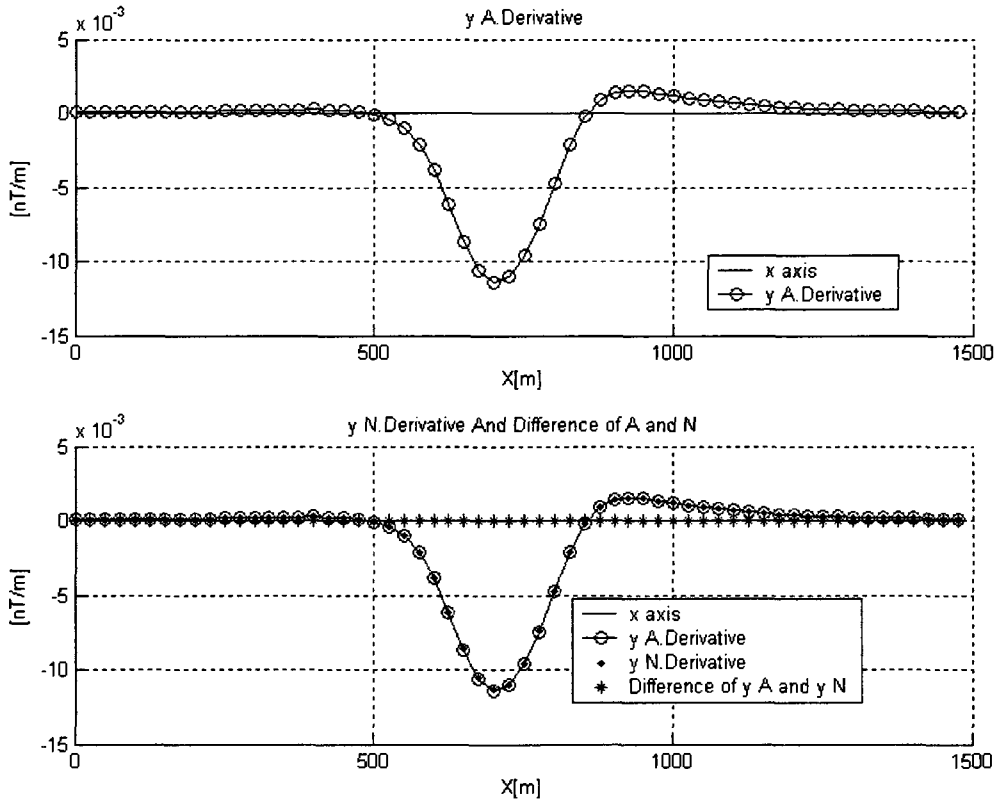

Fig.3.29 Profiles at y =800m of the calculated y derivative and numerical y derivative of third model

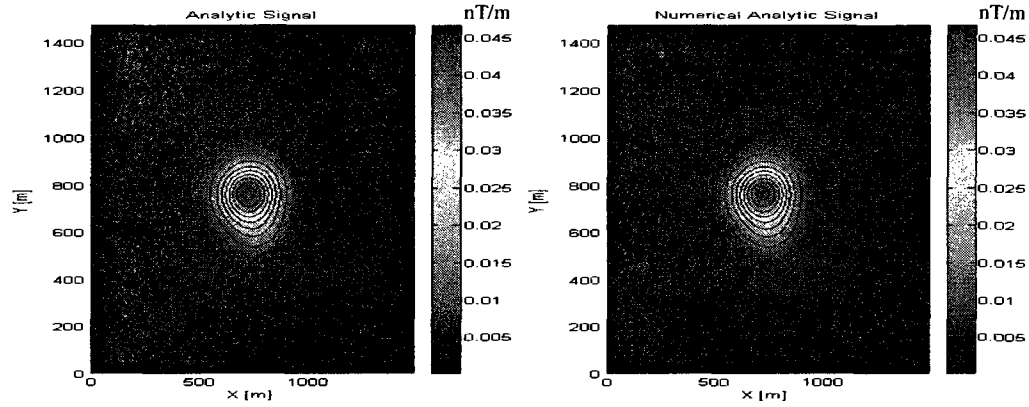

Fig.3.30 Contours of the calculated analytic signal and numerical analytic signal of third model

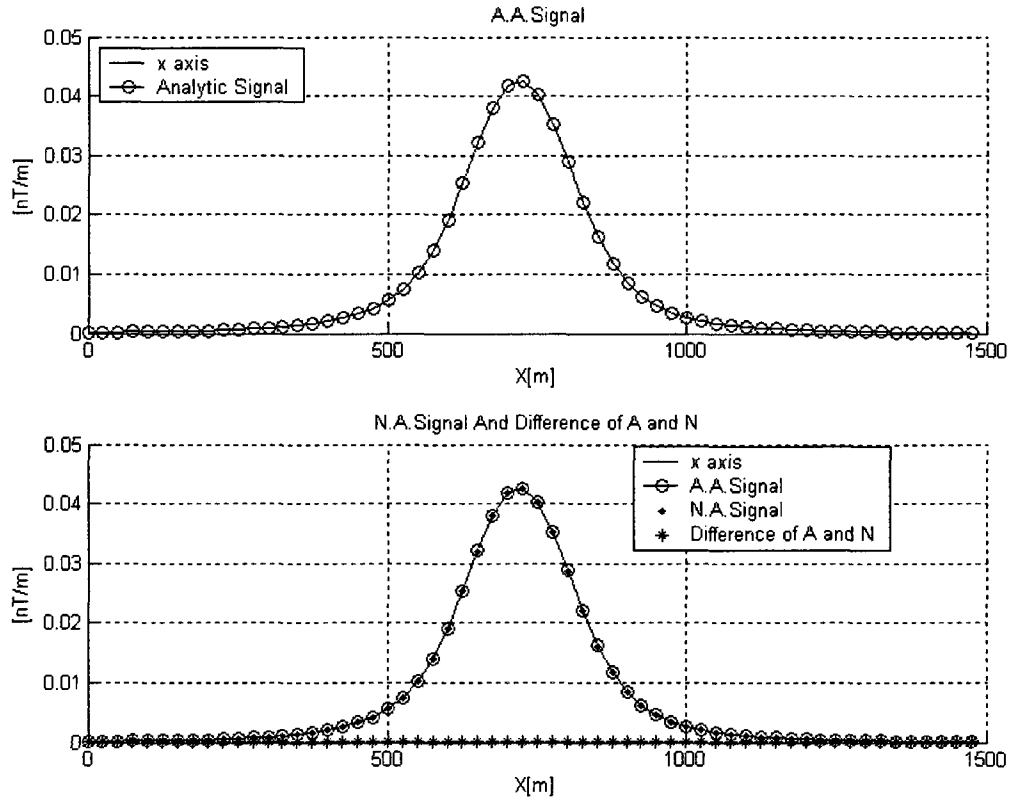

Fig.3.31 Profiles at y =800m of the calculated analytic signal and numerical analytic signal of third model

3.4.4 Comparison of the responses for fourth model

The fourth model with remanent magnetization is tested. It is a cylinder with Depth=58m, radius=101m, total inclination=-5° , total declination=-6°, remanent inclination=-43°, remanent declination=2°, J_{tot} $=33nT$ Q=1.576.

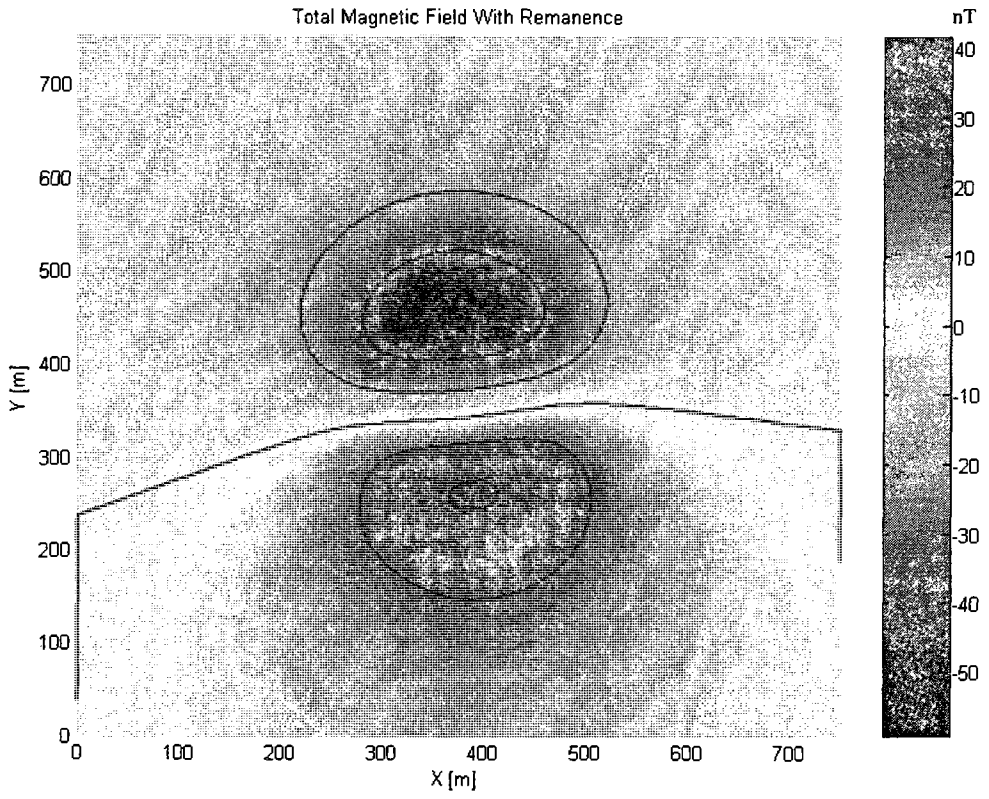

Fig.3.32 Contour of total magnetic field of fourth model

Figure3.32 to 3.41 shows the last model to be tested with remanent magnetization. The results from the two methods are the same, the difference of two profiles being zero; the profiles agree well with its source position (y =425m) on the corresponding contours. Annex F presents robustness of this calculation of the derivatives relative to the change of the remanent magnetization inclination. Figure F.1 to F.10 show the contours and profiles for a remanent inclination of -30° while Figure F.11 to F.20

show the contours and profiles for a remanent inclination of -10°. The figures show that the pattern of total magnetic field is almost insensitive to the changes of remanent magnetization inclination from $-43°$ to $-30°$ to $-10°$. For the vertical gradients, the patterns are almost the same, and the values show minimal variations. For horizontal gradients, there is a little increase for x gradients which results in an increase to the amplitude of analytic signal. The results from the analytic method and that from the numerical method are almost same.

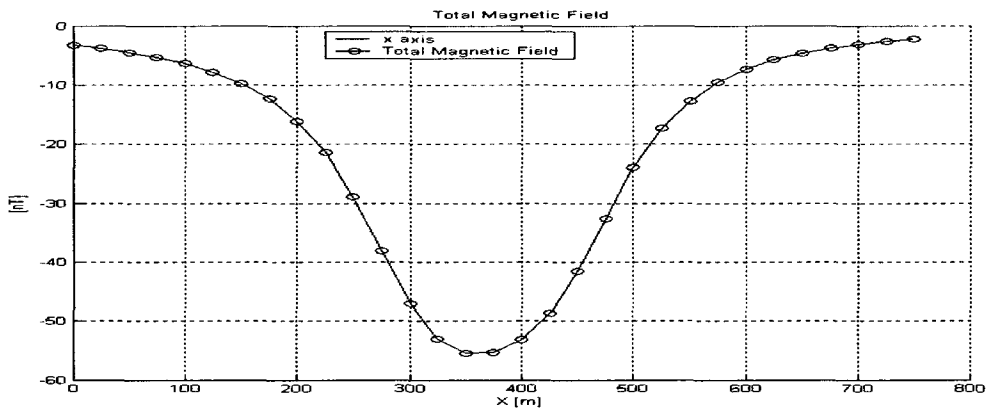

Fig.3.33 Profile at y =425m of total magnetic field of forth model

The results show that the results from the two methods are identical, that means the derivatives of the magnetic anomaly due to a vertical right circular with arbitrary polarization cylinder in the presence of remanent magnetization are also calculated successfully. The robustness of this calculation is also illustrated in Annex F. the results of the derivatives of the remanent inclination of -30° and of -10° are illustrated there. The results from two methods are always identical with the change of the remanent inclination. They show that it is robust to the change of remanent inclination.

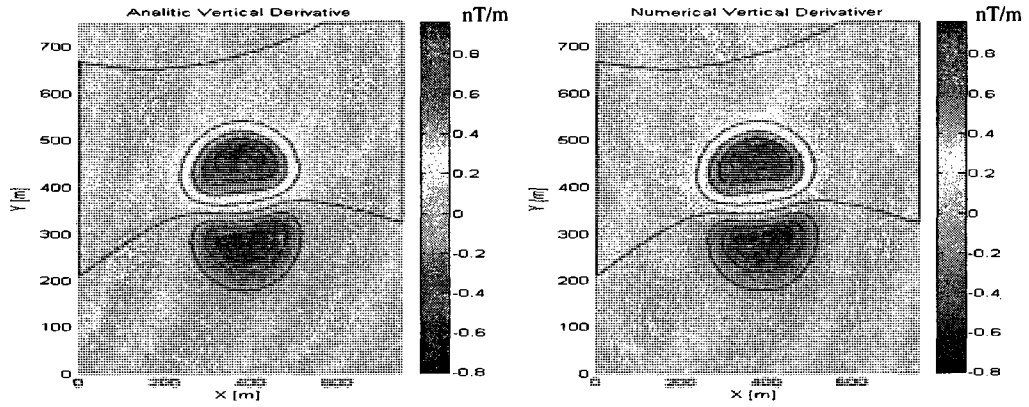

Fig.3.34 Contours of calculated vertical derivative and numerical vertical derivative of forth model

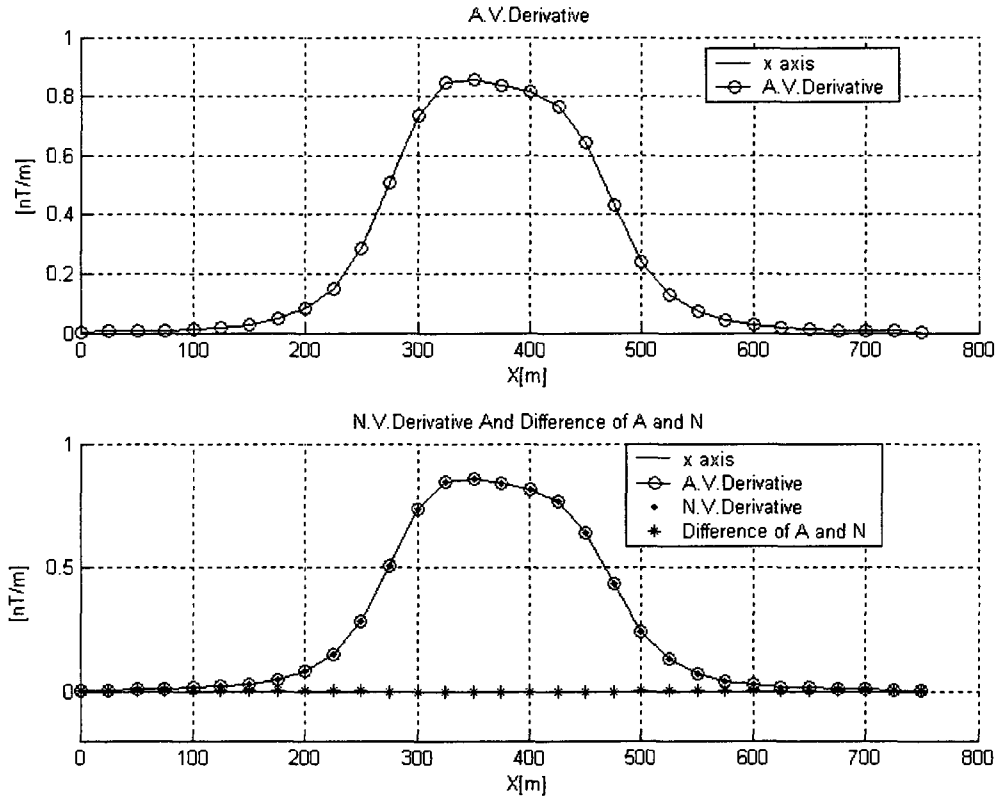

Fig.3.35 Profiles at y =425m of calculated vertical derivative and numerical vertical derivative of forth model

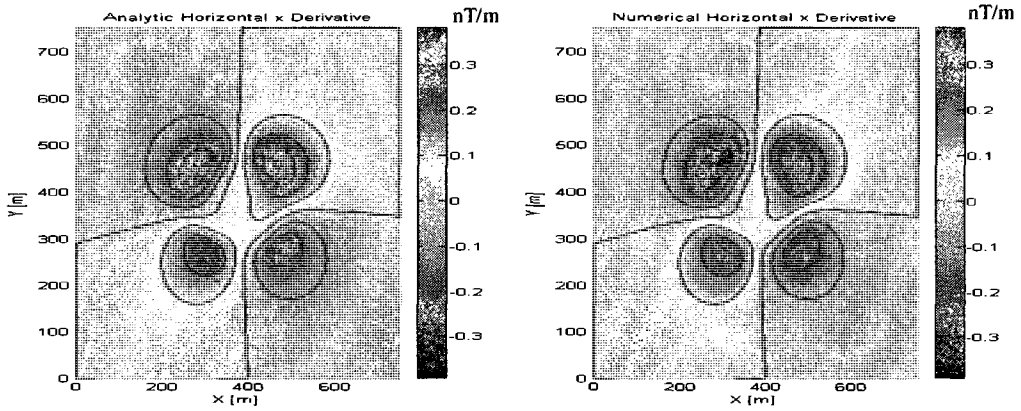

Fig.3.36 Contours of calculated x derivative and numerical x derivative of forth model

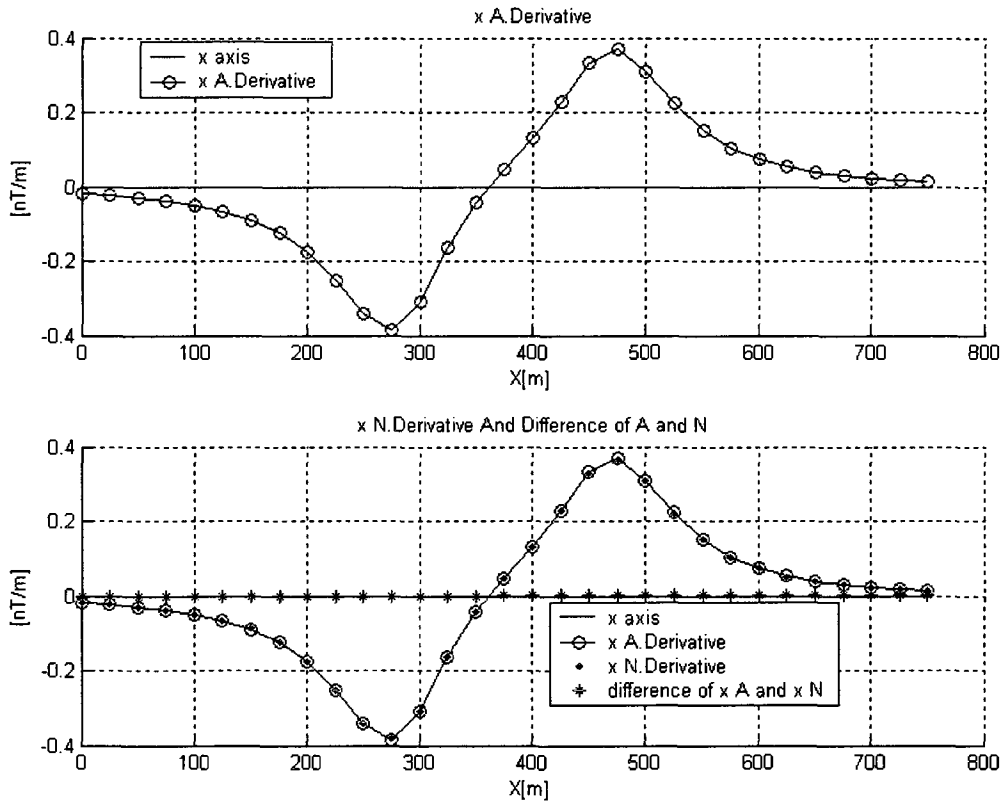

Fig.3.37 Profiles at y =425m of calculated x derivative and numerical x derivative of forth model

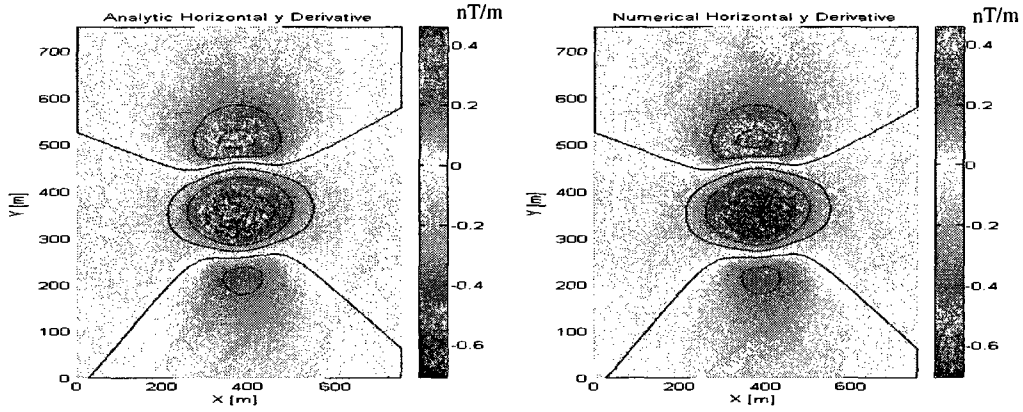

Fig.3.38 Contours of calculated y derivative and numerical y derivative of forth model

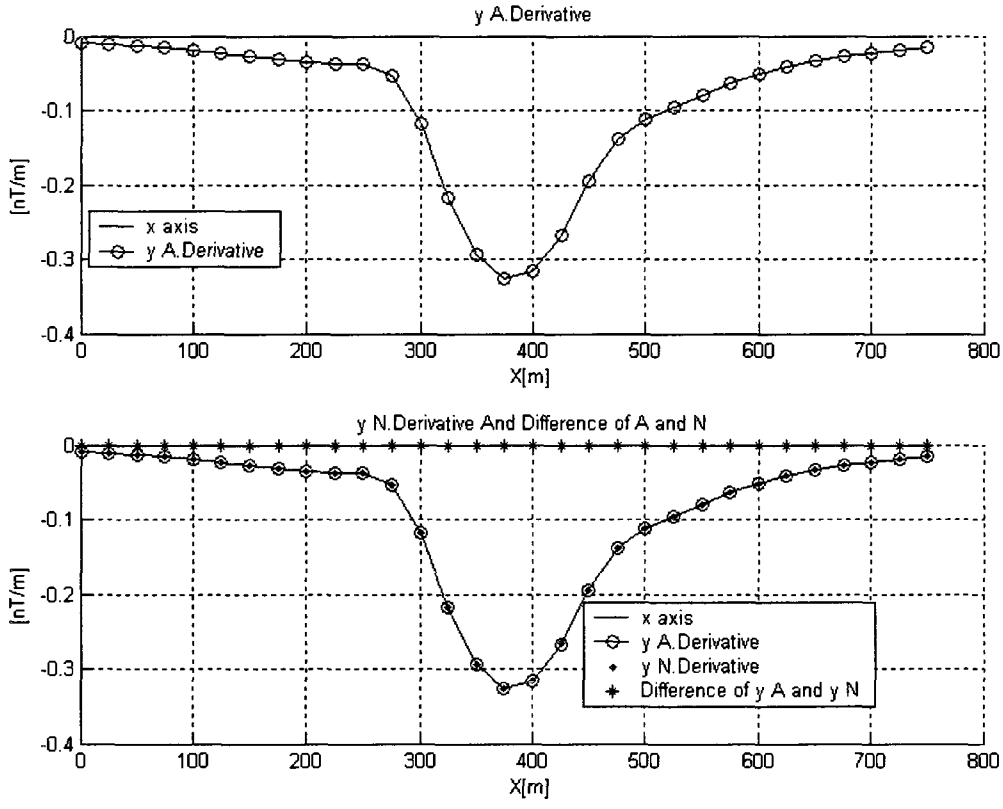

Fig.3.39 Profiles at y =425m of calculated y derivative and numerical y derivative of forth model

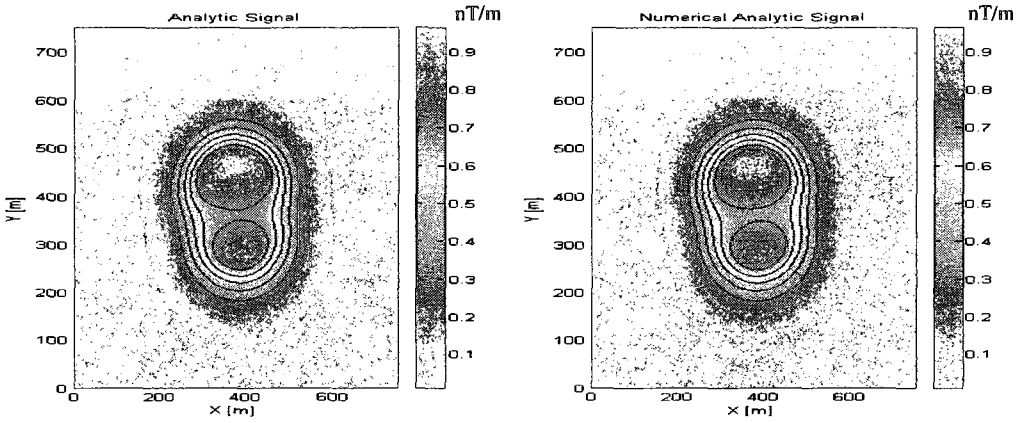

Fig.3.40 Contours of calculated analytic signal and numerical analytic signal of forth model

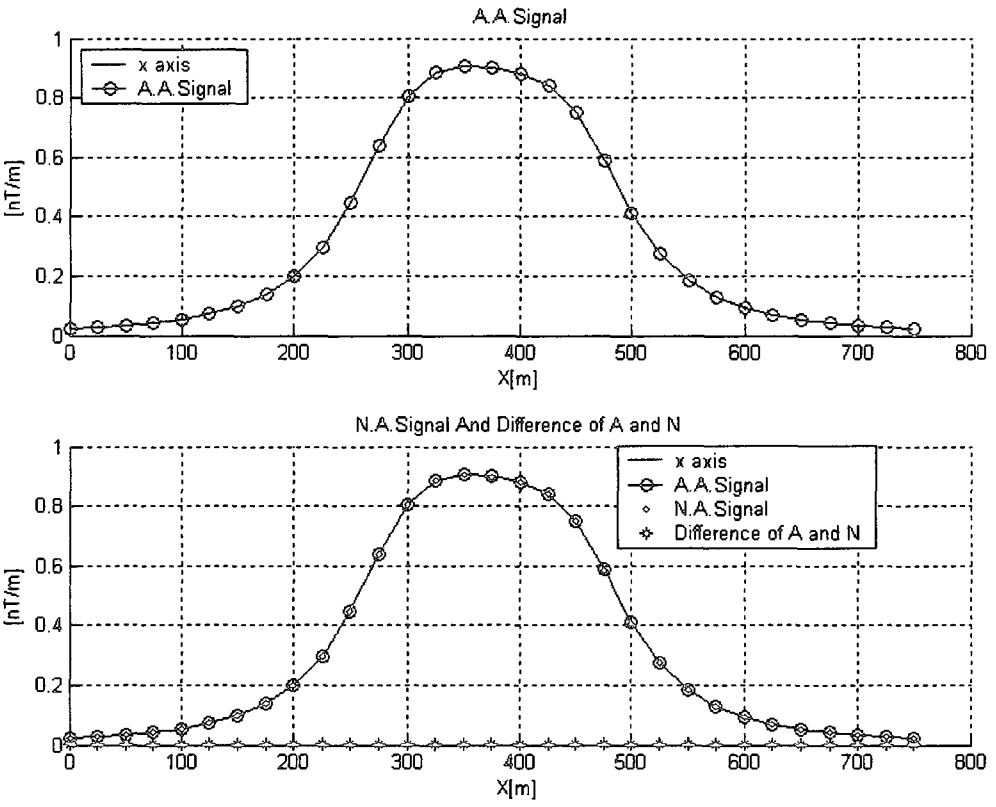

Fig.3.41 Profiles of y =425m of calculated analytic signal and numerical analytic signal of forth model

3.5 Conclusion

The calculation of the gradients and the analytic signal for magnetic anomalies due to the vertical cylinder is calculated successfully by the two methods, the analytic and the numerical methods. Their accuracies are evaluated by the sensibilities testing.

I compared the speed for the two methods, for the vertical derivative, the method of analytical derivative is faster than that of finite difference, and for the horizontal derivative, the later method is faster. As for the accuracy, the analytic derivative is superior, because for the method of finite difference, the size of Δ affects the results, for example, the vertical derivative of the magnetic field is obtained by computing the field at depth $z+\Delta z$ and $z-\Delta z$, dividing the difference by $2\Delta z$, I changed the value of Δz , the results of the z derivative is changed. The changes of Δx and Δy also affect the accuracy of x, y derivatives. The analytic derivative is stable. The analytic derivative is preferred for computation of the analytic signal and its derivatives. And the most important point is that I completed the task of computation of the vertical and the two horizontal derivatives of the magnetic field to construct the mathematical model for analytic signal inversion.

Chapter 4 Inversion of the magnetic field

4.1 Introduction of the magnetic field inversion

In the preceding chapter, I completed the calculations of the analytic expressions of x, y and z derivatives and of the analytic signal. These analytic expressions will be used for computing the Jacobian matrix needed in the inversion of the total magnetic field and in the direct problem for the analytic signal inversion. I now proceed to implement the inversion of the magnetic field, to develop an algorithm that inverts the magnetic data to recover the properties of the earth magnetic field and the geometry of the causative body. In this chapter, I introduce the originality of the problem and the methodology used to resolve the problem, the results from various tests will be illustrated.

Inversion is an automatic numerical procedure that constructs a model of subsurface geology from measured magnetic data and other information, under the condition that the input data are reproduced within a given error tolerance (Nabighian et al., 2005). The inversion of magnetic field data has been proposed for the estimation of the basement relief, to interpret dike (2D), rectangular prism (3D) and vertical cylinder. Pilkington and Crossley (1986) inverted magnetic anomalies to estimate basement relief by applying linear inverse theory and Parker's (1972) forward calculation technique. Pustisek (1990) developed a direct procedure to invert for the magnetic basement. For isolated anomalies, the models of the dike (2D) and the rectangular prism (3D) have been used (Whitehill, 1973; Ballantyne, 1980; Bhattacharyya, 1980; Silva and Hohmann, 1983; Zeyen and Pous, 1991). Causative bodies are usually represented as polygonal bodies in 2D or polyhedral bodies in 3D (Pedersen, 1979; Wang and Hansen, 1990). Most of these methods assume that the magnetization direction is known. As a result, their application is limited when strong remanent magnetization alters the total magnetization direction. To overcome this difficulty, Chemam (2006) implemented a 3D inversion with the model of cylinder

given by Singh and Sabina (1978).Here, not only the remanent magnetization is taken into account, but also the pipe like model that mimics the reality.

4.2 The problem

Before introducing the inversion of the magnetic field, it is necessary to introduce the work of Chemam (2006). Using the model of cylinder given by Singh and Sabina (1978), Chemam proposed a parametric inversion of the magnetic field caused by a vertical cylinder. This method was aimed at interpreting magnetic data in diamond prospecting context. His most important contribution is the evaluation of the direction of the magnetization by the method of magnetic moment obtained by the integration of the field components. The inversion requires knowing the magnetization direction. Using the wrong magnetization direction produces erroneous inversion results. So the evaluation of the magnetization direction is a very important prerequisite for the inversion to be successful. Secondly, he introduced methods for deriving the initial values of the parameters for the inversion, including the estimation of the direction of the remanent magnetization, the geometric parameters, such as the depth of the cylinder, the diameter of the cylinder, the intensity of the magnetization and the coordinates of the centre of the cylinder. Thirdly, the inversion of remanent magnetization has been implemented to separate the remanent magnetization from the total magnetization.

Yet, there remain problems to be solved in order to improve the magnetic parametric inversion of the anomaly due to the vertical right circular cylinder with arbitrary polarization. First of all, the inversion for the remanent magnetization is sometimes unstable. This is because the estimation of the direction of the remanent magnetization can be erroneous, which leads to erroneous estimation of geometric parameters. Secondly, the Jacobin matrix in the inversion of magnetic field given by Chemam is calculated by finite difference derivatives. The precision of the calculation of the Jacobian matrix is the key factor to obtain accurate inversion results. In the following inversion, it is replaced by the analytic derivatives to increase the stability.

4.3 The solutions

4.3.1 The relationship between the total magnetization intensity and the remanent magnetization.

The relationship between the induced magnetization intensity J_i, the remanent magnetization intensity J_r and the total magnetization is a key factor to obtain stable results from the inversion. I derive the formulation of the relationship between the induced magnetization intensity and the remanent magnetization to replace that used by Chemam (2006) to improve the results of the inversion. The formulation is given as follow:

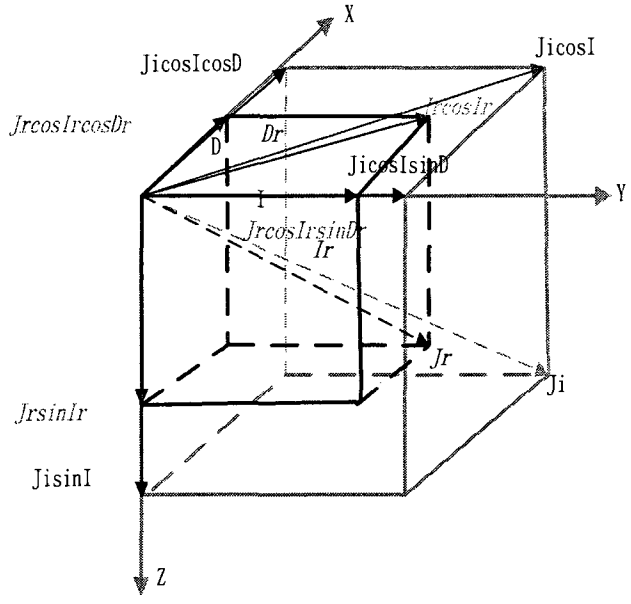

Fig.4.1 Relationship between the induced magnetization intensity J_i and remanent magnetization intensity J_r

$$J_r = J_i Q \quad (4.1)$$

$$J_x = J_i \cos I \cos D + J_r \cos I_r \cos D_r \quad (4.2)$$

$$J_y = J_i \cos I \sin D + J_r \cos I_r \sin D_r \quad (4.3)$$

$J_z = J_i \sin I + J_r \sin I_r$ (4.4)

$J_{tot}^2 = J_x^2 + J_y^2 + J_z^2$ (4.5)

Substitute equation 4.1 into 4.2, 4.3 and 4.4, after substitute equation 4.2, 4.3 and 4.4 into the equation 4.5, the equation 4.6 is derived:

$J_i^2 / J_{tot}^2 = 1/[1 + Q^2 + 2Q(a+b+c)]$ (4.6)

Included:

$a = \sin I \sin I_r$ (4.7)

$b = \cos I \cos D \cos I_r \cos D_r$ (4.8)

$c = \cos I \sin D \cos I_r \sin D_r$ (4.9)

4.3.2 The explicit derivatives to replace numerical derivatives in the calculation of the jacobian matrix.

I completed the calculation of the explicit x, y and z derivative of the anomaly due to the vertical right circular cylinder with arbitrary polarization, so numerical derivatives are replaced by analytic derivatives to increase the stability of the inversion and its precision.

4.4 Levenberg -marquardt method

4.4.1 Description of levenberg -marquardt method

Most of the problems in geophysics are ill-posed inverse problems. The Levenberg-Marquardt method is one of the popular methods for ill-posed inverse problems (Marquardt 1963; Morrison 1960). In order to give a description of the Levenberg-Marquardt method clearly, the general notation for inversion should be given:

The M data values $d_1, d_2, ..., d_M$, corresponding to M sample points, or instrument readings, are written as the vector

$$\vec{d} = (d_1, d_2, ...d_M)^T. \qquad (4.10)$$

the models are determined by N free parameters, which we write as the vector,

$$\vec{m} = (m_1, m_2, ...m_N)^T. \qquad (4.11)$$

the magnetic field intensity is generated by forward modeling for each setting of $\vec{m}$. This is denoted as a vector function by

$$F(\vec{m}) = (F_1(\vec{m}), F_2(\vec{m}), \ldots, F_M(\vec{m}))^T. \quad (4.12)$$

Here, $F_i(\vec{m})$ is the value predicted by the model, and corresponds to the observation d_i, the inverse problem determines values of $\vec{m}$ such that $F(\vec{m})$ matches $\vec{d}$ (Jupp, 1975).

Using the first order of Taylor's expansion to develop $F(\vec{m})$, we write:

$$\vec{d_i} - F_i(\vec{m}) = \sum_{j=1}^{N} \frac{\partial F_i(m)}{\partial m_j} \Delta m_j + e, \quad i = 1,2,\ldots,M \quad (4.13)$$

$$\Delta m_j = m_j - m_j^0 \quad (4.14)$$

m_j^0 is the initial value of the parameters of the models.

In matrix form

$$\varepsilon = A\Delta m + e \quad (4.15)$$

we call ε the error vector, A the Jacobian matrix.

Given the equation:

$$e = \varepsilon - A\Delta m \quad (4.16)$$

the Marquardt method is usually defined operationally as the solution that

minimizes $e^T e + \lambda \Delta m^T \Delta m$

λ is called the damping parameter, used to control the size and direction of the step Δm during the iteration (Marquardt, 1963).

Now, we define:

$$\phi = e^T e + \lambda \Delta m^T \Delta m \quad (4.17)$$

substitute equation (4.16) into equation (4.17)
we get:

$$\phi = (A\Delta m - \varepsilon)^T (A\Delta m - \varepsilon) + \lambda \Delta m^T \Delta m \quad (4.18)$$

minimization of ϕ, given $\partial\phi / \partial m^T = 0$, leads to :

$$\Delta m = (A^T A + \lambda I)^{-1} A^T \varepsilon \qquad (4.19)$$

4.4.2 Forward modeling

The first inversion is for deriving the geometric parameters such as the depth of the cylinder, the diameter of the cylinder etc. The functions are:

$$F1 = f(x, y, h, a, J_{tot}, I_m, D_m, x_0, y_0) \quad (4.20)$$

$$F2 = f(x, y, h+th, J_{tot}, I_m, D_m, x_0, y_0) \quad (4.21)$$

$$F = F1 - F2 \quad (4.22)$$

$F1$ and $F2$ are given by Singh and Sabina (1978), A17 and A18 are all the mathematical model for semi-infinite cylinder, their depths are h and $h+th$ separately. (I_m, D_m) is the inclination and declination of the total magnetization, J_{tot} is the total magnetization intensity, x, y are the coordinates of the observation, h is the depth, a is

The radius of the cylinder, (x_0, y_0) is the center position of the cylinder, th is the thickness of the cylinder.

The second inversion is for the separation of the remanent magnetization from total magnetization. The parameters relating to remanent magnetization such as the Koenigsberger ratio (Q), the induced magnetization (J_i), the remanent inclination (I_{rem}) and the remanent declination (D_{rem}) are substituted for the total magnetization (J_{tot}), total inclination (I_m) and total declination (D_m) to derive the mathematical model for remanent magnetization inversion as follow:

$$F1 = f(x, y, h, a, J_i, I_{rem}, D_{rem}, x_0, y_0) \quad (4.23)$$

$$F2 = f(x, y, h+th, a, J_i, I_{rem}, D_{rem}, x_0, y_0) \quad (4.24)$$

$$F = F1 - F2 \quad (4.25)$$

x, y are coordinates of the observations, h is depth of the cylinder, a is diameter of the cylinder, th is thick of the cylinder, J_i is the induced magnetization, I_{rem} is

inclination of the remanent magnetization, D_{rem} is declination of remanent magnetization, x_0, y_0 are coordinates of the centre of the cylinder.

4.4.3 The calculation of the jacobian matrix

The Jacobian matrix is a M×N sensitivity matrix. The number of row (M) is the number of observation data, while the number of the column (N) is the number of parameters.

For the inversion without remanent magnetization, we need to calculate the following derivatives to construct the Jacobian matrix: $\frac{\partial F}{\partial h}, \frac{\partial F}{\partial a}, \frac{\partial F}{\partial J_{tot}}, \frac{\partial F}{\partial I_m}, \frac{\partial F}{\partial D_m}, \frac{\partial F}{\partial x_0}, \frac{\partial F}{\partial y_0}, \frac{\partial F}{\partial th}$, where

(I_m, D_m) is the inclination and declination of the total magnetization, the J_{tot} is the total magnetization intensity, h is the depth, a is radius of the cylinder, (x_0, y_0) is the position of the cylinder.

The term $\frac{\partial F}{\partial h}$ is equal to $\frac{\partial F}{\partial z}$, which is given in the Chapter 3. $\frac{\partial F}{\partial a}$ is derived in Appendix B. $\frac{\partial F}{\partial J_{tot}}$ $\frac{\partial F}{\partial I_m}$ and $\frac{\partial F}{\partial D_m}$ are derived by Chemam (Chemam, 2006). $\frac{\partial F}{\partial x_0}$ is equal to $-\frac{\partial F}{\partial x}$, $\frac{\partial F}{\partial y_0}$ is equal to $-\frac{\partial F}{\partial y}$ and $\frac{\partial F}{\partial x}$, $\frac{\partial F}{\partial y}$ have been derived in the Chapter 3. The $\frac{\partial F}{\partial th}$ is derived by finite difference, see section 3.2.

For the inversion with remanent magnetization, we need to calculate $\frac{\partial F}{\partial J_i}, \frac{\partial F}{\partial I_{rem}}, \frac{\partial F}{\partial D_{rem}}, \frac{\partial F}{\partial Q}$, by finite difference. Where J_i is the intensity of the induced magnetization, I_{rem} is the inclination of the remanent magnetization, D_{rem} is the declination of the remanent magnetization, Q and is the Koenigsberger ration.

4.4.4 The evaluation of initial values

The problem of initial values is resolved by Chemam (2006)'s initial values determination technique. The initial values evaluated by his technique are always

close to the true values. The tests are showed in his thesis. The initial inclination and declination of the remanent magnetization are estimated from the total inclination and declination, the total inclination and declination are calculated by the method of magnetic moment (Mikov, 1962). The initial values of the depth and diameter of the cylinder are calculated by the relationship between the derivatives of maximum of l' amplitude of the analytical signal of l' anomaly RTP in the center of the pipe, and the coordinates of the center of the cylinder are obtained maximum of the amplitude of the analytic signal of the reduction to pole of the magnetic anomaly due to the right vertical cylinder with arbitrary polarization. The entire job was implemented by Chemam (2006).

4.4.5 The inversion technique

An outline of the Levenberg-Maquardt inversion method is described in the flow diagram 4.1 and the flow diagram 4.2. Firstly, the forward model of the inversion is implemented by formula 3.1; I call this inversion the inversion -1. The initial values for the parameters need to be estimated, and then, the initial model response $F^{cal}_{(x,y)}$ is calculated. We get δF, the difference between the initial model response and the observations and the root-mean-squares (rms) error criterion is calculated. The Jacobin matrix is then calculated. With the formula (4.19), the parameter changes from the initial responses estimates are determined, so that we get the new parameters which are then used to compute a new model response estimates. With the new model response, we start the second iteration of inversion. At each stage, the root-mean-squares (rms) error between the model response and observation values is monitored. With the changes of the rms, the damping factor λ is modified automatically; when rms is decreased, λ is decreased to $10\%\lambda$, when rms is increased, λ is increased to 10λ. The inversion is terminated whenever the number of iteration equals the specified value.

The second inversion is followed. Its forward model is implemented by formula 3.2. I call it inversion-2. The technique for the inversion-2 is same as the first inversion, only the elements of the parameter vector are changed.

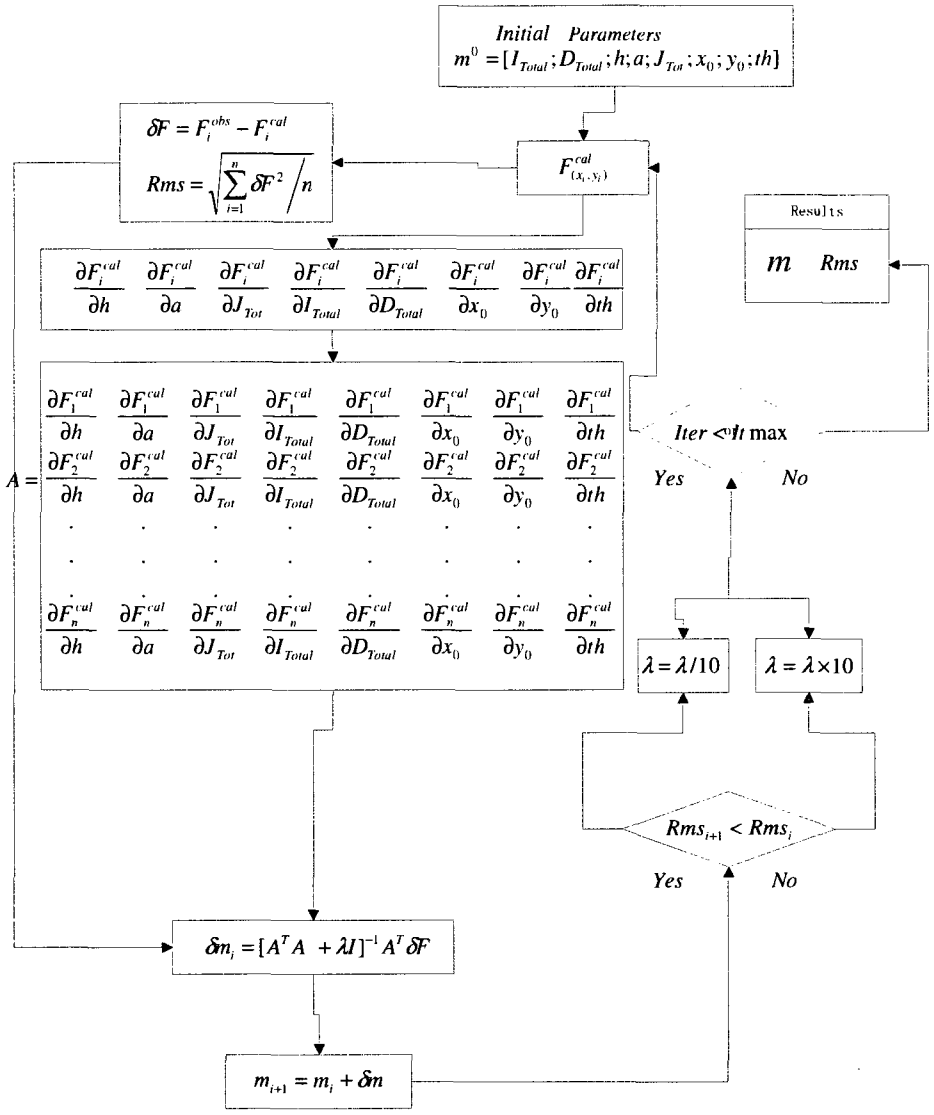

Flow Diagram 4.1: flow diagram for magnetic field inversion without remanent magnetization of the Levenberg- Maquardt (Inversion-1)

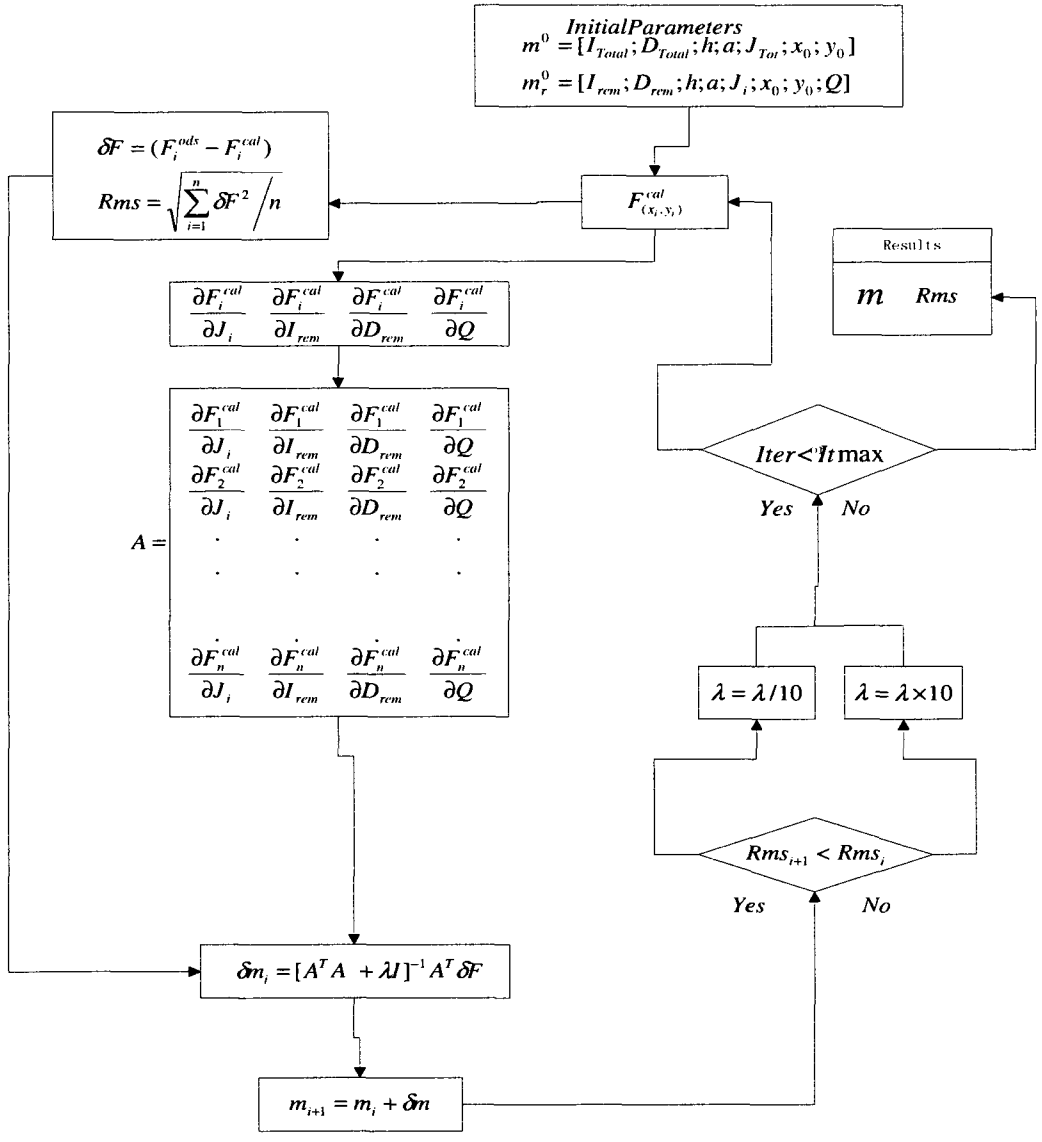

Flow Diagram 4.2: flow diagram for magnetic field inversion with remanent magnetization using Maquardt-Levenberg (Inversion-2)

4.6 The convergence

The convergence of successive iterations is monitored by the following root-mean-squares (rms) error criterion:

$$rms = \sqrt{\sum_{i=1}^{N} \varepsilon_i^2 / N}$$

where, N is the number of the data observations. The iteration procedure is terminated when the rms is smaller than the required value or when the number of iterations reached.

4.7 Tests for the magnetic inversion

The tests include two parts, the first part is tests for the magnetic inversion in absence of remanent magnetization and the second part is tests for the magnetic inversion in presence of remanent magnetization.

4.7.1 Tests for the magnetic inversion in absence of remanent magnetization

The tests for the magnetic inversion in absence of remanent magnetization include two sections; first section is the validation with models for the magnetic inversion in absence of remanent magnetization. In this section, the method of calculation of the initial values of Chemam (2006) is used to derive the initial values to start the inversion. Generally speaking, the initial values of Chemam are close to the solutions, so the second section, the robustness of the magnetic inversion in absence of remanent magnetization to initial values, is added to figure out the results of the inversion with initial values further from the solutions.

4.7.1.1 The validation with models for the magnetic inversion in absence of remanent magnetization

Here I give some results of some tests using the synthetic data generated by Potent, a modeling program of Geophysical Software Solution (G.S.S) in Australia. In the next figures the values for each parameter of the model are listed at left side, the results are listed at right side; in the parenthesis are the initial values. I used the grid dimension of $750 \times 750m$, $1000 \times 1000m$, $1500 \times 1500m$. The cell size is $25 \times 25m$. And

I changed the values for each parameter to estimate the change relative to the change in the parameter.

I tested several models to estimate the tendency of the changes of the results of the inversion; here I select a few examples to illustrate the results of the inversion. Three examples are selected; they are listed in the table 4.1. In. is the abbreviation of the inclination of the earth magnetic field, De. is the abbreviation of the declination of the earth magnetic field, Dep. is the abbreviation of the depth of the cylinder, Dia. is the abbreviation of the diameter of the cylinder, Th. is the abbreviation of thickness of the cylinder, MSu. is the abbreviation of magnetic susceptibility. For the model Defang2, Defang5, the earth field is 55278nT, for the model Atestm1, the earth field is 57170nT.

Table 4.1 Results of the tests with models without remanent magnetization

N.	Type	Dep. (m)	Dia. (m)	In. (°)	De. (°)	Th. (m)	MSu.(SI)
Defang 2	Model	50	160	69	12	200	0.01
	Initials	50	157	66	12	200	0.00900
	Results	50	160	69	12	200	0.01001
Defang 5	Model	50	160	30	12	200	0.01
	Initials	48	157	31	13	202	0.00860
	Results	50	160	30	12	202	0.00989
Atestm 1	Model	100	160	74	-12	300	0.01
	Initials	96	157	71	-11	304	0.00851
	Results	99	161	74	-12	304	0.00978

The inclination and declination are taken parts in the inversion; the reason is that we need to know these values when there is remanent magnetization. The model Defang2 is used to test the model with high inclination, the model Defang5 is used to test the validation of the algorithm used to the model with low inclination. Changing of the declination is not giving the big vibration of the results of the inversion. The model Atestm1 is for testing the deeper source.

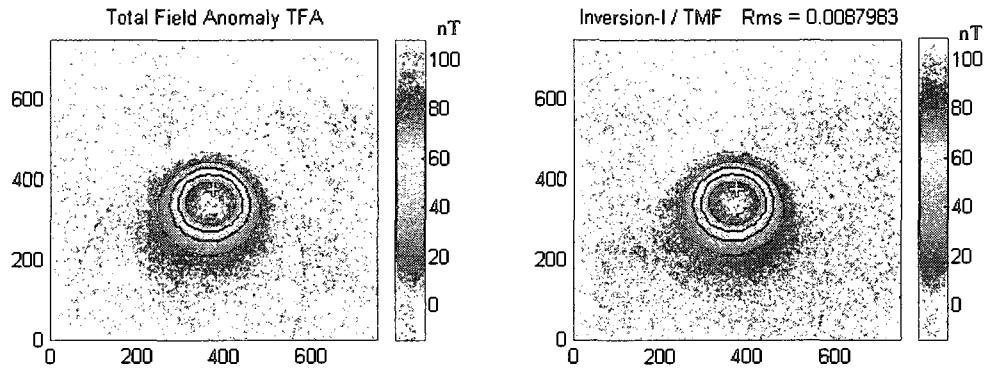

3D Model Defang2 :

- Depth = 50m
- Diameter = 160m
- Incl. $_{ter}$ = 69^0
- Decl. $_{ter}$ = 12^0
- Magnetic Suscept.= 0.01 SI
- Coord. of centre: (375, 375)
- Depth Extension = 200m

Results of Inversion :

- Depth = 50(50)m
- Diameter = 160(157)m
- Incl. $_{tot}$ = $69^0(66^0)$
- Decl. $_{tot}$ = $12^0(12^0)$
- Magnetic Suscept.= 0.010011 SI
- Coord. of centre: (375, 375)
- Depth Extension = 200(200)m

Fig.4.2 Model Defang2: Geomagnetic field intensity: 55278nT , inclination of geomagnetic field : 69^0 , declination of geomagnetic field : 12^0 , depth of the cylinder:50m, diameter of the model : 160, height: 200m, magnetic susceptibility:0.01 SI.

On the image, the left column is the model; the right column is results of the inversion, in the parentheses are the initial values for the inversion. The approaches to obtain the initial values are given by Chemam (2006). They are listed in the parenthesis. Here the inclination and declination of the earth field are inverted because we do not know if there is the remanent magnetization in the magnetic data, if there is remanent magnetization we do not know the inclination and declination.

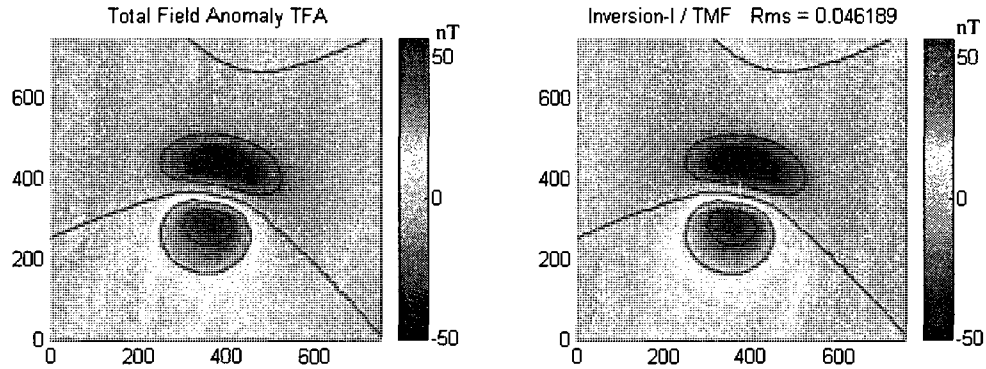

3D Model Defang5 :

- Depth = 50m
- Diameter = 160m
- Incl. $_{ter}$ = 30^0
- Decl. $_{ter}$ = 12^0
- Magnetic Suscept.= 0.01 SI
- Coord. of centre: (375, 375)
- Depth Extension = 200m

Results of Inversion :

- Depth = 50(48)m
- Diameter = 160(157)m
- Incl. $_{tot}$ = $30^0(31^0)$
- Decl. $_{tot}$ = $12^0(13^0)$
- Magnetic Suscept.= 0.0098978 SI
- Coord. of centre: (375, 375)
- Depth Extension = 202(202)m

Fig.4.3 Model Defang5: Geomagnetic field intensity: 55278nT , inclination of geomagnetic field : 30^0 , declination of geomagnetic field : 12^0 , depth of the cylinder:50m, diameter of the model : 160, height: 200m,magnetic susceptibility:0.01 SI.

Comparing Fig.4.2 and Fig.4.3, the inclination of geomagnetic field changes from 69^0 to 30^0, the results are stable. That means, no matter the inclination is higher, or is lower; the results of magnetic inversion are stable.

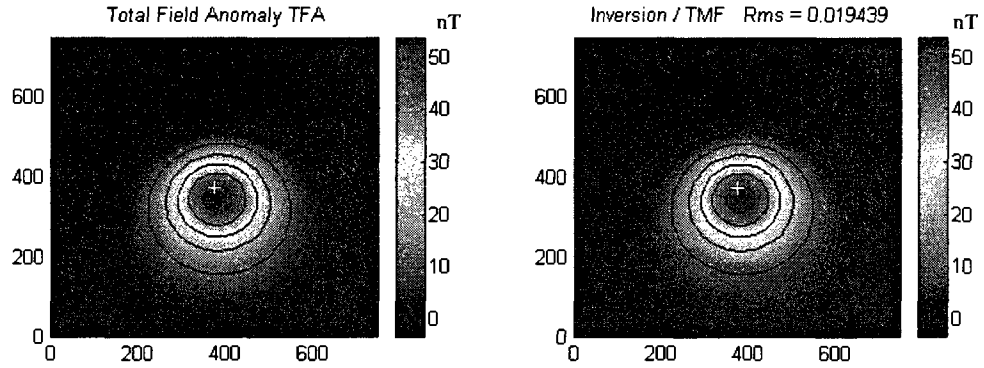

3D Model Atestm1 :

- Depth = 100m
- Diameter = 160m
- Incl. $_{ter}$ = 74^0
- Decl. $_{ter}$ = -12^0
- Magnetic Suscept.= 0.01 SI
- Coord. of centre: (375, 375)
- Depth Extension = 300m

Results of Inversion :

- Depth = 100 (96)m
- Diameter = 161(157)m
- Incl. $_{tot}$ = $74^0(71^0)$
- Decl. $_{tot}$ = $-12^0(-11^0)$
- Magnetic Suscept.= 0.009782 SI
- Coord. of centre: (375, 375)
- Depth Extension = 302(304)m

Fig.4.4 Model Atestm1: Geomagnetic field intensity: 57170nT , inclination of geomagnetic field : 74^0 , declination of geomagnetic field : -12^0 , depth of the cylinder:100m, diameter of the model : 160,height: 300m,magnetic susceptibility:0.01 SI.

Comparing Fig.4.3 and Fig.4.4, the declination of the model changes from 12^0 to -12^0, and the depth and diameter of the model are changed; the results of the inversion are stable.

4.7.1.2 Robustness of the magnetic inversion in absence of remanent magnetization to initial values

The accuracy and the stability of the inversion are related with the initials values. The closer, the initial values and the parameters of the model are, the more accurate, the results of the inversion are. If the differences between the initial values and the parameters of the model are bigger, the results of the inversion are supposed to be in

error. In this inversion algorithm, the methods of calculation of the initials are given by Chemam (2006). Generally speaking, the differences between the initial values calculated by Chemam's method and the parameters of the model are close to the solutions. Even though, I now test the robustness of the calculation to the initials to the parameters, such as depth, diameter, inclination, declination, and depth extension, I take the model Defang2 as an example, and the results of the tests are illustrated in the table below:

Table 4.2 Results of tests of sensibilities to the initial values without remanent magnetization

NI.	Initials of Parameters					Results of Inversions				
	Dep.	Dia.	In.	De.	Th.	Dep.	Dia.	In.	De.	Th.
Model	50	160	69	12	200					
IC	50	157	66	12	200	50	160	69	12	200
I 1	40	157	66	12	200	50	160	69	12	200
I 2	60	157	66	12	200	50	160	69	12	200
I 3	50	140	66	12	200	50	160	69	12	200
I 4	50	180	66	12	200	50	160	69	12	200
I 5	50	157	50	12	200	50	160	69	12	200
I 6	50	157	80	12	200	50	161	69	12	201
I 7	50	157	66	8	201	50	161	69	12	201
I 8	50	157	66	28	201	50	161	69	12	201
I 9	50	157	66	12	150	50	160	69	12	200
I 10	50	157	66	12	250	50	160	69	12	200

For the model Defang2: the depth is 50m, the diameter is 160m, the inclination 69°, the declination is 12° and the depth extent is 200. IC is the abbreviation for the initials values calculated. I1 is for the change of depth to 40m, 10m less than that calculated; I2 is for the change of depth to 60m, 10m more than that calculated; I3 is for the change of diameter to 140m, 17m less than that calculated; I4 is for the change of diameter to 180m, 23m more than that calculated; I5 is for the change of inclination to 50°, 16° less than that calculated; I6 is for the change of inclination to 80°, 14° more than that calculated; I7 is for the change of declination to 8°, 4° less than that

calculated; I8 is for the change of declination to 28°, 16° more than that calculated; I9 is for the change of depth extent to 150m, 50m less than that calculated; I10 is for the change of depth extent to 250m, 50m more than that calculated. In table 4.2, the results of the tests of the robustness to the initial values are illustrated. From I1 to I5, there are not any changes of the results with the changes of the initial values, I8 and I9; we have a little changed about diameters and depth extension, I9 and I10 no changes. It can be seen that the robustness of the algorithm of the magnetic field inversion in absence of remanent magnetization to initial values is good.

4.7.2 Tests for the magnetic inversion in presence of remanent magnetization

4.7.2.1 The validation with models for the magnetic inversion in presence of remanent magnetization

The examples below are for the inversion with remanent magnetization. Five models were tested. First of all, Vjina111t6 was tested for a low inclination of the remanent magnetization; secondly, the model AteR1 was tested for a high inclination of the remanent magnetization, thirdly, the model Vjina111t215n1 was tested for negative remanent magnetization, fourthly, the model Vjina111t21116 was tested for bigger depth of the cylinder, the bigger diameter of the cylinder and the bigger depth extension, at last, a special model was tested, the depth of this model is 150m, it is very deeper, its diameter is not bigger, and its depth extension is not bigger. The models and the results of the inversion are given in the table 4.3. The model of right vertical cylinder with oval cross-section is also tested and listed in table 4.3. After that, the model with the addition of noise was tested to estimate the robustness of the inversion in the presence of noise.

In the parenthesis are the parameters of the model on the image. The initial values calculated are listed.

Table 4.3 Results of the tests with models with remanent magnetization
T_0=57170nT, $I_0 = 74^0$ $D_0 = -12$

N.	Type	Dep. (m)	Dia. (m)	Inr. (°)	Der. (°)	Th. (m)	MSu.(SI)
Vjina111t6	Model	60	160	1	30	300	0.01
	Initials	58	158	6	32	302	0.00985
	Results	60	160	1	30	300	0.00989
AteR1	Model	60	200	70	-30	300	0.01
	Initials	57	196	74	-32	303	0.00990
	Results	60	200	70	-28	301	0.00988
Vjina111t215n1	Model	80	200	250	-30	300	0.01
	Initials	77	195	254	-37	303	0.01000
	Results	80	200	250	-30	299	0.01005
Vjina111t21116	Model	80	300	210	30	600	0.01
	Initials	82	304	205	37	598	0.00979
	Results	80	300	210	30	600	0.00989
Geomtest3	Model	150	160	65	-15	200	0.01
	Initials	127	166	63	-18	253	0.00337
	Results	141	174	65	-15	230	0.00717
Babneq (oval section)	Model	60	160/120	30	30	300	0.01
	Initials	61	133	37	45	299	0.00965
	Results	61	133	29	28	377	0.010

The Dep. is abbreviation of depth, Dia. is abbreviation of diameter. Inr. is abbreviation of inclination of remanent magnetization. Der. is abbreviation of declination of remanent magnetization. Th. is thickness of the cylinder. For the model Babneq, its cross-section is oval, it long axis is 160m while it short axis is 120m. The images for each model are illustrated below:

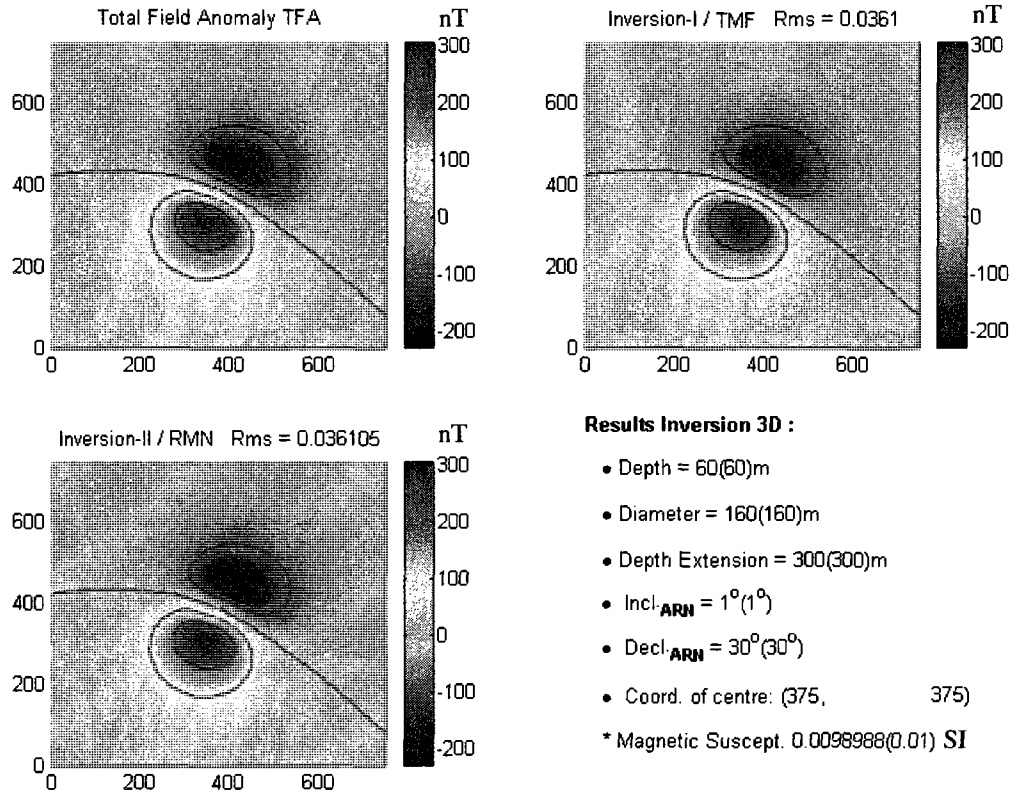

Fig.4.5 Model Vjina111t6: Geomagnetic field intensity: 57170nT , inclination of geomagnetic field : 74^0, declination of geomagnetic field : -12^0, depth of the cylinder: 60m, diameter of the model : 160, height: 300m, magnetic susceptibility: 0.01 SI. Inclination of remanent magnetization: 1^0, declination of the remanent magnetization: 30^0, position of the center of the cylinder: (375,375), konigsberger ratio parameter Q: 5

Initial Parameters of Model Vjina111t6 :

- Depth = 58m
- Diameter = 158m
- Depth Extension = 302m
- $Incl._{ARN} = 6^0$
- $Decl._{ARN} = 32^0$
- Coord. of centre: (375, 375)

* Magnetic Suscept. 0.009854 SI

In this model, the parameters of model are shown in parentheses, and the initial values are derived above, the results of the inversion are very precise.

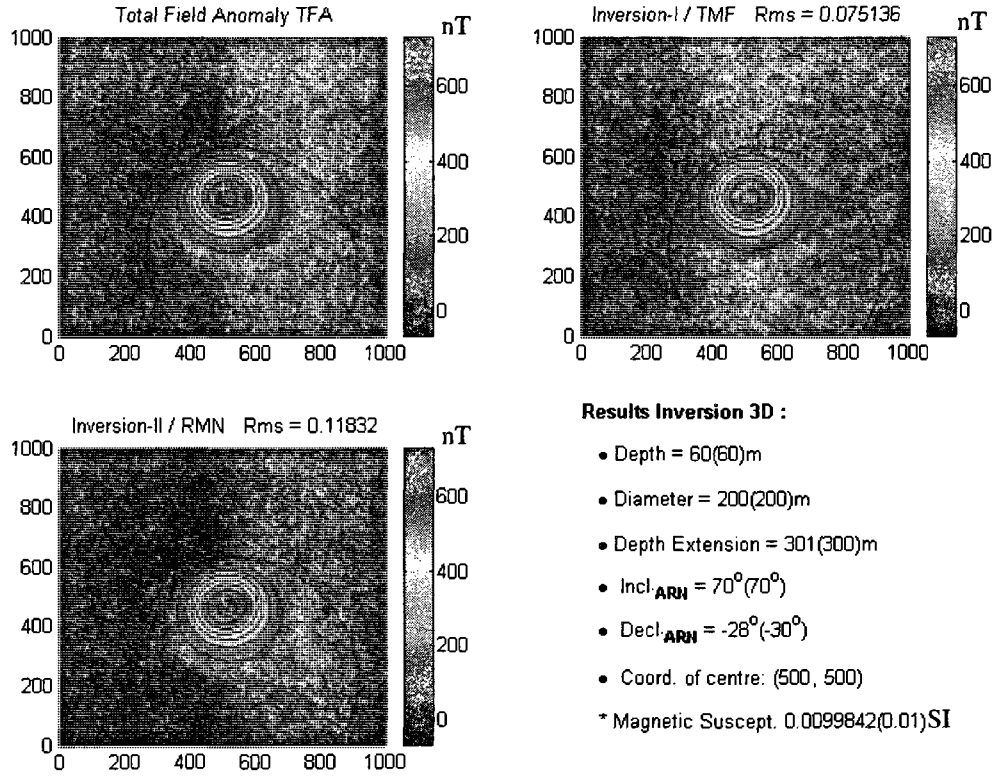

Fig.4.6 Model AteR1: Geomagnetic field intensity: 57170nT , inclination of geomagnetic field : 74^0 , declination of geomagnetic field : -12^0 , depth of the cylinder:60m, diameter of the model : 200, height: 300m, magnetic susceptibility:0.01 SI. Inclination of remanent magnetization: 70^0 , declination of the remanent magnetization: -30^0 , position of the center of the cylinder: (500,500) , konigsberger ratio parameter Q:5

Initial Parameters of Model AteR1 :

- Depth = 57m
- Diameter = 196m
- Depth Extension = 303m
- $Incl\cdot_{ARN} = 74^0$
- $Decl\cdot_{ARN} = -32^0$
- Coord. of centre: (500, 500)

* Magnetic Suscept. 0.0099744 SI

Comparing Fig.4.5 and Fig.4.6, the declination changes from 30^0 to -30^0 , the inclination changes from 1^0 to 70^0 and the diameter changes from 160m to 200m, the results are stable.

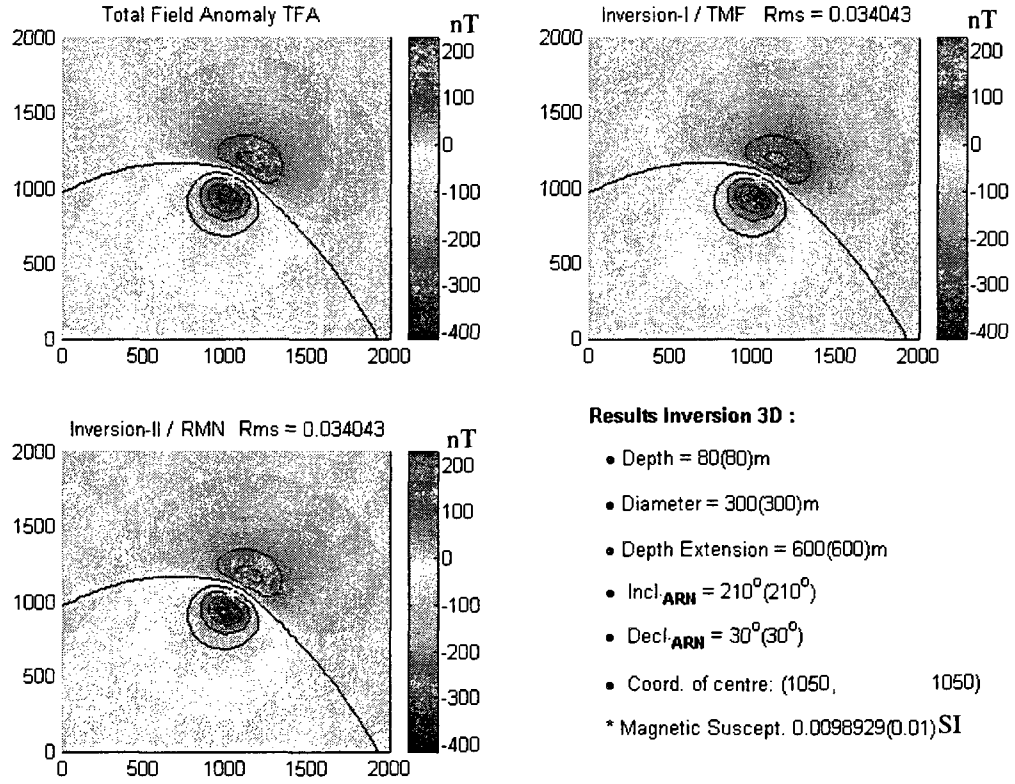

Fig.4.7 Model Vjina111t21116: Geomagnetic field intensity: 57170nT , inclination of geomagnetic field : 74^0 , declination of geomagnetic field : -12^0 , depth of the cylinder:80m, diameter of the model : 300, height: 600m, magnetic susceptibility:0.01 SI. Inclination of remanent magnetization: 210^0, declination of the remanent magnetization: 30^0, position of the center of the cylinder: (1050,1050), konigsberger ratio parameter Q:5

Initial Parameters of Model Vjina111t21116 :

- Depth = 82m
- Diameter = 304m
- Depth Extension = 598m
- Incl·$_{ARN}$ = 205°
- Decl·$_{ARN}$ = 37°
- Coord. of centre: (1050, 1050)

* Magnetic Suscept. 0.0097978 SI

Comparing the Fig 4.6 and the Fig 4.7, the depth is increased from 60m to 80m, the diameter is increased from 200m to 300m, the thickness of the cylinder is increased from 300m to 600m, and the remanent magnetization is negative, the grid

dimension is increased from 1000m to 2000m, the results of the inversion are stable and precise.

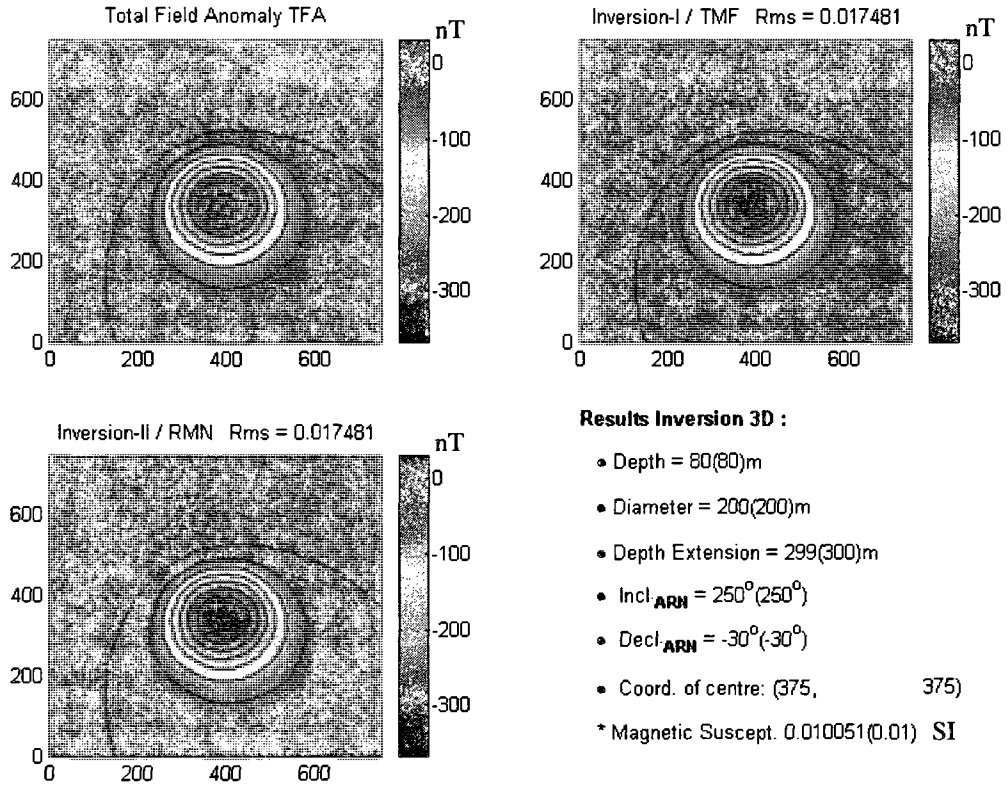

Fig.4.8 Model Vjina111t215n1: Geomagnetic field intensity: 57170nT , inclination of geomagnetic field : 74^0 , declination of geomagnetic field : -12^0 , depth of the cylinder:80m, diameter of the model : 200, height: 300m, magnetic susceptibility:0.01 SI. Inclination of remanent magnetization: 250^0, declination of the remanent magnetization: -30^0, position of the center of the cylinder: (375,375), konigsberger ratio parameter Q:5

Initial Parameters of Model Vjina111t215n1 :

- Depth = 77m
- Diameter = 195m
- Depth Extension = 303m
- $Incl._{ARN} = 254^o$
- $Decl._{ARN} = -37^o$
- Coord. of centre: (375, 375)

* Magnetic Suscept. 0.010014 SI

Fig 4.8 show the case of a negative remanent magnetization, generally, the inclination of the remanent magnetization in Canada is about $60^0 - 70^0$, and the direction of this model is antiparallel direction. The results of inversion are stable and precise too.

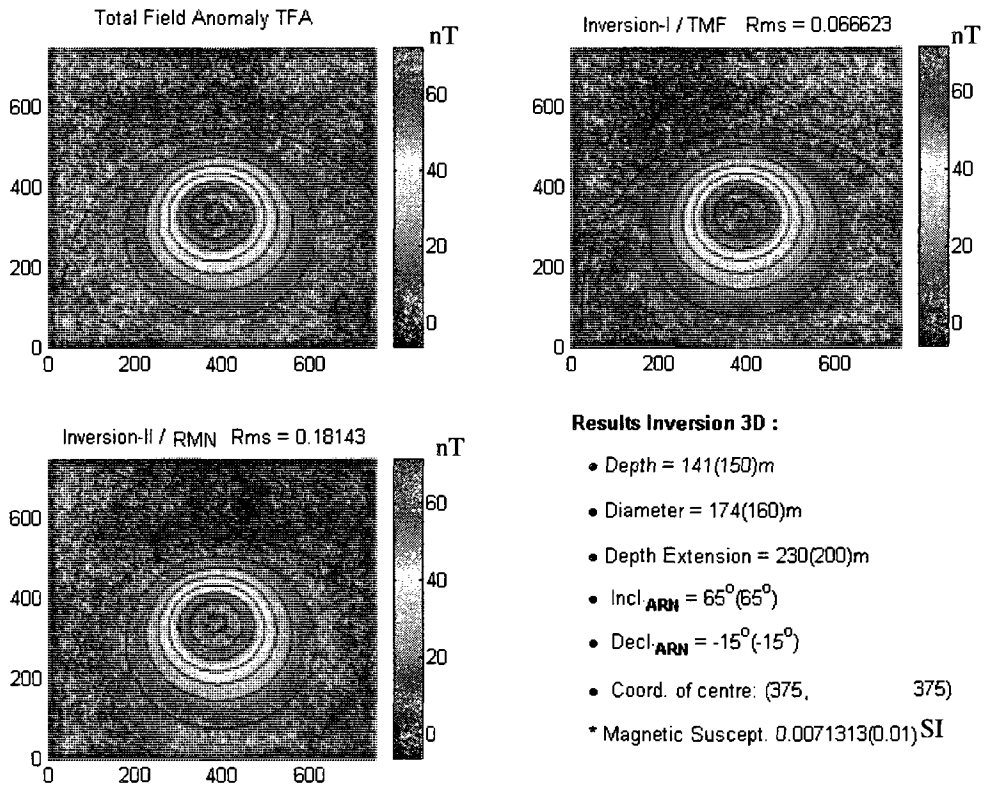

Fig.4.9 Model Geomtest3: Geomagnetic field intensity: 57170nT , inclination of geomagnetic field : 74^0, declination of geomagnetic field : -12^0, depth of the cylinder:150m, diameter of the model : 160, height: 200m,magnetic susceptibility:0.01 SI. Inclination of remanent magnetization: 65^0 , declination of the remanent magnetization: -15^0, position of the center of the cylinder: (375,375), konigsberger ratio parameter Q:2

Initial Parameters of Model Geomtest3 :

- Depth = 127m
- Diameter = 166m
- Depth Extension = 253m
- $Incl._{ARN} = 63^{o}$
- $Decl._{ARN} = -18^{o}$
- Coord. of centre: (375, 375)

* Magnetic Suscept. 0.0033711SI

With the increase of the depth of the cylinder, the result of the depth and the diameter are getting biased from the real values.

4.7.2.2 The robustness of the magnetic inversion in presence of remanent magnetization to initial values

For the sensibilities tests with initial values for magnetic inversion with remanent magnetization, I selected the model Vjina111t6 (Model1) and Vjina111t3 (Model2) to figure out the results of the inversion with the changes of parameters (Table 4.4).

Table 4.4 Results of tests of sensibilities with initials values with remanent magnetization

NI.	Parameters					Inversions Results				
	Dep.	Dia.	Inr.	Der.	Th.	Dep.	Dia.	Inr.	Der.	Th.
Model	60	160	1	30	300					
IC	58	158	6	32	302	60	160	1	30	300
I 1	50	158	6	32	310	60	160	1	30	300
I 2	70	158	6	32	290	60	160	1	30	300
I 3	58	151	6	32	302	60	160	1	30	300
I 4	58	170	6	32	302	60	160	1	30	300
I 5	58	158	12	32	302	60	160	1	30	300
I 6	58	158	-12	32	302	60	160	0	30	300
I 7	58	158	6	20	302	60	160	1	30	300
I 8	58	158	6	40	302	60	160	1	30	300
I 9	58	158	6	32	250	60	160	1	30	300
I 10	58	158	6	32	350	60	160	1	30	300
Model2	60	160	30	30	300					
IC1	59	158	32	32	301	60	160	30	30	300
I11	80	158	32	32	301	63	156	30	30	279
I12	59	158	80	32	301	60	160	26	32	300
I11a	30	80	15	15	150	68	196	26	30	155
I12a	120	320	60	60	600	34	119	30	33	600

IC is the test where the initial values are calculated by chemam's technique. for test I1 of model1, the initial value of depth is changed to 50m; for test I2, the initial value is increased to 70m; for test I3, the initial value of diameter is decreased to 151m; for test I4, the initial value of diameter is increased to 170m; for test I5, the initial value of inclination is 12°; for test I6, the initial value of inclination is -12°; for test I7, the initial value of declination is 20°; for test I8, the initial value of declination is changed to 40°; for test I9, the initial value of thickness of cylinder is decreased to 250m; for test I10, the initial value of thickness of cylinder is increased to 350m. IC1 is the test of the model2 where the initial values are calculated by chemam's technique. I11 is the test where the initial value of depth is 80m (increase of 20m); I12 is the test where the initial value of inclination is 80° (increase of 50°); I11a is a test where all of the parameters are decreased to 50%; I12a is a test where all of the parameters are increased to 200%. From the results of the testing, we see that when the initial values are changed closely to the true values, the results are stable. When the initial values are far from the true values, the results are less accurate. When all of the initial values are far from the true values, the results of the inversion are more inaccurate.

4.7.3 Tests for addition of noise

In this section, I will test the robustness of magnetic field inversion with the method Levenberg-Marquardt; the models to be tested are illustrated in the table 4.5 below:

Table 4.5 Model of the inversion with remanent magnetization with addition of noise
T_0=57170nT, $I_0 = 74^0, D_0 = -12$

Addition of random noise: 2nT/5nT

N^0	Inr.	Der.	Dep. (m)	Dia. (m)	Th. (m)	MSu. (SI)
Vjina111t3	30^0	30^0	60	160	300	0.01

Table 4.6 Results of the inversion with remanent magnetization with addition of noise (2nT)

N^0	Inr.	Der.	Dep. (m)	Dia. (m)	Th. (m)	MSu. (SI)
Vjina111t3	30^0	30^0	60	160	300	0.0099
Vjina111t3 (2nT)	30^0	30^0	62	159	288	0.01
Vjina111t3 (5nT)	28^0	31^0	77	145	352	0.01678

The results show that the noise affects the precision of the inversion, and the stability of the inversion is also affected by the addition of noise. The depth of the cylinder of the model is 60m, see to figure 4.10, while the result for it is 62m, see to figure 4.11; the diameter of the cylinder of the model is 160m while the result for it is 159, though the error is relatively small. When the noise is added to 5nT, the results of magnetic inversion are less accurate, especially for the geometry. I added the noise to 10nT, the results of direction of magnetization are less affected, and the results of magnetic inversion in related to the geometry are more affected.

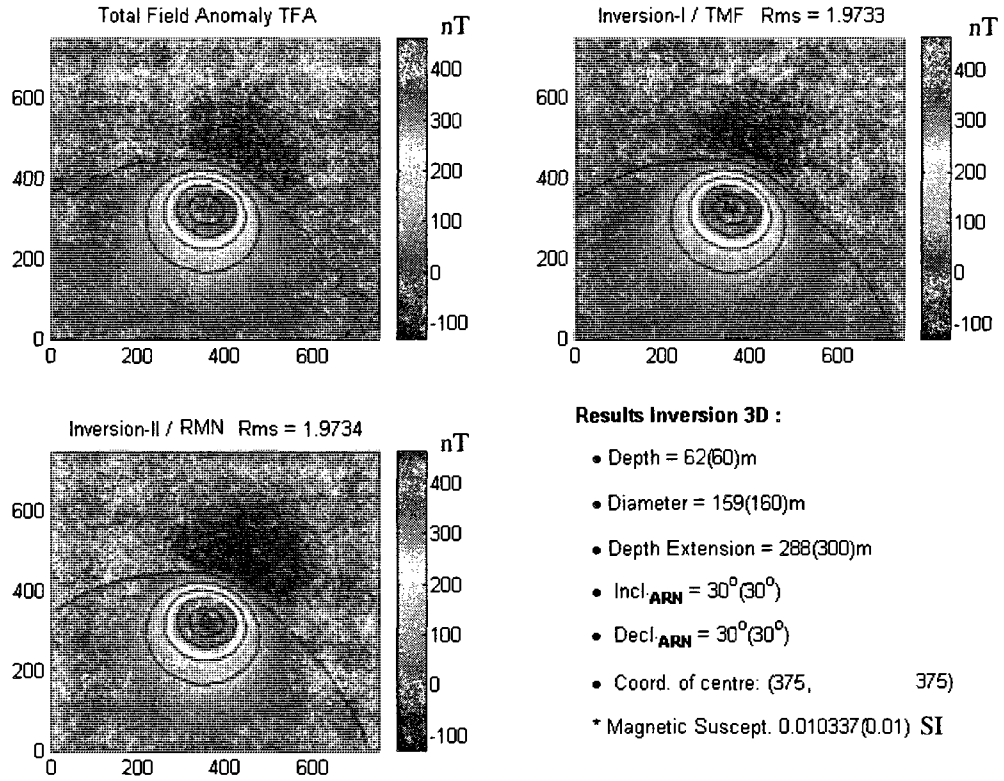

Fig.4.10.1 Model Vjina111t3: Geomagnetic field intensity: 57170nT , inclination of geomagnetic field : 74^0 , declination of geomagnetic field : -12^0 , depth of the cylinder:60m, diameter of the model : 160, height: 300m, magnetic susceptibility:0.01 SI. Inclination of remanent magnetization: 30^0 , declination of the remanent magnetization: 30^0 , position of the center of the cylinder: (375,375) , konigsberger ratio parameter Q:5 addition of random noise: 2nT

Initial Parameters of Model Vjina111t3 With 2nT Noise :

- Depth = 40m
- Diameter = 156m
- Depth Extension = 340m
- $Incl._{ARN} = 32^0$
- $Decl._{ARN} = 32^0$
- Coord. of centre: (375 375)

* Magnetic Suscept. 0.0096509 SI

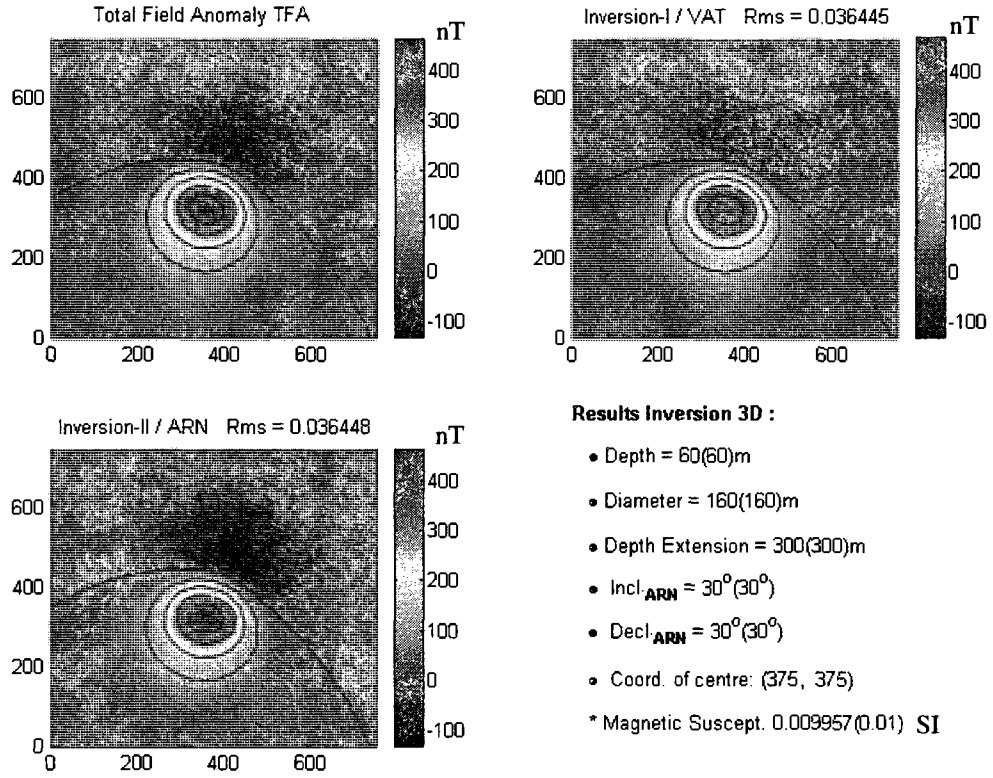

Fig.4.11.2 Model Vjina111t3, no addition of noise

Initial Parameters of Model Vjina111t3 :

- Depth = 59m
- Diameter = 158m
- Depth Extension = 321m
- $Incl._{ARN} = 32^{o}$
- $Decl._{ARN} = 32^{o}$
- Coord. of centre: (375, 375)

* Magnetic Suscept. 0.0099472 SI

4.8 Discussion and conclusions

4.8.1 Discussion

Several models have been tested to validate the algorithm. For the models without remanent magnetization, the tested models are Defang2 for high inclination of the induced magnetization, the model Defang5 for a low inclination, and model Atestm1

for a deeper magnetic body. The results of the inversion are precise and they are not change with the changes of the initial values within a given range. For the models with remanent magnetization, the tested models are Vjina111t6, AteR1, Vjina111t215n1, Vjina111t21116, and Geomtest3. From the table 4.3 and figure 4.5-figure4.9, we see that the results for models Vjina111t6 for a low inclination of remanent magnetization, Vjina111t215n1 for a negative remanent magnetization, Vjina111t21116 for a deeper body with bigger diameter are very precise except the model AteR1 for a high inclination of the remanent magnetization, that is not so precise, the result of the declination of the remanent magnetization is -28°, the model is -30°.

The model of right vertical cylinder with oval cross-section, Babneq was tested. The depth of the model is 60m, the long axis of oval cross-section is 160m, the short axis of oval cross-section is 120m, and the depth extension is 300m. The direction of the remanent magnetization is 30° inclination and declination. The magnetic susceptibility is 0.01SI. And the position of cylinder is (375m, 375m). The results of the magnetic inversion are close the true values.

The sensibility of the algorithm to the changes of the initial values was tested for the model with remanent magnetization. The results are not changed with the changes of the initial values, but when the initial values are changed a lot, the results of the inversion are erroneous. For example, in the table 4.4, the model Vjina111t3, I11, the initial value of the depth is 80m (60m of the model); the result of the inversion of depth is 63m, 3m more than the depth of the model (60m), the result of the inversion of diameter is 156m, 4m less than that of the model (160m). For I12, the initial value of the inclination of remanent magnetization is 80° (30° of the model); the result of the inversion of inclination is 26°, 4° less than that of the model, the results of the declination of the remanent magnetization is 32°, 2° more than that of the model.

Especially for the tests where all of the parameters are changed far away from the true values, the results of magnetic inversion are affected a lot.

The results of the inversion in presence of the noise are evaluated by the addition of noise. They are listed in the table 4.6. From this, we could see that the addition of the noise affects the results of the inversion in contrast to that of the inversion without addition of the noise, especially for the results related to the geometry.

With the increase of the depth of the cylinder, the results of the inversion are biased, such as the model Geomtest3, the depth of the model is 150m, the diameter of the model is 160m, the result of the depth is 141m, and the result of the diameter is 174m.

4.8.2 Conclusions

From these results, we conclude that, in most of the cases, whether the inversion is with or without remanent magnetization, the stability and the precision of the results are better. But the problem has not yet solved totally. Sometimes, the results of the magnetic inversion are not stable; as for the precision of the results of the magnetic inversion, it is not perfect. For example, if the depth of the target is too deep, the results of the inversion are not precise enough. The noise affects the results of the inversion, and for the inversion of remanent magnetization, the results are in error with higher inclination of the remanent magnetization. The results of the inversion are affected by the initial values, if the initial values are too far from the true solution; the results of the inversion are also not accurate.

Chapter 5 Inversion of the analytic signal

5.1 Introduction of the analytic signal

In the preceding chapter, the magnetic field inversion has been implemented and tested successfully; the precision and stability of the inversion is improved. But we still have a few problems to be resolved. Firstly, for the remanent inversion, a high inclination of the remanent magnetization causes erroneous results. Secondly, the initial values affect the results of the inversion. Thirdly, the noise affects the results of the inversion. I now develop the inversion of the analytic signal, which is expected to improve the results further.

The 3D analytic signal is also called the amplitude of the total gradient. The amplitude of the total gradient is formulated as follows:

$$g = \|\nabla F\| = \sqrt{(\partial F/\partial x)^2 + (\partial F/\partial y)^2 + (\partial F/\partial z)^2} \quad (5.1)$$

where F is total magnetic field anomaly, g is the analytic signal (the amplitude of total gradient). The analytic signal was introduced by Nabighian (1974) who showed how it can be used to determine the depth to the top and the horizontal position of thin, elongated bodies. This concept was extended to 3D by Nabighian (1984). Roest et al. (1992) used 3D analytic signal to outline magnetic sources and to estimate depth using a simple amplitude half width rule. Hsu et al. (1996) used the nth-order enhanced analytic signal to outline the boundaries of contacts and faults and to estimate the depth. To identify anomalies that could be caused by kimberlite pipes, Keating and Sailhac (2004) proposed a simple pattern recognition technique, based on a first-order regression over a moving window, between the analytic signal of the observed magnetic field and the theoretical analytic signal of a magnetic vertical cylinder to identify potential targets. The standard error between the estimated values of the analytic signal and the values of the analytic signal of the observed magnetic field within the moving window is calculated, as is the correlation coefficient between the analytic signal within the moving window and the analytic signal of the model.

Results where the correlation coefficient between the analytic signal and the theoretical analytic signal within a moving window are above a certain threshold are retained.

The advantage to use the absolute value of analytic signal is that its shape over linear structures is almost independent of the earth's magnetic field parameters and of the direction of magnetization of the anomaly source. Therefore, the use of the magnitude of the analytic signal allows the determination of source characteristics without making any assumptions on the direction of source body magnetization. This can be very important, especially in areas where the contribution of remanent magnetization to the observed anomalies is not known (Roest et al., 1992). Xiong (2006) noted that in three dimensions, the analytic signal depends on the direction of the inducing field, the direction of the remanent magnetization, the dipping angle of the source body and the depths to the top and bottom of the source body. Nevertheless, the shape of the analytic signal is still nearly independent of the direction of magnetization and of the earth's field direction. Agarwal and Shaw (1996) calculate the analytic signal of a single magnetic pole anomaly and conclude that, in general, the analytic signal is not symmetric for arbitrary values of inclinations and declinations. A circular symmetry is observed for a field inclination of 90°, and at an inclination of 0° the anomaly is symmetric along the axis of the declination (Keating & Saihac, 2004).

In chapter 3, I calculated the analytic signal produced by the anomaly due to a vertical circular cylinder with arbitrary polarization; the results show that, in most cases, the shape of the analytic signal is symmetric. When the total inclination is higher than 60°, it is circular symmetric, when the total inclination is smaller, it is symmetric along the axis of the total declination. So when the total inclination is higher, it is nearly independent of the total inclination and total declination, including remanent magnetization and inducing field. Even if the total inclination is smaller, its change from the change of the inclination and declination is smaller than that of the

magnetic field. In contrast to the magnetic field, the analytic signal has a weak dependence of inducing magnetization and remanent magnetization. This is the reason why many geophysicists used it to magnetic interpretation.

5.2 Forward modeling

In the analytic signal inversion, two forward models are used: the first one is a semi-infinite vertical cylinder and the second one a finite-extent vertical cylinder. For the first model, I will use $g = \|\nabla f(x, y, h, a, J_{tot}, I_m, D_m, x_0, y_0)\|$, which I call Method-1.

For the second model, suppose:

$$F_1 = f(x, y, h, a, J_{tot}, I_m, D_m, x_0, y_0) \quad (5.2)$$

$$F_2 = f(x, y, h + th, J_{tot}, I_m, D_m, x_0, y_0) \quad (5.3)$$

and:

$$g = \|\nabla(F_1 - F_2)\| \quad (5.4)$$

here, thickness of the cylinder is a variable in the inversion; I call it Method-2

For the inversion with remanent magnetization, Method-1:

$$g_r = \|\nabla f(x, y, h, a, J_i, I_{rem}, D_{rem}, x_0, y_0)\| \quad (5.5)$$

for the inversion with remanent magnetization Method-2:

$$F_{r1} = f(x, y, h, a, J_i, I_{rem}, D_{rem}, x_0, y_0) \quad (5.6)$$

$$F_{r2} = f(x, y, h + th, a, J_i, I_{rem}, D_{rem}, x_0, y_0) \quad (5.7)$$

$$g_r = \|\nabla(F_{r1} - F_{r2})\| \quad (5.8)$$

5.3 Method of inversion

The method used is still Levenberg-Marquardt method, presented in the previous chapter.

5.3.1 Jacobian matrix

Here, there is a very important problem that is the calculation of Jacobian Matrix needed for the inversion of the analytic signal data. In the inversion of magnetic field, we got

$\frac{\partial F}{\partial h}, \frac{\partial F}{\partial a}, \frac{\partial F}{\partial J_{tot}}, \frac{\partial F}{\partial I_m}, \frac{\partial F}{\partial D_m}, \frac{\partial F}{\partial x_0}, \frac{\partial F}{\partial y_0}$ for inversion without remanent magnetization, and $\frac{\partial F}{\partial J_i}, \frac{\partial F}{\partial I_{rem}}, \frac{\partial F}{\partial D_{rem}}, \frac{\partial F}{\partial Q}$, for inversion with remanent magnetization. J_i is intensity of inductive magnetization, I_{rem} is the inclination of the remanent magnetization, D_{rem} is the declination of the remanent magnetization, Q is the Koenigsberger ration. Here, we need to derive $\frac{\partial g}{\partial h}, \frac{\partial g}{\partial a}, \frac{\partial g}{\partial J_{tot}}, \frac{\partial g}{\partial I_m}, \frac{\partial g}{\partial D_m}, \frac{\partial g}{\partial x_0}, \frac{\partial g}{\partial y_0}$ for inversion without remanent magnetization, and $\frac{\partial g}{\partial J_i}, \frac{\partial g}{\partial I_{rem}}, \frac{\partial g}{\partial D_{rem}}, \frac{\partial g}{\partial Q}$, for inversion with remanent magnetization, where $g = \|\nabla F\| = \sqrt{(\partial F/\partial x)^2 + (\partial F/\partial y)^2 + (\partial F/\partial z)^2}$. additionally, for Method-2, $\frac{\partial g}{\partial th}$ is needed.

I use formula 5.1 to derive the formula as below:

$$\frac{\partial g}{\partial z} = \frac{1}{g}\left\{\frac{\partial^2 g}{\partial x \partial z}\frac{\partial g}{\partial x} + \frac{\partial^2 g}{\partial y \partial z}\frac{\partial g}{\partial y} + \frac{\partial^2 g}{\partial z^2}\frac{\partial g}{\partial z}\right\} \quad (5.9)$$

For other derivatives, the method is the same as formula (5.9).

5.3.2 Convergence

The control of the convergence is also the same as for the inversion of the magnetic field described in the chapter before.

5.3.3 Technique of the inversion

The technique for the inversion of analytic signal is the same as that of the inversion of the magnetic field inversion.

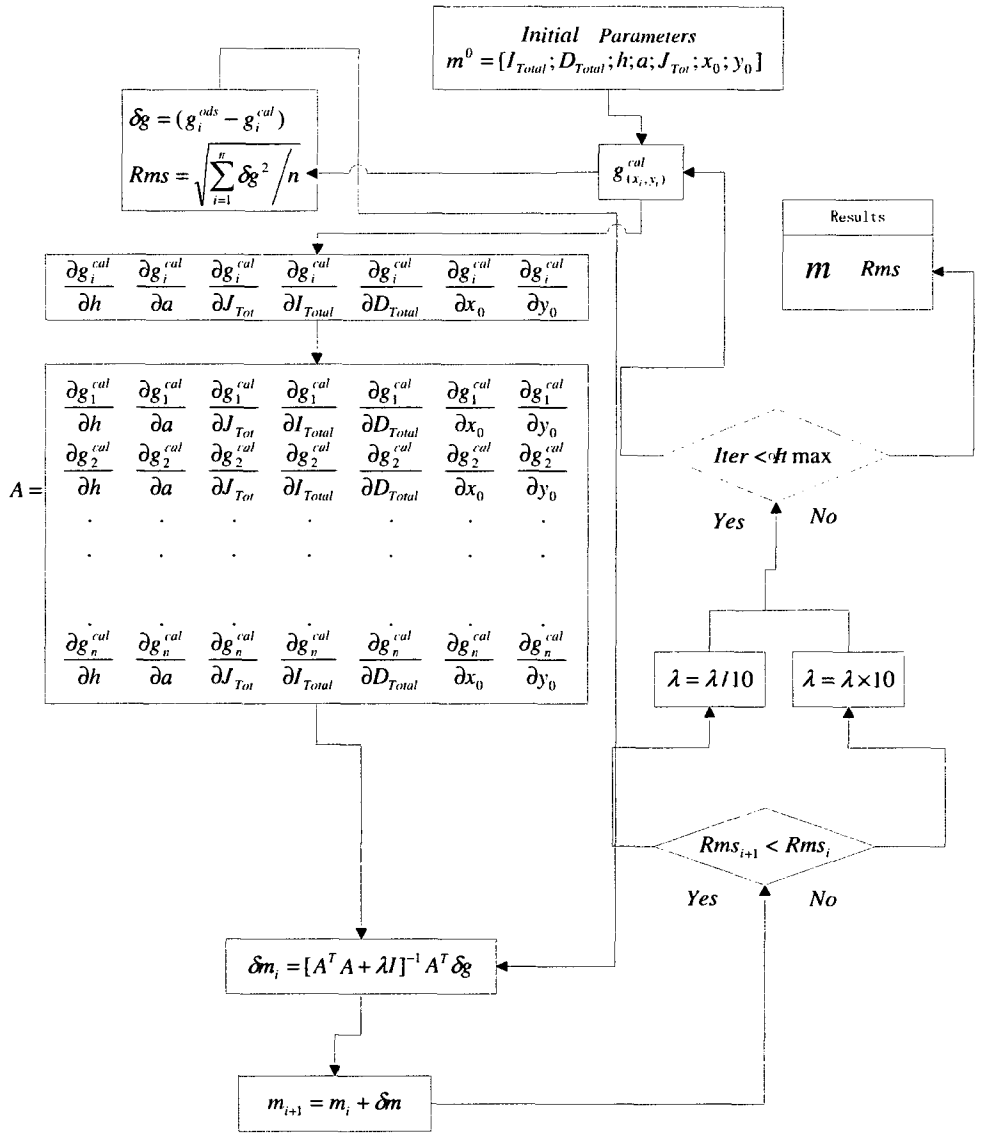

Flow Diagram 5.1 the flow diagram for analytic signal inversion without remanent magnetization using Levenberg- Maquardt (Method-1)

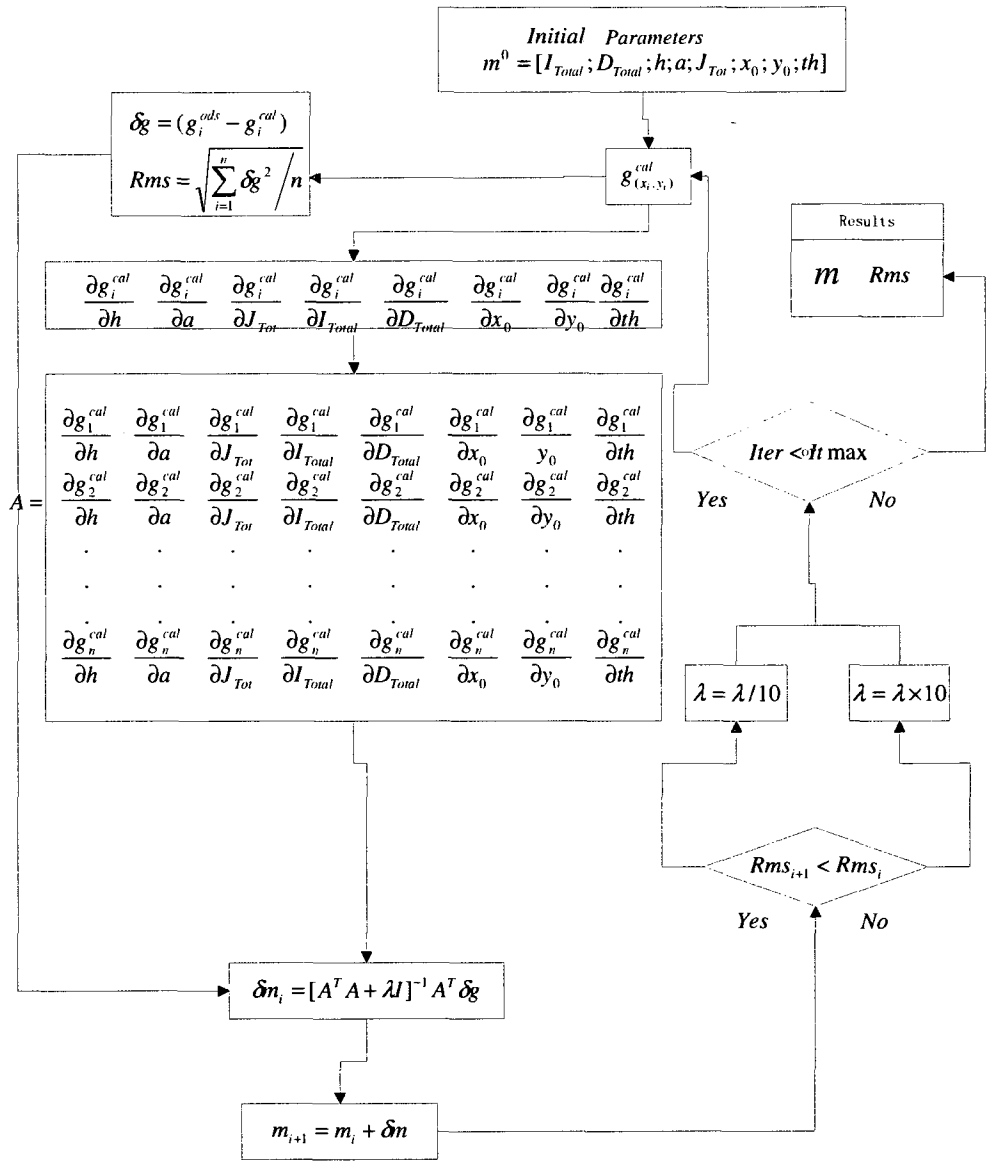

Flow Diagram 5.2 the flow diagram for analytic signal inversion without remanent magnetization using Levenberg- Maquardt (Method-2)

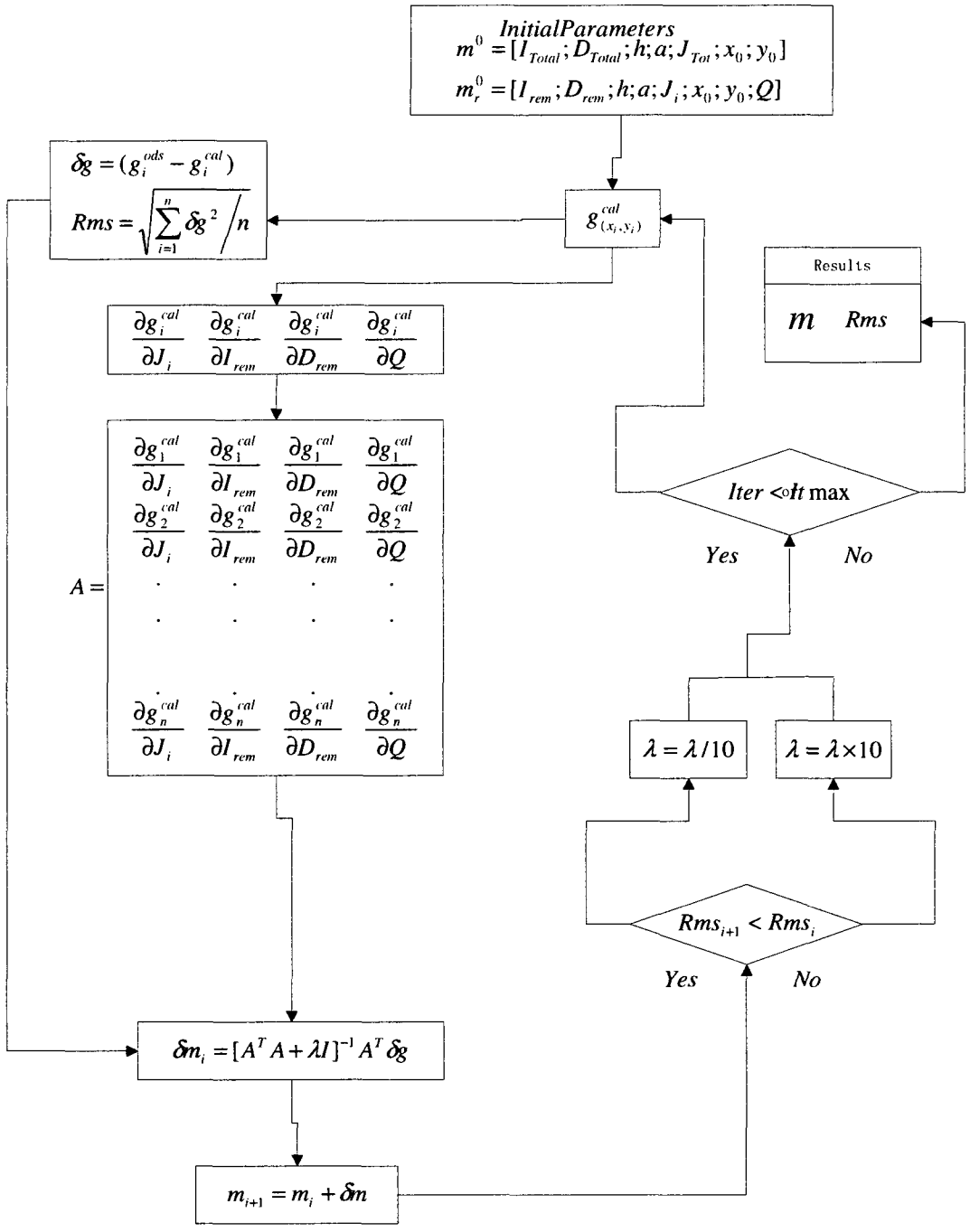

Flow Diagram 5.3 the flow diagram for analytic signal inversion with remanent magnetization using Levenberg- Maquardt (Method-1 and Method-2)

5.4 Tests

5.4.1 Tests for the analytic signal inversion with method-1

Firstly, I test the models for Method-1, and then, I will test the models for Method-2. I will test the models presented in the inversion of magnetic field in order to compare the results of the inversion obtained with the magnetic field inversion with that of the analytic signal inversion.

5.4.1.1 Tests for the analytic signal inversion in absence of remanent magnetization with method-1

The models to be tested are detailed below:

Table 5.1 Results for analytic signal inversion without remanent magnetization (Method-1)

N.	Type	Dep. (m)	Dia. (m)	In. (°)	De. (°)	Th. (m)	MSu.(SI)
Defang2	Model	50	160	69	12	200	0.01
	Initials	50	157	66	12		0.00900
	Results	49	160	66	12		0.00950
Defang5	Model	50	160	30	12	200	0.01
	Initials	48	157	31	13		0.00860
	Results	47	161	31	12		0.00880
Atestm1	Model	100	160	74	-12	300	0.01
	Initials	96	157	71	-11		0.00851
	Results	95	161	62	-9		0.00920

Here I select three models, Defang2, Defang5 and Atestm1. They are the same as the models tested in the magnetic field inversion. The earth magnetic field strength for Defang2 is 55278 nT; the inclination of the earth magnetic field is 69^0, the declination of the earth magnetic field is 12^0, the grid dimension are 750×750m, the coordinates of the center of the cylinder are (375m, 375m), the depth of the cylinder is 50m, the diameter of the cylinder is 160m, the thickness of the cylinder is 200m and the susceptibility is 0.01 (SI). Defang5 is for the change of the inclination of the earth magnetic field to figure out the tendency of the changes of the results of the parameters of the inversion. And, the model Atestm1, the declination of the earth

magnetic field is changed, and the depth and the thickness of the cylinder are also changed to figure out the precision and the stability of the results of the inversion with the changes of the parameters concerned.

The images are illustrated below:

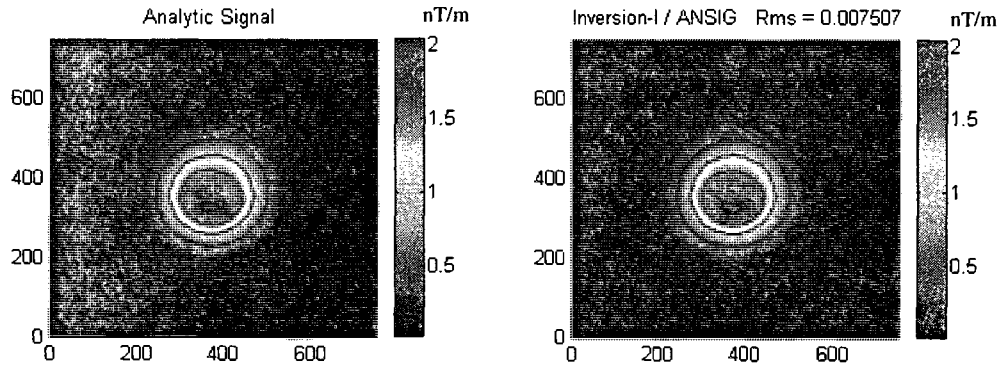

3D Model Defang2 :

- Depth = 50m
- Diameter = 160m
- Incl. $_{ter}$ = 69°
- Decl$_{ter}$ = 12°
- Magnetic Suscept.= 0.01 SI
- Coord. of centre: (375, 375)
- Depth Extension = 200m

Results of Inversion :

- Depth = 49(50)m
- Diameter = 160(157)m
- Incl. $_{tot}$ = 66°(66°)
- Decl$_{tot}$ = 12°(12°)
- Magnetic Suscept.= 0.0094689 SI
- Coord. of centre: (377, 375)

Fig.5.1 Model Defang2: Geomagnetic field intensity: 55278nT , inclination of geomagnetic field : 69^0 , declination of geomagnetic field : 12^0 , depth of the cylinder:50m, diameter of the model : 160, height: 200m, magnetic susceptibility:0.01 SI.

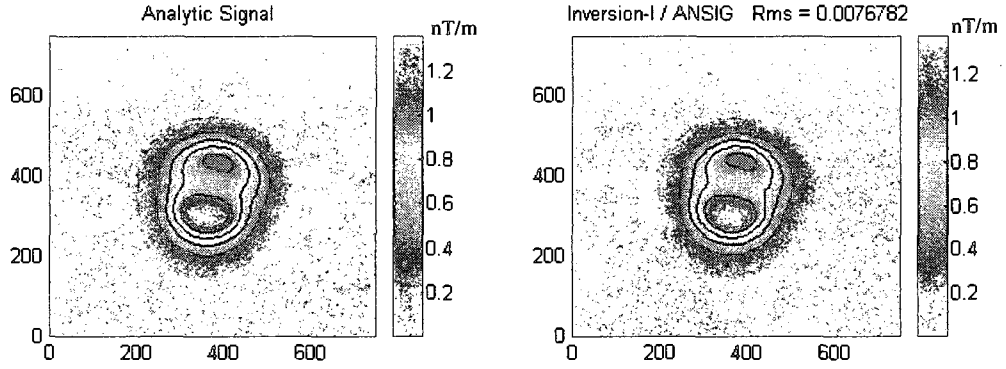

3D Model Defang5 :

- Depth = 50m
- Diameter = 160m
- $Incl._{ter} = 30^{o}$
- $Decl._{ter} = 12^{o}$
- Magnetic Suscept.= 0.01 SI
- Coord. of centre: (375, 375)
- Depth Extension = 200m

Results of Inversion :

- Depth = 47(48)m
- Diameter = 161(157)m
- $Incl._{tot} = 31^{o}(31^{o})$
- $Decl._{tot} = 12^{o}(13^{o})$
- Magnetic Suscept.= 0.0088452 SI
- Coord. of centre: (375, 375)

Fig.5.2 Model Defang5: Geomagnetic field intensity: 55278nT , inclination of geomagnetic field : 30^{0} , declination of geomagnetic field : 12^{0} , depth of the cylinder:50m, diameter of the model : 160, height: 200m, magnetic susceptibility:0.01 SI.

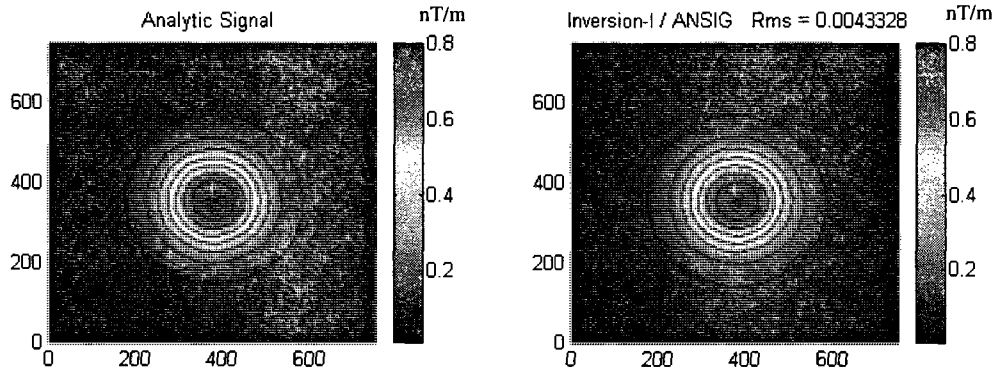

3D Model Atestm1 :

- Depth = 100m
- Diameter = 160m
- Incl. $_{ter}$ = 74°
- Decl $_{ter}$ = -12°
- Magnetic Suscept.= 0.01 SI
- Coord. of centre: (375, 375)
- Depth Extension = 300m

Results of Inversion :

- Depth = 95(96)m
- Diameter = 161(157)m
- Incl. $_{tot}$ = $62^{o}(71^{o})$
- Decl $_{tot}$ = $-9^{o}(-11^{o})$
- Magnetic Suscept.= 0.0091982 SI
- Coord. of centre: (383, 374)

Fig.5.3 Model Atestm1: Geomagnetic field intensity: 57170Nt , inclination of geomagnetic field : 74^{0} , declination of geomagnetic field : -12^{0} ,depth of the cylinder:100m, diameter of the model :160, height: 300m,magnetic susceptibility:0.01 SI.

Fig.5.1, Fig.5.2, and Fig.5.3 show that for the geometry of the model, such as the depth and diameter of the models, the results of the analytical signal inversion with Method-1 are better than that of the magnetic field: for the model Defang2, the result of magnetic inversion with method-1 of depth is 28m, the result of analytic signal inversion with method-1 of depth is 49m; the result of diameter inversed from magnetic inversion is 166m while that from analytic signal is 160m. For model Defang5, the result of depth inversed from magnetic inversion is 30m while that from analytic signal inversion is 47m, the diameter inversed from magnetic field inversion is 168 while that from analytic signal inversion is 161m. For the model Atestm1, the depth inversed from magnetic field inversion is 72m while that from analytic signal

inversion is 95m, the diameter from magnetic field inversion is 170m while that from analytic signal inversion is 161m. In addition to that, in appendix A, more models are tested to show that the results of analytic signal inversion in geometry are stable. For the inclination and declination of the earth's field, the results of the magnetic field inversion are better than that of the analytic signal inversion.

5.4.1.2 Tests for the analytic signal inversion in presence of remanent magnetization with method-1

The models Vjina111t6, AteR1 and Vjina111t21116 are tested as follows:

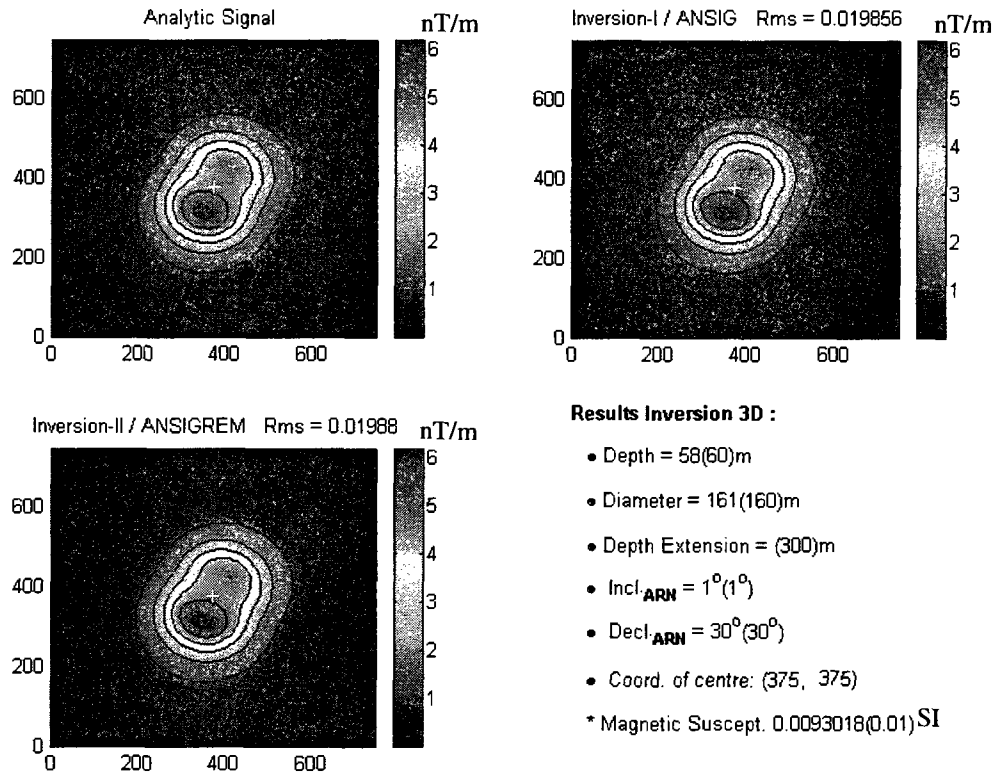

Fig.5.4 Model Vjina111t6: Geomagnetic field intensity: 57170nT , inclination of geomagnetic field : 74^0 , declination of geomagnetic field : -12^0 , depth of the cylinder:60m, diameter of the model : 160, height: 300m, magnetic susceptibility:0.01 SI. Inclination of remanent magnetization: 1^0, declination of the remanent magnetization: 30^0, position of the center of the cylinder: (375,375), konigsberger ratio parameter Q:5

From Fig.5.4, it shows that when the inclination is low, the results of the inversion are more precise for the inclination and declination, and the results of the geometry, such as the depth and diameter is more precise than that of magnetic inversion.

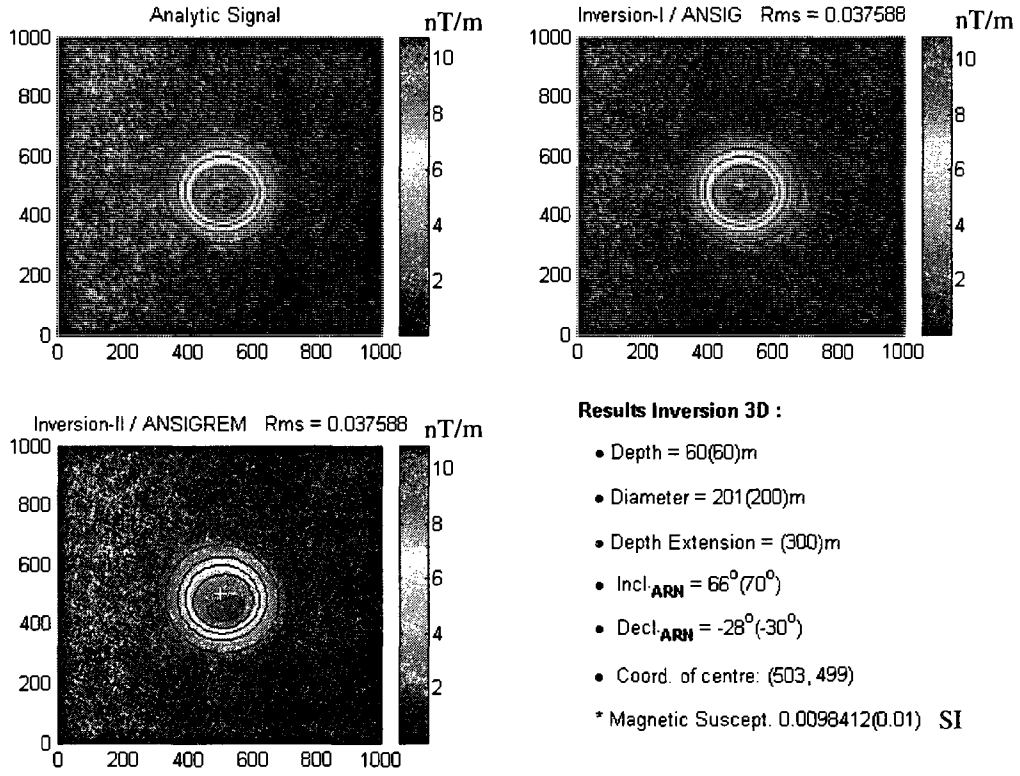

Fig.5.5 Model AteR1: Geomagnetic field intensity: 57170nT , inclination of geomagnetic field : 74^0, declination of geomagnetic field : -12^0, depth of the cylinder:60m, diameter of the model : 200, height: 300m, magnetic susceptibility:0.01 SI. Inclination of remanent magnetization: 70^0, declination of the remanent magnetization: -30^0 , position of the center of the cylinder: (500,500), konigsberger ratio parameter Q:5

Fig.5.5 shows that when the inclination of the remanent magnetization is higher than 60^0, the results of the inversion for the inclination and the declination are less accurate, but for the depth of the cylinder and the diameter of the cylinder they are always stable.

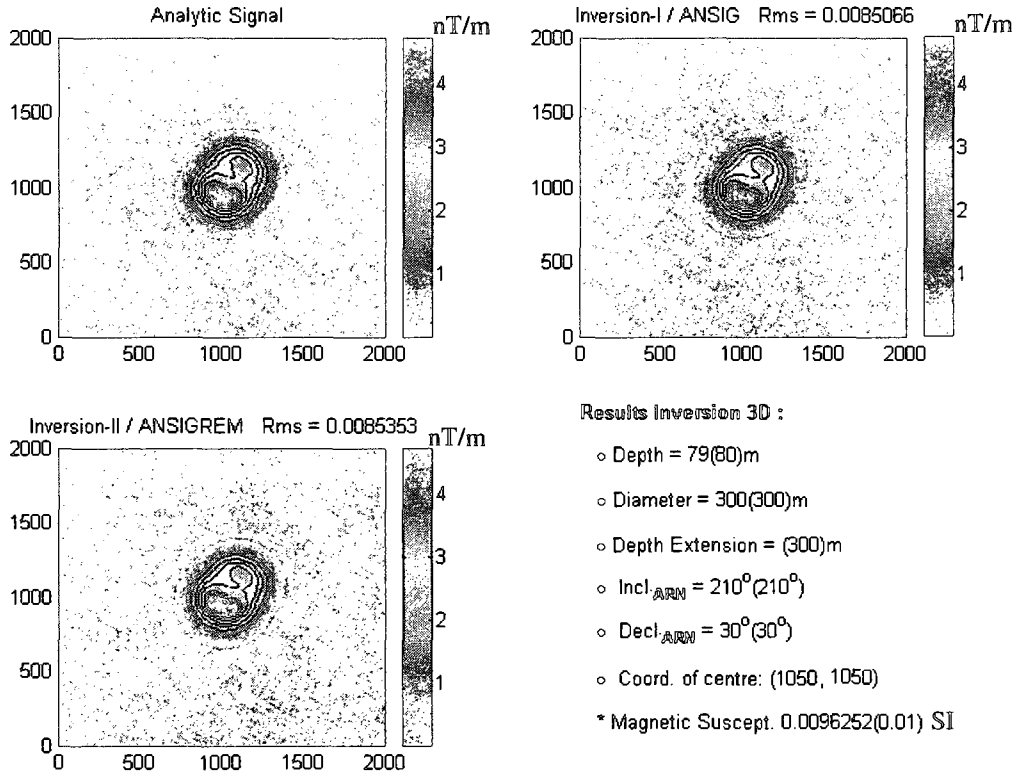

Fig.5.6 Model Vjina111t21116: Geomagnetic field intensity: 57170nT , inclination of geomagnetic field : 74^0, declination of geomagnetic field : -12^0, depth of the cylinder:80m, diameter of the model : 300, height: 600m, magnetic susceptibility:0.01 SI. Inclination of remanent magnetization: 210^0, declination of the remanent magnetization: 30^0, position of the center of the cylinder: (1050,1050), konigsberger ratio parameter Q:5

Here, the depth of the cylinder, its diameter and the grid dimension are all increased; the results of the inversion are also stable and precise.

Table 5.2 Results of analytic signal inversion with remanent magnetization (Method-1)

N.	Type	Dep. (m)	Dia. (m)	Inr. (°)	Der. (°)	Th. (m)	MSu.(SI)
Vjina111t6	Model	60	160	1	30	300	0.01
	Initials	58	158	6	32		0.00985
	Results	58	161	1	30		0.00930
AteR1	Model	60	200	70	-30	300	0.01
	Initials	57	196	74	-32		0.00990
	Results	60	201	66	-28		0.00984
Vjina111t21116	Model	80	300	210	30	600	0.01
	Initials	82	304	205	37		0.00979
	Results	79	300	210	30		0.00962

5.4.1.3 Conclusion

The analytic signal inversion with Method-1 is implemented successfully. Defang5 and Atestm1 are tested for analytic signal inversion without remanent magnetization. Vjina11t6, AteR1 and Vjina111t21116 are tested for analytic signal inversion with remanent magnetization. Compared with magnetic inversion with the semi-infinite model, the inversion results related with geometric parameters are more stable and precise. AteR1 is taken as an example, the result of depth from inversion of analytic signal of semi-infinite model is 60m, and from magnetic inversion of semi-infinite model is 37m; the result of diameter from inversion of analytic signal of semi-infinite model is 201m, and from magnetic field inversion is 207m. However, when the inclination of remanent magnetization is high, the inversion results related to the direction of magnetization are less precise.

5.4.2 Tests for analytic signal inversion with method-2

As tests in the section of magnetic inversion, tests for analytic signal inversion proceeds by two steps. First step is to test the models in absence of remanent magnetization; second step is to test the models in presence of remanent magnetization.

5.4.2.1 Tests for the analytic signal inversion in absence of remanent magnetization with method-2

The tests include the validation tests, where the initial values are calculated by Chemam (2006)'s method automatically. And then, the robustness of the algorithms are tested by changing the initial values manually.

5.4.2.1.1 Validation with models for the analytic signal inversion in absence of remanent magnetization (Method-2)

I tested the same models Defang2, Defang5 and Atestm1 with Method-2, the results are as follows:

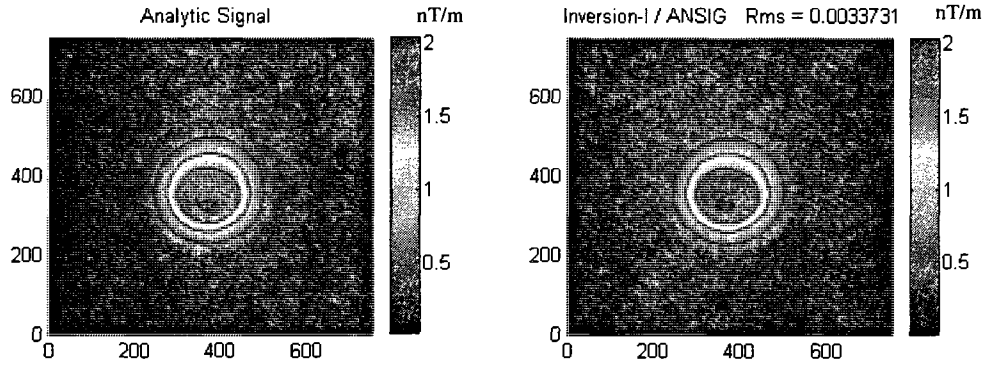

3D Model Defang2 :

- Depth = 50m
- Diameter = 160m
- Incl. $_{ter}$ = 69°
- Decl. $_{ter}$ = 12°
- Magnetic Suscept.= 0.01 SI
- Coord. of centre: (375, 375)
- Depth Extension = 200m

Results of Inversion :

- Depth = 50(50)m
- Diameter = 160(157)m
- Incl. $_{tot}$ = 68°(66°)
- Decl. $_{tot}$ = 12°(12°)
- Magnetic Suscept.= 0.010012 SI
- Coord. of centre: (376, 375)
- Depth Extension = 223(200)m

Fig.5.7 Results of inversion for model Defang2 with Method-2

For the model Defang2, the depth and diameter are exactly equal to the parameter of the model, and the inclination is 68°, is more accurate than the result of the analytic signal inversion with method-1. For the model Defang5, the depth of the analytic

signal inversion with method-2 is 49m, more accurate than the interpreted depth from the method-1 (47m), the diameter is 160m, exactly equal to the parameter of the model while interpreted diameter from method-1 is 161m, 1m more than the model; and the inclination is 30°, exactly equal to the that parameter of the model; magnetic susceptibility is 0.0098SI, is more accurate than that inverted by the method-1.

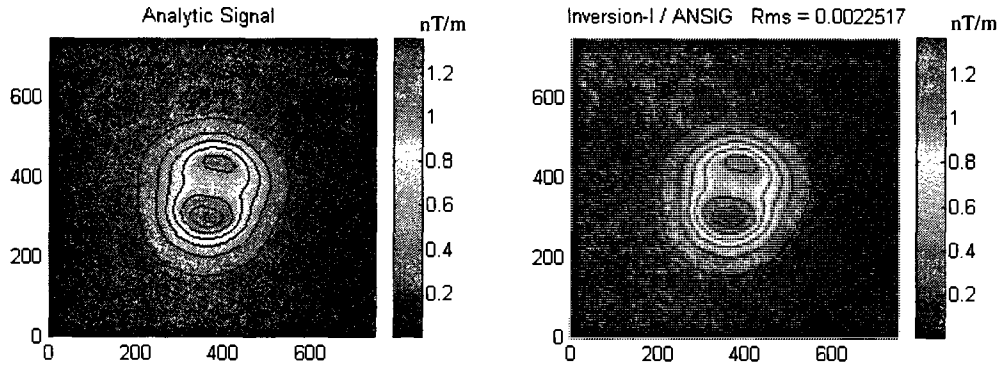

3D Model Defang5 :

- Depth = 50m
- Diameter = 160m
- $Incl._{ter} = 30^{o}$
- $Decl._{ter} = 12^{o}$
- Magnetic Suscept.= 0.01 SI
- Coord. of centre: (375, 375)
- Depth Extension = 200m

Results of Inversion :

- Depth = 49(48)m
- Diameter = 160(157)m
- $Incl._{tot} = 30^{o}(31^{o})$
- $Decl._{tot} = 12^{o}(13^{o})$
- Magnetic Suscept.= 0.0098045 SI
- Coord. of centre: (375, 375)
- Depth Extension = 202(202)m

Fig.5.8 Results of inversion for model Defang5 with Method-2

Table 5.3 Results of the analytic signal inversion without remanent magnetization (Method-2)

N.	Type	Dep. (m)	Dia. (m)	In. (°)	De. (°)	Th. (m)	MSu.(SI)
Defang2	Model	50	160	69	12	200	0.01
	Initials	50	157	66	12	200	0.00900
	Results	50	160	68	12	223	0.01001
Defang5	Model	50	160	30	12	200	0.01
	Initials	48	157	31	13	202	0.00860
	Results	49	160	30	12	202	0.00980
Atestm1	Model	100	160	74	-12	300	0.01
	Initials	96	157	71	-11	304	0.00851
	Results	100	159	66	-12	305	0.01025

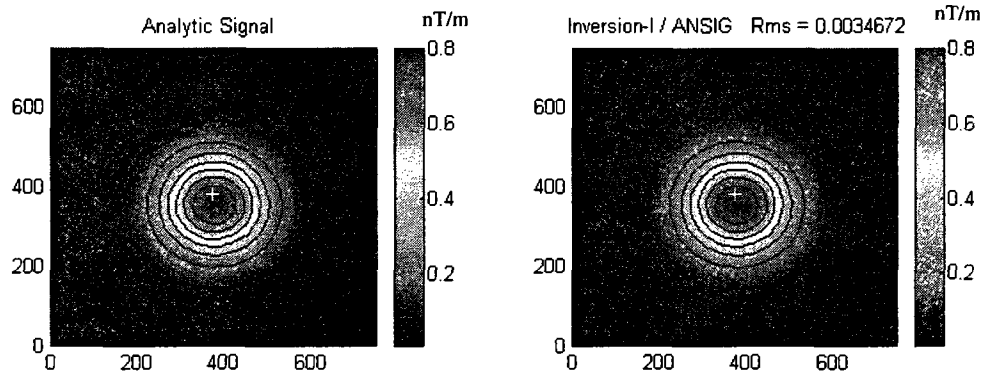

3D Model Atestm1 :

- Depth = 100m
- Diameter = 160m
- $Incl._{ter} = 74^{o}$
- $Decl._{ter} = -12^{o}$
- Magnetic Suscept.= 0.01 SI
- Coord. of centre: (375, 375)
- Depth Extension = 300m

Results of Inversion :

- Depth = 100(96)m
- Diameter = 159(157)m
- $Incl._{tot} = 66^{o}(71^{o})$
- $Decl._{tot} = -12^{o}(-11^{o})$
- Magnetic Suscept.= 0.010247 SI
- Coord. of centre: (380, 374)
- Depth Extension = 305(304)m

Fig.5.9 Results of inversion for model Atestm1 with Method-2

Comparing the figure 5.1 and 5.7 and figure 5.2 and 5.8, we notice that, for the inversion without remanent magnetization, the precision of the results of the inversion with Method-2 is better that of inversion with Method-1, especially for the inclination and declination of the terrestrial magnetic field, the results are improved.

5.4.2.1.2 The robustness of the analytic signal inversion in absence of remanent magnetization to the initial values (method-2)

In order to compare the sensibility of the inversion to the initial values for models with and without remanent magnetization, the same geometric model was selected. The results are showed in table 5.4. The obvious change is that the depth extension is less precise than that of magnetic inversion.

Table 5.4 Results of tests of sensibilities to the initial values without remanent magnetization

NI.	Initials of Parameters					Results of Inversions				
	Dep.	Dia.	In.	De.	Th.	Dep.	Dia.	In.	De.	Th.
Model	50	160	69	12	200					
IC	50	157	66	12	200	50	160	68	12	223
I 1	40	157	66	12	210	51	160	68	12	219
I 2	55	157	66	12	195	50	160	68	12	224
I 3	50	151	66	12	200	50	160	68	12	223
I 4	50	170	66	12	200	50	160	68	12	224
I 5	50	157	60	12	200	50	160	68	12	224
I 6	50	157	80	12	200	51	160	68	13	217
I 7	50	157	66	6	200	50	160	68	12	223
I 8	50	157	66	18	200	50	160	68	12	223
I 9	50	157	66	12	150	50	160	68	12	222
I 10	50	157	66	12	250	50	160	68	12	222

5.4.2.2 Tests for the analytic signal inversion in presence of remanent magnetization with method-2

Also the tests are included two sections. The first section is testing of validation using the initial values calculated automatically while second section is testing of robustness of the algorithm to the initial values using initial values entered manually.

5.4.2.2.1 The validation with models for the analytic signal inversion in presence of remanent magnetization (method-2)

The models and results of the analytic signal inversion are listed in table 5.5. In the table, Inr. is abbreviation of the inclination of remanent magnetization, Der. is abbreviation of the declination of remanent magnetization. Compared with results of Method-1 for Vjina111t6, the results of the inversion in terms of depth and diameter are improved. The results of the analytic signal inversion are exactly equal to true values.

Table 5.5 Results of the analytic signal inversion with remanent magnetization (Method-2)

N.	Type	Dep. (m)	Dia. (m)	Inr. (°)	Der. (°)	Th. (m)	MSu.(SI)
Vjina111t6	Model	60	160	1	30	300	0.01
	Initials	58	158	6	32	302	0.00985
	Results	60	160	1	30	305	0.01
AteR1	Model	60	200	70	-30	300	0.01
	Initials	57	196	74	-32	303	0.00990
	Results	60	201	68	-29	448	0.00988
Vjina111t21116	Model	80	300	210	30	600	0.01
	Initials	82	304	205	37	598	0.00979
	Results	80	300	210	30	598	0.00985
Babneq	Model	60	160/120	30	30	300	0.01
	Initials	61	133	37	45	299	0.00965
	Results	62	144	35	43	300	0.00959

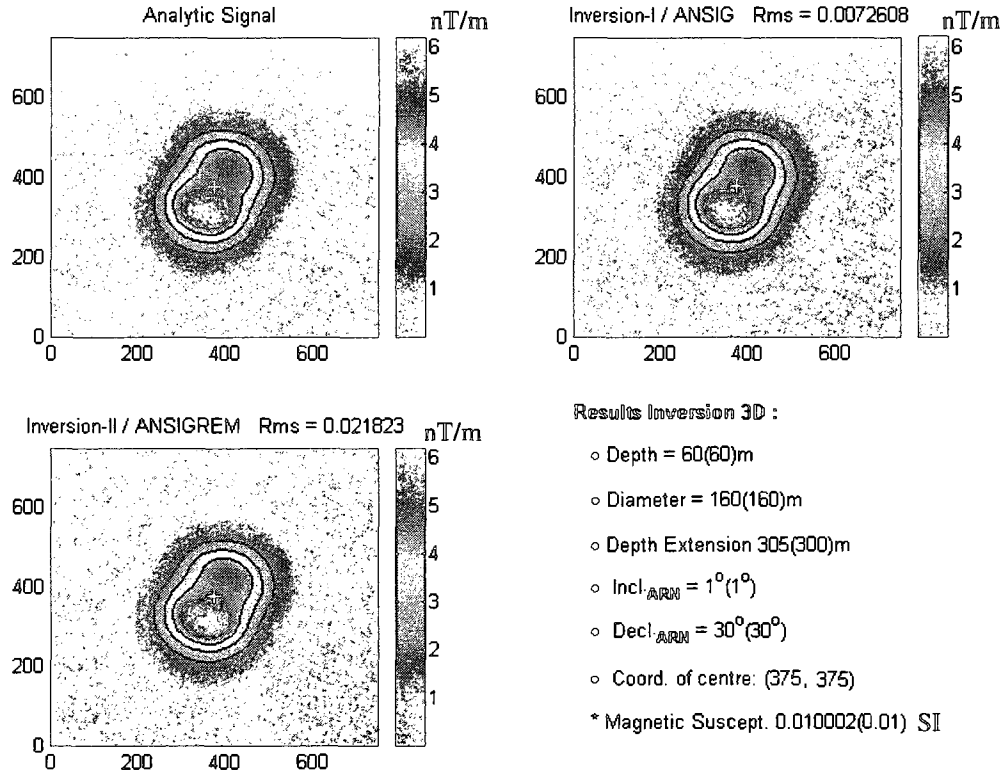

Fig.5.10 Results of inversion for model Vjina111t6 with Method-2

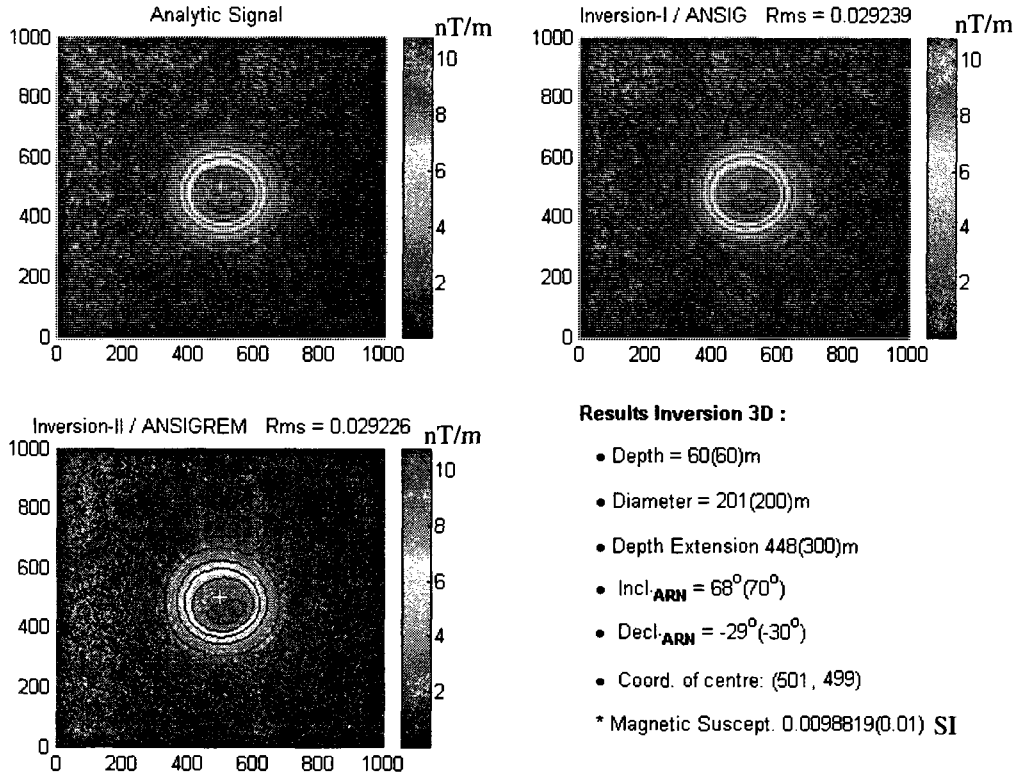

Fig.5.11 Results of inversion for model AteR1 with Method-2

Compared with results of Method-1 for AteR1, the results of the inversion in terms of inclination and declination of the remanent magnetization are improved; they are more precise than before. The model of right vertical cylinder of oval cross-section is tested, the long axis of it is 160m, and the short axis is 120m. The results of inversion of analytic signal relative to the direction of magnetization are less accurate than that of magnetic field inversion, but the results of the geometry are not changed greatly.

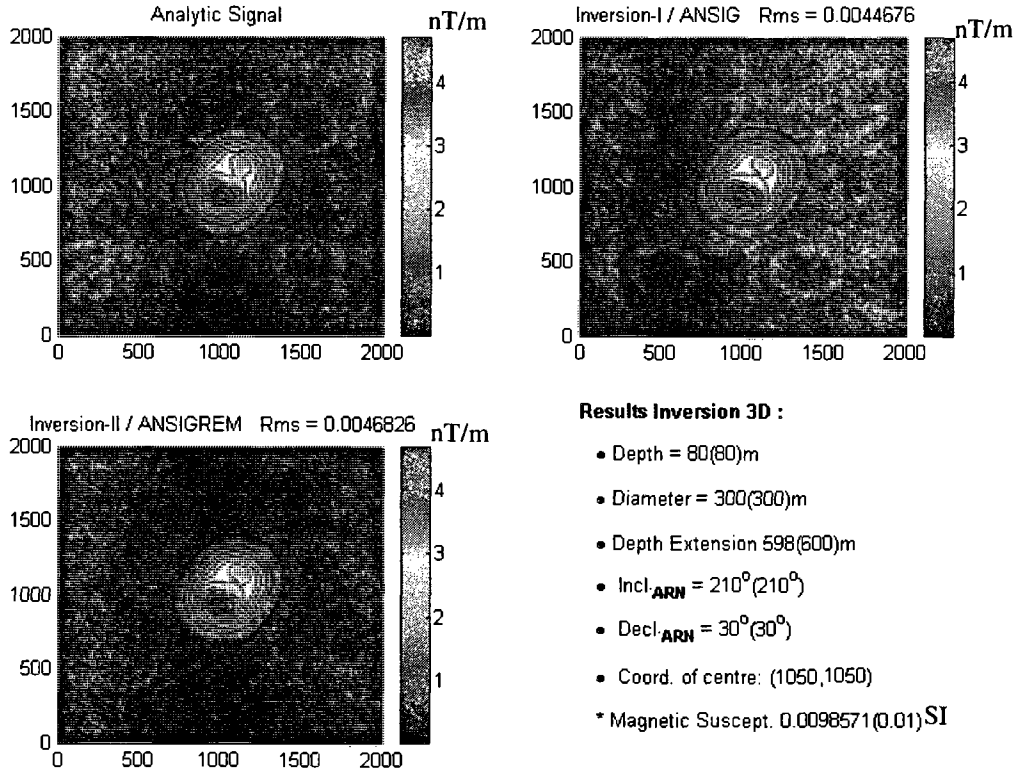

Fig.5.12 Results of inversion for model Vjina111t21116 with Method-2

Compared with results of Method-1 for Vjina111t21116, the result of the inversion in terms of depth is improved.

5.4.2.2.2 The robustness of the analytic signal inversion in presence of remanent magnetization to the initial values (method-2)

In order to compare the results of the tests with that of magnetic inversion, the same models Vjina111t6 and Vjina111t3 are selected to be tested. Obviously, the depth extension is less precise than that of magnetic inversion. When the initial values are changed not far from the true values, the results of the inversion of analytic signal are stable, when the initial values are changed greatly, especially when all of the parameters are changed a lot, the results of the inversion of analytic signal are not stable and not accurate. See to the table 5.6.

Table 5.6 Results of tests of sensibilities with initials values with remanent magnetization

NI.	Initials of Parameters					Results of Inversions				
	Dep.	Dia	Inr.	Der.	Th.	Dep	Dia.	Inr.	Der.	Th.
Model 1	60	160	1	30	300					
IC	58	158	6	32	302	60	160	1	30	305
I 1	50	158	6	32	310	60	160	1	30	314
I 2	70	158	6	32	290	60	160	1	30	300
I 3	58	151	6	32	302	60	160	1	30	306
I 4	58	170	6	32	302	60	160	1	30	307
I 5	58	158	12	32	302	60	160	1	30	305
I 6	58	158	-12	32	302	60	160	1	30	305
I 7	58	158	6	20	302	60	160	1	30	305
I 8	58	158	6	40	302	60	160	1	30	305
I 9	58	158	6	32	250	60	160	1	30	307
I 10	58	158	6	32	350	59	160	1	30	348
Model 2	60	160	30	30	300					
IC1	59	158	32	32	301	60	160	30	30	323
I11	80	158	32	32	301	60	160	29	30	325
I12	59	158	80	32	301	60	160	28	32	323
I11a	30	80	15	15	150	93	146	36	34	182
I12a	120	320	60	60	600	131	268	91	62	598

5.4.2.3 Tests for addition of noise

Noise is tested in this section to figure out the sensitivity of the algorithm of analytic signal inversion to noise, the model is tabled below

Table 5.7 Model to be tested with addition of noise

N^0	Inr. (°)	Der.(°)	Dep.(m)	Dia. (m)	Th.(m)	MSu. (SI)
Vjina111t3	30^0	30^0	60	160	300	0.01

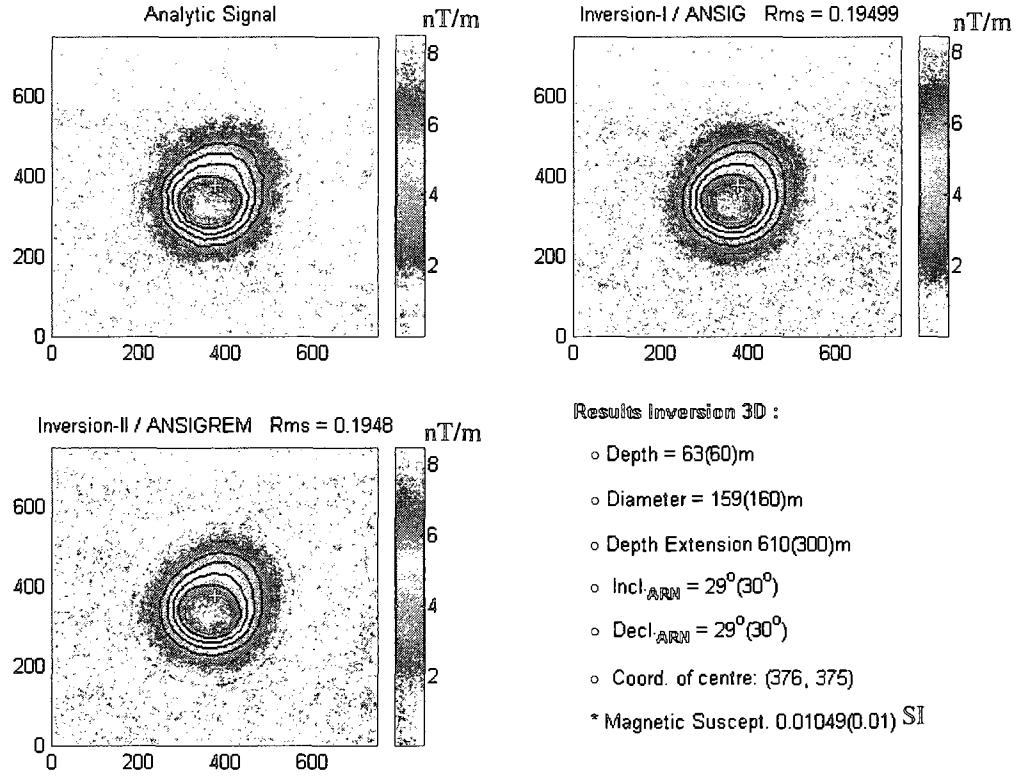

Fig.5.13.1 Model Vjina111t3: Geomagnetic field intensity: 57170nT , inclination of geomagnetic field : 74^0, declination of geomagnetic field : -12^0, depth of the cylinder:60m, diameter of the model : 160, height: 300m, magnetic susceptibility:0.01 SI. Inclination of remanent magnetization: 30^0 , declination of the remanent magnetization: 30^0, position of the center of the cylinder: (375,375), konigsberger ratio parameter Q:5 addition of random noise: 2nT

Table 5.8 Results tested with addition of noise

N^0	Inr.	Der.	Dep. (m)	Dia. (m)	Th. (m)	MSu. (SI)
Vjina111t3	30^0	30^0	60	160	323	0.01
Vjina111t3 (2nT)	29^0	29^0	63	159	610	0.01
Vjina111t3 (5nT)	28^0	25^0	52	147	353	0.00665

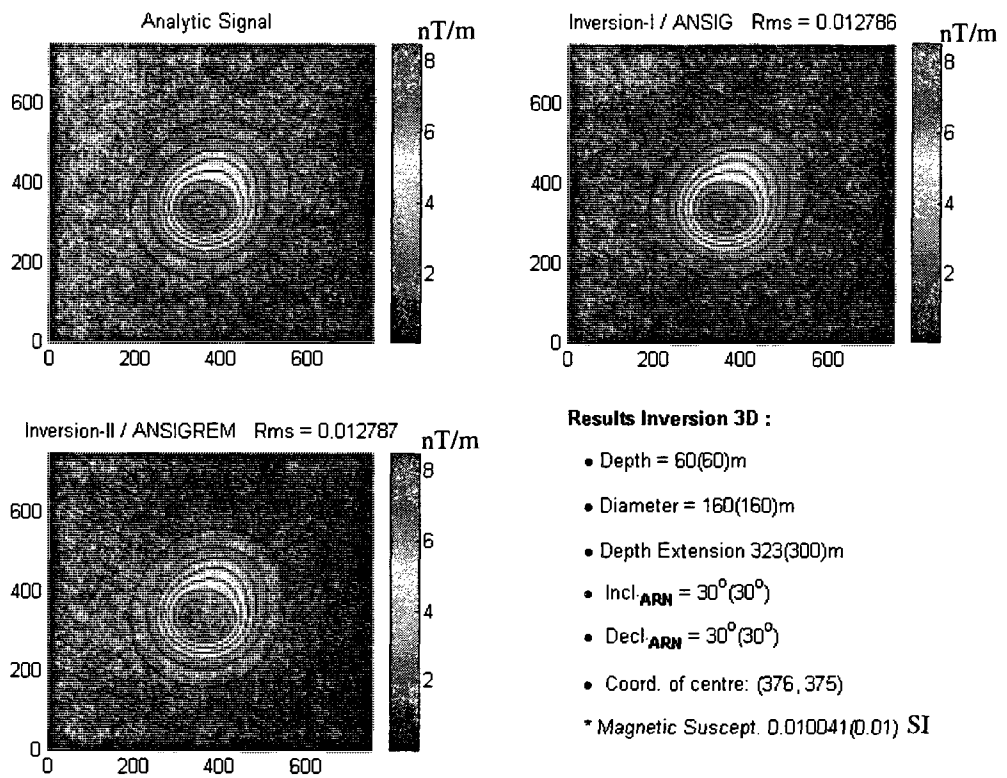

Fig.5.14.2 Model Vjina111t3, without addition of the noise

Comparison of the results illustrated in figure 5.13.1 and figure 5.14.2, suggests that the random noise affects the precision and the stability of the analytic signal inversion. The inclination and the declination of the model is 30^0 while the results of the inversion is 29^0, the depth of the model is 60m while that of the result of the inversion is 63m, the diameter of the model is 160m while that of the result is 159m, the depth extent of the cylinder is 300m while that of the result of the inversion is 610m, especially for the depth extent of the cylinder, the error is large. In the table 5.8, the results of magnetic data of same model added 5nT random noise are listed. The results of geometry and magnetic susceptibility are more inaccurate that of inversion of analytic signal of the same model added to 2nT random noise.

5.5 Conclusions

The analytic signal inversion is implemented for two basic models, the method-2 is better than method-1 in terms of the precision. With method-1, when the inclination of the remanent magnetization is near vertical, the results of the inversion of inclination and declination are less precise, but with method-2, the results are improved. The advantages of the analytic signal inversion is that the results of the inversion in terms of the geometry are less dependent on the remanent magnetization, which could give a results of inversion more precise on the condition that the initial values for starting inversion in terms of remanent magnetization are not precise. The addition of the noise affects the results of the analytic signal inversion.

5.6 Discussion

For the analytic signal inversion of a semi-infinite (method-1) without remanent magnetization, models Defang2, Defang5 and Atestm1 were tested. Their parameters are given in table 5.1. The results for Defang5 are precise while results for Defang2 and Atestm1 are not precise, especially for the inclination, i.e. for Defang2, the result for the inclination is 66°, 3° less than that of model; for Defang5, the result of inclination is 62°, 12° less than that of the model.

For the analytic signal inversion (method-1) with remanent magnetization, models Vjina111t6, AteR1 and Vjina111t2116 were tested. The results of inversion for Vjina111t6 and Vjina111t21116 are precise, and the results of inversion for AteR1 are less precise, especially for the inclination and the declination of the remanent magnetization. For example, the result of inclination is 66°, 4° less than that of the model.

For the analytic signal inversion of a finite extent model (method-2) without remanent magnetization, Defang2, Defang5 and Atestm1 were also tested. Results are presented in table 5.4. In contrast to that of method-1 without remanent magnetization, the results are improved, but for the model with a high inclination and a deeper target,

the results are still not good, for the model Atestm1, the result of inclination is 66°, 8° less than that of the model.

For the analytic signal inversion of method-2 with remanent magnetization, Vjina111t6, AteR1 and Vjina111t2116 were tested. The results of inversion for Vjina111t6 and Vjina111t21116 are good, and the results of the inversion for AteR1 are not good, especially for the results of inclination and declination, the result of inclination is 68°, 2°less than that of the model, the result of declination is -29°, -1°more than that of the model.

In addition, robustness of the algorithm to the initial values for method-2 was studied. For the inversion with and without remanent magnetization, when the changes of the initial values are limited to a small range, the results are not affected (table 5.4 and table 5.6). In contrast to the magnetic field inversion, the robustness of the analytic signal inversion to the initial values is better. For example, For model Vjina111t3, the initial value for depth is 80m (60m of model), the results of analytic inversion are 60m of depth, 160m of diameter, 29° of inclination, 30° of declination, they are improved in contrast to that of magnetic inversion, that are 63m of depth, 156m of diameter, 30° of inclination, 30° of declination. For the same model, the initial value of the inclination of remanent magnetization is 80° (the model is 30°), the results of analytic inversion are 60m of depth, 160m of diameter, 28° of inclination, and 32° of declination, they are also improved in contrast to that of magnetic inversion, that are 60m of depth, 160m of diameter, 26° of inclination, 32° of declination. But for the analytic inversion, the estimation of the depth is not as precise as that of magnetic inversion. When all of the parameters are changed greatly, the results of inversion of analytic signal are not better.

The results of the analytic signal inversion in presence of noise are tested; the result is that the noise affects the results of the analytic inversion. Results are

presented in table 5.8. Without addition of noise 2nT, the results are 60m of depth (that of model is 60m), 160m of diameter (that of model is 160m), 30° of inclination (that of model is 30°), 30° of declination (that of model is 30°), 323m of depth (that of model is 300m); with addition of noise, the results are 63m of depth, 159m of diameter, 29° of inclination, 29° of declination and 610m of depth extension. 5nT random noise was added. The more the noise is added, the more inaccurate, the results of inversion of analytic signal are.

Chapter 6 Joint inversion of the magnetic field and its analytic signal

6.1 Introduction of joint inversion

In the preceding chapter, the analytic signal inversion was proposed. The advantage of the analytic signal inversion is that the results of the inversion in terms of the geometry are less dependent on the remanent magnetization, which could give a results of inversion more precise on the condition that the initial values for starting inversion in terms of remanent magnetization are not precise. The results of the analytic signal inversion relative to the inclination are not precise, especially, when the inclination is high. When the initial values are far away from the solutions, the analytic signal inversion is better than the magnetic field inversion. I now proceed the joint inversion of the magnetic field and the analytic signal

In an attempt to improve the results by taking advantage of the strength of both methods, Vozoff and Jupp (1975) demonstrated the joint inversion of two types of data, DC resistivity and Ultra Low Frequency electromagnetic (magnetotelluric) measurements in horizontally-layered conditions. Since then, the joint inversion has received more and more attention. Raiche et al. (1985) do a joint inversion of coincident loop transient electromagnetic and schlumberger sounding to resolve layered structures. Meju (1996) developed the joint inversion of TEM and MT sounding data. Dobroka (1991) jointly inverted the vertical seismic profiles data and electric data to determine the physical properties parameters of the underground coal mine etc.

Benech et. al (2002) completed a joint inversion of EM and magnetic data for near surface studies. They incorporated the two types of data to enhance the quality of the interpretation by the simultaneous use of EM and magnetic data.

For potential field methods, Gallardo-Delgado et.al (2003) implemented a joint inversion of gravity and magnetic data in terms of 3D structures. The algorithm combines a number of features that have proven useful in other algorithms. It defines

the subsurface using a large number of prisms, with the depths to the tops and bottoms as unknowns to be determined by optimization. This joint inversion helps constrain the structure of a basin and helps extend offshore the interpretation of known surface faults to the offshore.

Pilkington (2006) implemented joint inversion of gravity and magnetic data for two layer models. The damped least-squares inversion is used to determine the topography of the interface. The effect of this inverse is closely related to a downward continuation of the field to the average interface depth. The method is used to map the base of the Sept-Iles mafic intrusion, Quebec, Canada, and the shape of the central uplift at the Chicxulub impact crater, Yucatan, Mexico.

For the joint inversion of gravity and magnetic data, several approaches have been used. Menichetti and Guillen (1983) use a generalized inversion technique to determine body shapes for the 2.5D case with specified densities and magnetization. A stable inversion is achieved by removing the effects of small eigenvalues, providing a suggested improvement over separate inversion of either data set. Serpa and Cook (1984) use a least- squares inversion method to solve for the vertices and physical properties of a 2.5D model. Their method does not include damping or regularization, so stabilizing the solution is effected by holding some parameters fixed while inverting for others. Zeyen and Pous (1993) use a 3D subsurface model comprising of an ensemble of vertical prisms and solved for physical properties and the tops and bottoms of each prism. They control solution stability by specifying a priori parameter and data covariances (Pilkington, 2006).

The joint inversion provides better results than the separate inversion of each data set. Firstly, the resolution is increased; secondly, the stability of the results is enhanced.

6.2 The model of the joint inversion

The joint inversion of the magnetic field anomaly and its analytic signal is a kind of inversion with two data sets for one model geometry and physical parameters; the parameters to be inverted are same for each set of the data:

$$\vec{m} = (m_1, m_2, ... m_N)^T. \qquad (6.1)$$

Here, we have two inverse problems:

$$\varepsilon_1 = A_1 \Delta m + e_1 \qquad (6.2)$$

$$\varepsilon_2 = A_2 \Delta m + e_2 \qquad (6.3)$$

Given :

$$A = [A_1; A_2] \qquad (6.4)$$

$$\varepsilon = [\varepsilon_1; \varepsilon_2] \qquad (6.5)$$

We get:

$$\varepsilon = A\Delta m + e \qquad (6.6)$$

The problem of joint inversion is to derive the solution of equation (6.6)

6.3 Forward modeling

As for the inversion of the magnetic field and the inversion of its analytic signal separately, the kimberlite model is that of a pipe, and the vertical cylinder model is used. Singh and Sabina (1978) found the mathematical expressions of magnetic anomaly for this model. Chemam (2006) gives the mathematical expressions of the magnetic anomaly with remanent magnetization for this model. For the inversion of the analytic signal, I derived the mathematical expressions of the analytic signal of the magnetic anomaly without and with remanent magnetization due to the vertical right circular cylinder with arbitrary polarization. I calculated the partial derivatives of the total magnetic field (F) without and with remanent magnetization to x, y and z direction, and realize the model forwarding

$$g = \|\nabla F\| = \sqrt{(\partial F/\partial x)^2 + (\partial F/\partial y)^2 + (\partial F/\partial z)^2} \quad (6.7)$$

Where F is total magnetic field anomaly, g is the analytic signal (amplitude of total gradient). So for joint inversion of the magnetic field and its analytic signal, the forward modeling is implemented as follow:

$$\Phi = \lambda F + (1-\lambda) g \qquad (6.8)$$

In the latter, F and g need to be normalized to remove the units for them.

6.4 Formulation of the joint inversion

For the joint inversion problem; there are two inverse problems involved:

$$F[m] + \varepsilon_1 = d_1^{obs} \qquad (6.9)$$

$$g[m] + \varepsilon_2 = d_2^{obs} \qquad (6.10)$$

Included m are the parameters to be inversed. We have:

$$d_{1i} - F_i[m] = \sum_{j=1}^{k} \frac{\partial F_i}{\partial m_j} \Delta m_j + e, \quad i = 1,2,\ldots,N_1 \qquad (6.11)$$

and

$$d_{2i} - g_i[m] = \sum_{j=1}^{k} \frac{\partial g_i}{\partial m_j} \Delta m_j + e, \quad i = 1,2,\ldots,N_2 \qquad (6.12)$$

or in a matrix form:

$$\varepsilon = A\Delta m + e \qquad (6.13)$$

where: $\varepsilon = [\varepsilon_{1i}, \varepsilon_{2i}]^T$, $\Delta m = [\Delta m_1, \Delta m_2, \ldots, \Delta m_k]^T$ is defined as a modification vector which is added to m^0 (initial parameters values to start the inversion) to form a new vector. N_1 and N_2 are the number of the data of two sets respectively. k is the number of the parameters. A is a $N \times k$ matrix of partial derivative whose elements:

$A_{ij} = \frac{\partial F_i[m]}{\partial m_j}$ or $\frac{\partial g_i[m]}{\partial m_j}$. The final formats of the elements of the matrix A are as follows:

$$A_{ij} = \left(\frac{\partial F_i[m]}{\partial m_j}\right) \times w_1, \quad i = 1,2,...,N_1 \quad \text{and} \quad j = 1,2,...,k \quad (6.14)$$

$$A_{ij} = \left(\frac{\partial g_i[m]}{\partial m_j}\right) \times w_2 \ , i = N_1 + 1, N_1 + 2,...,N_1 + N_2, \ j = 1,2,...,k \quad (6.15)$$

where w_1 and w_2 are the weighting factors of the data. And in order to keep the equilibrium in equation (6.6), I need to weight ε of the two sets of data as follows:

$$\varepsilon_i = (d_{1i} - F_i[m]) \times w_1 \text{ , for } i = 1,2,...N_1 \quad (6.16)$$

and

$$\varepsilon_i = (d_{2i} - g_i[m]) \times w_2 \text{ , for } i = N_1 + 1, N_1 + 2,...,N_1 + N_2 \quad (6.17)$$

vector m^i is considered as solution to the unknowns when vector ε_i is sufficiently small.

For the equation (6.13), we have the solution normally:

$$\delta m = \left(A^T A\right)^{-1} A^T \varepsilon, \qquad (6.18)$$

In order to overcome the problem of singular value, I select the method of Marquardt-Levenberg to decrease the instability due to the singular value by adding the parameter λ to the diagonal of the matrix of sensibility A, so the solution is as follows:

$$\delta m = \left(A^T A + \lambda I\right)^{-1} A^T \varepsilon \ , \qquad (6.19)$$

where I is unit matrix. The convergence is monitored by the root-mean-squares (rms) error criterion

$$rms = \sqrt{\sum_{i=1}^{N} \varepsilon_i^2 / N} \qquad (6.20)$$

6.5 Normalization

Each set of data is normalized by the formula as follow:

$$Nor = \sqrt{\frac{\sum_{i=1}^{N} d_i^2}{N}}, \; i = 1,2,\ldots,N \qquad (6.21)$$

where d_i is measurement of the points, M is the number of the measurements of the points.

6.6 Weighting of the two sets of the data

As mentioned above, the weighting of the two sets of the data is very important for the joint inversion. With the L-curve idea (Christian, 2008), I derive the weighting parameters from the equation below:

$$\Phi = w_1 F + (1 - w_1) g \qquad (6.22)$$

in this equation , F is the signal of magnetic field, g is the analytic signal of the magnetic field, w_1 is weighting parameter for first set of data F , I propose a new equation :

$$w_1 \|F\| = (1 - w_1) \|g\| \qquad (6.23)$$

From (6.23), we derive the equation:

$$w_1 = \frac{\|g\|}{\|F\| + \|g\|}, \qquad (6.24)$$

$$w_2 = 1 - w_1 = \frac{\|F\|}{\|F\| + \|g\|} \qquad (6.25)$$

6.7 The convergence

The convergence of successive iterations for the joint inversion is also monitored by the root-mean-squares (rms) error criterion:

$$rms = \sqrt{\frac{\sum_{i=1}^{N_1}(Nor_1 W_1 \delta F)^2 + \sum_{i=1}^{N_2}(Nor_2 W_2 \delta g)^2}{N_1 + N_2}} \quad (6.26)$$

$$\delta F_i = F_i^{cal} - F_i^{ods} \quad (6.27)$$

$$\delta g_i = g_i^{cal} - g_i^{ods} \quad (6.28)$$

N_1 , N_2 are the numbers of the points of observations for two sets of data. Nor_1 and Nor_2 are respectively the normalizations for the two sets of the data while the W_1 and W_2 are respectively the weighting matrices for the two sets of the data. F_i^{cal}, F_i^{ods} are respectively the model responses and the observations for total magnetic field strength while g_i^{cal} and g_i^{ods} are respectively the model responses and observations for the analytic signal. The iteration procedure is terminated when rms reaches a fixed value or the number of iterations fixed.

6.8 The technique of the joint inversion

The technique for the joint inversion is almost same as that of the magnetic field inversion except that the convergence of the joint inversion is not same as that of the magnetic field, see to formula (6.26), and after that, the Jacobian matrix for joint inversion is constructed by combining the Jacobian matrix of the magnetic field and Jacobian matrix of the analytic signal by the formula below

$$A = [A_1 Nor_1 W_1 ; A_2 Nor_2 W_2] \quad (6.29)$$

The discrepancy vector for joint inversion is constructed by the differences between the initial model response and observed data of magnetic field and the

differences between the initial model response and observed data of analytic signal by the formula below

$$\delta p = [Nor_1 W_1 \delta F; Nor_2 W_2 \delta g] \qquad (6.30)$$

The outline of the joint inversion-1 is described in the flow diagram 6.1 while the outline of the joint inversion -2 is described in the flow diagram 6.2. Firstly, the initial values of parameters are estimated, and after, the initial model responses are determined, and then we could calculate the initial *rms* and initial discrepancy vector and calculate the Jacobian matrix for the two sets of the data to construct the Jacobian matrix for the joint inversion, and to start the inversion. For each iteration, the rms error is calculated to monitor λ. The inversion is terminated whenever the number of iteration becomes more than specified value or the rms becomes less than specified value.

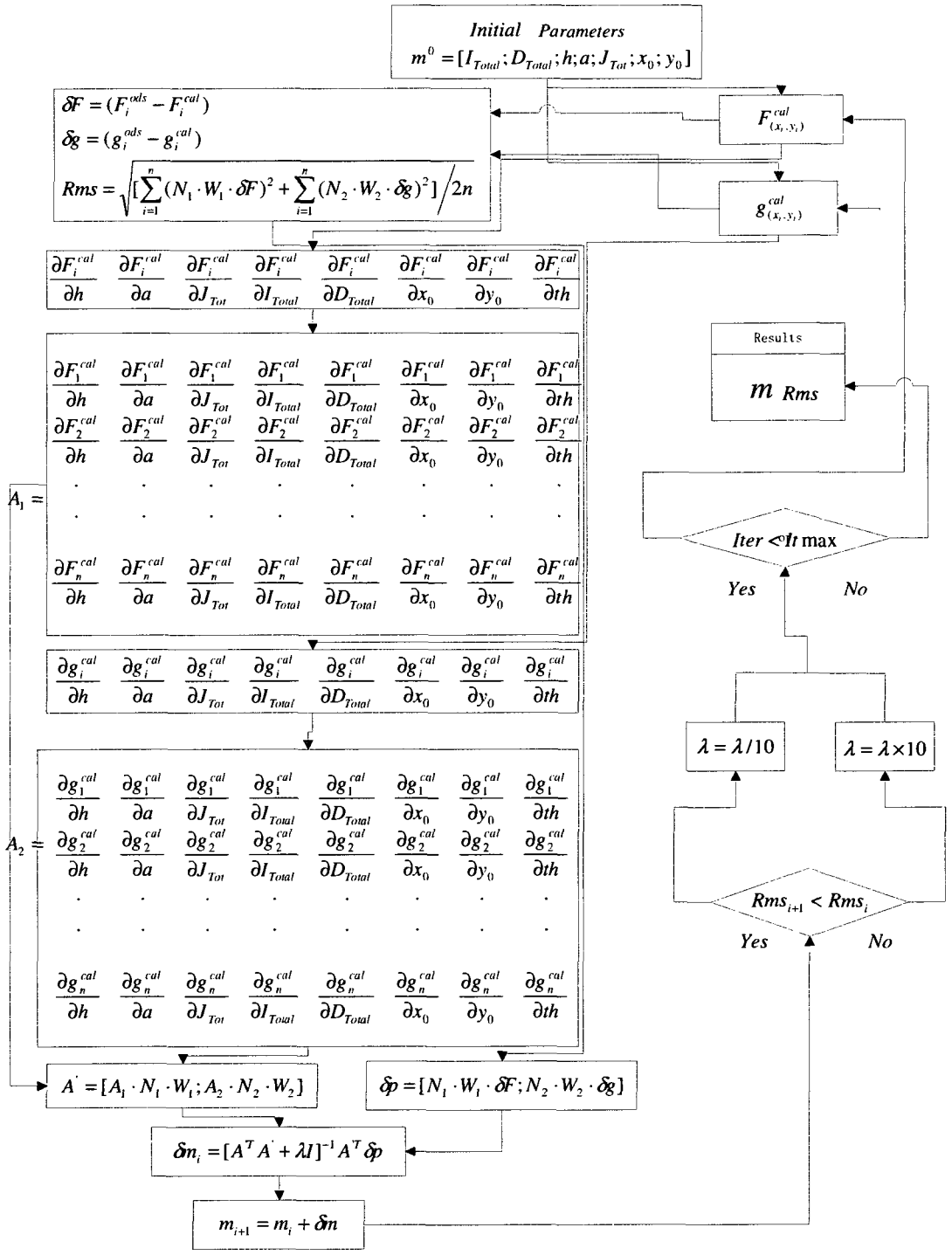

Flow Diagram 6.1 Flow diagram for joint inversion of magnetic field and analytic signal of magnetic field without remanent magnetization using Levenberg-Maquardt

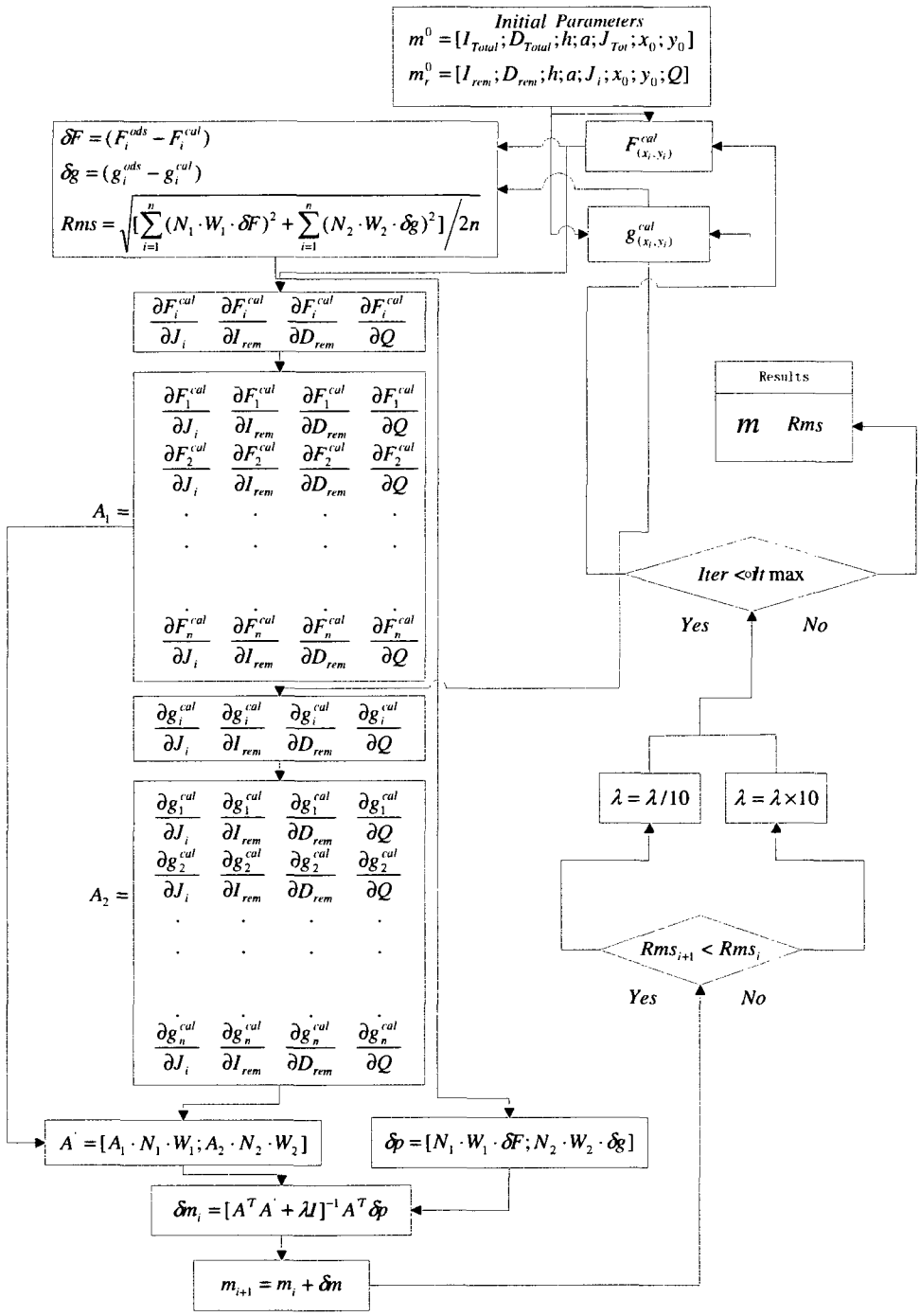

Flow Diagram 6.2 Flow diagram for joint inversion of magnetic field and analytic signal of magnetic field with remanent magnetization using Levenberg-Maquardt

6.9 Tests

The tests proceed in two steps. The first one is to test the models in absence of remanent magnetization; second step is to test the models in presence of remanent magnetization.

6.9.1 Tests for joint inversion in absence of remanent magnetization

in this section, I test the models in absence of remanent magnetization. Firstly, the validation of the algorithm of joint inversion is to be tested using the initial values calculated by Chemam (2006)'s method automatically. And after that, the robustness of this algorithm of joint inversion to changes of initial values entered manually is going to be tested.

6.9.1.1 The validation with models for joint inversion of the magnetic field and its analytic signal in absence of remanent magnetization

The models to be tested are also Defang2, Defang3 and Atestm1.

Table 6.9 Results of the joint inversion without remanent magnetization

N.	Type	Dep. (m)	Dia. (m)	In. (°)	De. (°)	Th. (m)	MSu.(SI)
Defang2	Model	50	160	69	12	200	0.01
	Initials	50	157	66	12	200	0.00900
	Results	51	160	69	12	197	0.01012
Defang5	Model	50	160	30	12	200	0.01
	Initials	48	157	31	13	202	0.00860
	Results	50	160	30	12	199	0.01005
Atestm1	Model	100	160	74	-12	300	0.01
	Initials	96	157	71	-11	304	0.00851
	Results	101	160	74	-12	296	0.01016

The images are illustrated below

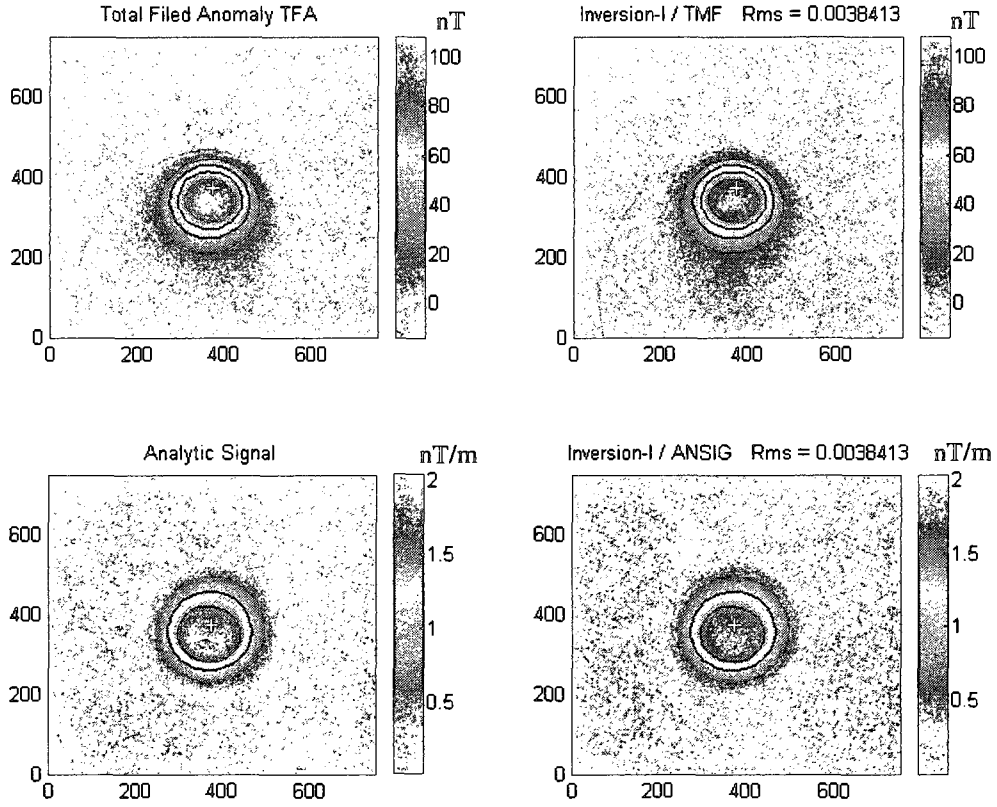

3D Model Defang2 :

- Depth = 50m
- Diameter = 160m
- Incl. $_{ter}$ = 69°
- Decl $_{ter}$ = 12°
- Magnetic Suscept.= 0.01 SI
- Coord. of centre: (375, 375)
- Depth Extension = 200m

Results of Inversion :

- Depth = 51(50)m
- Diameter = 160(157)m
- Incl. $_{tot}$ = 69°(66°)
- Decl $_{tot}$ = 12°(12°)
- Magnetic Suscept.= 0.010123 SI
- Coord. of centre: (375,375)
- Depth Extension = 197(200)m

Fig.6.1 Results of joint inversion for model Defang2

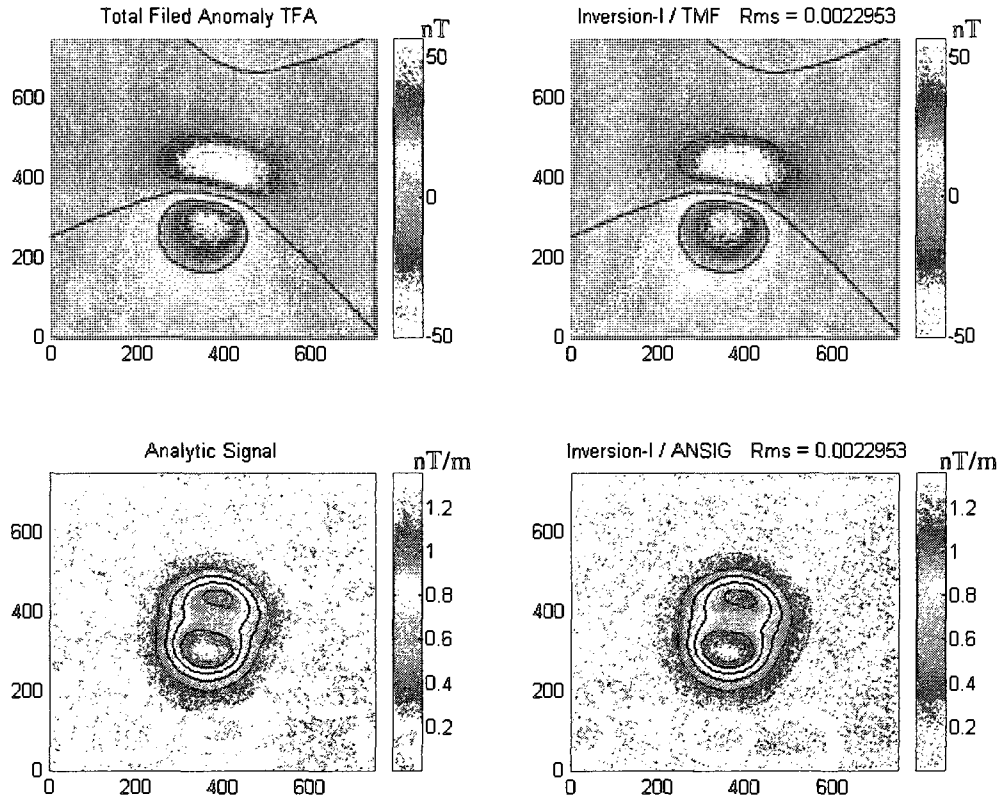

3D Model Defang5 :

- Depth = 50m
- Diameter = 160m
- Incl.$_{ter}$ = 30°
- Decl.$_{ter}$ = 12°
- Magnetic Suscept.= 0.01 SI
- Coord. of centre: (375, 375)
- Depth Extension = 200m

Results of Inversion :

- Depth = 50(48)m
- Diameter = 160(157)m
- Incl.$_{tot}$ = 30°(31°)
- Decl.$_{tot}$ = 12°(13°)
- Magnetic Suscept.= 0.010057 SI
- Coord. of centre: (375, 375)
- Depth Extension = 199(202)m

Fig.6.2 Results of joint inversion for model Defang5

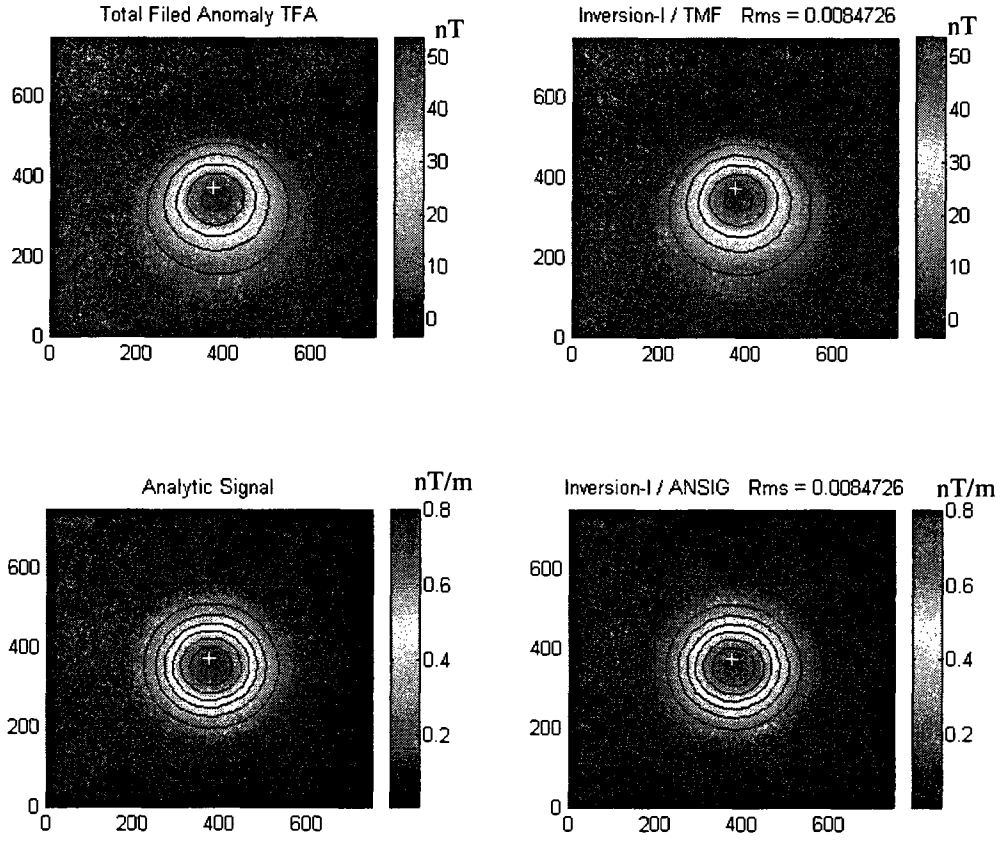

3D Model Atestm1 :

- Depth = 100m
- Diameter = 160m
- Incl. $_{ter}$ = 74°
- Decl. $_{ter}$ = -12°
- Magnetic Suscept.= 0.01 SI
- Coord. of centre: (375, 375)
- Depth Extension = 300m

Results of Inversion :

- Depth = 101(96)m
- Diameter = 160(157)m
- Incl. $_{tot}$ = 74°(71°)
- Decl. $_{tot}$ = -12°(-11°)
- Magnetic Suscept.= 0.010173 SI
- Coord. of centre: (375, 375)
- Depth Extension = 296(304)m

Fig.6.3 Results of joint inversion for model Atestm1

Table 6.10 Comparison of results of inversions without remanent magnetization

N.	Type	Dep. (m)	Dia. (m)	In. (^{0})	De. (^{0})	Th. (m)	MSu.(SI)
Defang2	Model	50	160	69	12	200	0.01
	Field Inversion	50	160	69	12	200	0.01001
	AS Inversion(1)	49	160	66	12		0.00950
	AS Inversion(2)	50	160	68	12	223	0.01001
	Joint inversion	51	160	69	12	197	0.01012
Defang5	Model	50	160	30	12	200	0.01
	Field Inversion	50	160	30	12	202	0.00989
	AS Inversion (1)	47	161	31	12		0.00880
	AS Inversion (2)	49	160	30	12	202	0.00980
	Joint inversion	50	160	30	12	199	0.01005
Atestm1	Model	100	160	74	-12	300	0.01
	Field Inversion	100	161	74	-12	304	0.00978
	AS Inversion (1)	95	161	62	-9		0.0092
	AS Inversion (2)	100	159	66	-12	305	0.01025
	Joint inversion	101	160	74	-12	296	0.01016

From the table above, the results of three models Defang2, Defang5 and Atestm1 were compared. The joint inversion of the magnetic field and its analytic signal is better than the analytic signal inversion because the results of the joint inversion are more stable and accurate than that of the analytic signal inversion, especially for the model Atestm1.The inclination of the model Atestm1 is 74° , the result of the analytic signal inversion (1) is 62°, 12° less than the solution; the result of the analytic signal inversion (2) is 66°, 8° less than the solution; the result of the joint inversion is 74°, equal to the solution. For the models with the low inclination, there are no big

differences between the results of the joint inversion and that of the analytic signal inversion. In contrast to the results of the magnetic field inversion, the accuracy of the results of the joint inversion has no obvious superiority.

6.9.1.2 The robustness of the joint inversion of the magnetic field and its analytic signal in absence of remanent magnetization to the initial values

The model Defang2 is to be tested to evaluate the sensibilities of joint inversion to initial values in the absence of remanent magnetization.

Table 6.11 Results of tests of sensibilities with initials values for joint inversion without remanent magnetization

NI.	Initials of Parameters					Results of Inversions				
	Dep.	Dia.	In.	De.	Th.	Dep.	Dia.	In.	De.	Th.
Model	50	160	69	12	200					
IC	50	157	66	12	200	51	160	69	12	197
I 1	40	157	66	12	210	51	160	69	12	196
I 2	59	157	66	12	195	51	160	69	12	197
I 3	50	151	66	12	200	51	160	69	12	197
I 4	50	170	66	12	200	51	160	69	12	197
I 5	50	157	60	12	200	50	160	69	12	197
I 6	50	157	80	12	200	51	160	69	12	196
I 7	50	157	66	6	200	51	160	69	12	197
I 8	50	157	66	18	200	51	160	68	12	197

Table 6.11 shows the robustness of the joint inversion without remanent magnetization. The model is Defang2. Compared with Table 5.4, the results of tests of sensibilities to the initial values without remanent magnetization, the robustness of joint inversion is better, especially for the results of the depth extent, the results of the analytic signal is far from the solution while the results of the joint inversion is near to the solution.

6.9.2 Tests for joint inversion in presence of remanent magnetization

In this section, the tests of the models in presence of remanent magnetization are going to be implemented. Firstly, I test the validation of the algorithm using Chemam

(2006)'s method to calculate the initial values automatically, and after, the initial values are going to be changed manually to test the robustness of the algorithm of the joint inversion of magnetic field and its analytic signal inversion to the changes of initial values.

6.9.2.1 The validation with models for joint inversion of the magnetic field and its analytic signal in presence of remanent magnetization

Results of the joint inversion for models with remanent magnetization are presented in the following table and figures: the models were tested are Vjina111t6, AteR1, Vjina111t21116 and Babneq.

Table 6.12 Results of joint inversion with remanent magnetization

N.	Type	Dep. (m)	Dia. (m)	Inr. (°)	Der. (°)	Th. (m)	MSu.(SI)
Vjina111t6	Model	60	160	1	30	300	0.01
	Initials	58	158	6	32	302	0.00985
	Results	60	160	1	30	298	0.00996
AteR1	Model	60	200	70	-30	300	0.01
	Initials	57	196	74	-32	303	0.00990
	Results	61	201	70	-30	297	0.01000
Vjina111t21116	Model	80	300	210	30	600	0.01
	Initials	82	304	205	37	598	0.00979
	Results	80	300	210	30	598	0.00995
Babneq	Model	60	160/120	30	30	300	0.01
	Initials	61	133	37	45	299	0.00965
	Results	60	137	30	29	300	0.01

The model Babneq is for testing the models other than right vertical circular cylinder. It is an oval cross-section right vertical cylinder. The long axis of it is 160m; the short axis is 120m. The results of joint inversion are better than that of each separated inversion. The depth of joint inversion is 60m, exactly equal to the true value, the depth of inversion of analytic signal is 62m and the depth of inversion of magnetic field is 61m; the result of inclination of remanent magnetization is 30°,

exactly equal to the true value, the result from inversion of analytic signal is 35° and that from inversion of magnetic field is 29°. The position of the cylinder from joint inversion is (375, 375), exactly equal to true value, that from inversion of analytic signal is (377, 379), and from inversion of magnetic field is (377, 374).

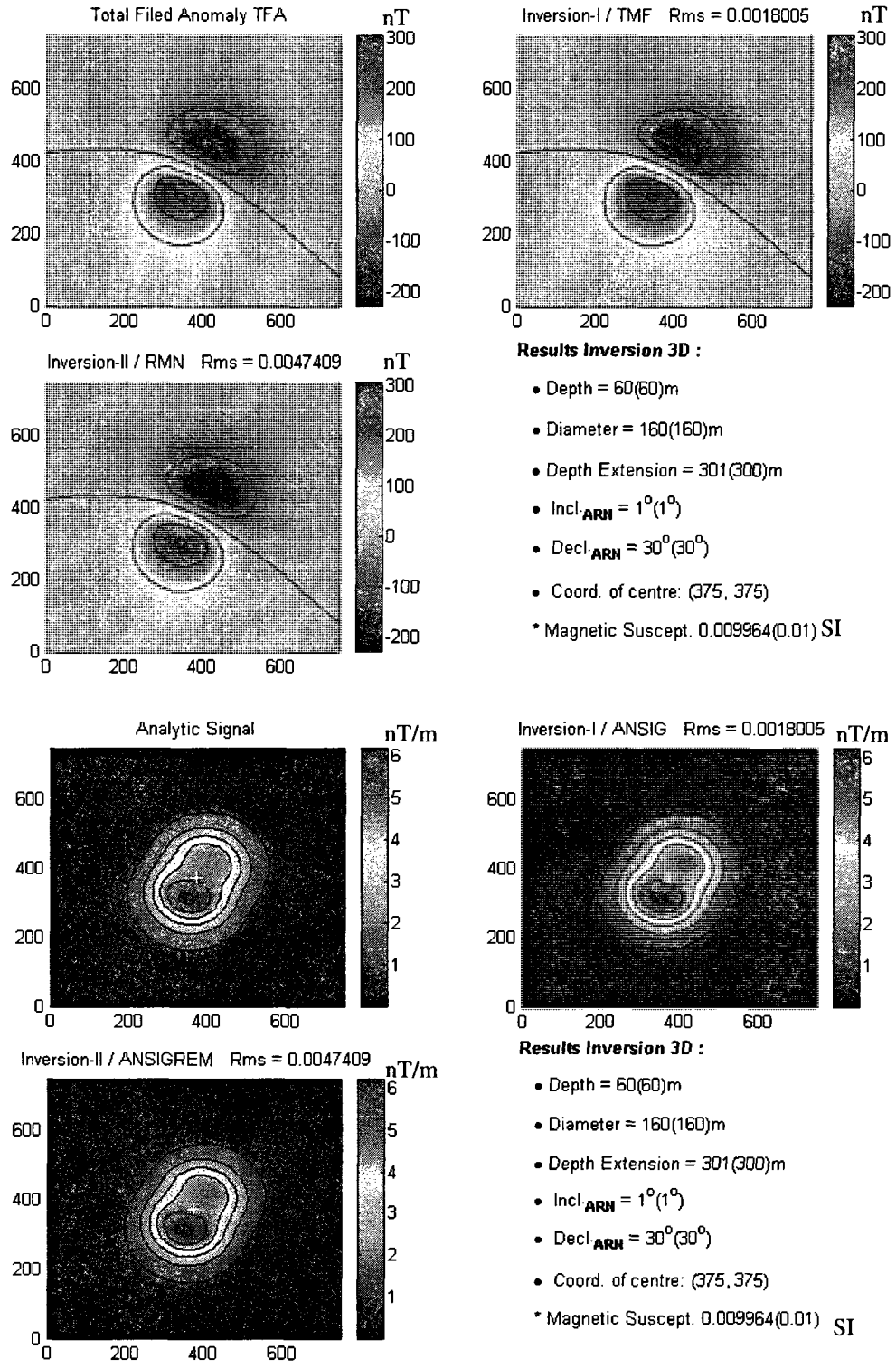

Fig.6.4 Results of joint inversion of the model Vjina111t6

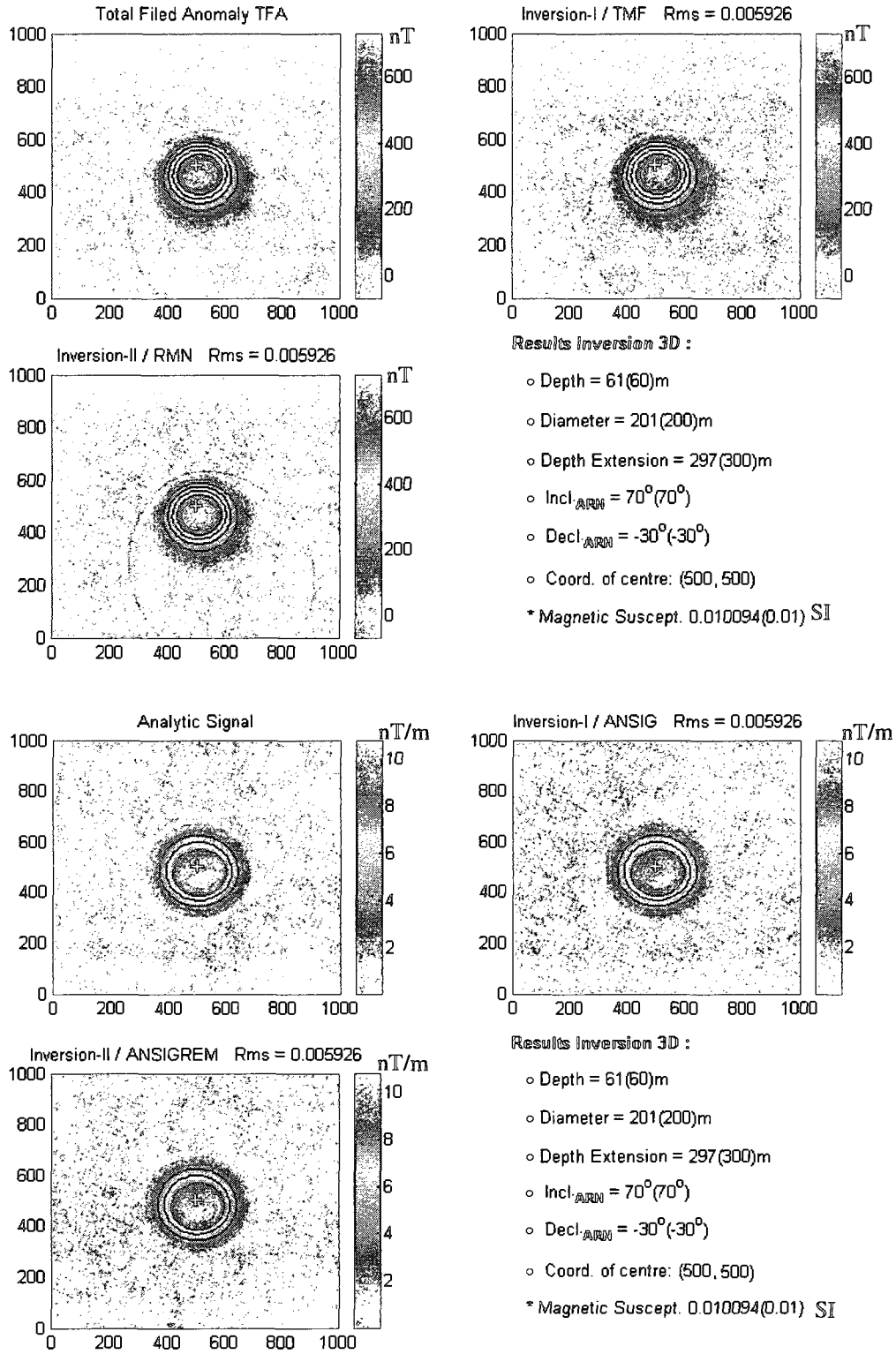

Fig.6.5 Results of joint inversion of the model AteR1

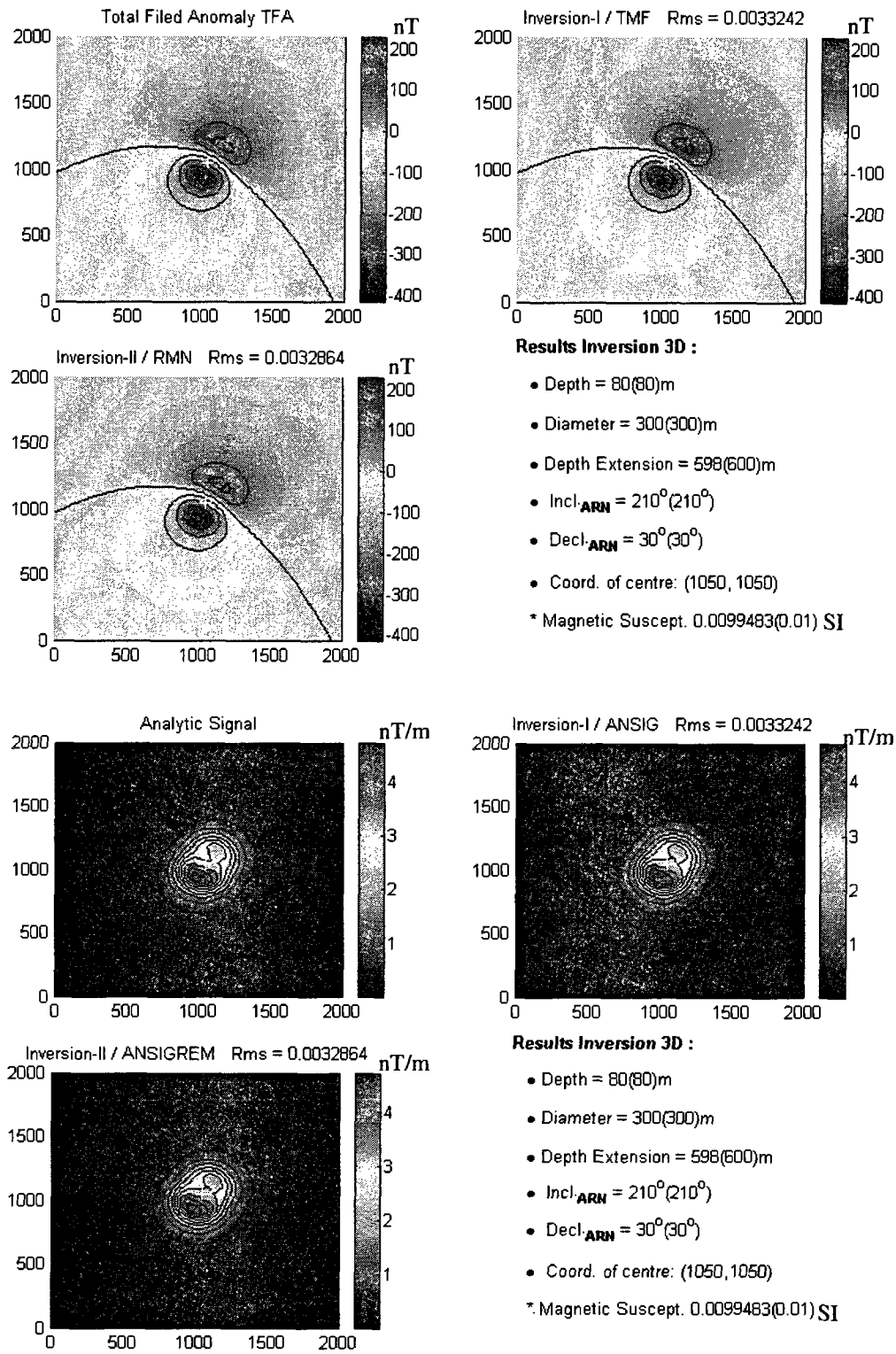

Fig.6.6 Results of joint inversion of the model Vjina111t21116

Table 6.13 Comparison of the results from all studied inversions in the presence of remanent magnetization

N.	Type	Dep. (m)	Dia. (m)	Inr. (^{0})	Der. (^{0})	Th. (m)	MSu.(m)
Vjina111t6	Model	60	160	1	30	300	0.01
	Field Inversion	60	160	1	30	300	0.00989
	AS Inversion(1)	58	161	1	30		0.00930
	AS Inversion(2)	60	160	1	30	305	0.01
	Joint inversion	60	160	1	30	298	0.00996
AteR1	Model	60	200	70	-30	300	0.01
	Field Inversion	60	200	70	-28	301	0.00988
	AS Inversion(1)	60	201	66	-28		0.00980
	AS Inversion(2)	60	201	68	-29	448	0.00988
	Joint inversion	61	201	70	-30	297	0.01
Vjina111t21116	Model	80	300	210	30	600	0.01
	Field Inversion	80	300	210	30	600	0.00989
	AS Inversion(1)	79	300	210	30		0.00962
	AS Inversion(2)	80	300	210	30	598	0.00985
	Joint inversion	80	300	210	30	598	0.00995

In the table above, we list the results for inversion of magnetic field; the results of inversion of analytic signal with method-1 (semi-infinite model); the results of inversion of analytic signal with method-2 (finite model) and the results of joint inversion. The comparison of the results of inversion by three methods is given in table 6.13. For the model Vijina111t6, Vjina111t21116, the results of the three

methods are in agreement with each other. For the model AteR1, the inclination of the remanent magnetization is high; the results of the joint inversion are more accurate than each separate inversion. The results of the three inversions in terms of geometry are agreement with each other also. The results of the joint inversion in terms of inclination and declination are more accurate than each separate inversion.

6.9.2.2 The robustness of joint inversion of the magnetic field and its analytic signal in presence of remanent magnetization to the initial values

In order to compare the results of the tests of the sensibility of joint inversion with remanent magnetization to the initial values, the same examples Vjina111t6 (Modle1) and Vjina111t3 (Model2) are tested, the results are presented in the table 6.14.

Table 6.14 Results of tests of sensibilities with initials values for joint inversion with remanent magnetization

NI.	Initials of Parameters					Results of Inversions				
	Dep	Dia.	Inr.	Der.	Th.	Dep.	Dia.	Inr.	Der.	Th.
Model.1	60	160	1	30	300					
IC	58	158	6	32	302	60	160	1	30	301
I 1	50	158	6	32	310	60	160	1	30	299
I 2	70	158	6	32	290	60	160	1	30	298
I 3	58	151	6	32	302	60	160	1	30	298
I 4	58	170	6	32	302	60	160	1	30	299
I 5	58	158	12	32	302	60	160	1	30	301
I 6	58	158	-12	32	302	60	160	1	30	301
I 7	58	158	6	20	302	60	160	1	30	301
I 8	58	158	6	40	302	60	160	1	30	301
I 9	58	158	6	32	250	60	160	1	30	298
I 10	58	158	6	32	350	60	160	1	30	298
Model.2	60	160	30	30	300					
IC	59	158	32	32	321	60	160	30	30	288
I11	80	158	32	32	321	63	158	30	30	272
I12	59	158	80	32	321	60	160	28	31	297
I11a	30	80	15	15	150	69	149	30	30	251
I11aa						62	150	30	30	275
I12a	120	320	60	60	600	46	125	24	20	599
I12aa						60	159	31	30	245

Compared with tables 5.6 and 4.4, the robustness of the joint inversion is better than that of the magnetic field inversion and the analytic signal inversion. For the model1, Vjina111t6, the results of the joint inversion of depth extent are improved, nearing the solution (300m). For the model2, Vjina111t3, when initial value of the inclination of remanent magnetization is 80°, 50° more than the solution, the result of the joint inversion is 28°, the result of the declination of joint inversion is 31°, they are more accurate that of each separate inversion (the results of the magnetic inversion are 26° and 32° while the results of the analytic signal inversion are 28° and 32°). The results of the joint inversion in terms of the inclination and declination are more accurate if the initial values of them are far away from the solution. Even all of the initial values are changed greatly (for test I11a, all of initial values are decreased to 50% of true values, for test I12a, all of initial values are increased to 200% of true values) the results of joint inversion are improved than each separated inversion. But results suggest that the initial values affect the results of inversion, the more the initial values are far from the true values, the more the results of the inversion are inaccurate.

I found a method to resolve this problem. I call this method as second inverting. The inaccuracy of the results of the inversion is due to the initial values which are far from the true values. So when I get the results of the inversion, I take these results as the initial values for the second inversion to put in the system to get the results more accurate than before. For example, the test I11aa, its initial values are the results of test I11a; the test I12aa, its initial values are the results of test I12a. We get the results of second inversion more accurate than the first inversion. Using this method to deal with the problem of initial values far away form true values needs the results of joint inversion of magnetic field and its analytic signal as the initial values, because the results of joint inversion are more stable than each separated inversion, which guarantees the results of the first inversion near the true values. By the second inversion method, we could get the results of inversion more accurate even the initial

values are far away from the true values, though by chemam' technique , we can get the initial values close to the true values.

6.9.3 Test for robustness to noise of the joint inversion

The robustness of the joint inversion in the presence of noise is tested in this section. The models tested are same as those tested previously for the inversion of the magnetic field anomaly and its analytic signal. The results of the joint inversion in the presence of noise presented in table 6.15 and the following figures:

Table 6.15 Comparison of results tested by magnetic field inversion (FI), analytic signal inversion (ASI) and joint inversion with addition of noise (2nT/5nT)

Model	Method	Inr.	Der.	Dep. (m)	Dia. (m)	Th. (m)	MSu (SI)
Vjina111t3 (2nT)	Model	30^0	30^0	60	160	300	0.01
	FI	30^0	30^0	62	159	288	0.01033
	ASI	29^0	29^0	63	159	610	0.01049
	Joint I	30^0	30^0	61	160	296	0.01016
Vjina111t3 (5nT)	FI	28^0	31^0	77	145	352	0.01678
	ASI	28^0	25^0	52	147	353	0.00665
	Joint I	32^0	30^0	61	161	339	0.00923

From Table 6.15, we conclude that the results of the magnetic inversion are as follows:

The inclination of the remanent magnetization equals to the solution (30°). The result of declination of the remanent magnetization also equals to the solution (30°). The depth of the cylinder is 62m, which is 2 meter more than that of the model. Diameter is 159 m, which is 1 meter less than that of the model; the thickness of the cylinder is 288m, which is 12 m less than that of the model. As for the analytic signal inversion, they are more in error than that of the results of the magnetic field inversion: the inclination and the declination of the remanent magnetization are 29^0,

which is 1^0 less than that of the model, the depth is 63m, 3m more than that of the model, the diameter is 159, 1m less than that of the model, and the thickness of cylinder is 610m, 310m more than that of the model. However, the joint inversion gives us better results for the inclination and the declination of the remanent magnetization. And there is 1 meter difference between the result of the inversion and that of the model for the depth, and the thickness of cylinder of 296 m is also the most precise result of the inversion. As for the susceptibility, they are always same as that of the model.

In the table 6.15, the results of inversion of the same model added 5nT of random noise are listed. The results of joint inversion are stable, and the results of inversion of magnetic field and analytic signal get more inaccurate than the results of the model added 2nT random noise. I added the random noise to 10nT, even with 10nT added, the joint inversion of magnetic field and its analytic signal get the results of inversion more accurate and stable than inversion of magnetic field and inversion of analytic signal. Off course, with increase of the noise added, the results of inversion are getting more inaccurate than before.

The method of continuation upward should be used to remove the noise when the noise level is high. I tested the model of Vjina111t3 added 10nT noise, when the data was continued upward to 30m, the noise was removed, and the good results of inversion are got.

Therefore, the results presented in the table 6.15 and figure 6.7 suggest that the robustness of the joint inversion of the magnetic field and its analytic signal, in the presence of noise, is stronger than if the magnetic field anomaly and its analytic signal are inverted separately.

Also the stability of the joint inversion in the presence of the random noise is better than that of magnetic inversion and the analytic signal inversion separately.

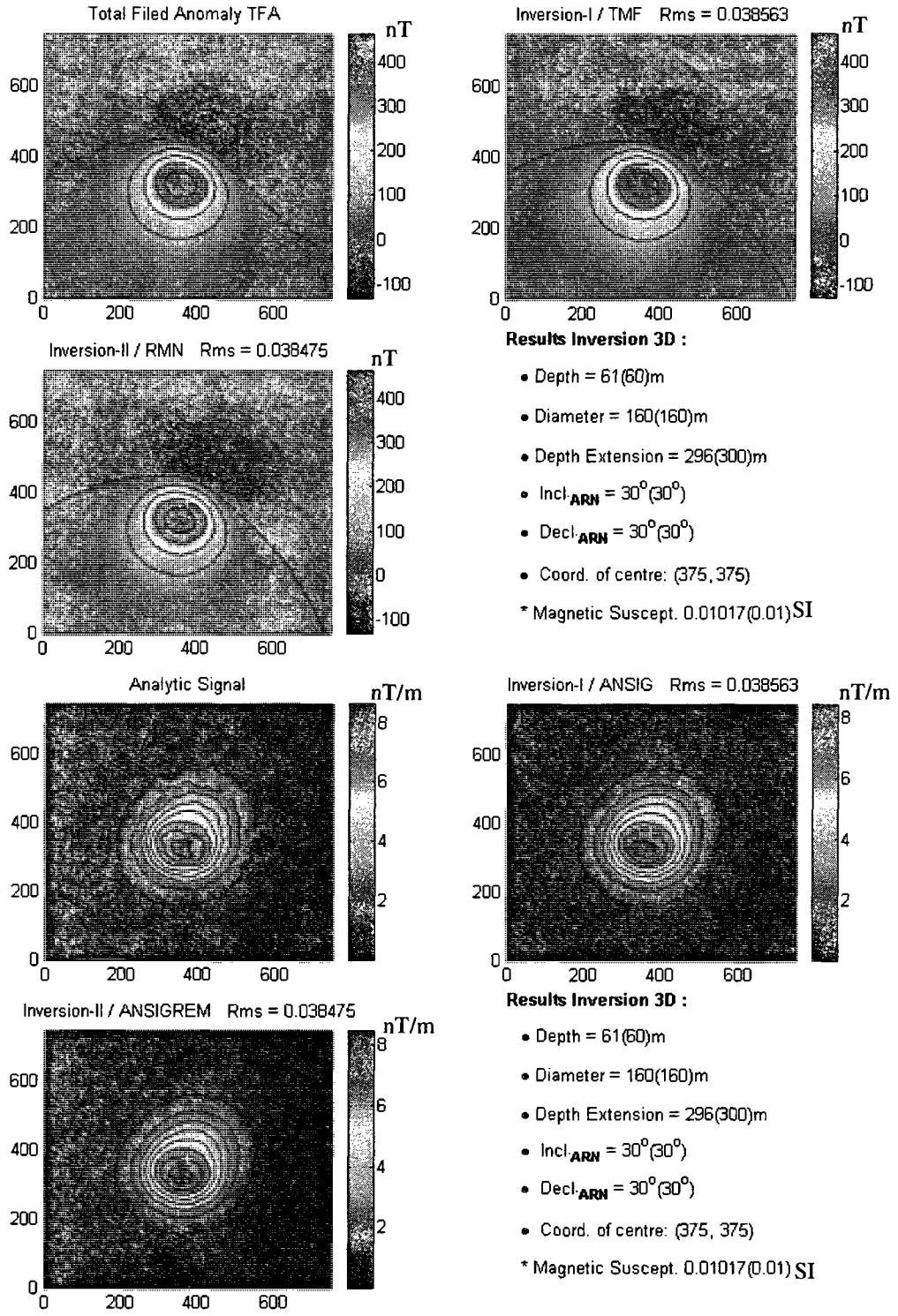

Fig.6.7 Results of joint inversion of the model Vjina111t3 with 2nT noise

6.10 Application to the real data

The Peddie kimberlite intruded Precambrian diabase sills and Paleozoic carbonate rocks approximately 153.6 Ma ago and consists of hypabyssal facies phlogopite macrocrystic monticellite kimberlite. The subcropping surface is covered by a thin (<4 m) sequence of glacial sediments consisting of 1 to 3 m of grey silty sand till overlain in places by up to 3 m of glaciolacustrine clay. The relative abundance of indicator minerals in the Peddie kimberlite is: olivine > Mg-ilmenite >> pyrope > chromite > Cr-diopside. This relative abundance is different from other kimberlites in the Lake Timiskaming field and can be used to distinguish the Peddie dispersal train from the relatively Cr-Ti-pyrope and Cr-diopside-rich dispersal trains from the Bucke and Gravel kimberlites. The high abundance of olivine in the Peddie pipe is due to it being a hypabyssal kimberlite with fresh (i.e. non-serpentinized) olivine. Olivine in the Peddie kimberlite has survived both in-situ weathering of the kimberlite and subsequent glacial transport. Unlike tropical and arid terrains of South Africa and Australia, olivine is an excellent kimberlite indicator mineral in this glaciated terrain. Mg-ilmenite in the Peddie kimberlite is characterized by extremely high MgO (most between 9 and 18 wt.%) similar to other kimberlites nearby (Gravel, Bucke) but unlike the Kirkland Lake kimberlites 80 km to the north. Till overlying the Peddie kimberlite contains a distinctive "kimberlitic" geochemical signature defined by Ni, Ba, Nb, MgO, and P2O5 which is most apparent in the coarse to very coarse sand (0.5 to 2.0 mm) size fraction.

The algorithm is applied to the Peddie Pipe found in the town of Haileybury of Ontario. The contours map of which shows a roughly circular anomaly. The grid dimension is 5×5 m, $T_0 = 56736nT$, $I_0 = 74^0$, $D_0 = -12^0$. The results of the inversion are imaged below. The method used to Peddie pipe is the method of finite model. The inversion proceeds by two steps. First step is to invert the geometry, such as the depth of the pipe, the diameter of the pipe and the depth extension of the pipe, we call it Inversion I. This is showed in the image. The second step is used to invert

the remanent magnetization, such as the direction of the remanent magnetization. We call it Inversion II. For the magnetic data of Peddie Pipe, firstly the inversion of magnetic field is used, after that, the inversion of analytic signal is used, and finally the algorithm of joint inversion of magnetic field and its analytic signal is used to it. For the joint inversion, *rms* is usually small, this is because in formula of calculation of *rms* for joint inversion (formula 6.26), the two sets of data firstly, have been normalized to remove the units of the data, and then the two sets of data are to be weighted. If the two sets of data are not normalized and weighted, like separated inversion, *rms* should be large.

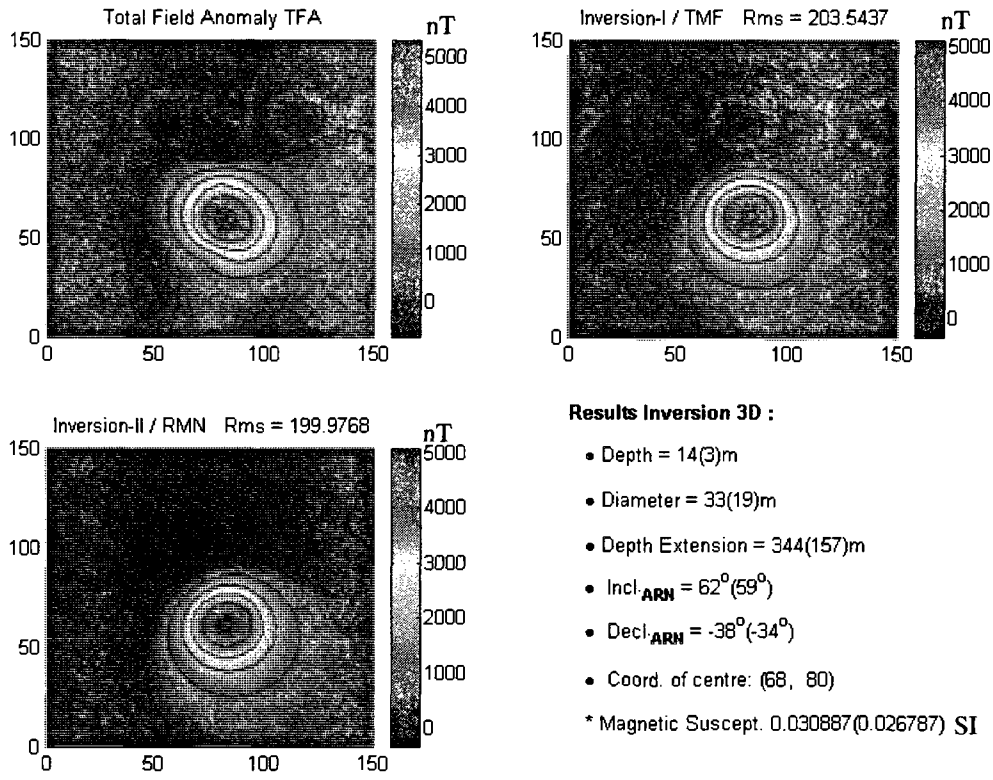

Fig.6.8 Results of the magnetic inversion for data of Peddie Pipe

Figure6.8 is for the magnetic field inversion, from the image we can see that the interpreted depth is 14m, 11m more than the initial value (3m); the interpreted

diameter is 33m, 14m more than the initial value (19m); the interpreted inclination of remanent magnetization is 62°, 3° more than the initial value (59°); the interpreted declination is -38°, -4° less than the initial value (-34°), the magnetic susceptibility is 0.0309SI. Figure 6.9 is for the analytic signal inversion, from the image we could see that there is noise with the magnetic data of Peddie Pipe, because the contour of the analytic signal is not circular there is small circular beside the big one. The inverted depth of analytic signal is 10m, the diameter is 26m, the inclination is 23°, and declination is 1°, which are from the results inverted magnetically. The results of joint inversion are better than each separated inversion (figure 6.10): The depth from joint inversion is 12m, the diameter is 34m, and inclination is 57° and declination is -28°, the magnetic susceptibility is 0.023SI.

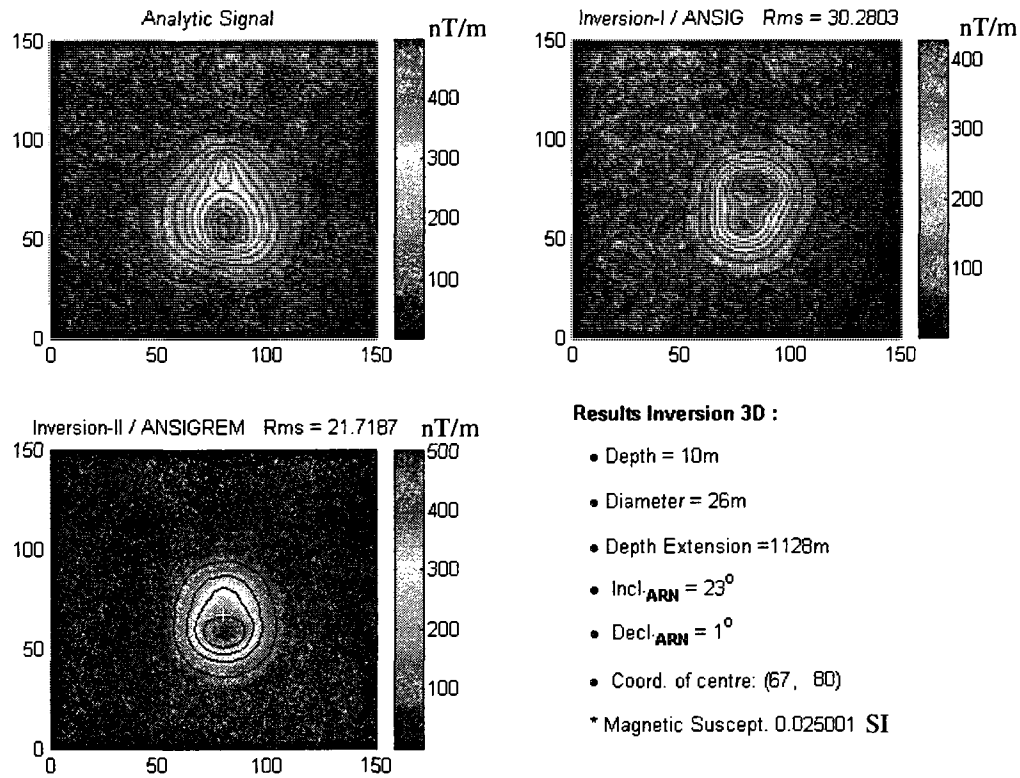

Fig.6.9 Results of the analytic signal inversion for data of Peddie Pipe

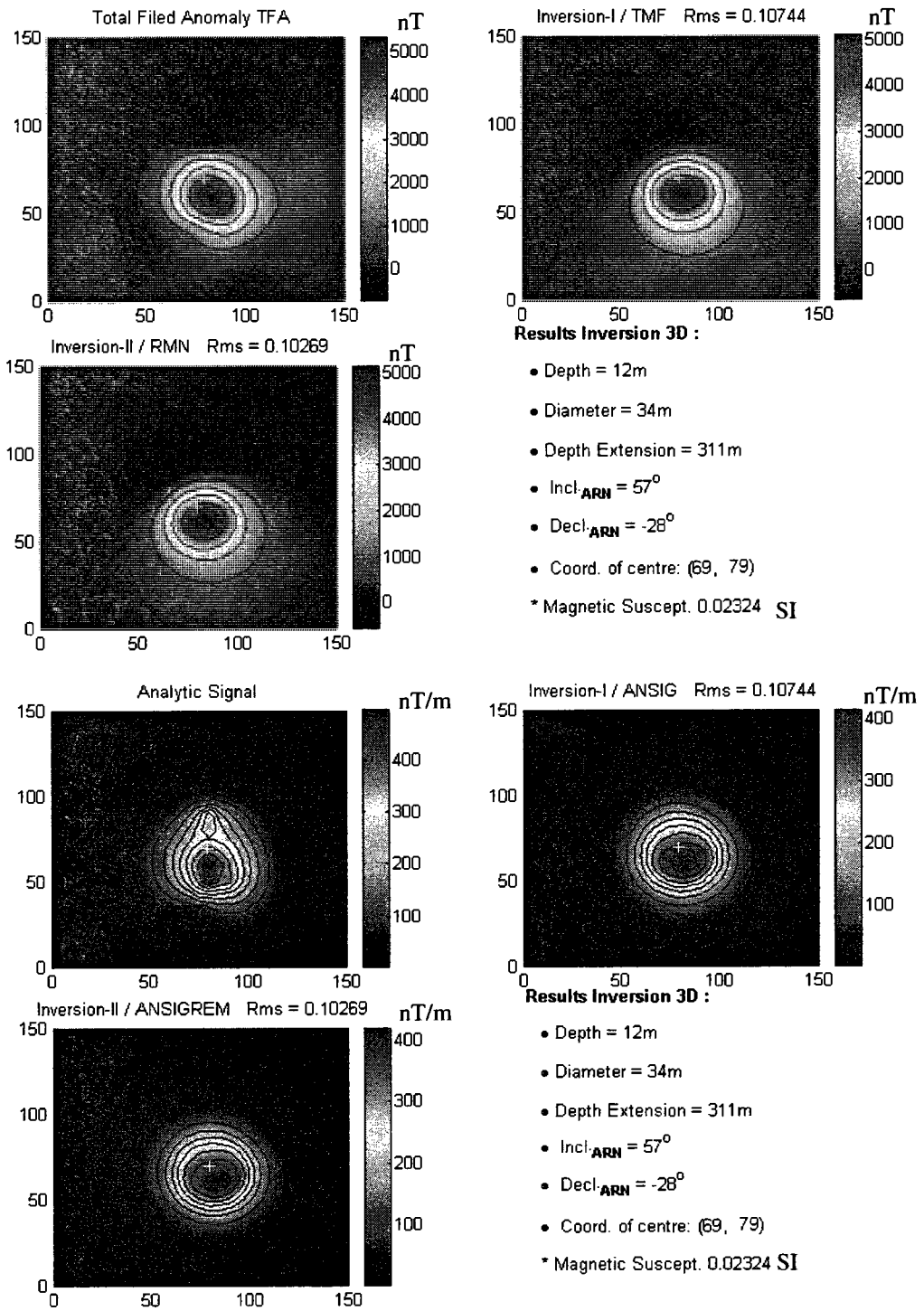

Fig.6.10 Results of the joint inversion for data of Peddie Pipe

Table 6.16 Inverted depths of magnetic data upward of Peddie Pipe

U	2	3	4	5	6	7	8	9	10	11	12	13	14	15	16	17	18
M	11	10	9	9	8	5	8	7	7	6	5	4	3	3	6	5	4
A	8	9	10	11	10	9	9	8	8	7	6	6	6	5	8	9	7
J	11	10	10	10	9	9	8	8	7	7	6	6	6	5	6	5	5

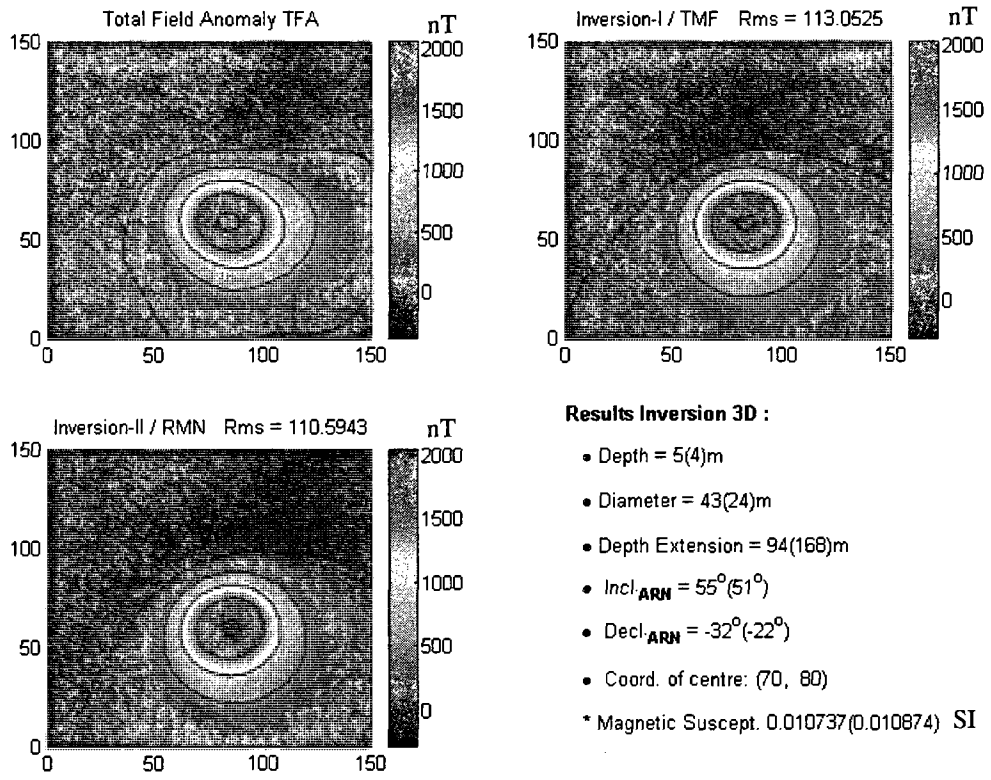

Fig.6.11 Results of the magnetic inversion for data of Peddie Pipe (12m up continuation)

There are influences which make the results of the inversion are not accurate. The Peddie Pipe is not a normal vertical circular cylinder, and there is another small source beside it. In order to reduce the influence of the influence, upward continuation of the data is implemented. The interpreted depths from the inversions of the upward continued performed magnetic data are listed in the table 6.16. In the table 6.16, U is

upward continued, M is the result of the depth of inversion of magnetic field, A is the result of the depth of inversion of analytic signal, and J is the result of the depth of joint inversion of magnetic field and its analytic signal. The magnetic data was continued upwardly by increment of 1m. The results of the joint inversion are more stable than the results of separate inversions. From the 12m of continuation upward, the interpreted depth is getting more stable, so data of 12m of continuation of upward is selected to be illustrated here in the figure 6.11, 6.12, 6.13.From Figure 6.11, 6.12 and 6.13, we can see that the influence of the noise is reduced. Figure 6.11 illustrates the results of the magnetic data for Peddie continued upward; the rms is 113, 90 less than that of inversion of original data. the interpreted depth is 5m, 1m more that the initial value of depth; the diameter is 43m ,19m more than that of the initial value of diameter; the inclination of the remanent magnetization is 55°, 4° more than initial value, and declination is -32, and the magnetic susceptibility is 0.011SI. Figure 6.12 illustrates the results of the analytic signal inversion of the data continued upward, the depth is 6m, which is 1m more that inverted by the magnetic inversion, the diameter is 33m, inclination is 28°, declination is -17°, and magnetic susceptibility is 0.011SI.

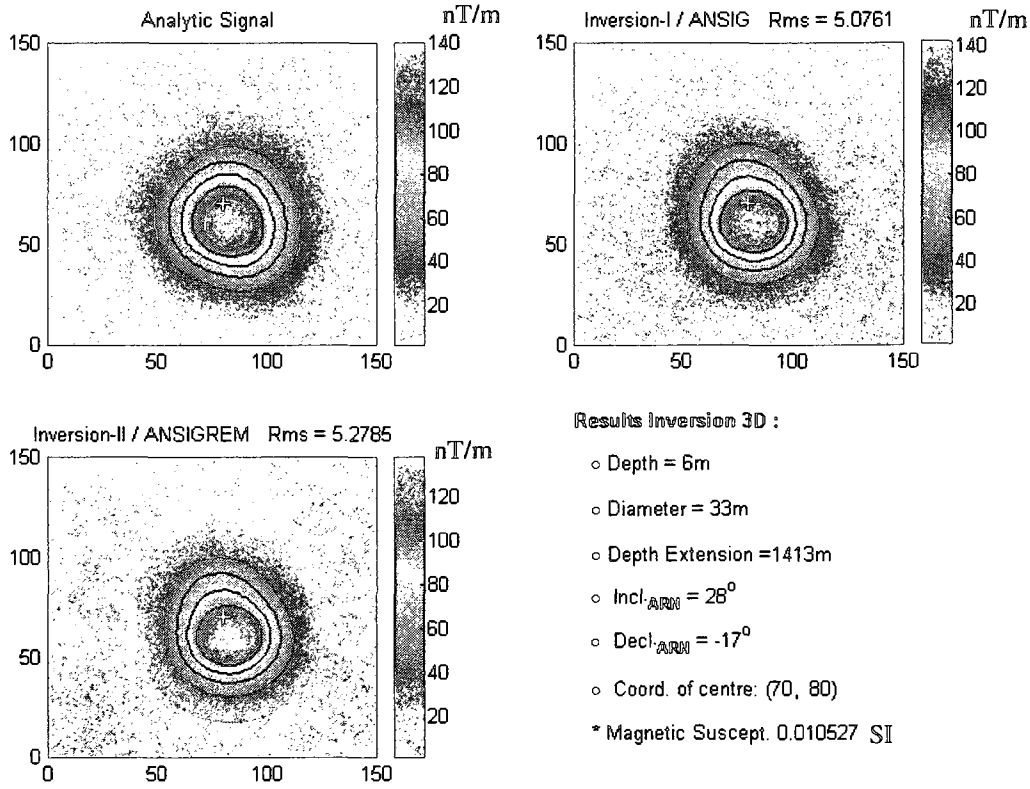

Fig.6.12 Results of the analytic signal inversion for data of Peddie Pipe (12m up continuation)

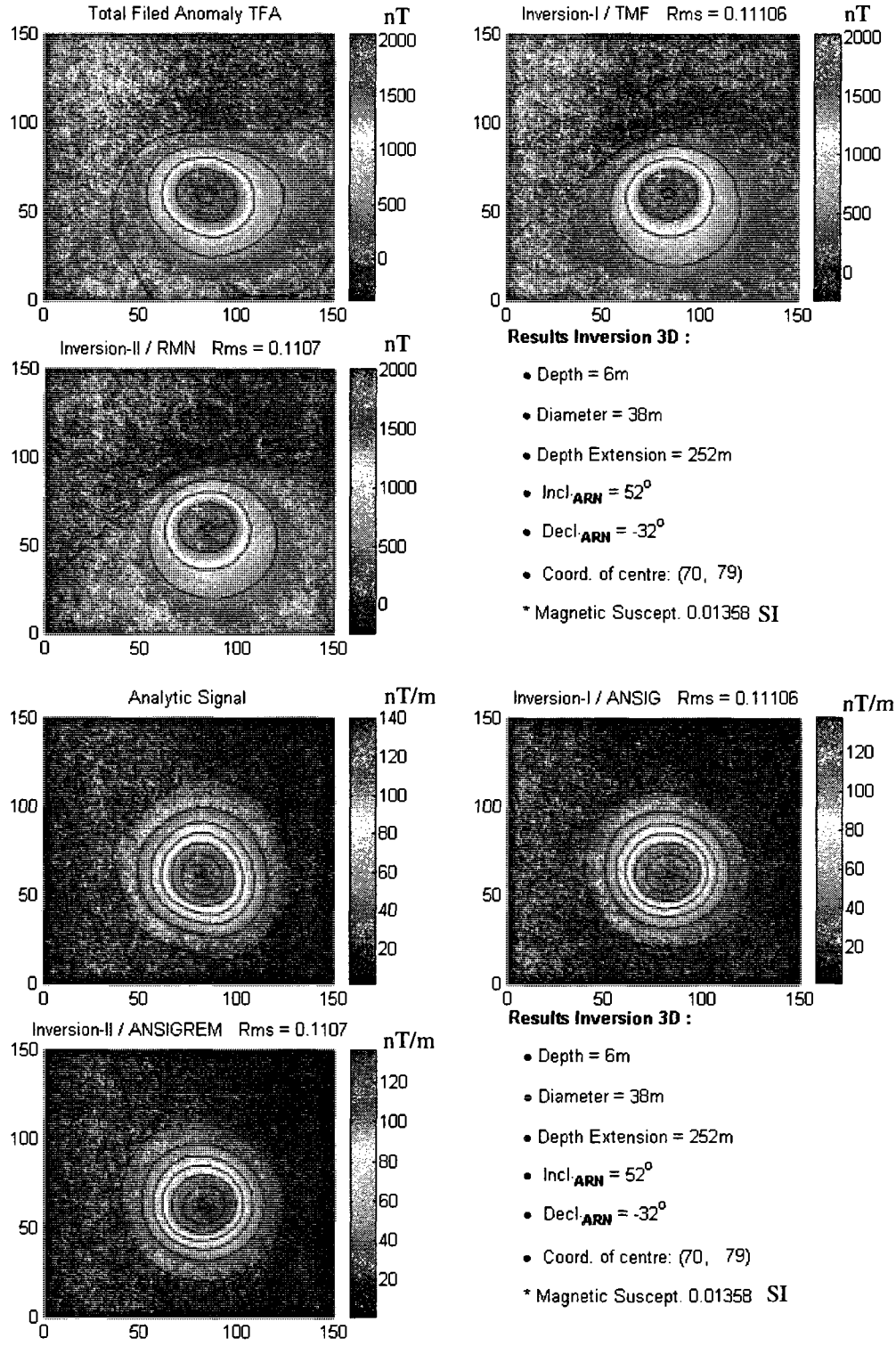

Fig.6.13 Results of the joint inversion for data of Peddie Pipe (12m up continuation)

Figure 6.13 is for joint inversion, the interpreted depth is 6m, equal to interpreted depth from analytic signal inversion, and 1m more than that of magnetic inversion; the interpreted diameter is 38m, 5m more than that of analytic signal inversion, 5m less than that of magnetic inversion; the inclination of remanent magnetization is 52°, 5° less than that inverted from the original data (57°), and the declination is -32°, 4° less than that inverted from the original data (-28°). They are comparable with each other, because the measurement point of continuation data is higher than the observation point of original data. By the analysis above, we got the results of the inversion for the Peddie Pipe are as follows: the depth of the Peddie Pipe is 6m, the diameter is 38m, the inclination of the remanent magnetization is 57^0, the declination of the remanent magnetization is -28^0, the magnetic susceptibility is 0.01358SI, and the position of the center of Peddie Pipe is (69m,79m), the depth extension is 252m.

6.11 Conclusions and discussion

Three approaches to inversion have been implemented successfully. The validation and robustness of the algorithm have been tested by synthetic and real data. The comparison of the three inversion methods shows that each one has its characteristics: the inversion of the magnetic field takes less time to compute, and the results of the inversion in terms of inclination and declination are more accurate than that derived from the analytic signal inversion alone. The inversion of the analytic signal gives the very accurate results for the geometry, such as the depth of the cylinder and the diameter. Also in the case with the remanent magnetization, it provides accurate results for the depth and diameter of the cylinder because of its weak dependence to the remanent magnetization. And for the joint inversion, with the two sets of data; the accuracy and stability of the results of the inversion are improved.

The joint inversion of magnetic field and its analytic signal is superior, in terms of stability and precision of the inversion, to the separate inversion and magnetic

anomaly and its analytic signal. Its superiority is shown when the inclination of remanent magnetization is high, the initial value of the inclination is far away from the solution and the magnetic body is deep. It is more robust in the presence of noise than the separate inversion of the magnetic field anomaly and its analytic signal.

For the joint inversion of the magnetic field and its analytic signal in absence of the remanent magnetization, the three models Defang2, Defang5 and Atestm1 that were used in the magnetic field inversion and the analytic signal inversion were tested. For the accuracy of the inversion, the joint inversion is better than that of the analytic signal inversion. For the stability, the joint inversion is superior to each separate inversion. The comparison of the results of the three inversions in absence of the presence is listed in the table6.10.

The robustness of the joint inversion in absence of the remanent magnetization was tested with the model Defang2. Compared with the analytic signal inversion, the robustness of the joint inversion in absence of the remanent magnetization is improved than that of the analytic signal inversion. The robustness of the joint inversion in absence of the remanent magnetization is detailed in the table6.11.

For the joint inversion in presence of the remanent magnetization, the three models Vjina111t6, Vjina111t21116, AteR1 and Babneq were tested. In contrast to each separate inversion, the stability of the joint inversion is better. For the results of the model Vjina111t6 and Vjina111t21116, the results of the three inversions are comparable to each other. For the model AteR1, its inclination is high; the results of the joint inversion are more accurate than that of each separate inversion. The model Babneq is used for testing the function of the algorithms of inversion to the models other than the right vertical circular cylinder. Its cross-section is oval other than circular, the joint inversion get the better results of the inversion than each separated inversion for the model Babneq. The comparison of the three inversions in presence of the remanent magnetization is detailed in the table 6.12.

The robustness of the joint inversion in presence of the remanent magnetization was tested with the same model Vjina111t6 with that used in the magnetic field inversion and the analytic signal inversion. In contrast with the magnetic field inversion and the analytic signal inversion, the joint inversion is more robust. In the test of the robustness for the analytic signal inversion, the accurate of the results of the depth extent is not good, in the test of the robustness for the joint inversion, the precision of the results of the depth extent is improved. For the model2, Vjina111t3, when the initial value of the inclination of remanent magnetization is $80°$, from away from the solution, the results of the joint inversion are most accurate. When all of the initial values of the parameters are far away from the true values, the joint inversion gets the better results of the inversion. The second inverting method is used to get the results of inversion more accurate when all of the initial values are far away from true values. The robustness test for the joint inversion is detailed in the table 6.14.

The robustness of the joint inversion in presence of the remanent magnetization and in presence of the noise was tested with the same model used in the magnetic field inversion and the analytic inversion. 2nT, 5nT random noise was added to the model Vjina111t3. The results of the joint inversion are demonstrated in the figure 6.15. The comparison of the results of the three inversions is listed in the table 6.15. It shows that the joint inversion has the best robustness in the presence of random noise, even the noise added is high to 10nT.

Chapter 7 Conclusions and discussion

7.1 Conclusions

The remanent magnetization is a factor that has hampered the magnetic method for a long time. This problem has been solved by two ways. The first one is given by Nabighian (1972, 1974) who applies the analytic signal concept to potential-field data in two dimensions and shows that the 2D analytic signal is independent of magnetization direction. But unfortunately, in three dimensions, the analytic signal is dependent on everything that the total magnetic intensity itself may depend (Xiong, 2006). The second method is given by an assumption that the remanent magnetization does not significantly alter the total magnetization direction (Li et al., 1996). They developed an algorithm, MAG3D (Li and Oldenburg, 1996) under an assumption that the remanent magnetization does not significantly alter the total magnetization direction. However, in applications such as archaeological investigations, mineral and resource exploration, and crustal and planetary studies, remanent magnetization is often strong and cannot be disregarded (Shearer, 2005).

In Canada, many of the kimberlites from the Northwest Territories have a strong remanent magnetization. So the separation of the remanent magnetization from the induced magnetization is necessary for improving the results of the interpretation of magnetic data. Chemam (2006) completed the parametric and physical property inversion of magnetic data due to a vertical right cylinder with arbitrary polarization in the presence of the remanent magnetization using the model of cylinder to separate the remanent magnetization successfully, but sometimes, the results of the inversion are not stable.

In this thesis, the derivatives of the magnetic field anomaly due to the right vertical circular cylinder with arbitrary polarization are calculated. The magnetic field inversion is improved by using calculated derivatives of the magnetic field used for

Jacobian matrix of the inversion of magnetic field and substitution a new formula for the relationship between the remanent magnetization and the induced magnetization.

An algorithm of analytic signal inversion due to a right circular vertical cylinder with arbitrary polarization in the presence of remanent magnetization is developed. The analytic signal is dependent on everything that the total magnetic intensity itself may depend, but it has a weak dependence on remanent magnetization. This makes the results of the inversion of analytic signal more stable and accurate with respect to the geometry of the cylinder and performs well in the case of remanent magnetization variations. Synthetic models and real data have been applied to this algorithm to validate its effectiveness.

Algorithm of joint inversion is developed for joint inversion of magnetic field intensity and analytic signal due to a vertical right circular cylinder with arbitrary polarization in the presence of remanent magnetization for separation of remanent magnetization. The joint inversion shows its superiority over the individual inversions of magnetic intensity and of analytic signal because of its better stability. It yields results that are more reliable and accurate especially for special situations, such as in the presence of noise, when the initial values far from the solutions, and for large inclination. The synthetic models and real data have been applied to validate the effectiveness of the joint inversion of magnetic intensity and its analytic signal.

7.2 Discussion

Each algorithm has its characteristics. For the magnetic field inversion, its advantage is a saving in computation time, but, it is not better than analytic signal inversion and joint inversion of magnetic field and its analytic signal inversion in respect of the stability and precision of the results. For analytic signal inversion, in many cases, it has superiority in respect of the stability and precision of the results of the inversion of geometry, but it has its own disadvantage, when the inclination is high, the results of inclination and declination of analytic signal inversion is getting

less accurate than magnetic field inversion. The joint inversion of magnetic field and its analytic signal is superior to each individual inversion because of its better stability; it yields the results of the inversion more reliable due to the increase of information, especially for some situations more complicated than normal, such as the high inclination of the remanent magnetization, initial values of inclination of remanent magnetization is far from the true value and in presence of noise.

With the introduction of my algorithms, it is now possible to derive the results of the inversion and interpretation of magnetic data more stable and precise than before for kimberlites survey because of the successful separation of the remanent magnetization from the induced magnetization.

The inversion algorithms that can be used in separation of the remanent magnetization are contributions to the magnetic interpretation of anomalies that are due to kimberlite pipes. The strengths and weaknesses of each inversion algorithms have been outlined.

The work of calculation of derivatives of the magnetic field presents improvements of the results of the magnetic intensity inversion and the possibility of implementing the inversion algorithm of analytic signal and the joint inversion of the magnetic inversion and its analytic signal. And, in the work of the joint inversion, the methods of normalization, the weighting of the two sets of the data have also enhanced the algorithms.

The algorithms are working for the models other than right vertical circular cylinder. The second inverting could be used to get the accurate results of inversion provided that the initial values are too far from the true values. The continuation upward could be used to get accurate results of inversion provided that the random noises are high.

The inversion algorithms that I have developed and improved are not without weaknesses. My inversion algorithms have been tested against numerous synthetic models, but the number of models is limited, and do not include all cases.

Finally, it is noted that application of inversion algorithms is needed the experience because that each inversion is unique and dependent. In each situation many factors must be studied, such as the geological condition, the incorporation of prior information, the causative body and the initial parameter values. The experience of the interpreter, such as the understanding of geology, and knowing well the circumstances of the survey, plays a very important role, it determines the final success of the works of inversion and interpretation of magnetic data.

References

Agarwal, B. N. P., and Shaw, R. K., 1996, Comment on "An analytic signal approach to the interpretation of total magnetic anomalies" by Shuang Qin: Geophysical prospecting, 44,911-914.

Atkinson, W.J. 1989. Diamond exploration philosophy, practice, and promises: A review. *Kimberlite and Related Rocks: Their Mantle-Crust Setting, Diamonds, and Diamond Exploration.*Vol.2. Edited by J.Ross, A.L.Jaques, J.Ferguson, D.H.Green, S.Y.O'Reilly, R.V. Duncan, and A.J.A.Janse.*Proceedings 4th International Kimberlite Conference, Perth, Australia, 1986.* Gelogical Society of Australia Special Publication 14.1075-1107.

Ballantyne Jr., E. J., 1980, Magnetic curve fit for a thin dike-Calculator program (TI-59): Geophysics, 45,447-455.

Barongo, J.O., 1985, Method for depth estimation and aeromagnetic vertical gradient anomalies: Geophysics, 50, 963-968.

Bhattacharyya, B. K., 1980, a generalized multibody model for inversion of magnetic anomalies: Geophysics, 45, 255-270.

Burley, A.J., and P.G. Greenwood. 1972. *Geophysical Survey over Kimberlite Pipes in Lesotho.* London: Institute of Geological Science, Geophysical Division, Applied Geophysics Unit.

Blakely, R. J., 1996, Potential theory in gravity and magnetic applications: Cambridge University Press.

Bolivar, S. L., and D. B. Brookins. 1979. Geophysical and Rb-Sr study of the prairie Creek, Arkansas, kimberlite. In Kimberlites, Diatremes and Diamonds. Edited by F.

R. Boyd and H. O. A. Meyer. Washington, DC: American Geophysical Union. 289-299.

Benech Christophe, Alain Tabbagh, and Guy Desvignes, Joint inversion of EM and magnetic data for near surface studies, Geophysics, 2002, 67(6):1729-1739.

Carlson, B. C (1979). Computing elliptic integrals by duplication. *Numerische Mathematik, 33*(1), 1-16.

Coopersmith, H.G., and R.G. Mitchell. 1989. Geology and exploration of the Rose lamproite, south-east Kansas. *Kimberlite and Related Rocks: Their Mantle-Crust Setting, Diamonds, and Diamond Exploration.* Vol.2. Edited by J. Ross, A.L.Jaques, J.Ferguson, D.H.Green, S.Y. O'Reilly, R.V. Duncan, and A.J.A. Janse.*Proceedings 4th International Kimberlite Conference, Perth, Australia.* Geological Society of Australia Special Publication 14. 1179-1191.

Cowan, D. R., Tompkins, L. A., and Cowan, C., 2000, screening kimberlite magnetic anomalies in magnetically active areas: Exploration Geophysics, 31, 66-72.

Clark, D.A., 1983. Comments on magnetic petrophysics. Bull. Aust. Soc. Explor. Geophys., 14(2):49-62.

Chemam, A., 2006, Inversion magnetique tridimensionnelle des anomalies circulaires "Kimberlitiques" isolees avec presence ou sans remanent magnetization. M.Sc A.,Ecole Polytechnique, Montréal (Canada).

Cordell, L., and A. E. McCafferty, 1989, a terracing operator for physical property mapping with potential field data: Geophysics, 54, 621-634.

Christian. H., 2008, a Matlab Package for Analysis and Solution of Discrete Ill-Posed Problems: Informatics and Mathematical Modeling Building 321, Technical University of Denmark DK-2800 Lyngby, Denmark.

Dobroka, Gyulai, A, Ormos, T, et al., Joint inversion of seismic and geo-electric data recorded in an underground coal mine. Geophysical Prospecting, 1991, 39: 643-665.

Erlich Edward I. and W. Dan Hausel, 2002. *Diamond Deposits, Origin, Exploration, and History of Discovery.*

Forrest, M., 2006. Diamond life diamond exploration in Canada. *Materials World,* 14(8), 25-27.

Gallardo-Delgado Luis A., Marco Antonio Perez-flores, and Enrique Gomez-Trevino, A versatile algorithm for joint 3D inversion of gravity and magnetic data. Geophysics, 2003, 68(3):949-959.

Gerryts, E.1967. Diamond prospecting by geophysical methods-A review of current practice. *Mining and Groundwater Geophysics.* Geological Survey of Canada Economic Report 26. 439-446.

Grant, F.S., and L. Martin, 1966, Interpretation of aeromagnetic anomalies by the use of characteristic curves: Geophysics, 31, 135-148.

Hansen, R.O., and L. Suciu, 2002, Multiple sources Euler deconvolution: Geophysics, 67, 525-535.

Hausel, W.D., and T.L.Woodzick.1981. *Geological and Geophysical Investigations of Kimberlite in the Laramie Range of Southeastern Wyoming.* Geological Survey of Wyoming Preliminary Report 18.

Hausel, W.D., M.E. McCallum, and T.L. Woodzick. 1979. *Exploration for Diamond-Bearing Kimberlite in Colorado and Wyoming: An Evaluation of Exploration Techniques.* Wyoming State Geological Survey Report of Investigations 19.

Hargraves, R.B., 1989. Paleomagnetism of Mesozoic kimberlites in Southern Africa and the Cretaceous apparent polar wander curve for Africa. J. Geophys. Res., 949B2 (:1851-1866.

Hawthorne, J. B., 1975. Model of a kimberlite pipe: Phys. And chem. of the earth. V.9, p.1-15

Hutchison, R.D., 1958, Magnetic analysis by logarithmic curves: Geophysics, 23, 749-769.

Henderson, R.G., and I.Zietz, 1948, Analysis of total magnetic intensity anomalies produced by point and line sources: Geophysics, 13,428-436.

Hsu, Shu-Kun, Sibuet, Jean-Claude, and Shyu, Chuen-Tien, 1996, High-resolution detection of geologic boundaries from potential-field anomalies: An enhanced analytic signal technique: Geophysics, 61, 373-386

Huixiang yu, Guoxiang huang, 1988, Magnetic prospecting, Central South University, Changsha, China.

Jaques, A. L., J.D. Lewis, and C.B. Smith. 1986. *The Kimberlites and Lamproites of Western Australia.* Geological Survey of Western Australia Bulletin 132

Janse, A.J.A., Downie, I.F., Reed, L.E. and Sinclair, I.G.L., 1989. Alkaline intrusions in the Hudson Bay Lowlands, Canada: exploration methods, petrology and geochemistry In: J. Ross (Editor), Kimberlites and Related Rocks. Blackwell, Melbourne, pp.1192-1202.

Jupp Vozoff K., D L, Joint inversion of geophysical data .Geophys. J.R.astr.Soc. 1975, 42: 977-991.

Jupp. D.L, Vozoff. K. Stable iterative methods for the inversion of geophysical data. Geophys.J.R.astr.Soc.1975, 42:957-976.

Keating, P., 1995, A simple technique to identify magnetic anomalies due to kimberlite pipes: Exploration and Mining Geology, 4, 121-125.

Keating, P., and M. Pilkington, 2000, Euler deconvolution of the analytic signal: 62nd Annual International Meeting, EAGE, Sonsion P0193.

Keating, P., & Sailhac, P. 2004. Use of the analytic signal to identify magnetic anomalies due to kimberlite pipes. *Geophysics*, 69(1), 180-190.

Koulomzine, T., Y. Lamontagne, and A. Nadeau, 1970, new methods for the direct interpretation of magnetic anomalies caused by inclined dikes of infinite length: Geophysics, 35, 821-830.

Litinskii, V.A. 1963a. Applications of metallometry and kappametry in prospecting for kimberlite bodies. *International Geology Review* 6:11; 2027-2035.

Litinskii, V.A. 1963b. Mesurement of magnetic susceptibility in prospecting for kimberlite pipes. *Mining Magazine* 109:137_146.

Li, Y., & Oldenbury, D.W (1996). 3-D inversion of magnetic data. *Geophysics* 61(2), 394

Menezes Paulo T.L.and Mauricio D.M.Garcia, 2007. Case History Kimberlite exploration at Serra da Canastra province, Brazil. *Geophysics* 72:3: p.M1-M5

Meju M A. Joint inversion of TEM and distorted MT sounding: some effective practical consideration, Geophysics, 1996, 61(1):56-65.

Marquardt, D.W., 1963. An algorithm for least-squares estimation of non-linear parameters, J.SIAM, 11,431-441.

Menichetti, V., and A. Guillen, 1983, Simultaneous interactive magnetic and gravity inversion: Geophysical Prospecting, 31, 929-944.

Mitchell, R.H., and S.C. Bergman.1991. *Petrology of Lamproites*. New York: Plenum Press.

Mitchell, R.H. 1986. *Kimberlites: Mineralogy, Geochemistry and Petrology*. New York: Plenum Press.

Macnae, C.J.1979.Kimberlite and exploration geophysics. Geophysics 44: 1395-1416.

Macnae, 1995.Applications of geophysics for the detection of kimberlites and lamproites, Journal of Geochemical Exploration 53:213-243.

Merrill, R. T., McElhinny, M.W., and McFadden, P. L., 1996, the magnetic field of the earth: paleomagnetism, the core, and the deep mantle: Academic Press, Inc.

Morrison, D.D., 1960. Methods for non-linear least-squares problems, and convergence proofs, tracking programs and orbit determination, proc.Jet propulsion Lab.Seminar, 1-9.

Mushayandebvu, M. F., P. van Driel, A. B. Reid, and J. D. Fairhead, 2001, Magnetic source parameters of two-dimensional structures using extended Euler deconvolution: Geophysics, 66, 814-823

Mushayandebvu, M. F., V. Lesur, A. B. Reid, and J. D. Fairhead, 2004, Grid Euler deconvolution with constraints for 2D structures: Geophysics, 69, 489-496.

Nabighian, M. N., 1972, the analytic signal of two-dimensional magnetic bodies with polygonal cross-section-Its properties and use for automated anomaly interpretation: Geophysics, 37, 507-517.

Nabighian, M.N (1974). Additional comments on the analytic signal of two dimensional magnetic bodies with polygonal cross section. *Geophysics*, 39(1), 85-92.

Nabighian, M. N., 1984, toward a three dimensional automatic interpretation of potential field data via generalized Hilbert transforms-Fundamental relations: Geophysics, 49, 780-786.

Nabighian, M. N., and R. O. Hansen, 2001, Unification of Euler and Werner deconvolution in three dimensions via the generalized Hilbert transform: Geophysics, 66, 1805-1810.

Nabighian, M. N., and V. J. S. Grauch, R. O. Hansen, T. R. LaFehr, Y. Li, J. W. Perice, J. D. Phillips, and M. E. Ruder, 2005, 75th Anniversary The historical development of the magnetic method in exploration: Geophysics, 70, No.6,P.33ND-61ND.

Naudy, H., 1971, Automatic determination of depth on aeromagnetic profiles: Geophusics, 36, 717-722.

Nixon, P.H.1981.Regional diamond exploration-Theory and practice. *Kimberlites and Diamonds.* Edited by J.D. Glover and D.I. University of Western Australia Extension Service Publication 5. 64-80

O'Brien, D. P., 1972, CompuDepth, a new method for depth-to-basement computation: Presented at the 42nd Annual International Meeting, SEG.

Parker, R. L., 1972, the rapid calculation of potential anomalies: Geophysical Journal of the Royal Astronomical Society, 31, 447-455.

Paterson, N.R., and D.A. MacFadyen.1984. An Airborne EM (INPUT)/Magnetometer Survey, State Line district, Colorado-Wyoming. Society of Mining Engineers of AIME Preprint 84-310.

Paterson, N.R., Racic, L. and Hearst, R.B., 1993. Cross-correlation of airborne EM and magnetic data for diamond exploration, In: LASI University of Arizona International conference on airborne electromagnetic method, Tucson, AZ.

Power, M., Belcourt. G., & Rockel, E (2004). Geophysical methods for kimberlite exploration in northern Canada. *Leading Edge (Tulsa, OK),* 23(11), 1124-1129

Paterson, N. R., Kwan, K. C. H., and Reford, S. W., 1991, use of Euler deconvolution in recognizing magnetic anomalies of pipe-like bodies: 61st Annual International Meeting Society Exploration Geophysicists, Expanded Abstracts, 642-645.

Pedersen, L. B., 1979, Constrained inversion of potential field data: Geophysical Prospecting, 27, 726-748

Peters, L.J., 1949, the direct approach to magnetic interpretation and its practical application: Geophysics, 14,290-320.

Pilkington, M., and D. J. Crossley, 1986, Determination of crustal interface topography from potential fields: Geophysics, 51, 1277- 1284.

Pustisek, A. M., 1990, Noniterative three dimensional inversion of magnetic data: Geophysics, 55, 782-785.

Reid, A. B., J. M. Allsop, H. Granser, A. J. Millett, and I. W. Somerton, 1990, Magnetic interpretation in three dimensions using Euler deconvolution: Geophysics, 55, 80-91.

Roest, W. R., J. Verhoef, and M. Pikington, 1992, Magnetic interpretation using the 3D analytic signal: Geophysics, 57, 116-125

Raiche A. P., Jupp. D. L. B, Rutter. H, Vozoff. K The joint use of coincident loop transient electromagnetic and schlumberger sounding to resolve layered structures. Geophysics, 50: 1618-1627.

Reynolds John M., 1997. An Introduction to Applied and Environmental Geophysics. Reynolds Geo-Sciences Ltd, U K.

Singh Krishna, S., & Sabina, F.J (1978), Magnetic anomaly due to a vertical right circular cylinder with arbitrary polarization. *Geophysics*, 43(1), 173-178.

Sarma, B. S. P., and Verma, B. K., 1996, Negative magnetization contrast in kimberlite search, Expl. Geophys. 26, 31-34.

Sarma, B.S., B.K. Verma, and S.V. Satyanarayana. 1999. Magnetic mapping of Majhgawan diamond pipe of central India. *Geophysics* 64:6:1735-1739

Sharma, P. V., 1997, Environmental and engineering geophysics: Cambridge University Press.

Serpa, L. F., and K. L. Cook, 1984, Simultaneous inversion modeling of gravity and aeromagnetic data applied to a geothermal study in Utah: Geophysics, 49, 1327-1337.

Silva, J. B. C., and G. W. Hohmann, 1983, nonlinear magnetic inversion using a random search method: Geophysics, 48, 1645-1658.

Shi, Z., 1991, an improved Naudy-based technique for estimating depth from magnetic profiles: Exploration Geophysics, 22, 357-362.

Smith, R.S., Annan, A.P/, Lemieux, J. and Pederson, R.N., 1996. Application of a modified Geotem system to reconnaissance exploration for kimberlites in the Point Lake Area, N.W.T., Canada. *Geophysics*, 61, 1, 82-92.

Skinner, E.M.W., 1986, Contrasting group 1 and group2 kimberlite petrology, towards a genetic model for kimberlites: 4th International Kimberlite Conference, Geological Society Australia, Extended Abstract Series, n.16, 202-204.

Smellie, D.W., 1956, Elementary approximations in aeromagnetic interpretation: Geophysics, 21, 1021-1040.

Shearer.E., 2005, Three- dimensional inversion of magnetic data in the presence of remanent magnetization, Masters Thesis, Department of Geophysics, Colorado School of Mines.

Telford, W. M., Geldart, L. P., and Sheriff, R. E., 1990, *Applied Geophysics* Second Edition: Cambridge University Press.

Talwani, M., 1965, Computation with the help of a digital computer of magnetic anomalies caused by bodies of arbitrary shape: Geophysics, 30, 797-817.

Thompson, D. T., 1982, EULDPH- A new technique for making computer-assisted depth estimates from magnetic data: Geophysics, 47, 31-37

Thurston, J. B., and R. S. Smith, 1997, Automatic conversion of magnetic data to depth, dip, and susceptibility contrast using the SPI method: Geophysics, 62, 807-813.

Thurston, J., J.-C. Guillon, and R. Smith, 1999, Model-independent depth estimation with the SPI method: 69th Annual International Meeting, SEG, Expanded Abstracts, 403-406.

Thurston, J. B., R. S. Smith, and J.-C. Guillon, 2002, a multimodel method for depth estimation from magnetic data: Geophysics, 67, 555-561.

Vacquier, V., N C.Steenland, R.G.Henderson, and I.Zietz, 1951, Interpretation of aeromagnetic maps: Geological Society of America, Memoir 47.

Wang, X., and R. O. Hansen, 1990, Inversion for magnetic anomalies of arbitrary three-dimensional bodies: Geophysics, 55, 1321-1326.

Werner,S., 1955,Interpretation of magnetic anomalies of sheet-like bodies, Sveriges Geologiska Undersokning, Series C, Arsbok 43, No.6.

Whitehill, D. E., 1973, Automated interpretation of magnetic anomalies using the vertical prism model: Geophysics, 38, 1070-1087.

Xiong, L., 2006, Understanding 3D analytic signal amplitude: Geophysics, 71, NO.2 P. L13-L16.

Zeyen, H., and Pous, J., 1991, A new 3D inversion algorithm for magnetic total field anomalies; Geophysical Journal International, 104, 583-591.

Zeyen, H., and J. Pous, 1993, 3D joint inversion of magnetic and gravimetric data with a priori information: Geophysical Journal International 112, 244-256.

Appendices

Appendix A: List of the models and results of the analytic inversion

Table A.17 -Parameters of the models of the vertical cylinders with remanent magnetization (1)

N^0	Parameters of IGRF $T_0 = 57170nT$; $I_0 = 74^0$; $D_0 = -12^0$						
	Parameters of the Models						
	Dep. (m)	Dia. (m)	k (SI)	$Incl._{RMN}$ (^{0})	$Decl._{RMN}$ (^{0})	Center (m)	Q
Vjina111	60	160	0.01	60	30	(375,375)	5
Vjina111t1	60	160	0.01	50	30	(375,375)	5
Vjina111t2	60	160	0.01	40	30	(375,375)	5
Vjina111t3	60	160	0.01	30	30	(375,375)	5
Vjina111t4	60	160	0.01	20	30	(375,375)	5
Vjina111t5	60	160	0.01	10	30	(375,375)	5
Vjina111t6	60	160	0.01	1	30	(375,375)	5
Vjina111t7	60	160	0.01	70	30	(375,375)	5
Vjina111t8	60	160	0.01	80	30	(375,375)	5
Vjina111t9	60	160	0.01	90	30	(375,375)	5
Vjina111t10	60	160	0.01	100	30	(375,375)	5
Vjina111t11	60	160	0.01	110	30	(375,375)	5
Vjina111t12	60	160	0.01	120	30	(375,375)	5
Vjina111t13	60	160	0.01	130	30	(375,375)	5
Vjina111t14	60	160	0.01	140	30	(375,375)	5
Vjina111t15	60	160	0.01	150	30	(375,375)	5
Vjina111t16	60	160	0.01	160	30	(375,375)	5
Vjina111t17	60	160	0.01	170	30	(375,375)	5
Vjina111t18	60	160	0.01	180	30	(375,375)	5
Vjina111t19	60	160	0.01	190	30	(375,375)	5
Vjina111t20	60	160	0.01	200	30	(375,375)	5
Vjina111t21	60	160	0.01	210	30	(375,375)	5
Vjina111t22	60	160	0.01	220	30	(375,375)	5
Vjina111t23	60	160	0.01	230	30	(375,375)	5
Vjina111t24	60	160	0.01	240	30	(375,375)	5
Vjina111t25	60	160	0.01	250	30	(375,375)	5
Vjina111t26	60	160	0.01	260	30	(375,375)	5
Vjina111t27	60	160	0.01	270	30	(375,375)	5

Table A.18 -Parameters of the models of the vertical cylinders with remanent magnetization (2)

Vjina111t28	60	160	0.01	280	30	(375,375)	5
Vjina111t29	60	160	0.01	290	30	(375,375)	5
Vjina111t29	60	160	0.01	290	30	(375,375)	5
Vjina111t31	60	160	0.01	310	30	(375,375)	5
Vjina111t32	60	160	0.01	320	30	(375,375)	5
Vjina111t33	60	160	0.01	330	30	(375,375)	5
Vjina111t34	60	160	0.01	340	30	(375,375)	5
Vjina111t35	60	160	0.01	350	30	(375,375)	5
Vjina111t36	60	160	0.01	360	30	(375,375)	5

Table A.19 -Parameters of the models of the vertical cylinders with remanent magnetization (1)

N^0	Parameters of IGRF $T_0 = 57170nT$; $I_0 = 74^0$; $D_0 = -12^0$						
	Parameters of the Models						
	Dep. (m)	Dia. (m)	k (SI)	$Incl._{RMN}$ (^{0})	$Decl._{RMN}$ (^{0})	Center (m)	Q
Dect1	60	160	0.01	30	0	(375,375)	5
Dect2	60	160	0.01	30	10	(375,375)	5
Dect3	60	160	0.01	30	20	(375,375)	5
Dect4	60	160	0.01	30	30	(375,375)	5
Dect5	60	160	0.01	30	40	(375,375)	5
Dect6	60	160	0.01	30	50	(375,375)	5
Dect7	60	160	0.01	30	60	(375,375)	5
Dect8	60	160	0.01	30	70	(375,375)	5
Dect9	60	160	0.01	30	80	(375,375)	5
Dect10	60	160	0.01	30	90	(375,375)	5
Dect11	60	160	0.01	30	100	(375,375)	5
Dect12	60	160	0.01	30	110	(375,375)	5
Dect13	60	160	0.01	30	120	(375,375)	5
Dect14	60	160	0.01	30	130	(375,375)	5
Dect15	60	160	0.01	30	140	(375,375)	5
Dect16	60	160	0.01	30	150	(375,375)	5
Dect17	60	160	0.01	30	160	(375,375)	5
Dect18	60	160	0.01	30	170	(375,375)	5
Dect19	60	160	0.01	30	180	(375,375)	5

Table A.20 -Parameters of the models of the vertical cylinders with remanent magnetization (2)

Dect20	60	160	0.01	30	-170	(375,375)	5
Dect21	60	160	0.01	30	-160	(375,375)	5
Dect22	60	160	0.01	30	-150	(375,375)	5
Dect23	60	160	0.01	30	-140	(375,375)	5
Dect24	60	160	0.01	30	-130	(375,375)	5
Dect25	60	160	0.01	30	-120	(375,375)	5
Dect26	60	160	0.01	30	-110	(375,375)	5
Dect27	60	160	0.01	30	-100	(375,375)	5
Dect28	60	160	0.01	30	-90	(375,375)	5
Dect29	60	160	0.01	30	-80	(375,375)	5
Dect30	60	160	0.01	30	-70	(375,375)	5
Dect31	60	160	0.01	30	-60	(375,375)	5
Dect32	60	160	0.01	30	-50	(375,375)	5
Dect33	60	160	0.01	30	-40	(375,375)	5
Dect34	60	160	0.01	30	-30	(375,375)	5
Dect35	60	160	0.01	30	-20	(375,375)	5
Dect36	60	160	0.01	30	-10	(375,375)	5

Table A.21 -Results of analytic signal inversions of the models (1)

N^0	Parameters of IGRF $T_0 = 57170nT$; $I_0 = 74^0$; $D_0 = -12^0$				
	Parameters of the Models				
	Depth (m)	Diameter (m)	$Incl._{RMN}$ (^{0})	$Decl._{RMN}$ (^{0})	Center (m)
Vjina111	60/60	160/160	60/56	30/26	(377,375)
Vjina111t1	60/60	160/160	50/47	30/28	(377,375)
Vjina111t2	60/59	160/160	40/38	30/29	(376,375)
Vjina111t3	60/59	160/160	30/28	30/29	(376,375)
Vjina111t4	60/59	160/160	20/19	30/29	(376,375)
Vjina111t5	60/58	160/161	10/10	30/30	(375,375)
Vjina111t6	60/58	160/161	1/1	30/30	(375,375)
Vjina111t7	60/60	160/160	70/65	30/23	(378,375)
Vjina111t8	60/61	160/160	80/75	30/16	(378,374)
Vjina111t9	60/61	160/160	90/85	30/-9	(378,375)
Vjina111t10	60/62	160/160	100/97	30/57	(377,374)
Vjina111t11	60/62	160/160	110/110	30/37	(376,374)

Table A.22 -Results of analytic signal inversions of the models (2)

Vjina111t12	60/61	160/160	120/124	30/32	(374,373)
Vjina111t13	60/61	160/160	130/135	30/30	(373,373)
Vjina111t14	60/59	160/158	140/133	30/31	(375,375)
Vjina111t15	60/60	160/159	150/153	30/30	(374,374)
Vjina111t16	60/59	160/159	160/162	30/30	(375,375)
Vjina111t17	60/58	160/160	170/169	30/32	(375,375)
Vjina111t18	60/58	160/161	180/180	30/30	(375,375)
Vjina111t19	60/58	160/160	190/190	30/30	(375,375)
Vjina111t20	60/57	160/162	200/200	30/30	(375,375)
Vjina111t21	60/58	160/161	210/210	30/30	(375,375)
Vjina111t22	60/59	160/160	220/219	30/30	(376,375)
Vjina111t23	60/59	160/159	230/228	30/29	(376,375)
Vjina111t24	60/60	160/159	240/237	30/28	(377,375)
Vjina111t25	60/59	160/158	250/254	30/33	(375,375)
Vjina111t26	60/59	160/158	260/261	30/32	(375,375)
Vjina111t27	60/59	160/158	270/269	30/-8	(375,375)
Vjina111t28	60/62	160/159	280/281	30/33	(375,374)
Vjina111t29	60/61	160/159	290/294	30/29	(373,374)
Vjina111t30	60/60	160/159	300/304	30/29	(373,374)
Vjina111t31	60/60	160/159	310/313	30/30	(374,374)
Vjina111t32	60/59	160/159	320/322	30/30	(375,375)
Vjina111t33	60/59	160/160	330/331	30/30	(375,375)
Vjina111t34	60/58	160/161	340/340	30/30	(375,375)
Vjina111t35	60/58	160/161	350/350	30/30	(375,375)
Vjina111t36	60/58	160/161	360/360	30/30	(375,375)

Table A.23 -Results of analytic signal inversions of the models (1)

N^0	Parameters of IGRF $T_0 = 57170nT$; $I_0 = 74^0$; $D_0 = -12^0$				
	Parameters of the Models				
	Depth (m)	Diameter (m)	$Incl._{RMN}$ (^{0})	$Decl._{RMN}$ (^{0})	Center (m)
Dect1	60/59	160/160	30/28	0/0	(376,375)
Dect2	60/59	160/160	30/28	10/10	(376,375)
Dect3	60/59	160/160	30/28	20/20	(375,375)
Dect4	60/59	160/160	30/28	30/29	(376,375)
Dect5	60/59	160/160	30/28	40/39	(376,375)

Table A.24 -Results of analytic signal inversions of the models (2)

Dect6	60/59	160/160	30/28	50/49	(376,375)
Dect7	60/59	160/160	30/28	60/59	(376,375)
Dect8	60/58	160/159	30/34	70/69	(375,375)
Dect9	60/59	160/160	30/28	80/79	(376,376)
Dect10	60/60	160/160	30/28	90/90	(376,376)
Dect11	60/60	160/160	30/28	100/100	(375,375)
Dect12	60/60	160/159	30/27	110/110	(375,375)
Dect13	60/60	160/159	30/27	120/120	(375,375)
Dect14	60/60	160/159	30/27	130/130	(374,376)
Dect15	60/60	160/159	30/27	140/140	(374,376)
Dect16	60/60	160/159	30/27	150/150	(374,376)
Dect17	60/60	160/159	30/27	160/160	(374,375)
Dect18	60/60	160/159	30/27	170/170	(374,375)
Dect19	60/60	160/159	30/27	180/180	(374,375)
Dect20	60/60	160/159	30/27	-170/-170	(374,375)
Dect21	60/60	160/159	30/27	-160/-160	(374,374)
Dect22	60/60	160/159	30/27	-150/-150	(374,374)
Dect23	60/60	160/159	30/27	-140/-140	(374,374)
Dect24	60/60	160/160	30/27	-130/-130	(375,374)
Dect25	60/60	160/160	30/28	-120/-120	(375,374)
Dect26	60/59	160/160	30/28	-110/-109	(375,374)
Dect27	60/59	160160	30/28	-100/-99	(375,374)
Dect28	60/59	160/160	30/28	-90/-89	(376,374)
Dect29	60/59	160/160	30/28	-80/-79	(376,374)
Dect30	60/59	160/160	30/28	-70/-69	(376,374)
Dect31	60/59	160/160	30/28	-60/-59	(376,374)
Dect32	60/59	160/160	30/28	-50/-50	(376,375)
Dect33	60/59	160/160	30/28	-40/-40	(376,375)
Dect34	60/59	160/160	30/28	-30/-30	(376,375)
Dect35	60/59	160/160	30/28	-20/-20	(376,375)
Dect36	60/59	160/160	30/28	-10/-10	(376,375)

Appendix B: Analytic expressions of the *a* derivative of the anomaly due to a vertical right circular cylinder with arbitrary polarization

(Please see to the original article Magnetic Anomaly Due To a Vertical Right Circular Cylinder with Arbitrary Polarization from Geophysics Vol.43, No1, and P.173-178)

The main expression is as follow:

$F = 2\pi a J_{tot}[(C-A)I(1,0;0)-(E-A)I(1,1;1)-BI(1,1;0)]$, Included:

$C = nN$,

$A = lL\cos^2\theta + (lM+mL)\sin\theta\cos\theta + mM\sin^2\theta$,

$E = lL\sin^2\theta - (lM+mL)\sin\theta\cos\theta + mM\cos^2\theta$,

$B = (lN+nL)\cos\theta + (mN+nM)\sin\theta$,

$l = \cos I\cos D$,

$m = \cos I\sin D$,

$n = \sin I$,

$L = \cos I_m \cos D_m$,

$M = \cos I_m \sin D_m$,

$N = \sin I_m$,

$$I(1,0;0) = \begin{cases} I100u1 + I100u2 + I100u3, & (a > r) \\ I100m1 + I100m2, & (a = r) \\ I100d1 + I100d2, & (a < r) \end{cases}$$

Included:

$$I100u1 = -\frac{kz}{4a\sqrt{ar}}F_0(k),$$

$$I100u2 = -\frac{1}{2a}\Lambda_0(\beta,k),$$

$$I100u3 = \frac{1}{a},$$

$$I100m1 = -\frac{kz}{4a^2}F_0(k),$$

$$I100m2 = \frac{1}{2a},$$

$I100d1 = I100u1$,

$I100d2 = -I100u2$,

$$I(1,1;1) = \begin{cases} I111u1 + I111u2 + I111u3 + I111u4, & (a > r) \\ I111m1 + I111m2 + I111m3, & (a = r) \\ I111d1 + I111d2 + I111d3 + I111d4, & (a < r) \end{cases}$$

Included:

$$I111u1 = \frac{zE_0(k)}{2k\sqrt{ar}},$$

$$I111u2 = -\frac{kz}{4ar\sqrt{ar}}(a^2 + r^2 + \frac{z^2}{2})F_0(k),$$

$$I111u3 = \frac{a^2 - r^2}{4ar}\Lambda_0(\beta, k),$$

$$I111u4 = \frac{r}{2a},$$

$$I111m1 = \frac{zE_0(k)}{2ka},$$

$$I111m2 = -\frac{kz}{4a^3}(2a^2 + \frac{z^2}{2})F_0(k),$$

$$I111m3 = \frac{1}{2},$$

$$I111d1 = I111u1,$$
$$I111d2 = I111u2,$$
$$I111d3 = -I111u3,$$

$$I111d4 = \frac{a}{2r},$$

$$I(1,1;0) = I110$$

Included:

$$I110 = \frac{1}{k\sqrt{ar}}[(1 - \frac{k^2}{2})F_0(k) - E_0(k)],$$

Now, the task is to get a derivatives of $I100u1$, $I100u2$, $I100u3$, $I100m1$, $I100m2$, $I100d1$, $I100d2$, $I111u1$, $I111u2$, $I111u3$, $I111u4$, $I111m1$, $I111m2$, $I111m3$, $I111d1$, $I111d2$, $I111d3$, $I111d4$ and $I110$.

In order to get them, first of all, we need to get the a derivatives of k, β and $K(k)$, $E(k)$.

$$k^2 = \frac{4ar}{(a+r)^2 + z^2},$$

$$\sin^2\beta = \frac{z^2}{(a-r)^2 + z^2},$$

$$F_0(k) = \frac{2}{\pi}K(k),$$

$$E_0(k) = \frac{2}{\pi} E(k),$$

$$K(k) = K(\frac{\pi}{2}, k) = \int_0^{\frac{\pi}{2}} \frac{d\varphi}{\sqrt{1 - k^2 \sin^2 \varphi}},$$

$$E(k) = E(\frac{\pi}{2}, k) = \int_0^{\frac{\pi}{2}} \sqrt{1 - k^2 \sin^2 \varphi} d\varphi,$$

And:

$$\Lambda_0(\beta, k) = \frac{2}{\pi}[K(k)E(\beta, \sqrt{1-k^2}) + (E(k) - K(k))K(\beta, \sqrt{1-k^2})],$$

$$dka = \frac{\partial k}{\partial a} = \frac{1}{2\sqrt{k}} \frac{4r[(a+r)^2 + z^2] - 8ar(a+r)}{[(a+r)^2 + z^2]^2},$$

$$dEa = \frac{\partial E(k)}{\partial a} = \frac{dka[E(k) - K(k)]}{k},$$

$$dKa = \frac{\partial K(k)}{\partial a} = \frac{dka[E(k) - (1-k^2)K(k)]}{k(1-k^2)},$$

$$d1k2a = \frac{\partial(\sqrt{1-k^2})}{\partial a} = -\frac{dka \cdot k}{\sqrt{1-k^2}},$$

$$d\beta a = \frac{\partial \beta}{\partial a} = \sqrt{\frac{(a-r)^2 + z^2}{(a-r)^2}} \cdot \sqrt{\frac{(a-r)^2 + z^2}{z^2}} \cdot \frac{(r-a)z^2}{[(a-r)^2 + z^2]^2},$$

$$dE\beta 1k2a = \frac{\partial E(\beta, \sqrt{1-k^2})}{\partial a} = \frac{\partial E(\beta, \sqrt{1-k^2})}{\partial \beta} \cdot \frac{\partial \beta}{\partial a} + \frac{\partial E(\beta, \sqrt{1-k^2})}{\partial(\sqrt{1-k^2})} \cdot \frac{\partial(\sqrt{1-k^2})}{\partial a},$$

$$dK\beta 1k2a = \frac{\partial K(\beta, \sqrt{1-k^2})}{\partial a} = \frac{\partial K(\beta, \sqrt{1-k^2})}{\partial \beta} \cdot \frac{\partial \beta}{\partial a} + \frac{\partial K(\beta, \sqrt{1-k^2})}{\partial(\sqrt{1-k^2})} \cdot \frac{\partial(\sqrt{1-k^2})}{\partial a},$$

$$d\Lambda 1 = dka \cdot E(\beta, \sqrt{1-k^2}) + K(k) \cdot dE\beta 1k2a,$$

$$d\Lambda 2 = (dEa - dKa) \cdot K(\beta, \sqrt{1-k^2}) + [E(k) - K(k)] \cdot dK\beta 1k2a,$$

$$d\Lambda a = \frac{2}{\pi}(d\Lambda 1 + d\Lambda 2),$$

$$dI100u1a = \frac{\partial I100u1}{\partial a} = -\frac{z}{2\pi\sqrt{r}}[(-\frac{3}{2})\cdot a^{(-\frac{5}{2})}\cdot K(k)\cdot k + a^{(-\frac{3}{2})}\cdot dKa\cdot k + a^{(-\frac{3}{2})}\cdot K(k)\cdot dka]$$

$$dI100u2a = \frac{\partial I100u2}{\partial a} = \frac{1}{2a^2}\cdot\Lambda_0(\beta,k) - \frac{1}{2a}\cdot d\Lambda a,$$

$$dI100u3a = \frac{\partial I100u3}{\partial a} = -\frac{1}{a^2},$$

$$dI100u = dI100u1a + dI100u2a + dI100u3a,$$

$$dI100m1a = -\frac{z}{2\pi}[(\frac{-2}{a^3})\cdot k\cdot K(k) + (\frac{1}{a^2})\cdot dka\cdot K(k) + (\frac{1}{a^2})\cdot k\cdot dKa],$$

$$dI100m2a = -\frac{1}{2a^2},$$

$$dI100m = dI100m1a + dI100m2a,$$

$$dI100d = dI100u1a - dI100u2a,$$

Now, I proceed to derive the a derivative of I(1,1;1):

Given:

$$Eak = \frac{E(k)}{\sqrt{a}\cdot k}, \text{ so that:}$$

$$dEaka = [-\frac{a^{(-\frac{3}{2})}}{2}]\cdot\frac{1}{k}\cdot E(k) + \frac{1}{\sqrt{a}}\cdot(-\frac{dka}{k^2})\cdot E(k) + \frac{1}{\sqrt{a}}\cdot\frac{1}{k}\cdot dEa,$$

$$dI111u1a = \frac{\partial I111u1}{\partial a} = \frac{z\cdot dEaka}{\pi\sqrt{r}},$$

for the a derivative of the $I111u2$, we write :

$$arz = \sqrt{a} + a^{(-\frac{3}{2})}(r^2 + \frac{z^2}{2}),$$

so that,

$$d(arz)a = \frac{\partial(arz)}{\partial a} = \frac{1}{2\sqrt{a}} + (-\frac{3}{2})\cdot a^{(-\frac{5}{2})}\cdot(r^2 + \frac{z^2}{2}),$$

$$dI111u2a = \frac{\partial I111u2}{\partial a} = -\frac{z}{2\pi r\sqrt{r}}[d(arz)a\cdot k\cdot K(k) + arz\cdot dka\cdot K(k) + arz\cdot k\cdot dKa],$$

$$dI111u3a = \frac{a^2 + r^2}{4a^2 r}\cdot\Lambda_0(\beta,k) + \frac{a^2 - r^2}{4ar}\cdot d\Lambda a,$$

$$dI111u4a = \frac{\partial I111u4}{\partial a} = -\frac{r}{2a^2},$$
$$dI111u = dI111u1a + dI111u2a + dI111u3a + dI111u4a;$$
$$dI111m1a = \frac{\partial I111m1}{\partial a} = \frac{z}{\pi}[(-\frac{1}{a^2})\cdot\frac{1}{k}\cdot E(k) + \frac{1}{a}\cdot(-\frac{dka}{k^2})\cdot E(k) + \frac{1}{a}\cdot\frac{1}{k}\cdot dEa],$$

for a derivative of the $I111m2$, we write:

$$az = \frac{2}{a} + \frac{z^2}{2a^3}, \text{ so that:}$$
$$d(az)a = \frac{\partial(az)}{\partial a} = -\frac{2}{a^2} + \frac{3z^2}{2a^4},$$
$$dI111m2a = \frac{\partial I111m2}{\partial a} = -\frac{z}{2\pi}[d(az)a\cdot k\cdot K(k) + az\cdot dka\cdot K(k) + az\cdot k\cdot dKa],$$
$$dI111m3a = \frac{\partial I111m3}{\partial a} = 0,$$
$$dI111m = dI111m1a + dI111m2a + dI111m3a,$$
$$dI111d1a = dI111u1a,$$
$$dI111d2a = dI111u2a,$$
$$dI111d3a = -dI111u3a,$$
$$dI111d4a = \frac{\partial I111d4}{\partial a} = \frac{1}{2r},$$
$$dI111d = dI111d1a + dI111d2a + dI111d3a + dI111d4a,$$

For a derivative of the I (1, 1; 0),

We write:

$$akk1 = \frac{1}{\sqrt{a}}\cdot\frac{1}{k}\cdot K(k),$$
$$akk2 = \frac{1}{\sqrt{a}}\cdot k\cdot K(k),$$
$$akk3 = \frac{1}{\sqrt{a}}\cdot\frac{1}{k}\cdot E(k),$$

so that :

$$d(akk1)a = \frac{\partial(akk1)}{\partial a} = [-\frac{a^{(-\frac{3}{2})}}{2}]\cdot\frac{1}{k}\cdot K(k) + \frac{1}{\sqrt{a}}\cdot(-\frac{dka}{k^2})\cdot K(k) + \frac{1}{\sqrt{a}}\cdot\frac{1}{k}\cdot dKa,$$

$$d(akk2)a = \frac{\partial(akk2)}{\partial a} = [-\frac{a^{(-\frac{3}{2})}}{2}] \cdot k \cdot K(k) + \frac{1}{\sqrt{a}} \cdot dka \cdot K(k) + \frac{1}{\sqrt{a}} \cdot k \cdot dKa ,$$

$$d(akk3)a = \frac{\partial(akk3)}{\partial a} = [-\frac{a^{(-\frac{3}{2})}}{2}] \cdot \frac{1}{k} \cdot E(k) + \frac{1}{\sqrt{a}} \cdot (-\frac{dka}{k^2}) \cdot E(k) + \frac{1}{\sqrt{a}} \cdot \frac{1}{k} \cdot dEa ,$$

$$d110 = \frac{\partial I110}{\partial a} = \frac{2d(akk1)a}{\pi\sqrt{r}} - \frac{d(akk2)a}{\pi\sqrt{r}} - \frac{2d(akk3)a}{\pi\sqrt{r}}$$

Hence, the task is completed successfully, the analytic expressions of the *a* derivatives of the magnetic anomalies due to the right vertical cylinder with arbitrary polarization has been derived successfully. It is used to calculate the analytic Jacobian matrix in the inversion to increase the precision.

Appendix C: Sensibility of the results of calculations of the derivatives to the changes of depth

In order to figure out the sensibility of the results of my calculations to the changes of depth, the depth of the first model is increased to figure out the sensitivity of the function to the depth:

Depth=80m

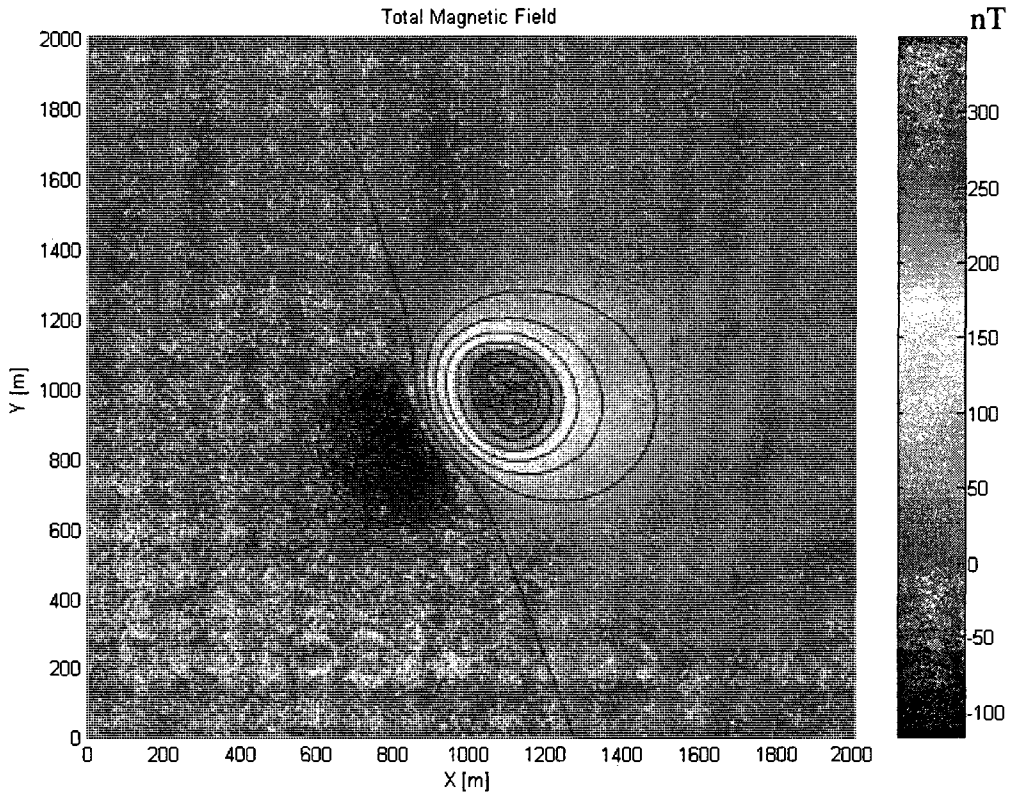

Fig.C.1 Contour of the total magnetic field of first set of data Depth =80m

Comparing with Fig.3.2, the values of anomalies is less, but the shape of the contour is not changed. Fig.C.2 is the profile of the total magnetic field, compared with Fig.3.3, its form is not changed, and the value of its peak is less than before.

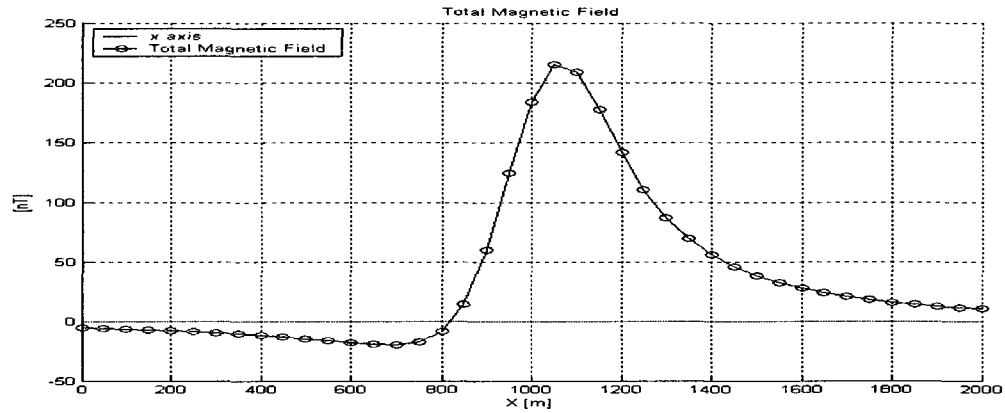

Fig.C.2 profile at y =1175m of the total magnetic field of first model Depth =80m

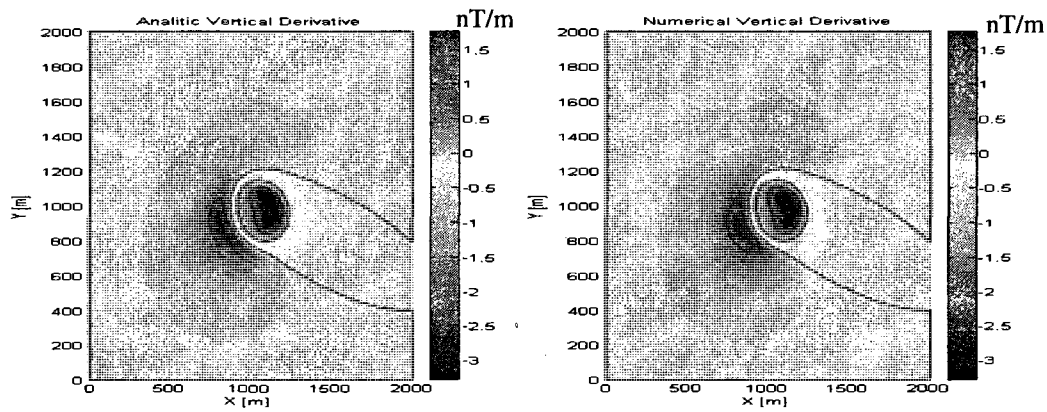

Fig.C.3 Contours of the analytic vertical derivative and the numerical vertical derivative of first model Depth =80m.

It can be noticed that the shape of Fig.C.3 is same as Fig3.4; the values of anomalies are decreased. Fig.C.4. shows that the two profiles drawn at the positions y =1175m from the analytic method and numerical method are identical. Comparing with Fig.3.5, their forms are not different, the values are getting less. Fig.C.5 is for the contours of the analytic x derivative and numerical x derivative of variation of depth of 80m compared to the first model. The results from the two methods are same. Comparing with Fig.3.6, the pattern has changed a little with depth; the values of anomalies have decreased. Fig.C.6 shows that the two profiles drawn at positions y =1175 from the analytic and numerical methods are almost identical in terms of

form and value. Comparing with Fig.3.7, the values are less than that of Fig.3.7. Fig.C.7 shows contours of the analytic y derivative and the numerical y derivative of model with an increase of depth of 17m. The results from the two methods are same, compared with Fig.3.8, the contours have changed a little, and values are smaller than before.

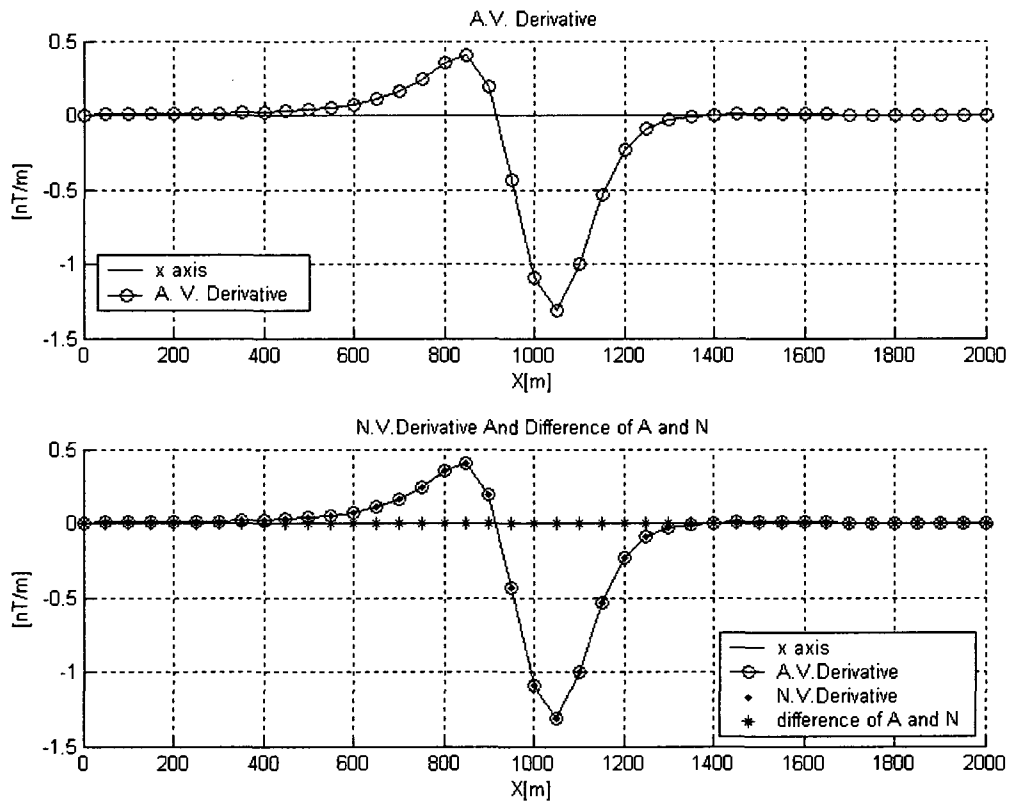

Fig.C.4 Profiles at y =1175m of the analytic vertical derivative and the numerical vertical derivative of first model Depth =80m

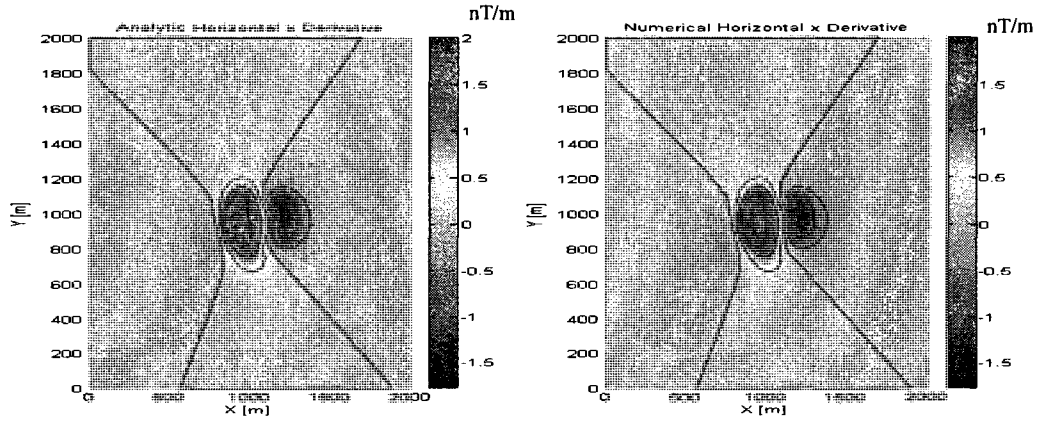

Fig.C.5 Contours of the analytic x derivative and the numerical x derivative of first model Depth =80m.

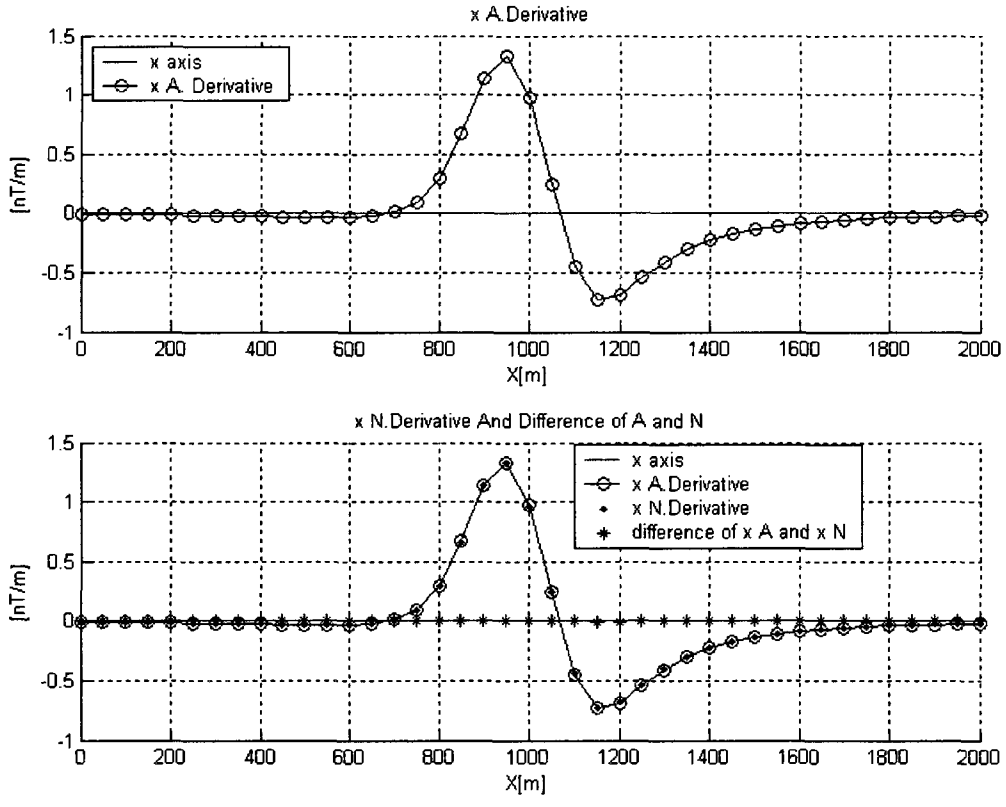

Fig.C.6 Profiles at y =1175m of the analytic x derivative and the numerical x derivative of first model Depth =80m

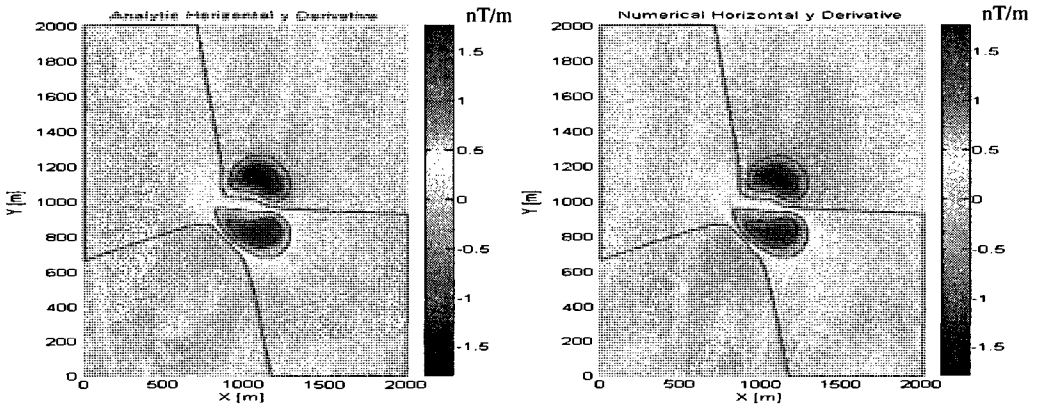

Fig.C.7 Contours of the analytic y derivative and the numerical y derivative of first model Depth =80m.

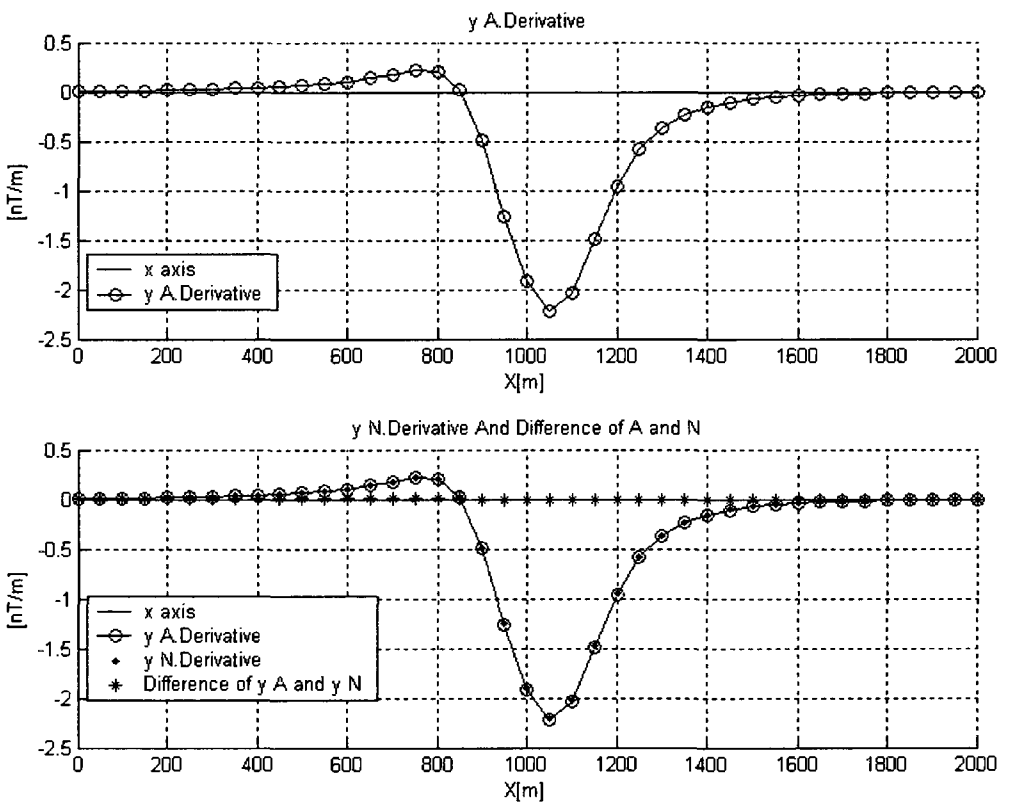

Fig.C.8 Profiles at y =1175m of the analytic y derivative and the numerical y derivative of first model Depth =80m

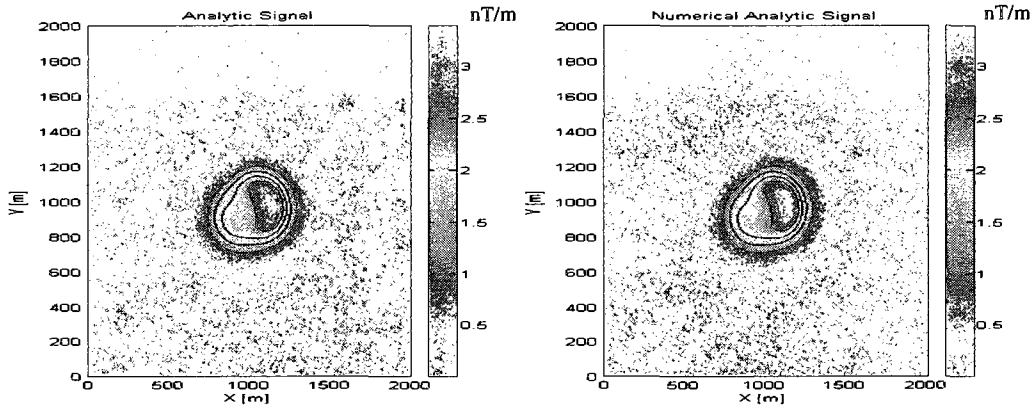

Fig.C.9 Contours of the analytic signal and numerical analytic signal of first model Depth =80m

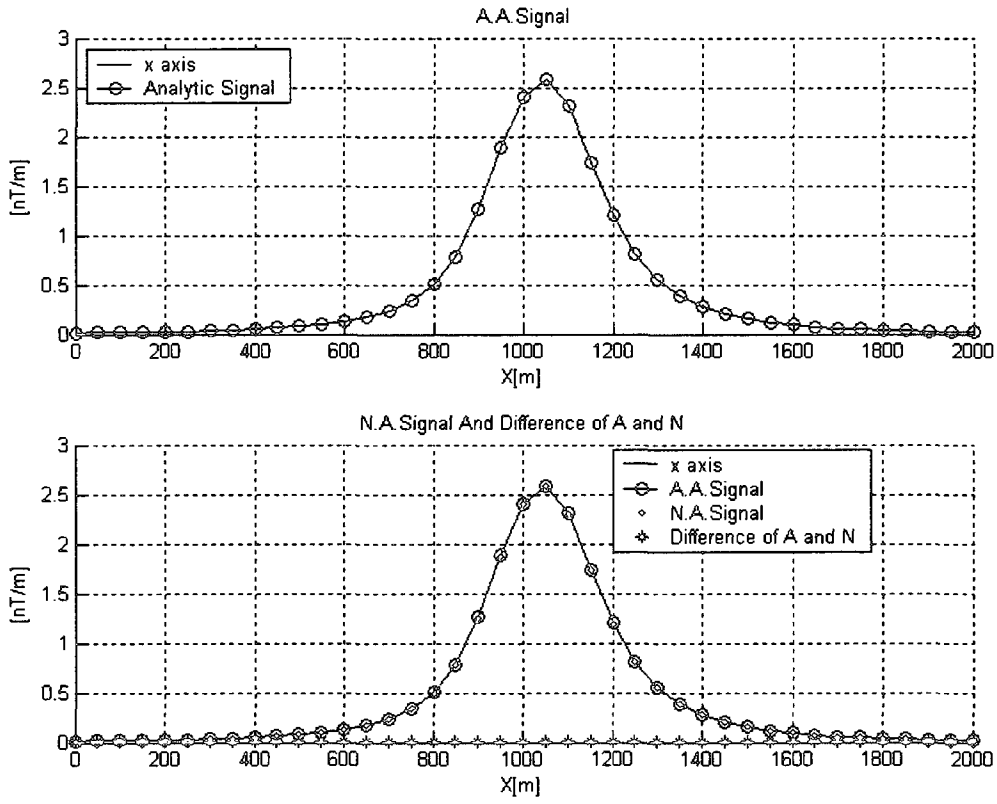

Fig.C.10 Profiles at y =1175m of the analytic signal and numerical analytic signal of first model Depth =80m

Fig.C.8 shows the profiles of the analytic y derivative and the numerical y derivative of first data, Depth is increased to 80m. The results from two methods are identical. The amplitudes of the profiles are decreased. Fig.C.9 shows the contours of analytic and numerical signal of first model, compared with before, and the values are smaller. The profiles from Fig.C.10 are in conformity with the contours concerned.

Depth=100m

Next we test for a depth of 100m. From the Fig.C.11 to Fig.C.20, it can be noticed that the tendencies of the changes from the increase of the depth from 80m to 100m for the total magnetic field, the gradients and the analytic signal are same as to that of the changes from the increase of the depth from original depth to 80m. There is no change in terms of shapes of the contours and profiles; there are decreases in terms of values of total magnetic values, gradients, and analytic signal. The results from the analytic method and the numerical method are identical.

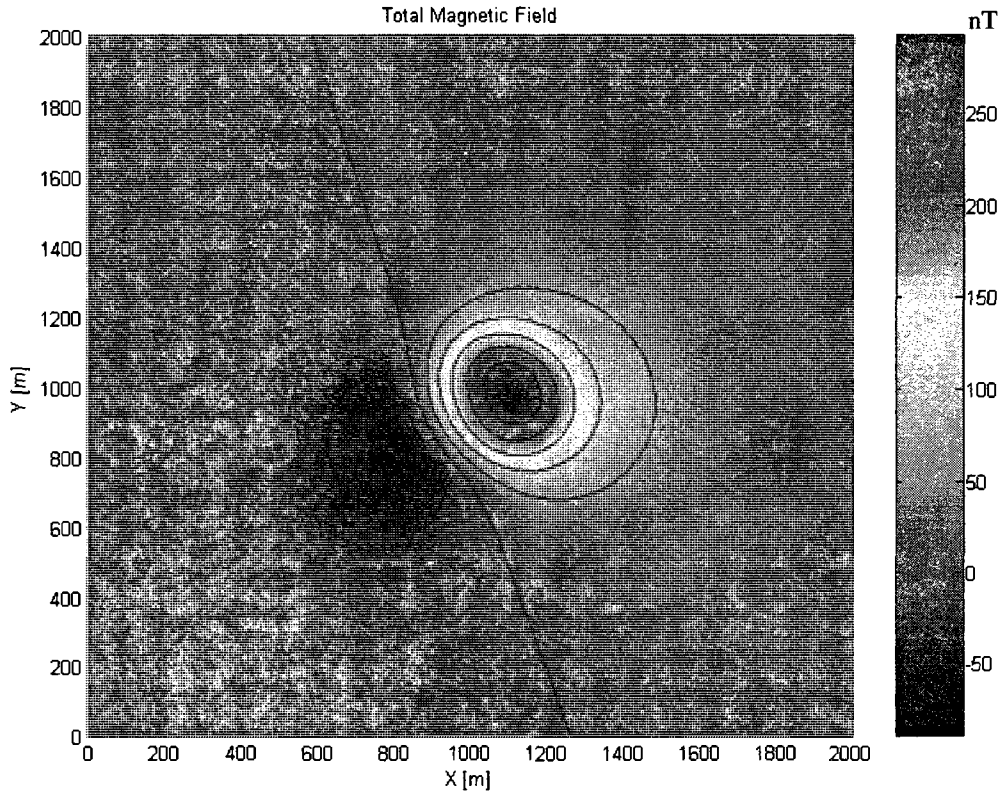

Fig.C.11 Contour of the total magnetic field of first model Depth =100m.

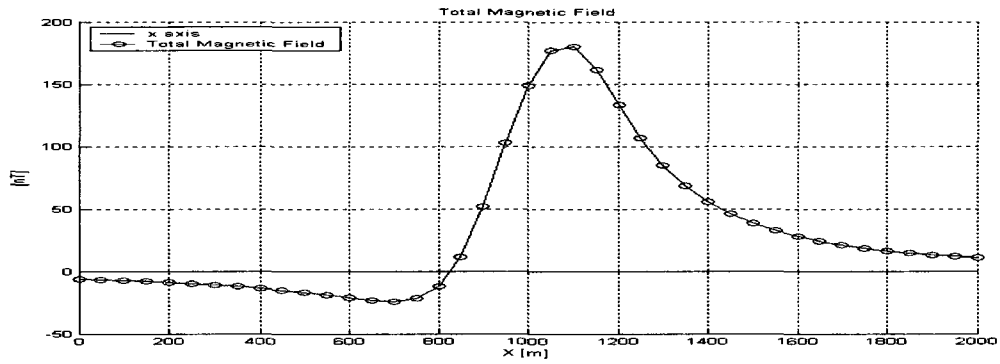

Fig.C.12 Profile at y =1175m of the total magnetic field of first model Depth =100m

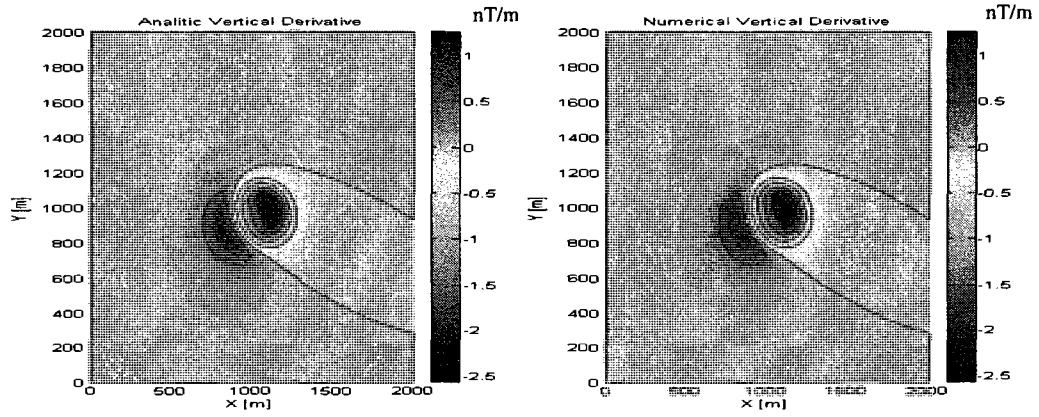

Fig.C.13 Contours of the analytic vertical derivative and numerical vertical derivative of first model Depth =100m

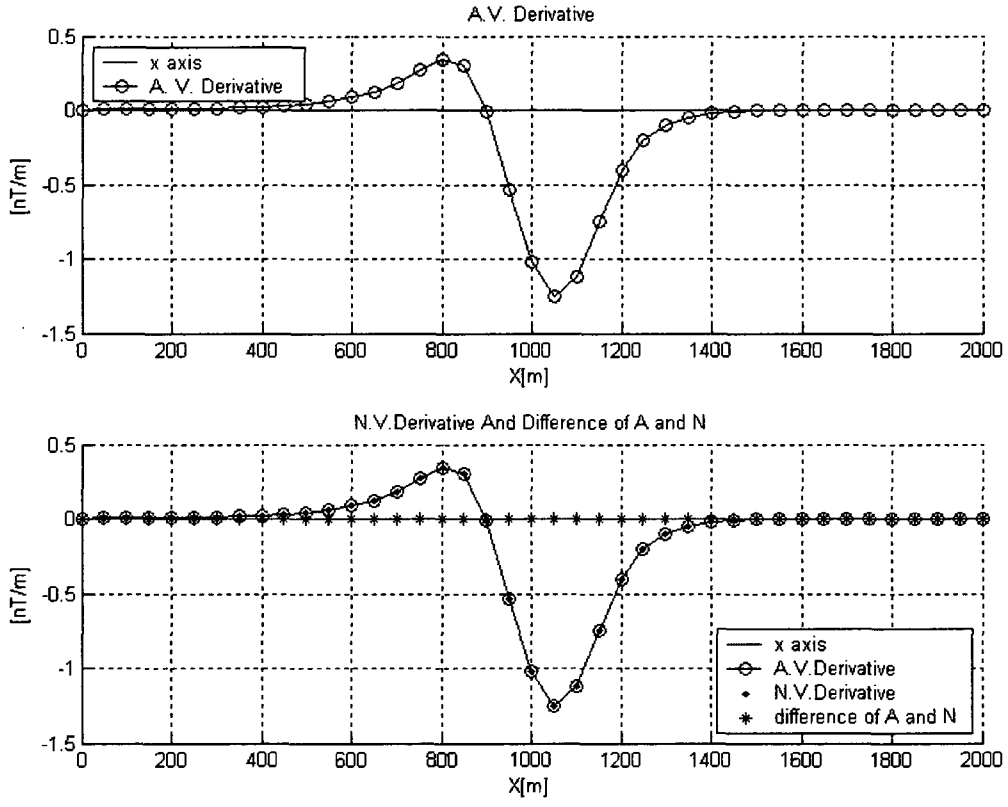

Fig.C.14 Profiles at y =1175m of the analytic vertical derivative and numerical vertical derivative of first model Depth =100m

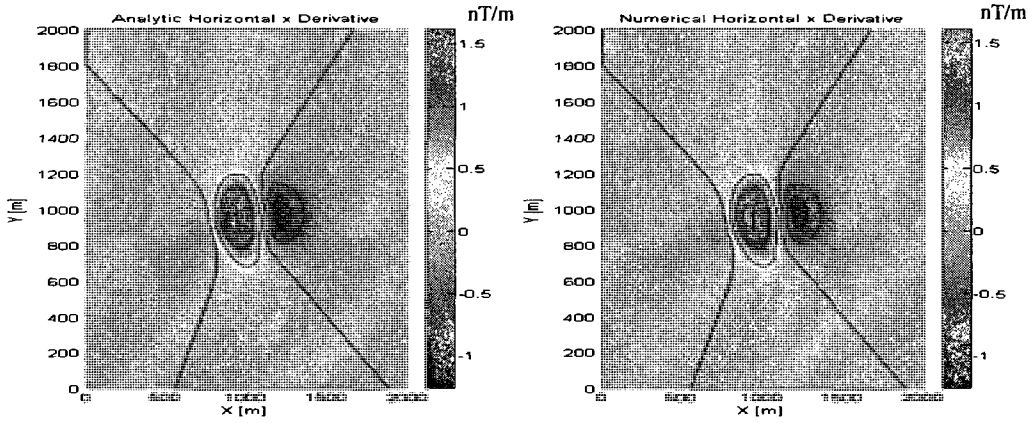

Fig.C.15 Contours of the analytic x derivative and numerical x derivative of first model Depth =100m

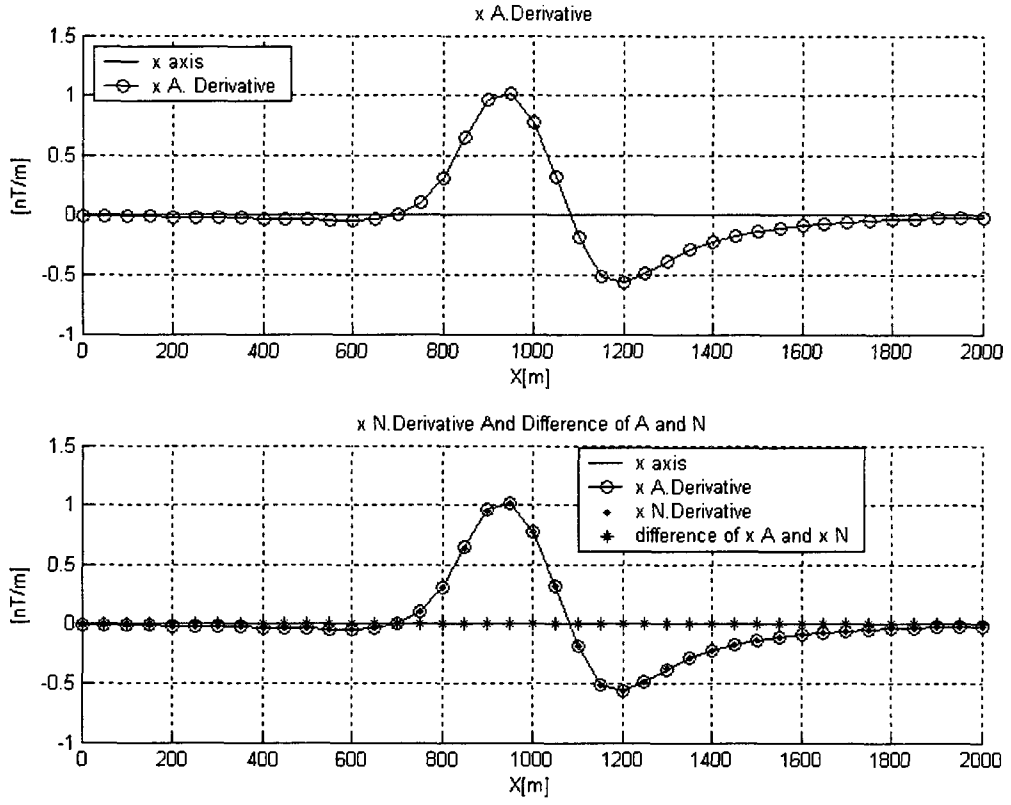

Fig.C.16 Profiles at y =1175m of the analytic x derivative and numerical x derivative of first model Depth =100m

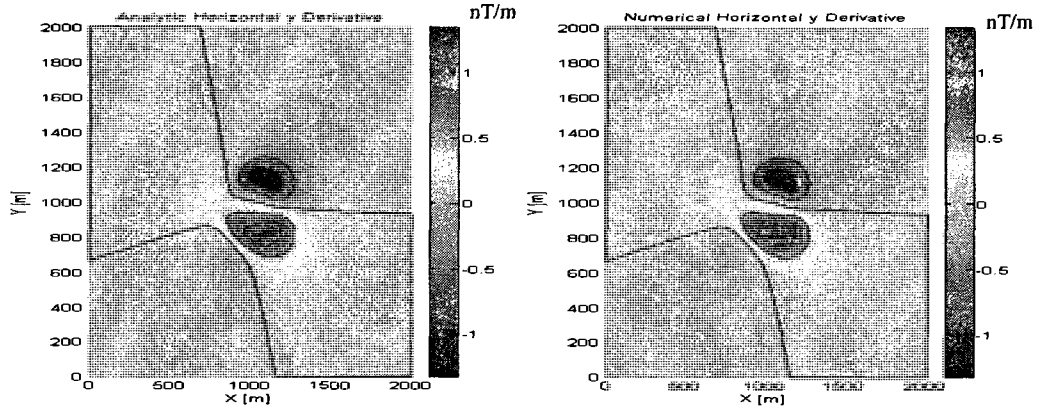

Fig.C.17 Contours of the analytic y derivative and numerical y derivative of first model Depth =100m

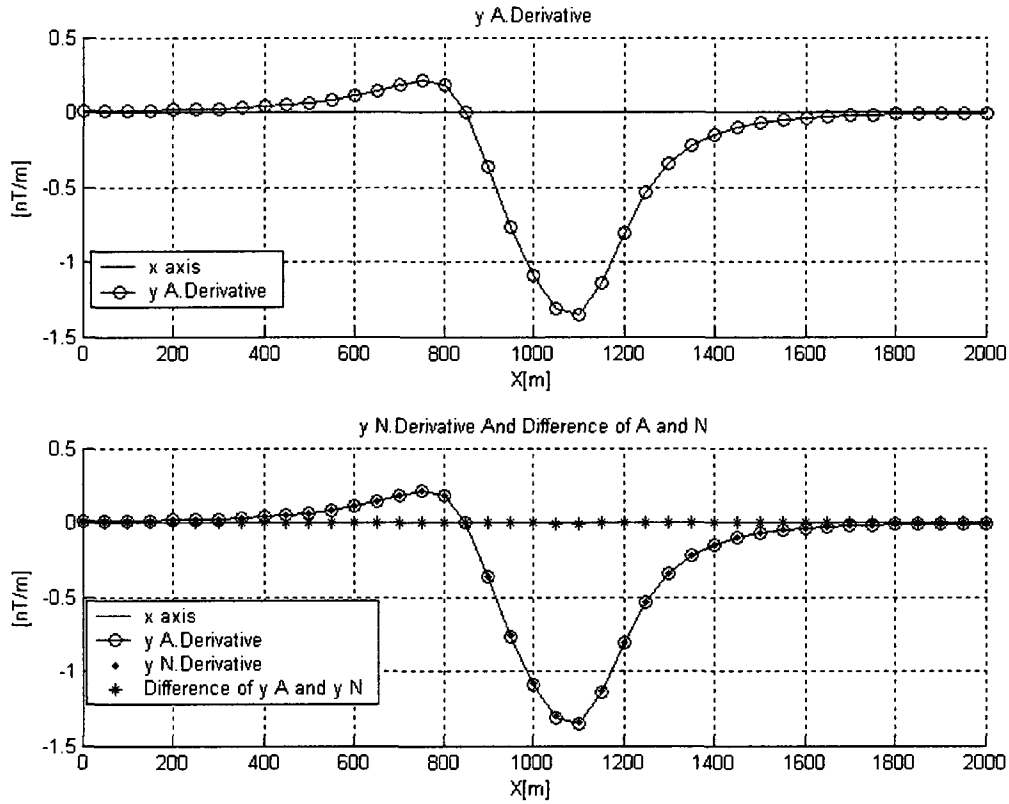

Fig.C.18 Profiles at y =1175m of the analytic y derivative and numerical y derivative of first model Depth =100m

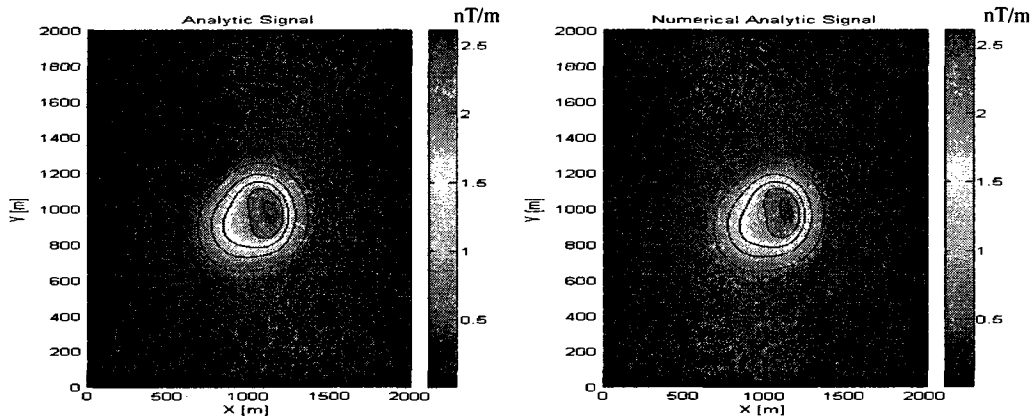

Fig.C.19 Contours of the analytic signal and numerical analytic signal of first model Depth =100m

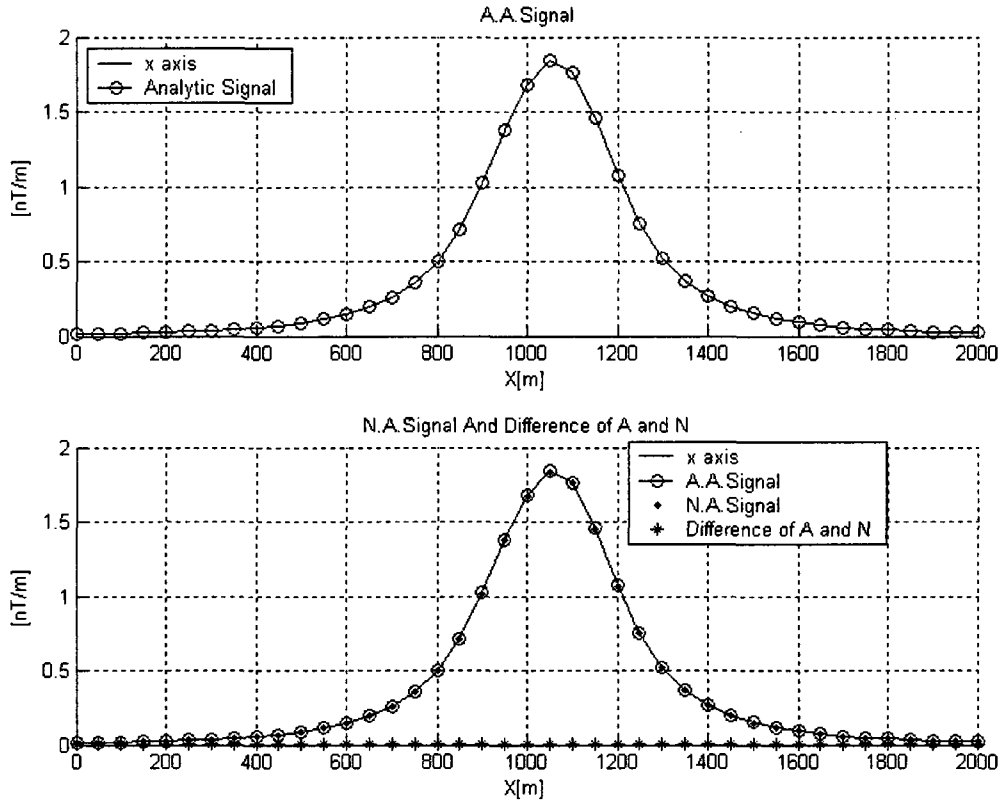

Fig.C.20 Profiles at y =1175m of the analytic signal and numerical analytic signal of first model Depth =100m

For a depth of 63m, the peak of the analytic signal equals 4.0 nT / m; for a depth of 80m, the peak of the analytic signal equals 3.0 nT / m; for a depth of 100m, the peak of the analytic signal equals 2.5 nT / m.

Appendix D: Sensibility of the results of calculations of derivatives to changes of radius

The radius of second model is increased to figure out the sensitivity of this function to radius: Radius=200m.

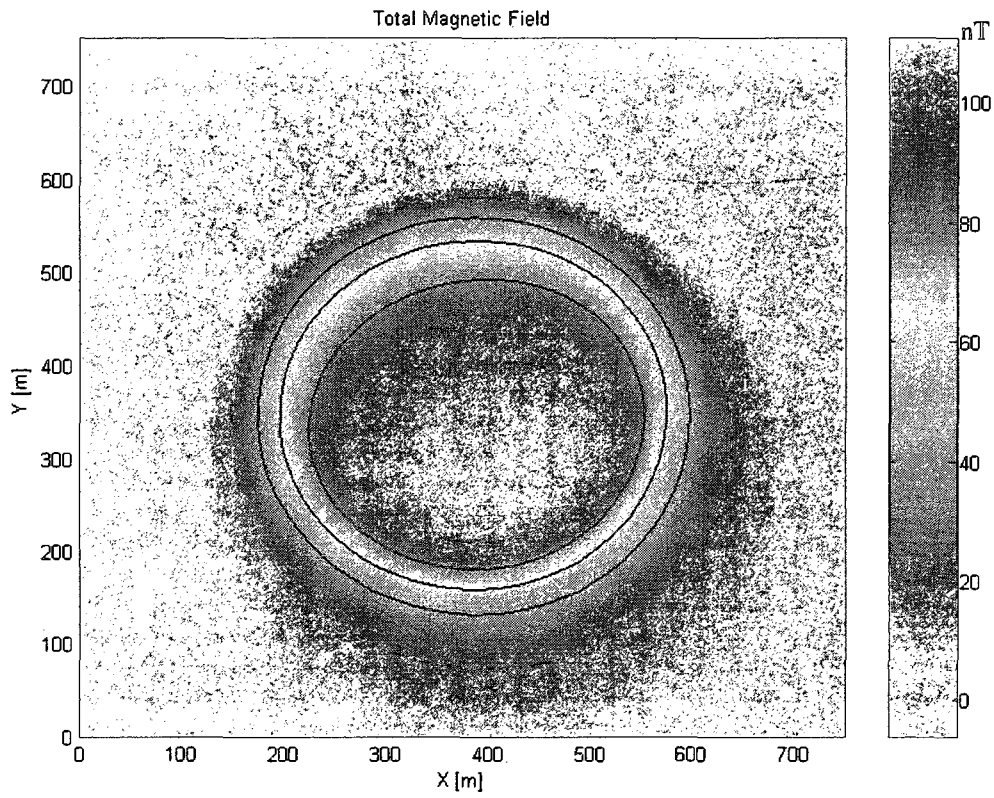

Fig.D.1 Contour of the total magnetic field of second model Radius=200m.

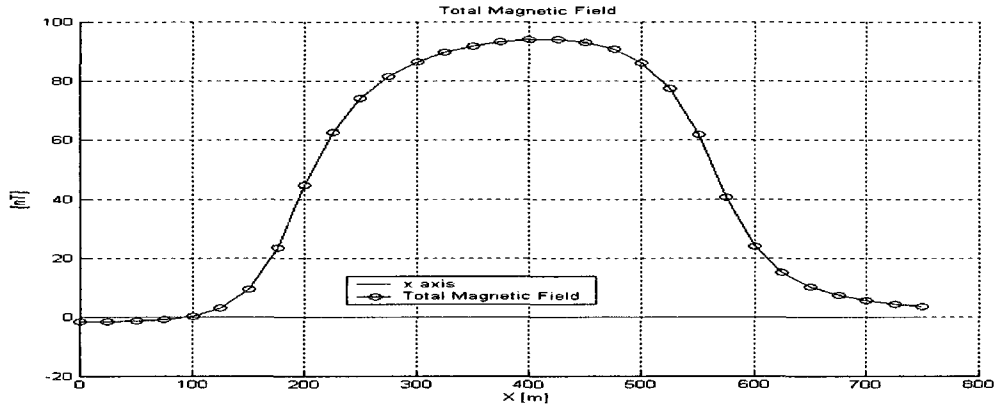

Fig.D.2 Profile at y =425m of the total magnetic field of second model Radius=200m

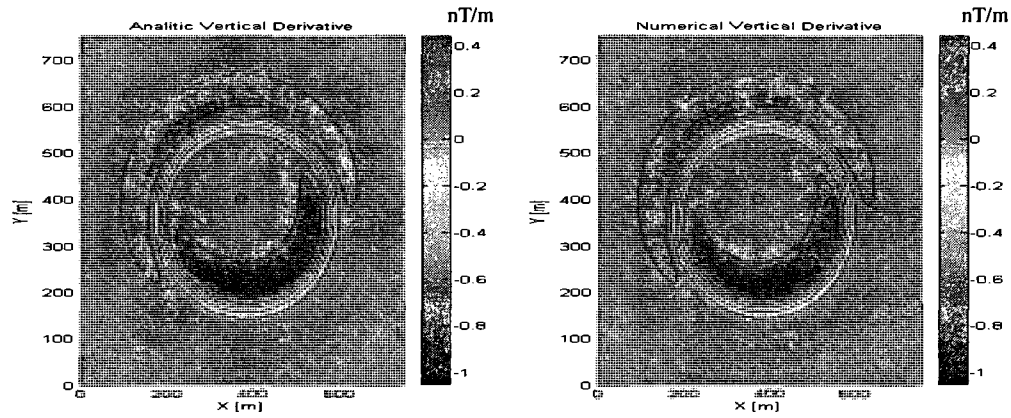

Fig.D.3 Contours of the analytic vertical derivative and numerical vertical derivative of second model Radius=200m.

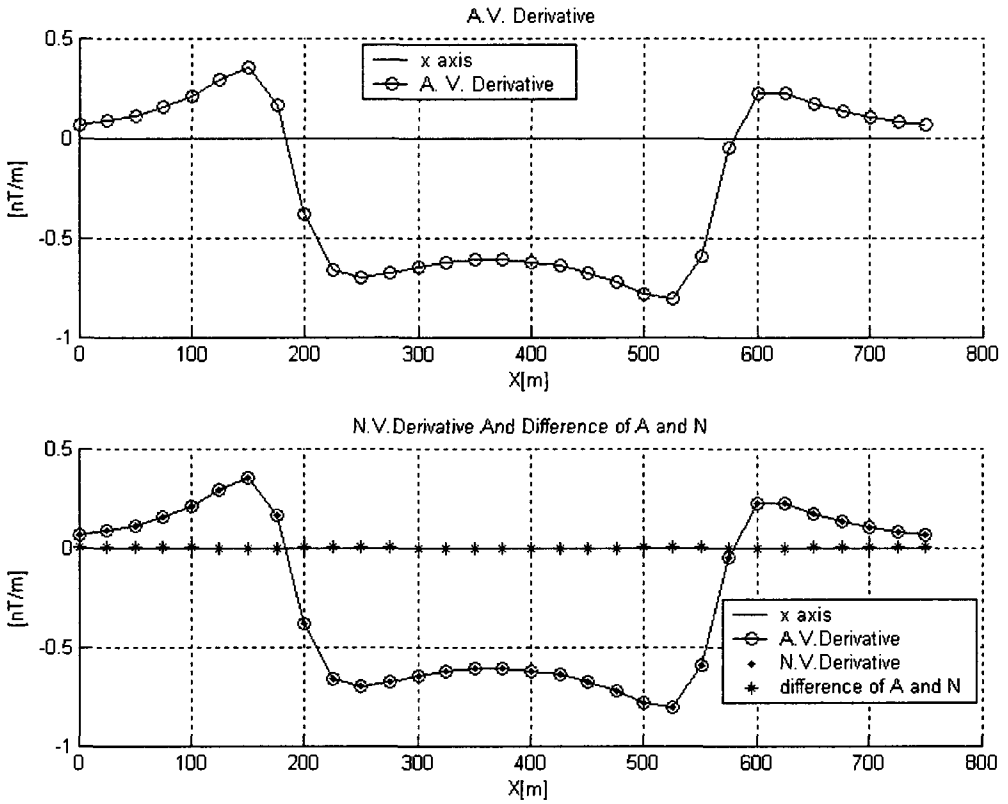

Fig.D.4 Profiles at y =425m of the analytic vertical derivative and numerical vertical derivative of second model Radius=200m

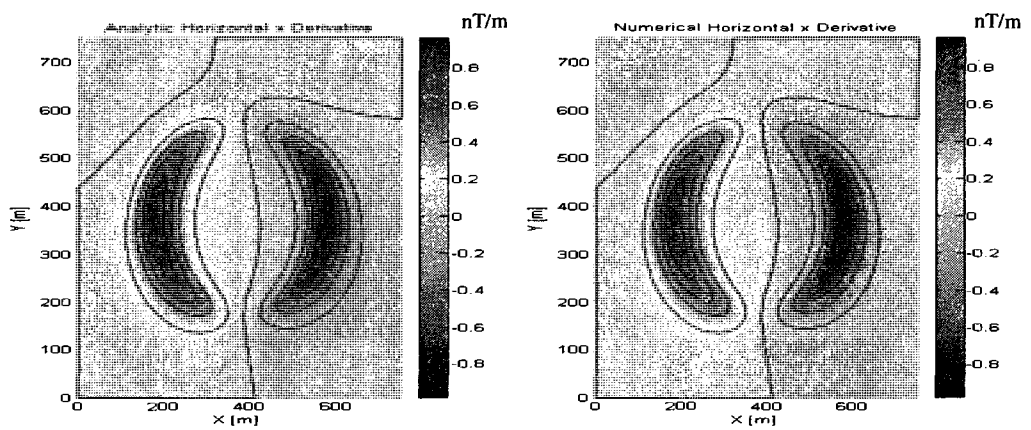

Fig.D.5 Contours of the analytic x derivative and numerical x derivative of second model Radius=200m.

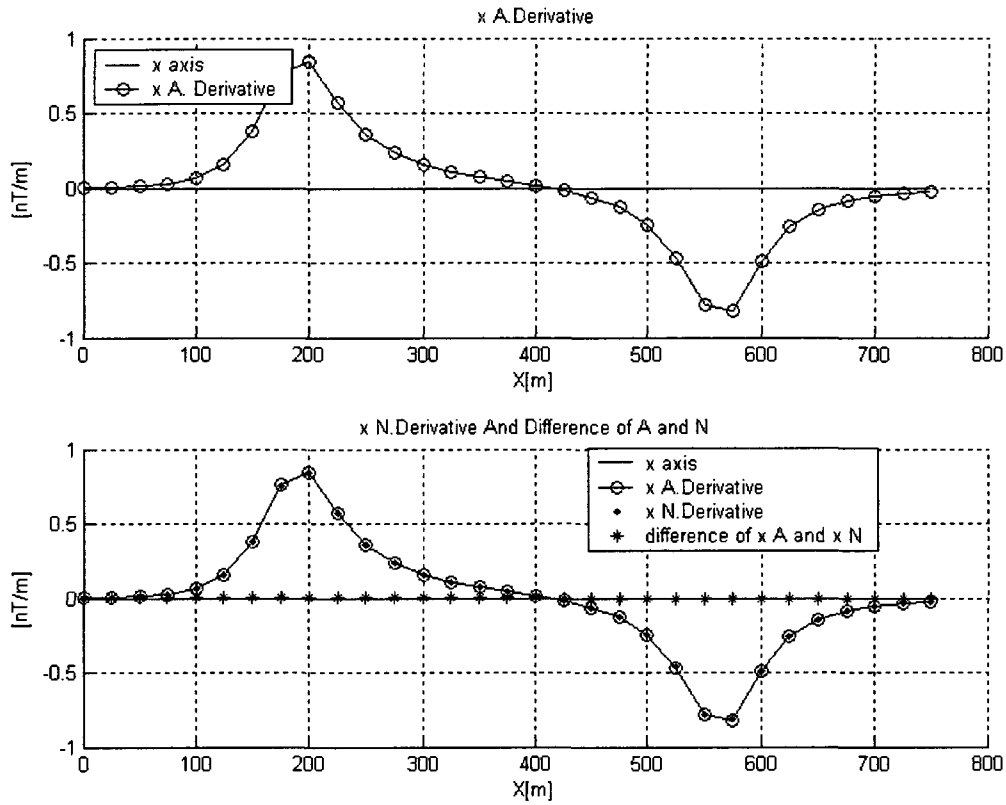

Fig.D.6 Profiles at y =425m of the analytic x derivative and numerical x derivative of second model Radius=200m

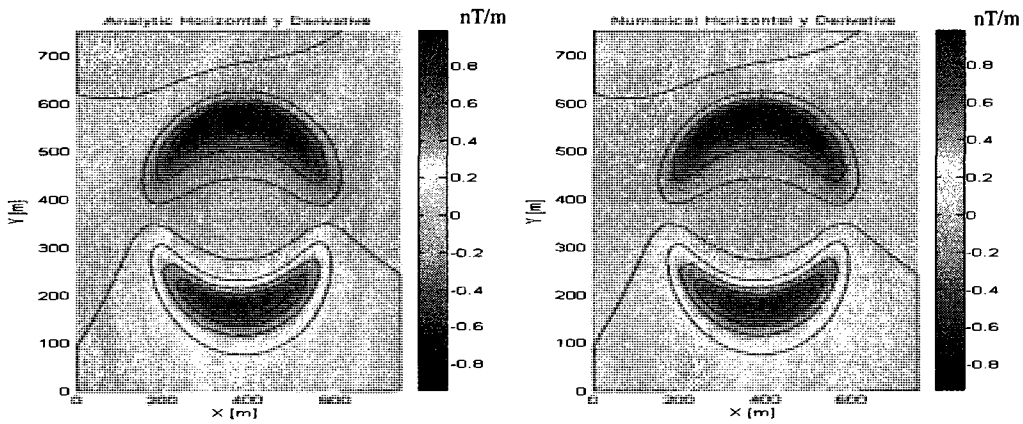

Fig.D.7 Contours of the analytic y derivative and numerical y derivative of second model Radius=200m.

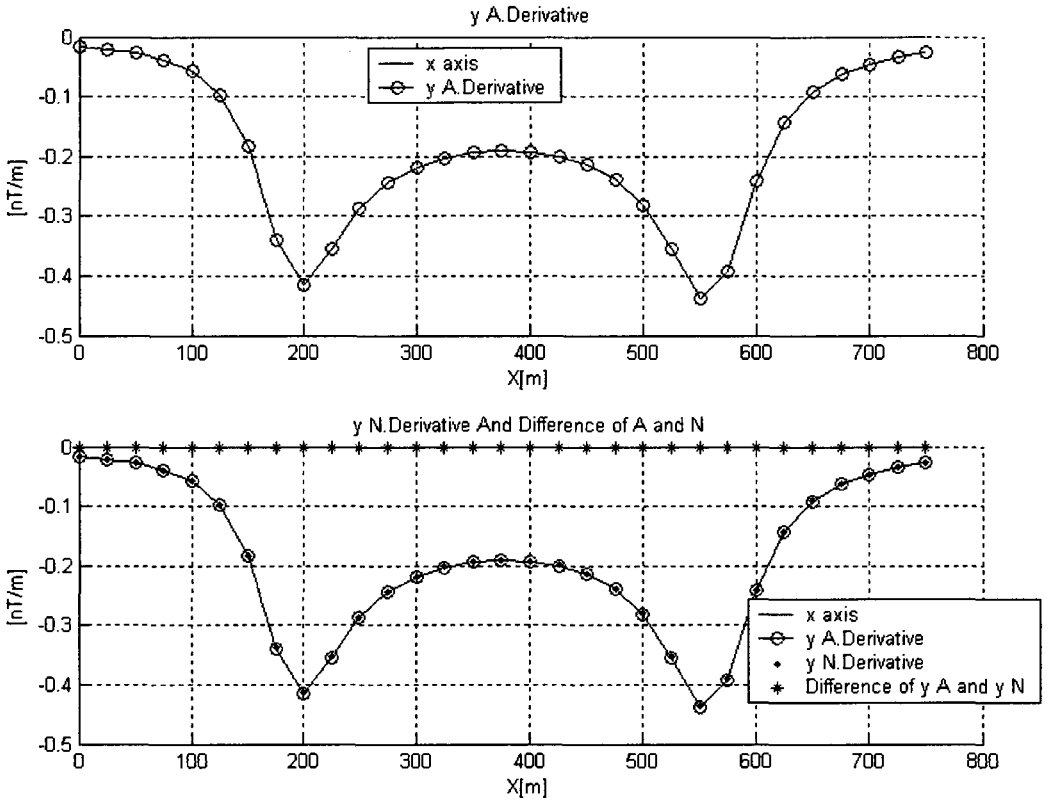

Fig.D.8 Profiles at y =425m of the analytic y derivative and numerical y derivative of second model Radius=200m

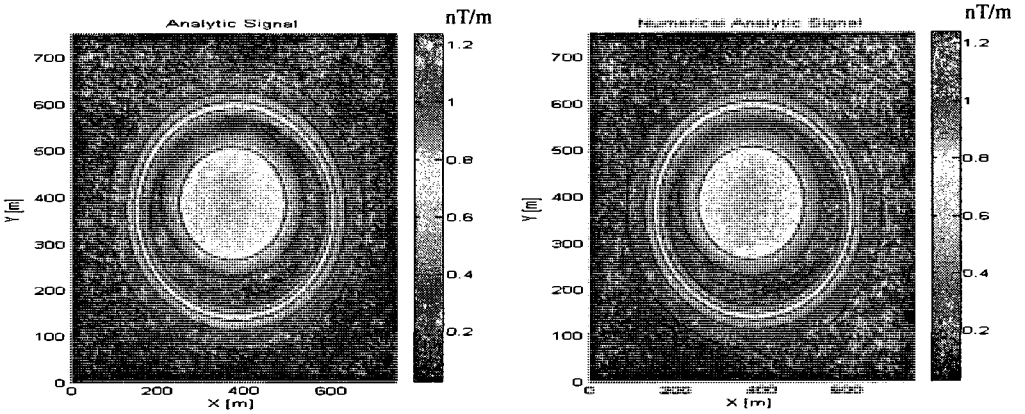

Fig.D.9 Contours of the analytic signal and numerical analytical signal of second model Radius=200m

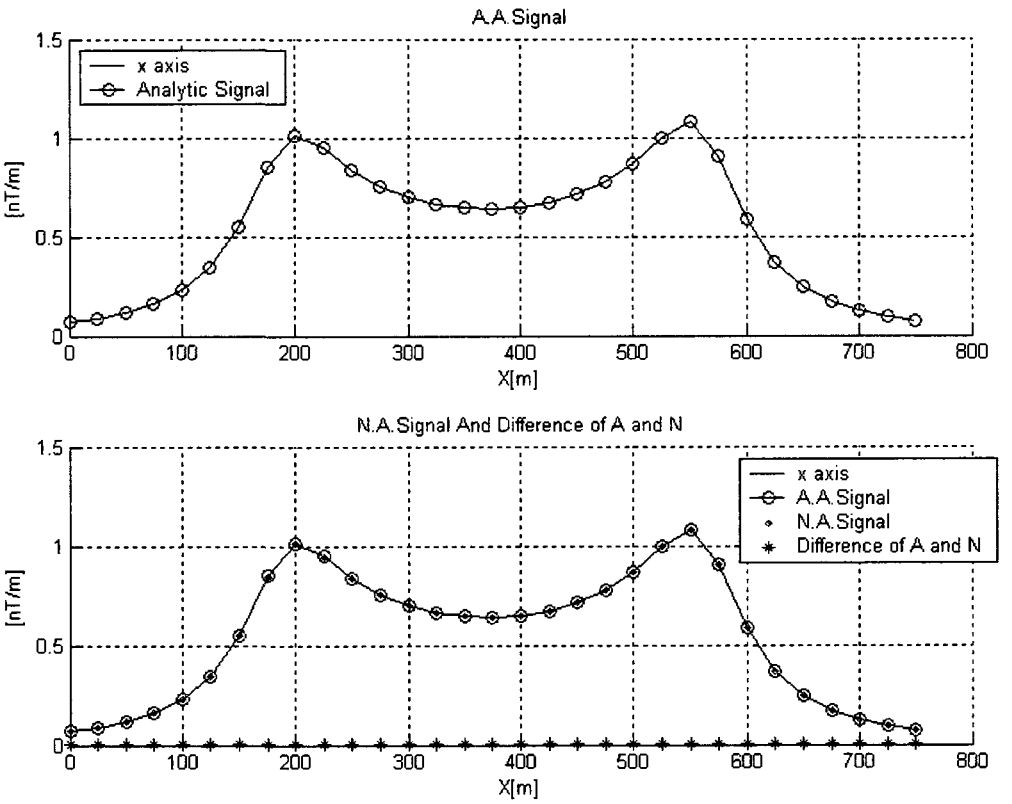

Fig.D.10 Profiles of y =425m of the analytic signal and numerical analytical signal of second model Radius=200m

Fig.D.1 to Fig.D.10 shows the tendencies of changes from the increase of radius from 133m to 200m while Fig.D.11 to Fig.D.20 shows the tendencies of changes from the increase of radius from 200 to 300. With increases of radius, the anomalies are increased, but the values of the gradients do not have big changes except that the amplitudes of y Gradients are decreased with the increases of radius. The forms of contours of gradients are changed.

The ranges of the anomalies and gradients are increased with the increase of the radius while the width of the profiles is increased with increases of the radius. The two methods agree well.

Next group of figures is for the change of radius=300m.

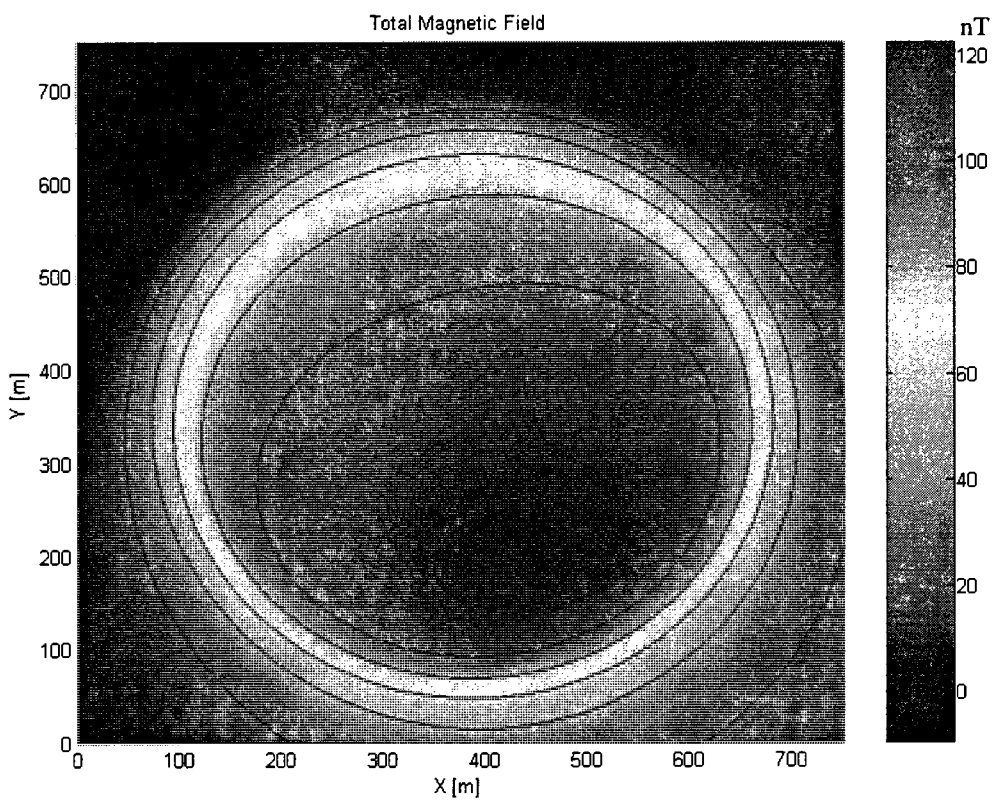

Fig.D.11 Contour of the total magnetic field of second set of data Radius=300m.

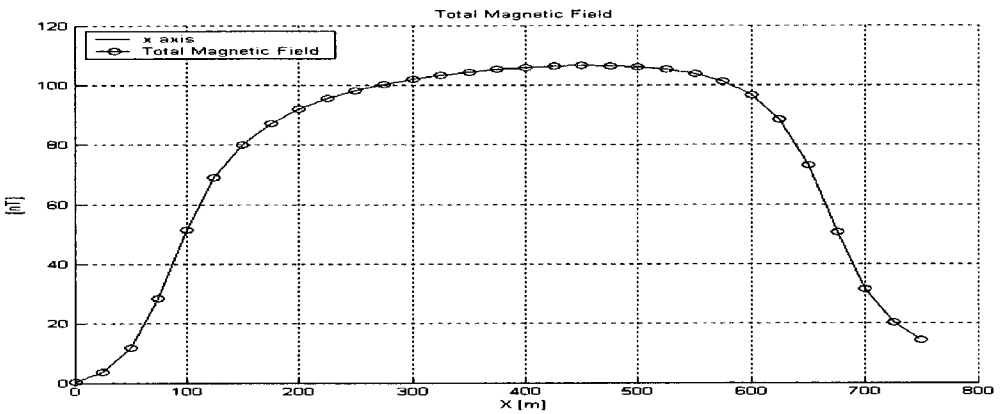

Fig.D.12 Profile at y =425m of the total magnetic field of second model Radius=300m

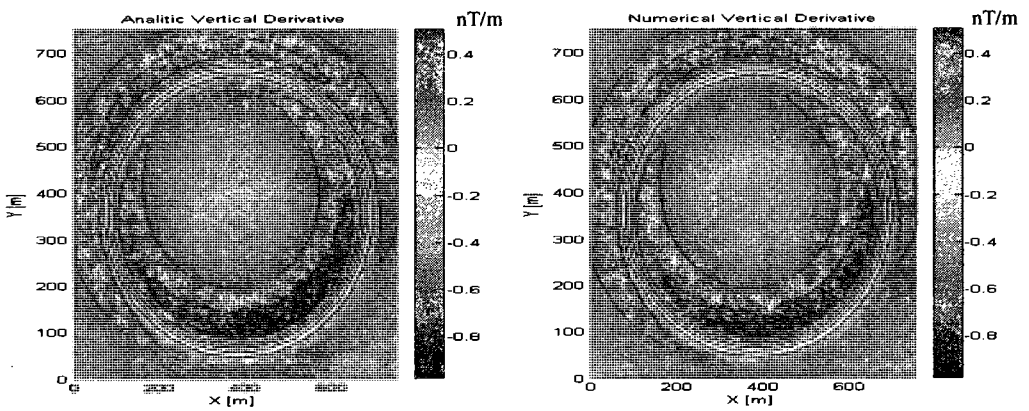

Fig.D.13 Contours of the analytic vertical derivative and numerical vertical derivative of second model Radius=300m

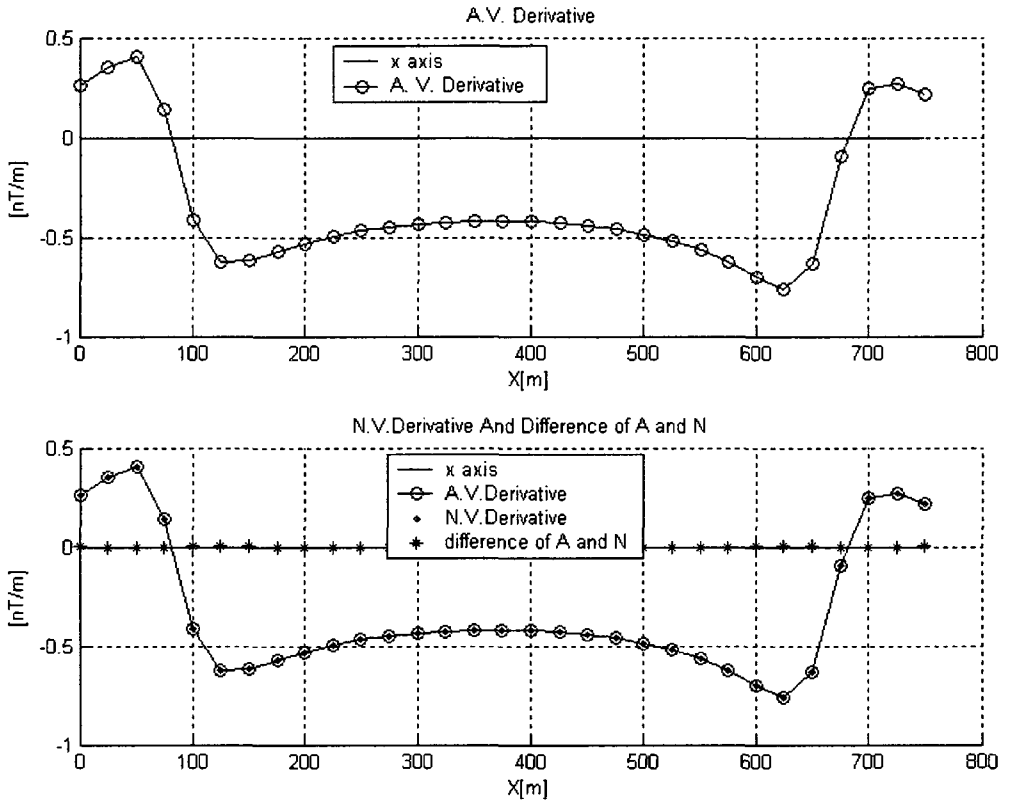

Fig.D.14 Profiles at y =425m of the analytic vertical derivative and numerical vertical derivative of second model Radius=300m

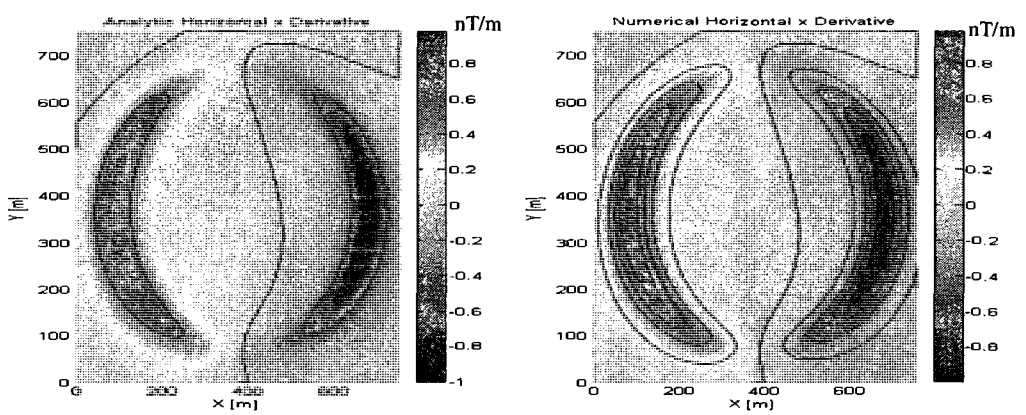

Fig.D.15 Contours of the analytic x x derivative and numerical x derivative of second model Radius=300m.

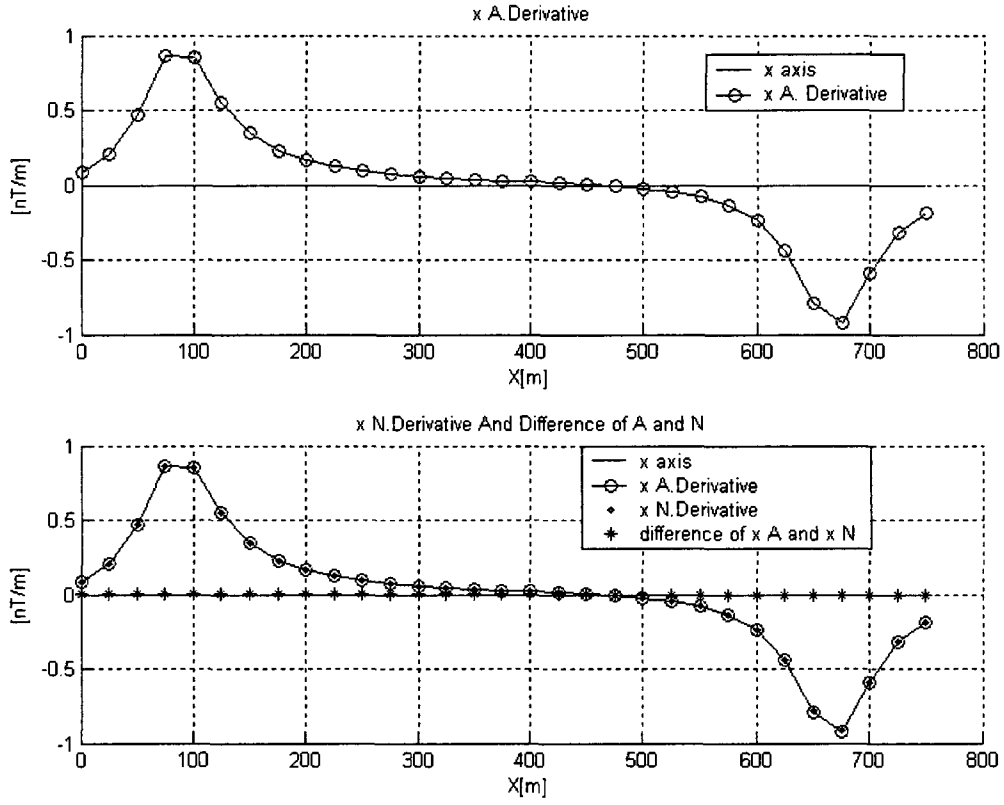

Fig.D.16 Profiles of y =425m of the analytic x derivative and numerical x derivative of second model Radius=300m

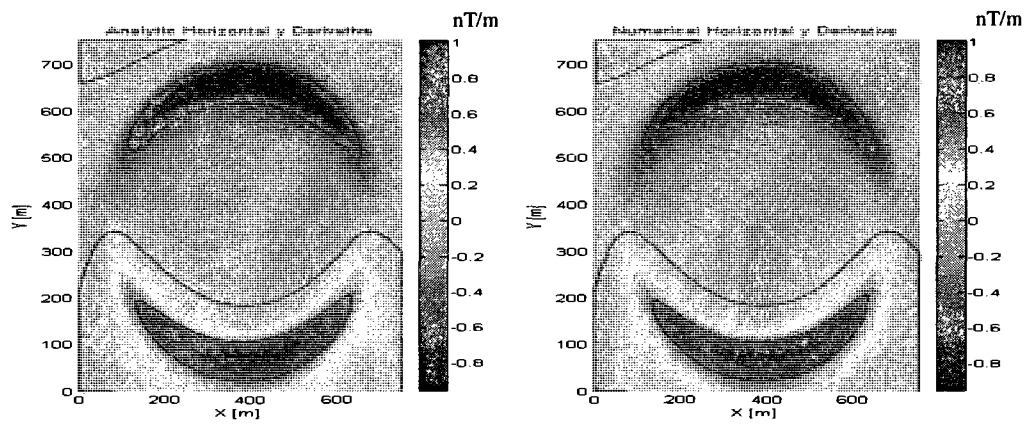

Fig.D.17 Contours of the analytic y derivative and numerical y derivative of second model Radius=300m.

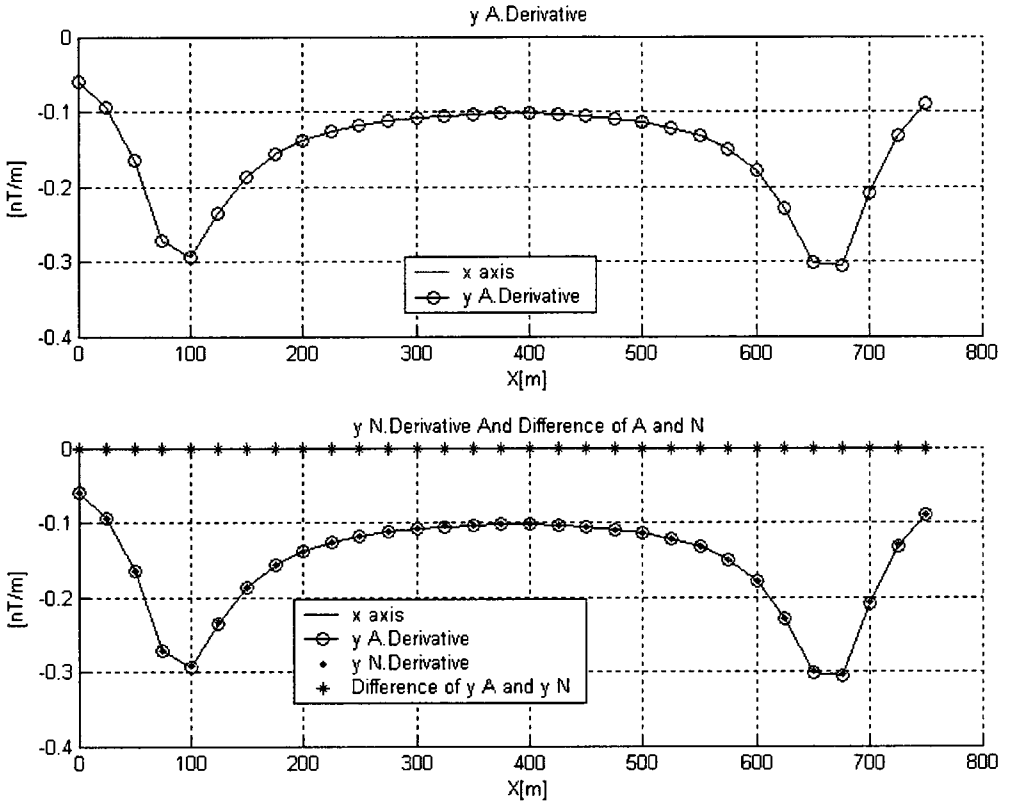

Fig.D.18 Profiles at y =425m of the analytic y derivative and numerical y derivative of second model Radius=300m

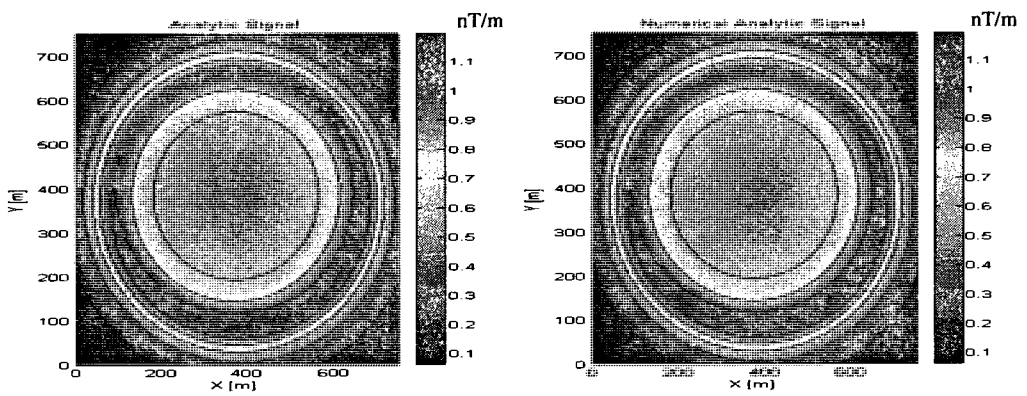

Fig.D.19 Contours of the analytic signal and numerical analytic signal of second model Radius=300m.

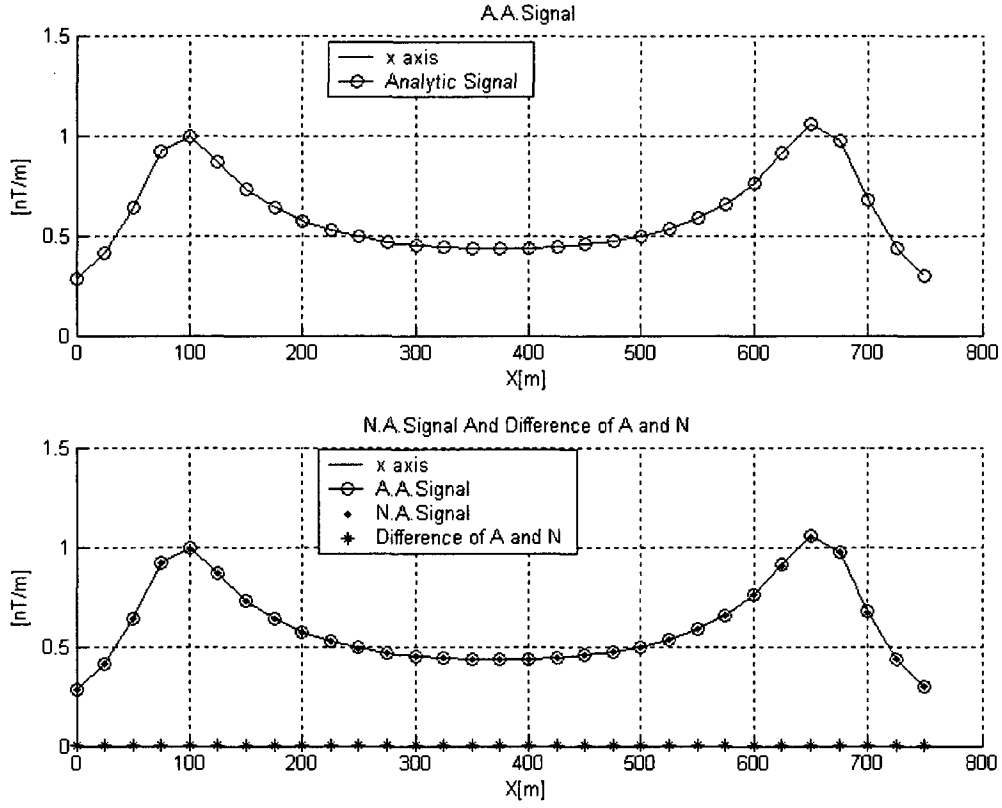

Fig.D.20 Profiles at y =425m of the analytic signal and numerical analytic signal of second model Radius=300m

With the change of the value of the radius of the cylinder, there are no changes about the derivatives and the analytic signal, but the peaks are in conformity with the position of the edge of the body. There are the differences between the peaks of the values and edges of the positions that are because the profiles are not in the middle.

Appendix E: Sensibility of the results of calculations of the derivative to changes of the inclination

The total inclination for third model is decreased to 40° to figure out the sensitivity to the change of inclination, total inclination = 40°

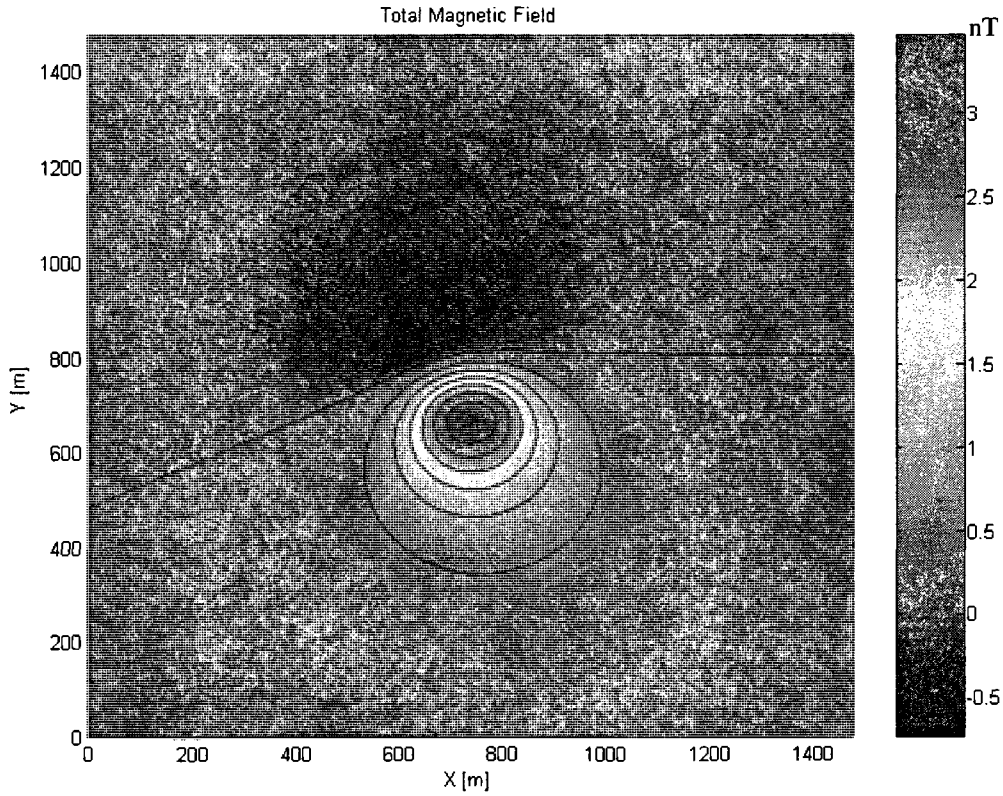

Fig.E.1 Contour of the total magnetic field of third set of data, total inclination = 40°

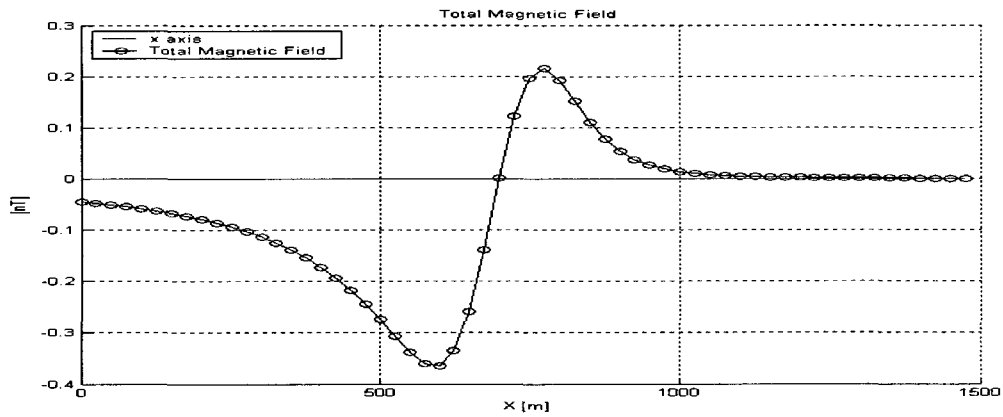

Fig.E.2 Profile y =800m of the total magnetic field of third model total inclination = 40°

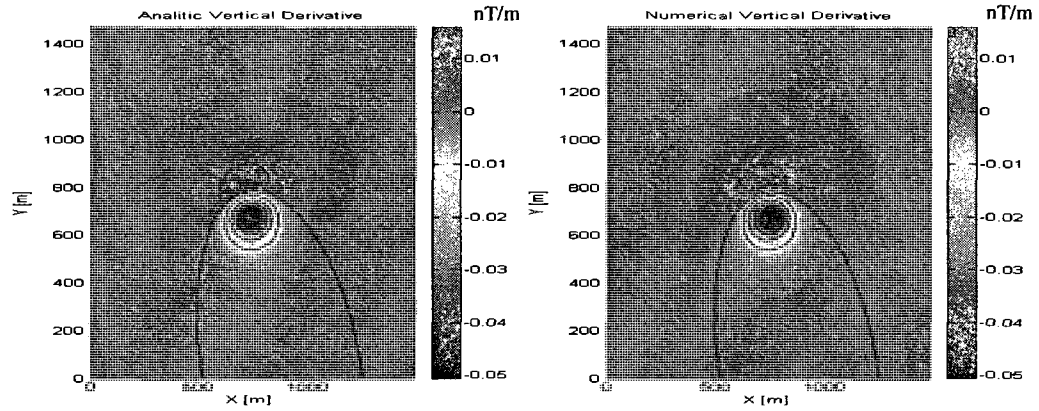

Fig.E.3 Contours of the analytic vertical derivative and numerical analytic vertical derivative of third model, total inclination = 40°

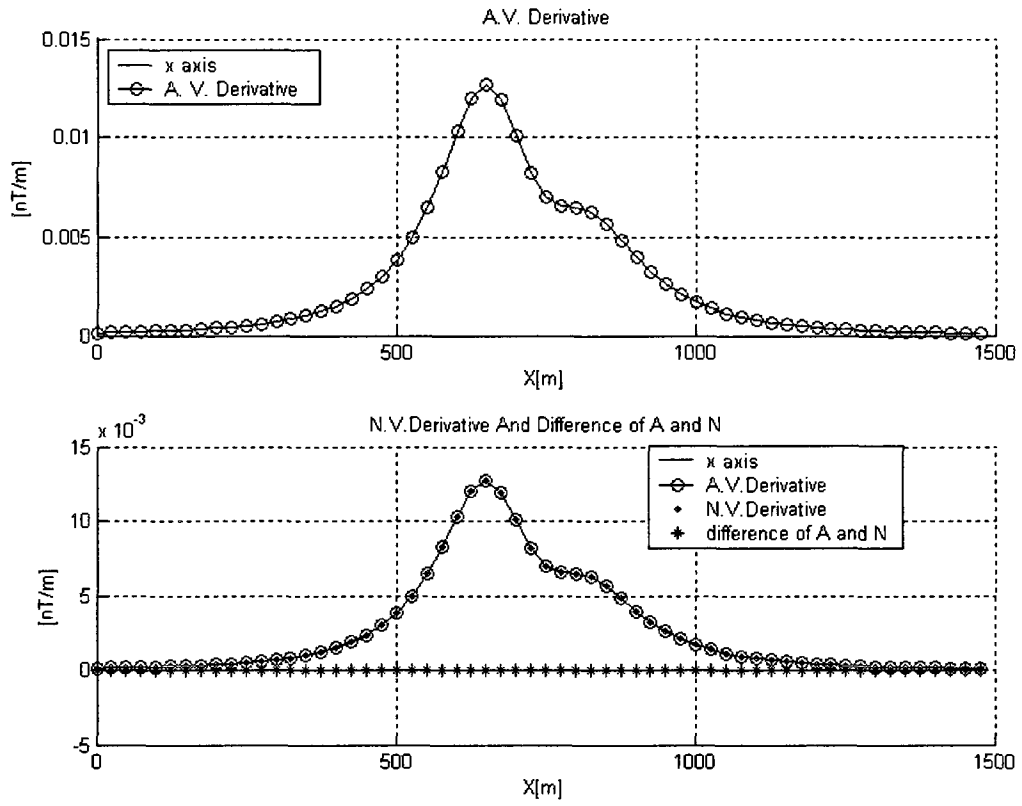

Fig.E.4 Profiles at y =800m of the analytic vertical derivative and numerical analytic vertical derivative of third model, total inclination = 40°

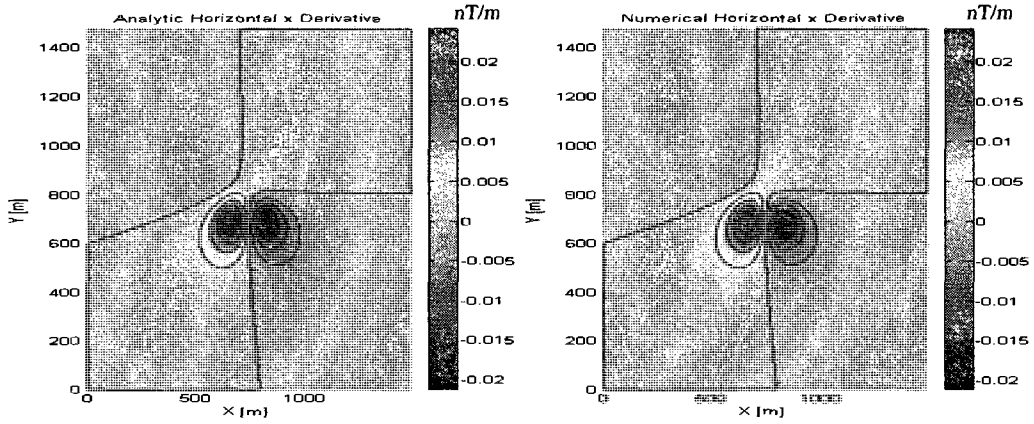

Fig.E.5 Contours of the analytic x derivative and numerical analytic x derivative of third model, total inclination = 40°

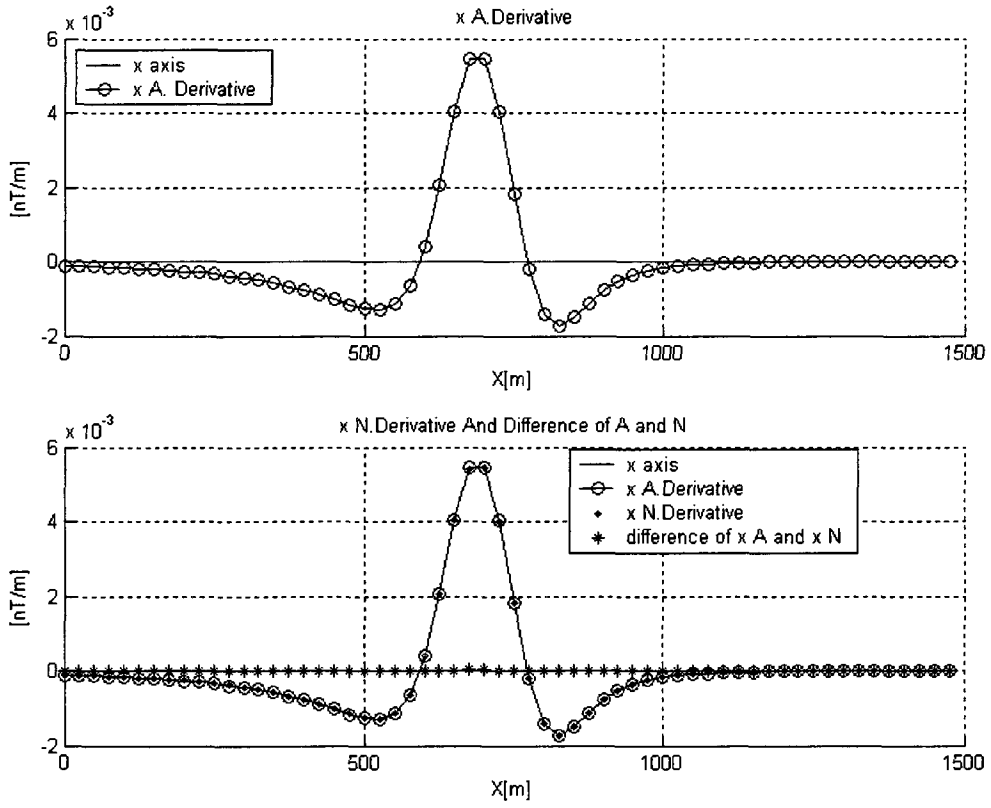

Fig.E.6 Profiles at y =800m of the analytic x derivative and numerical analytic x derivative of third set of data, total inclination = 40°

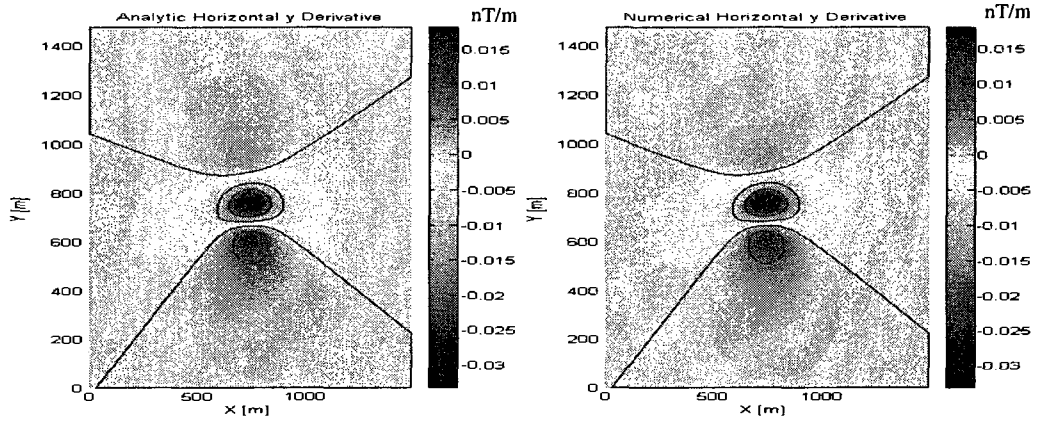

Fig.E.7 Contours of the analytic y derivative and numerical analytic y derivative of third model, total inclination = 40°

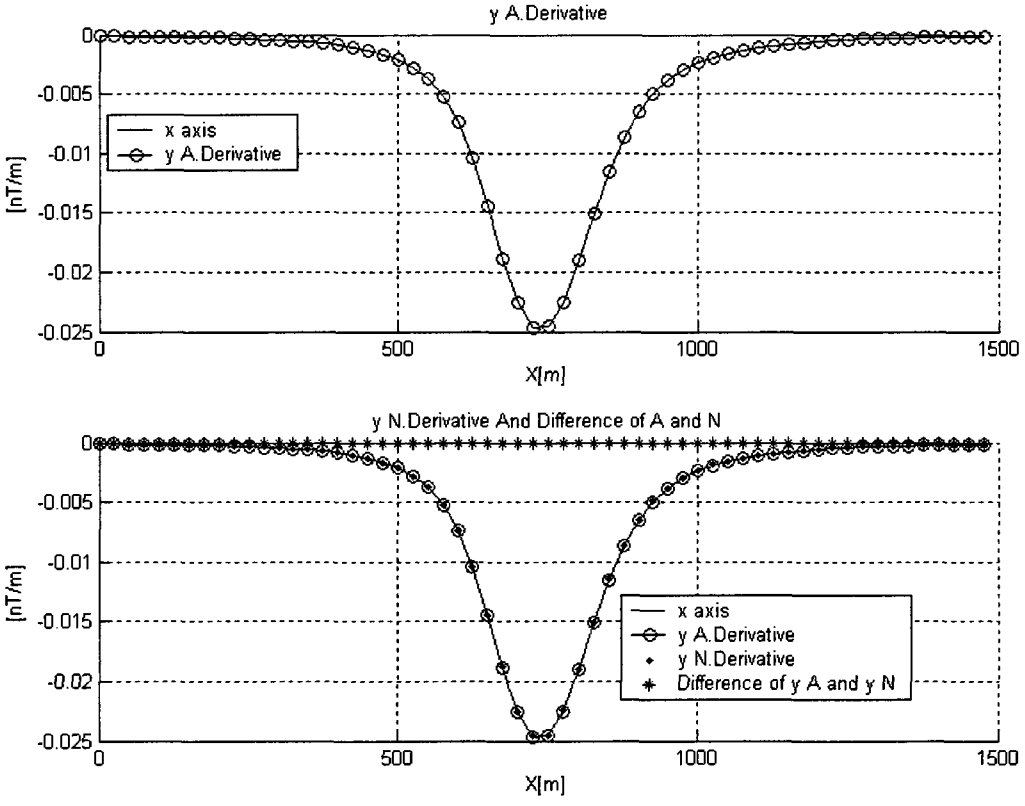

Fig.E.8 Profiles of y =800m of the analytic y derivative and numerical analytic y derivative of third model, total inclination = 40°

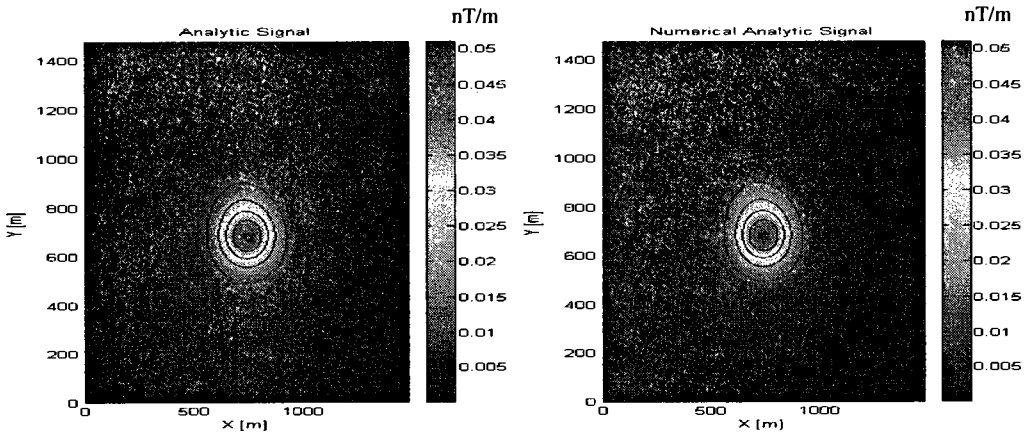

Fig.E.9 Contours of the analytic signal and numerical analytic signal of third model, total inclination $=40^{\circ}$.

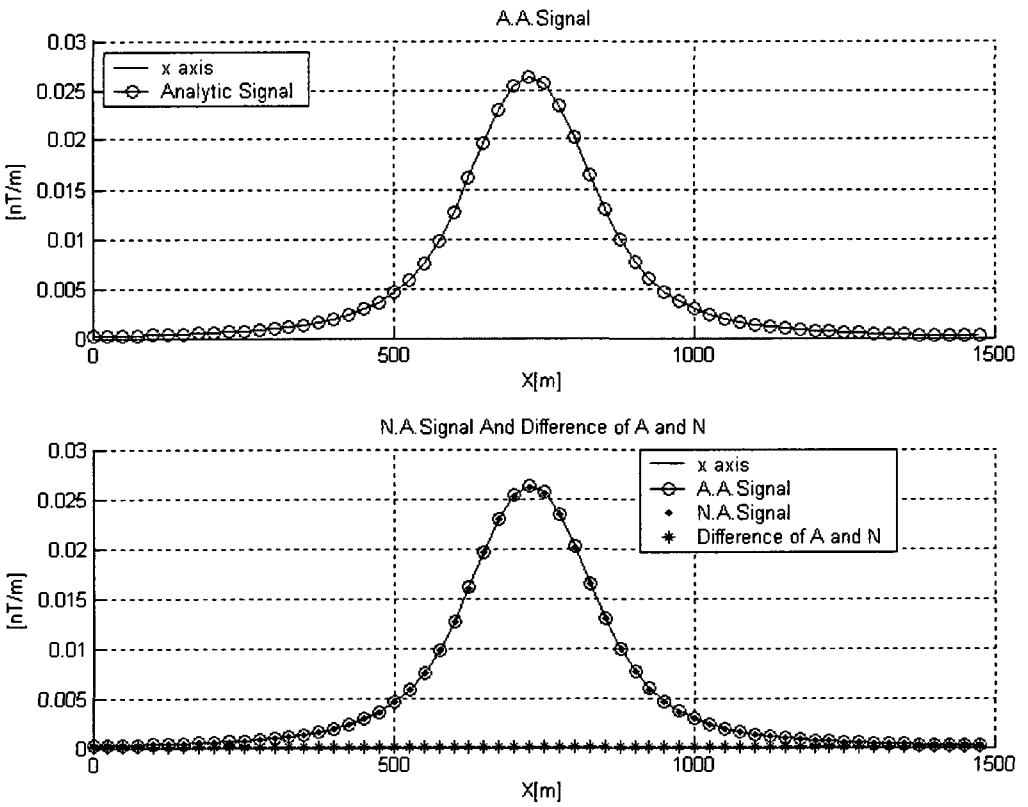

Fig.E.10 Profiles of y =800m of the analytic signal and numerical analytic signal of third set of data, total inclination $=40^{\circ}$.

Next group of images shows contours and profiles for total inclination = 30°

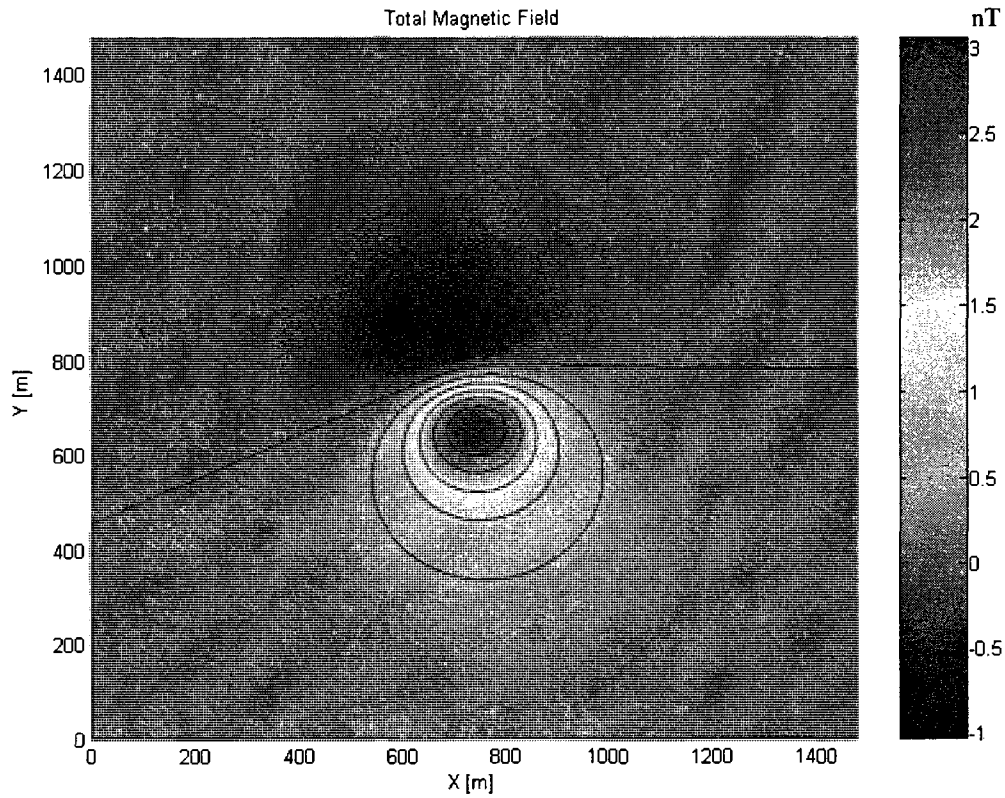

Fig.E.11 Contour of total magnetic field of third set of data, total inclination = 30°

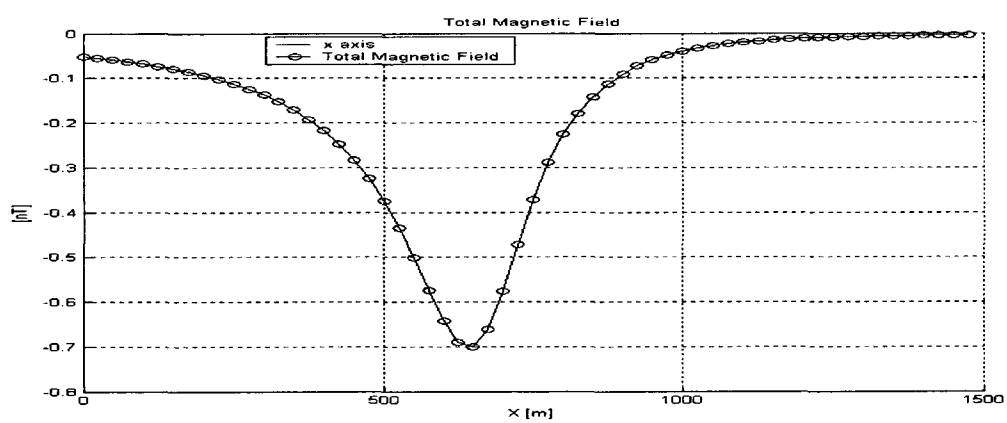

Fig.E.12 Profile y =800m of total magnetic field of third model, total inclination = 30°

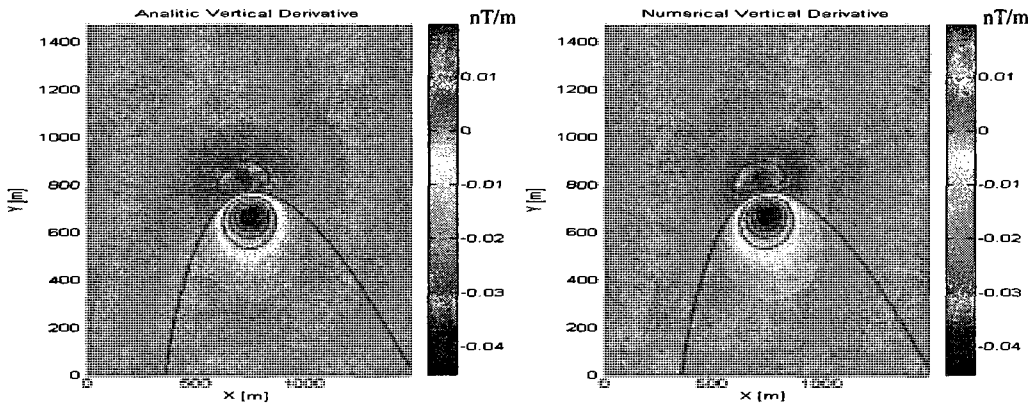

Fig.E.13 Contours of analytic vertical derivative and numerical vertical derivative of third model, total inclination $=30^{\circ}$

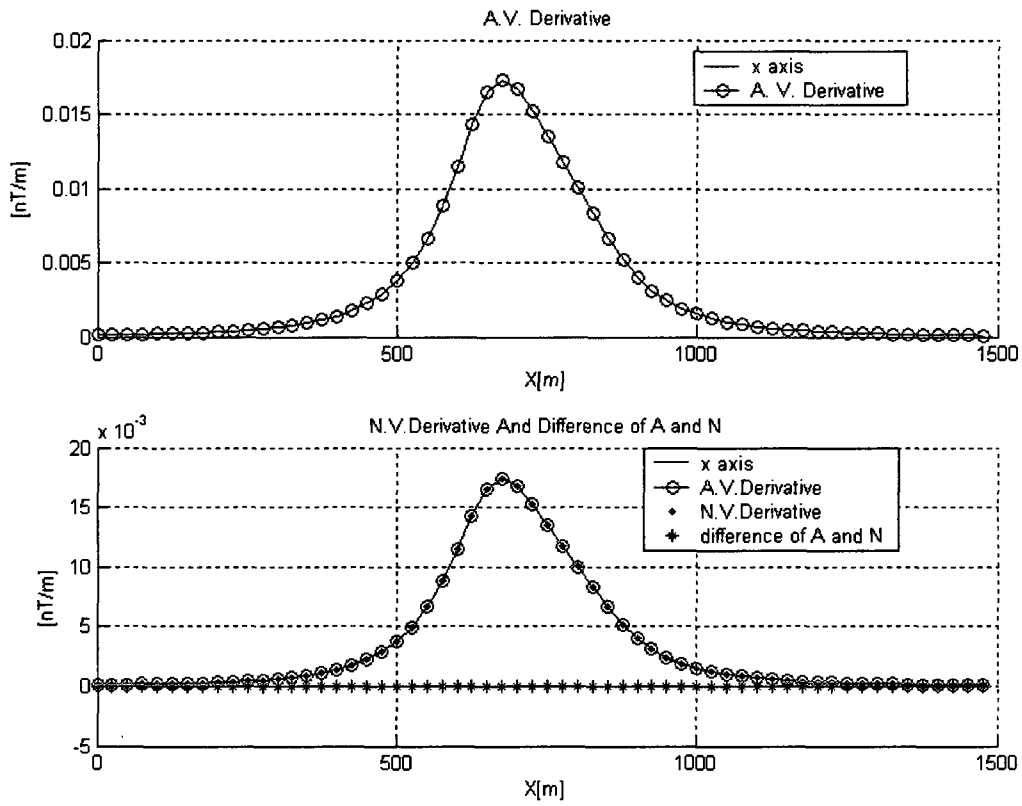

Fig.E.14 Profiles at y = 800m of analytic vertical derivative and numerical vertical derivative of third model, total inclination $=30^{\circ}$

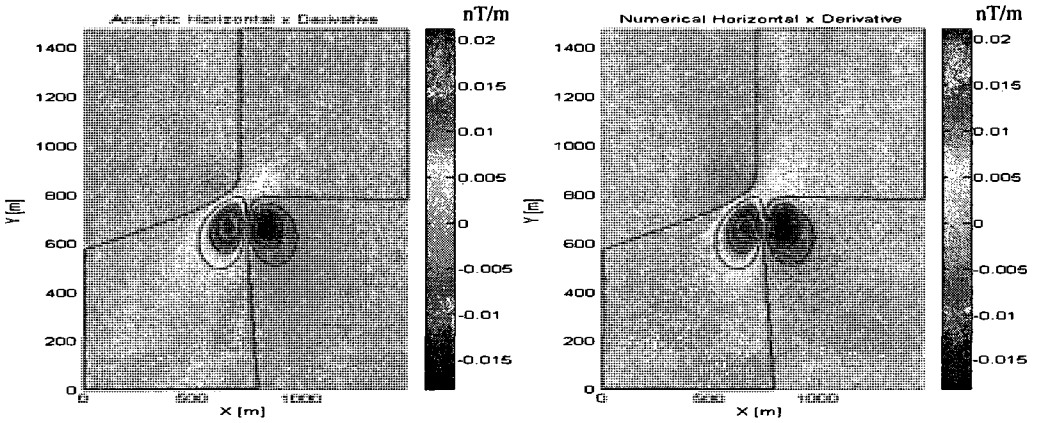

Fig.E.15 Contours of analytic x derivative and numerical x derivative of third model, total inclination $=30^{\circ}$.

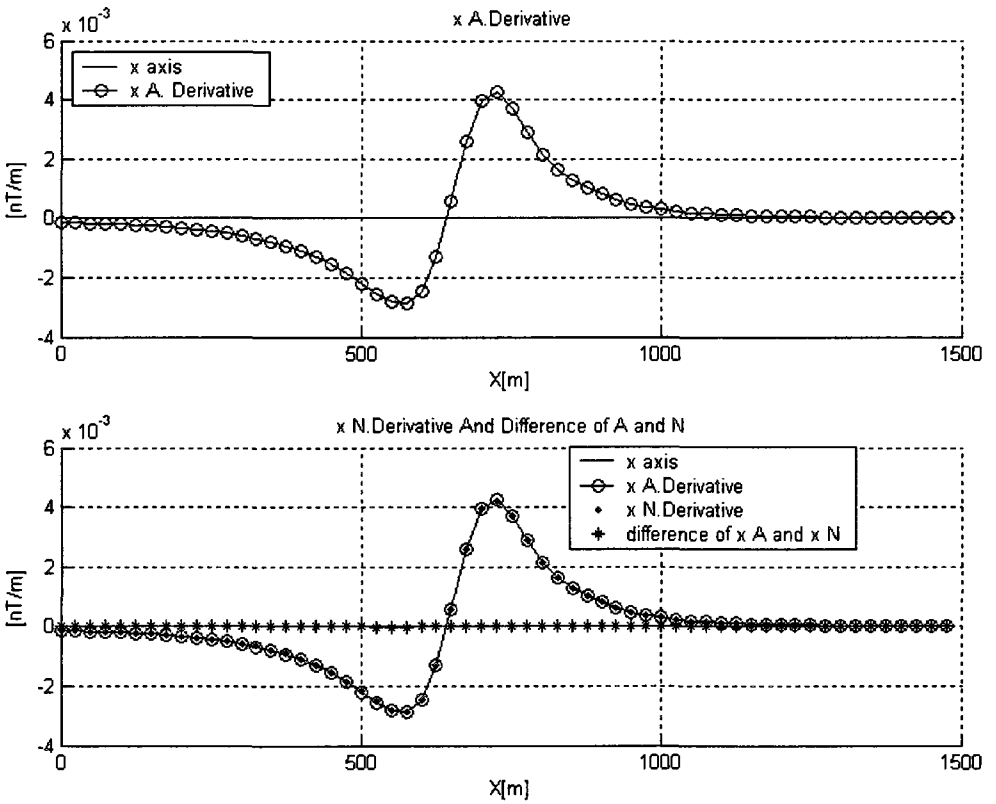

Fig.E.16 Profiles at y = 800m of analytic x derivative and numerical x derivative of third model, total inclination $=30^{\circ}$

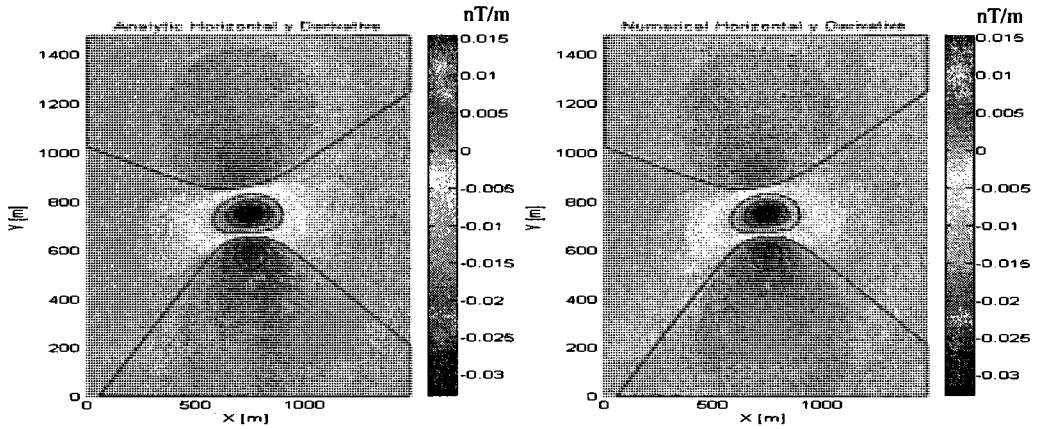

Fig.E.17 Contours of analytic y derivative and numerical y derivative of third model, total inclination $=30^{\circ}$

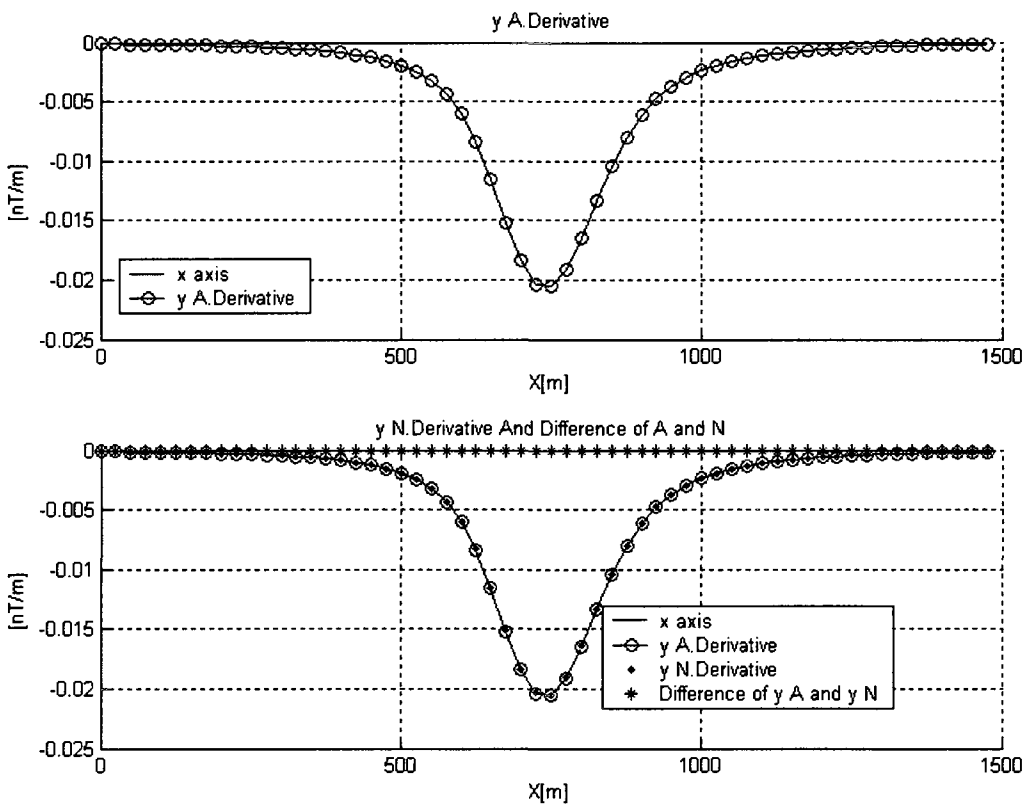

Fig.E.18 Profiles at y = 800m of analytic y derivative and numerical y derivative of third model, Total inclination $=30^{\circ}$

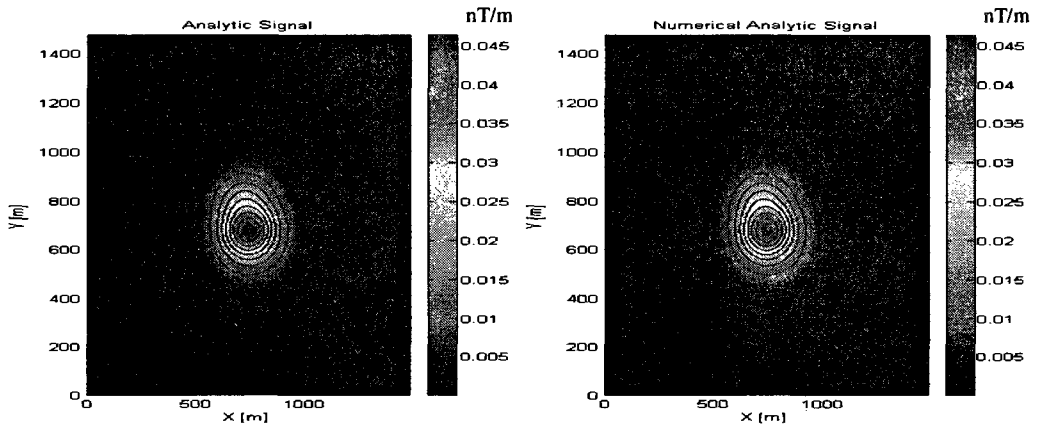

Fig.E.19 Contours of analytic signal and numerical analytic signal of third model, total inclination $=30^{\circ}$

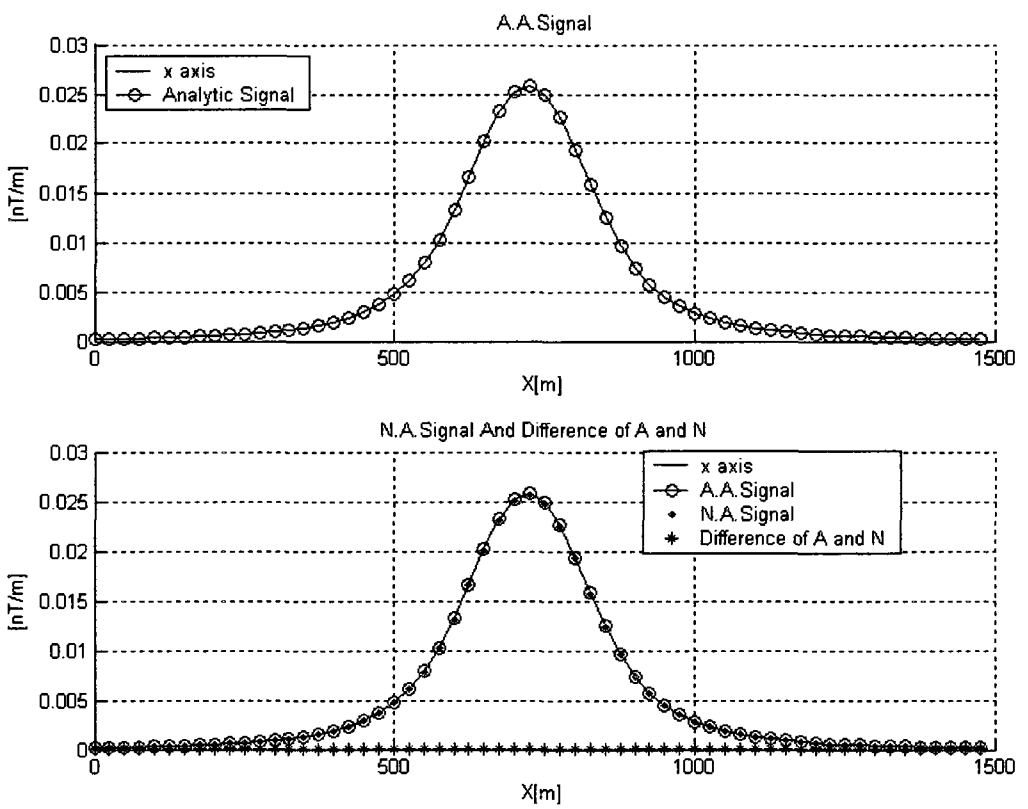

Fig.E.20 Profiles at y = 800m of analytic signal and numerical analytic signal of third model, total inclination $=30^{\circ}$

From Fig.E.1 to Fig.E.20 shows the changes of the total magnetic field, gradients and analytic signal because of the changes of total inclination of the magnetic field. Originally, the total inclination is 152°, it is changed to 40° and 30° subsequently. From 152° of total inclination to 40° of total inclination, the direction of magnetization is almost opposite, so the forms of the contours of total magnetic field, the gradients are changed. The values of anomalies, the vertical gradients and x gradients are almost same; there are differences for y gradients. The analytic signal is stable, no changes in terms of shapes and values. The two methods yield the same results.

From 40° of total inclination to 30° of total inclination, the two methods also yield the same results.

Appendix F: Sensibility of the results of calculations of derivatives to changes of remanent inclination

The remanent inclination of fourth model is increased to -30° to figure out the sensitivity to of the results of calculations of derivatives to changes of remanent magnetization:

Remanent inclination = -30°

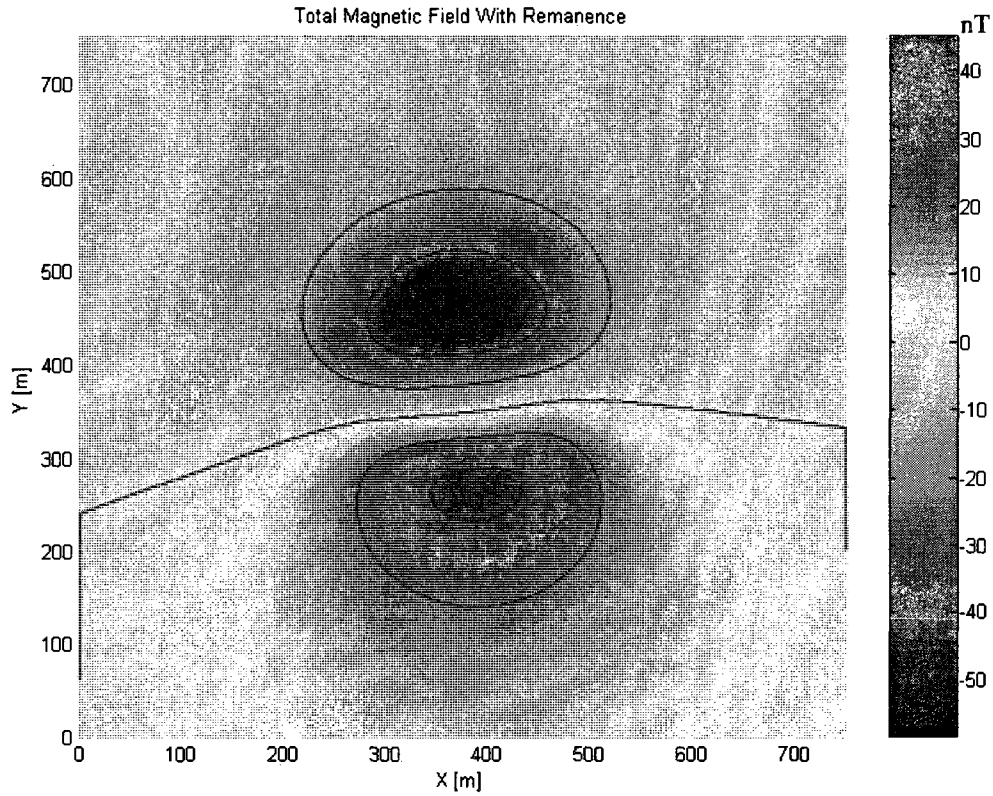

Fig.F.1 Contour of total magnetic field of forth model, Remanent inclination $= -30^{\circ}$

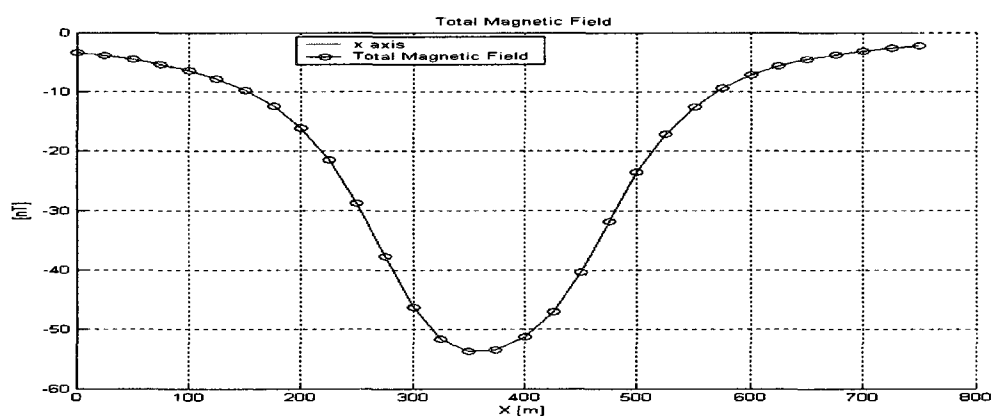

Fig.F.2 Profile at y =425m of total magnetic field of forth set of data, remanent inclination $= -30^{\circ}$

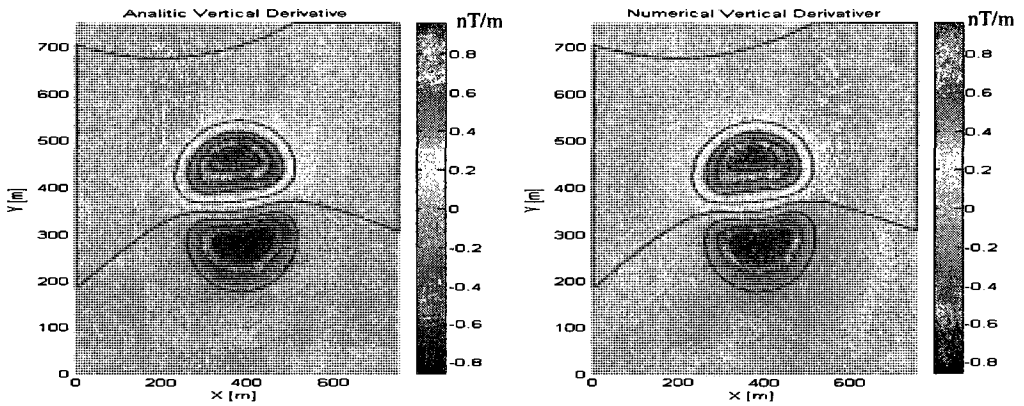

Fig.F.3 Contours of analytic vertical derivative and numerical vertical derivative of forth model, remanent inclination $= -30^{\circ}$

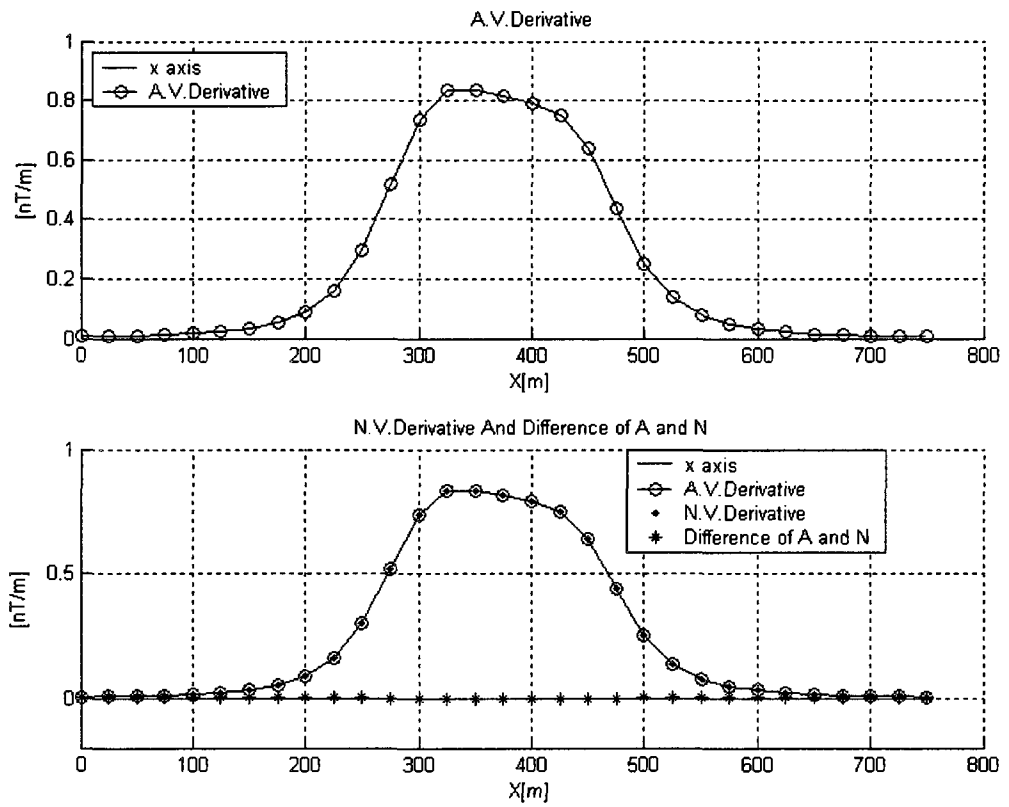

Fig.F.4 Profiles at y =425m of analytic vertical derivative and numerical vertical derivative of forth model, remanent inclination $= -30^{\circ}$

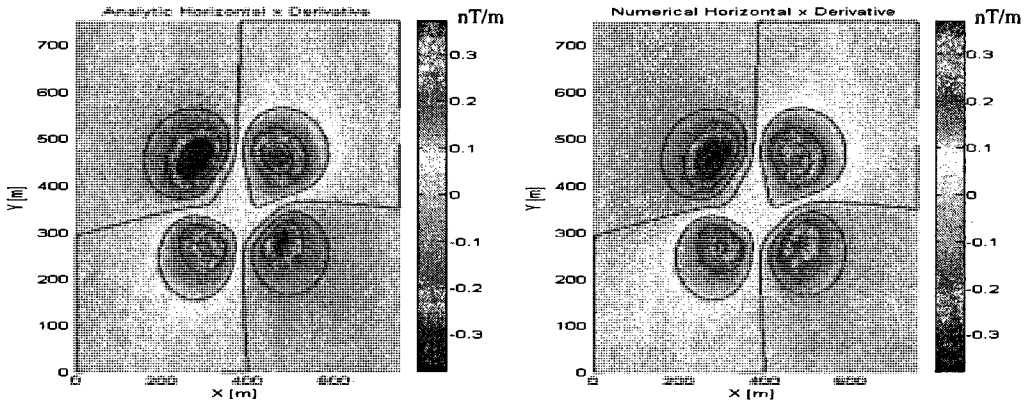

Fig.F.5 Contours of analytic x derivative and numerical x derivative of forth set of data. Remanent inclination $= -30^{\circ}$.

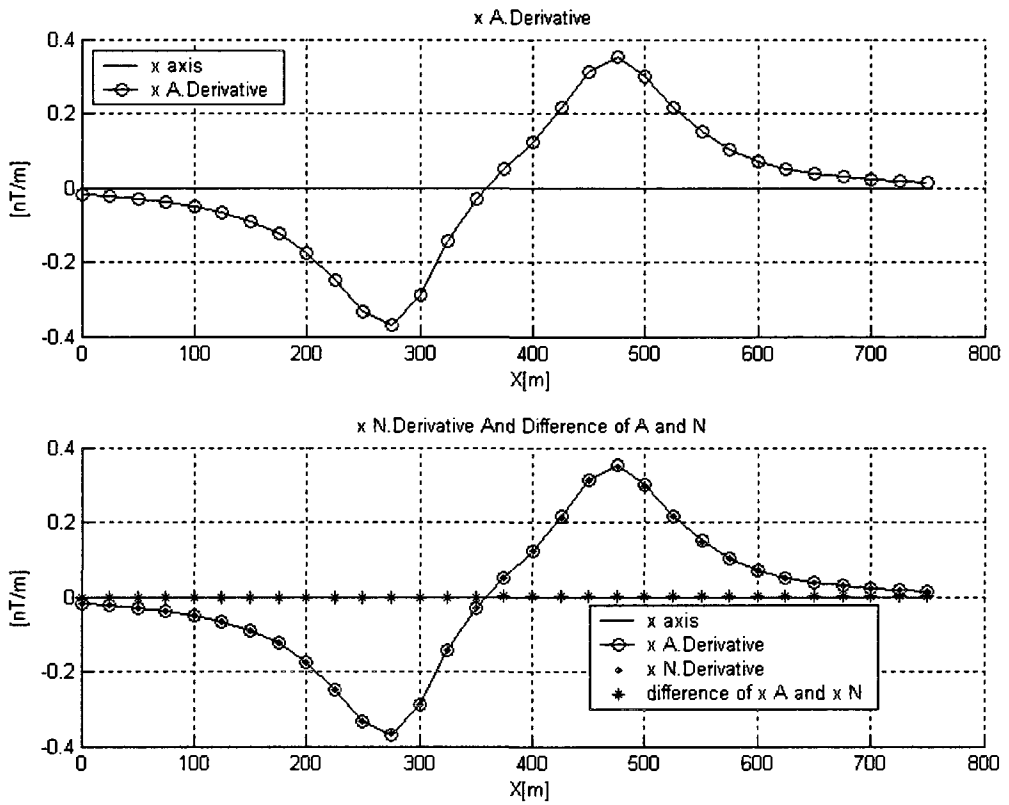

Fig.F.6 Profiles at y =425m of analytic x derivative and numerical x derivative of forth model, remanent inclination $= -30^{\circ}$

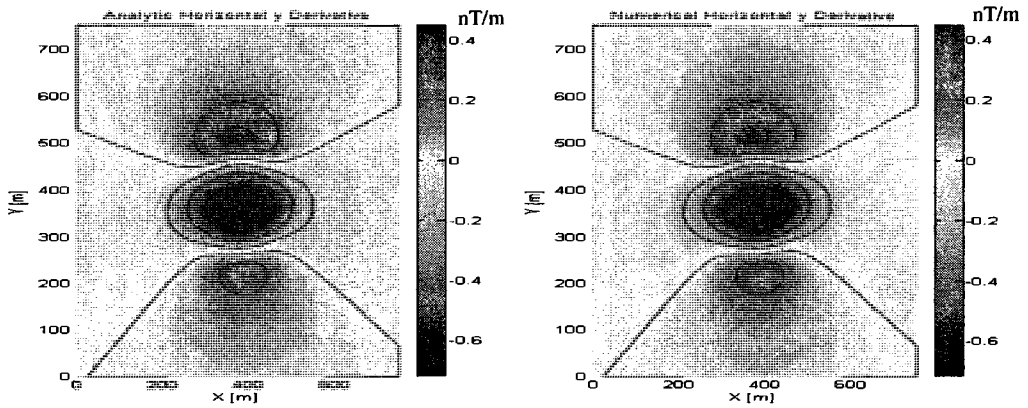

Fig.F.7 Contours of analytic y derivative and numerical y derivative of forth model remanent inclination $= -30^{\circ}$

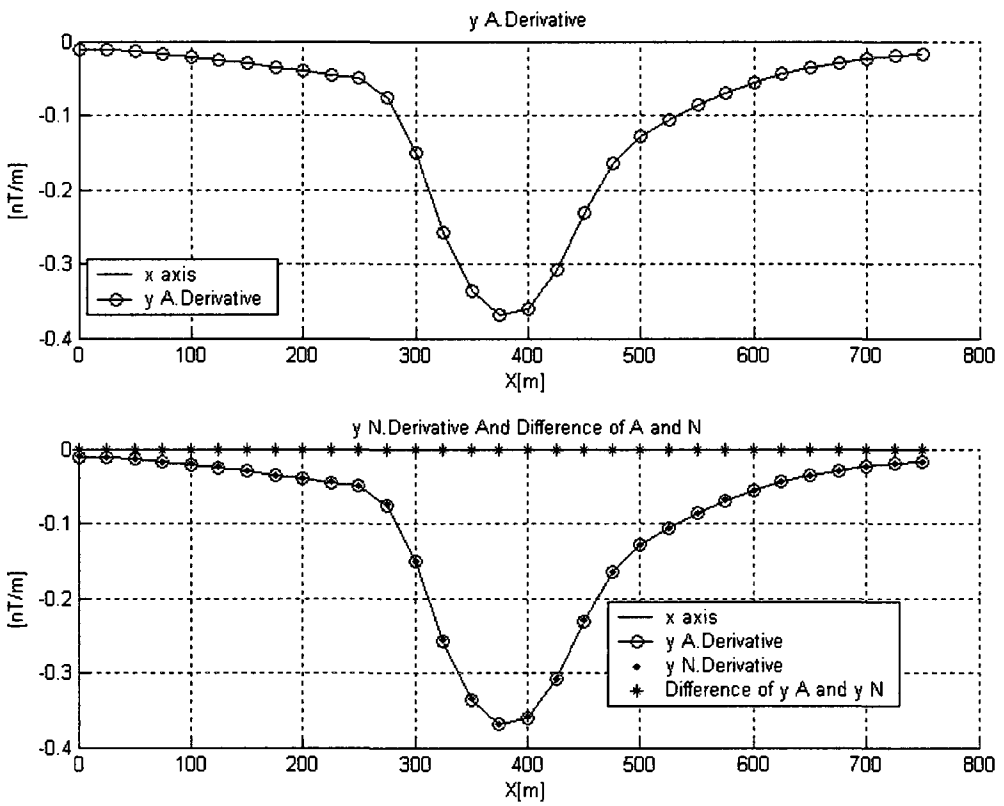

Fig.F.8 Profiles at y =425m of analytic y derivative and numerical y derivative of forth model, remanent inclination $= -30^{\circ}$

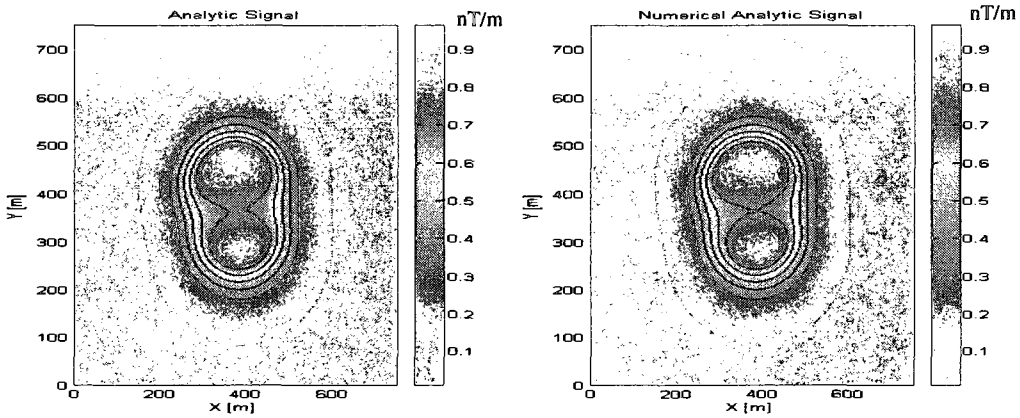

Fig.F.9 Contours of analytic signal and numerical analytic signal of forth model remanent inclination $= -30^{\circ}$.

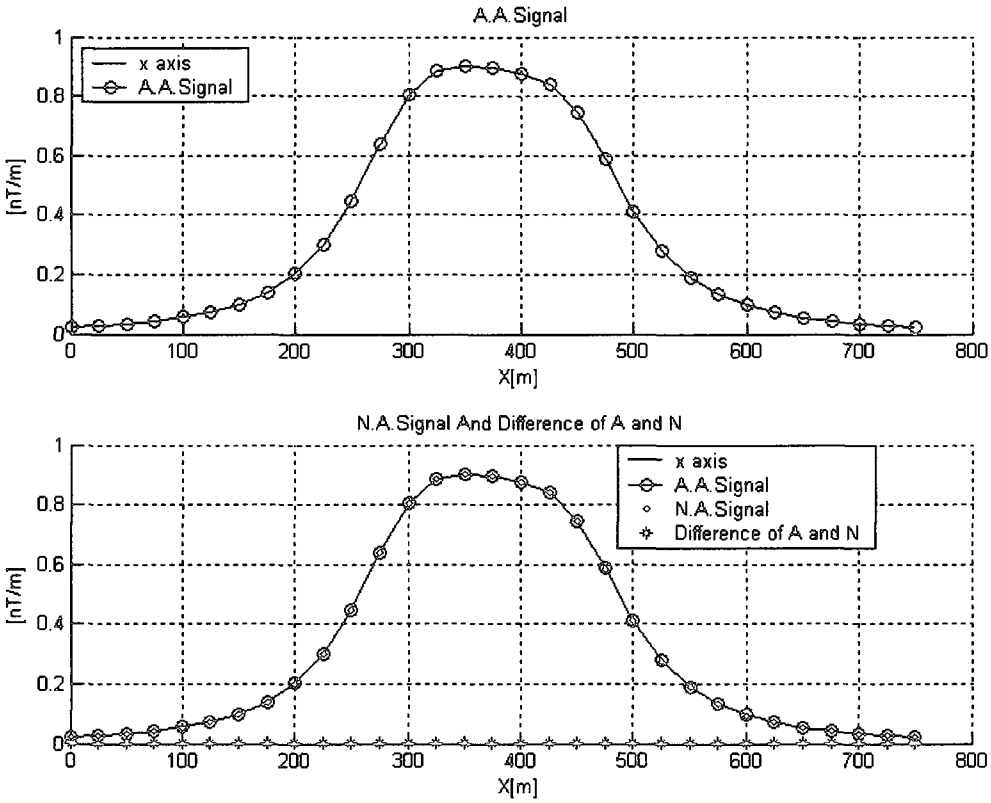

Fig.F.10 Profiles at y =425m of analytic signal and numerical analytic signal of forth model remanent inclination $= -30^{\circ}$

The last groups of figures show the results for remanent inclination = -10°

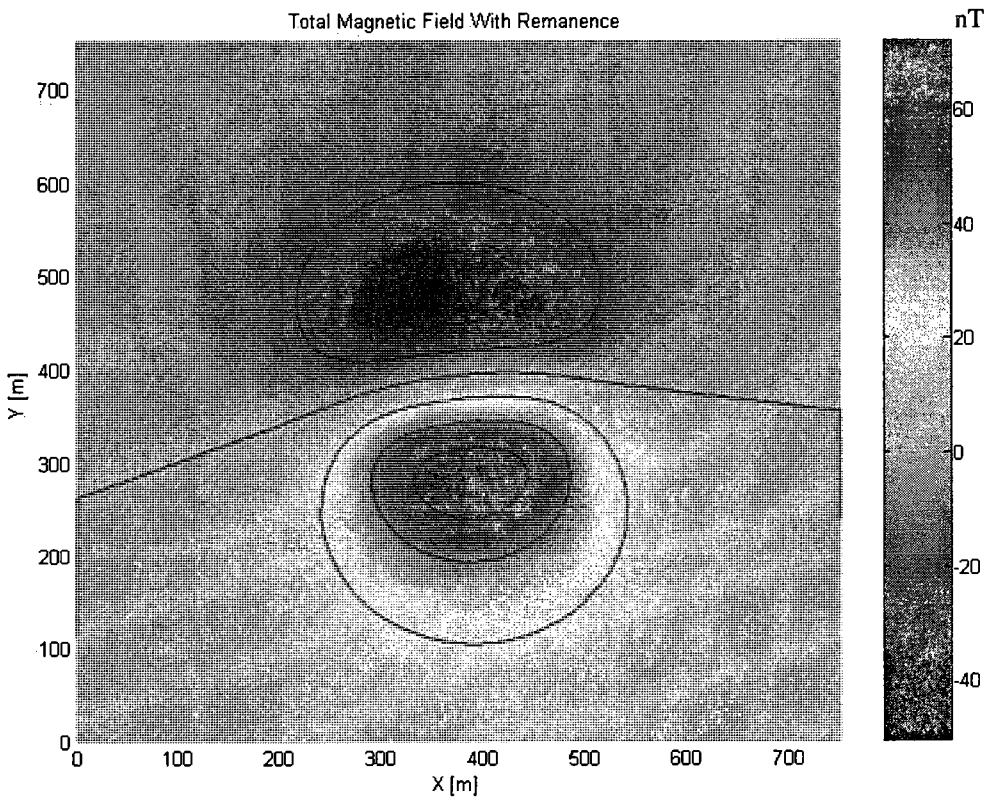

Fig.F.11 Contour of total magnetic field of forth model remanent inclination=-10°

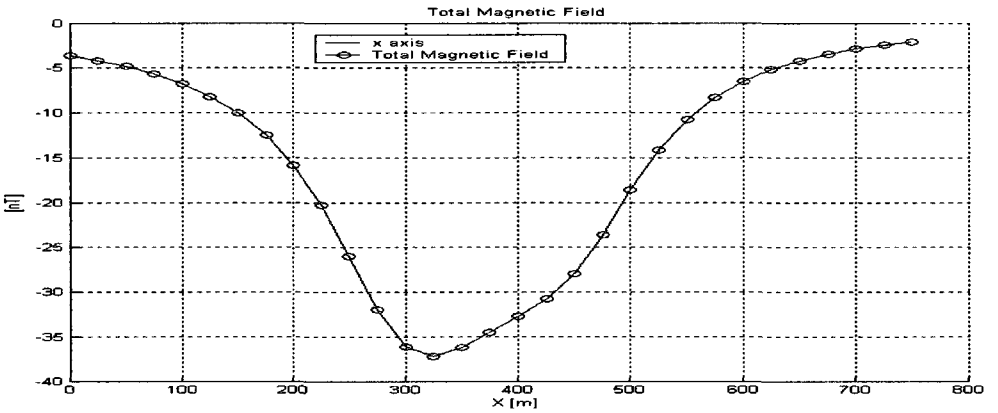

Fig.F.12 Profile at y =425m of total magnetic field of forth model, remanent inclination= -10°

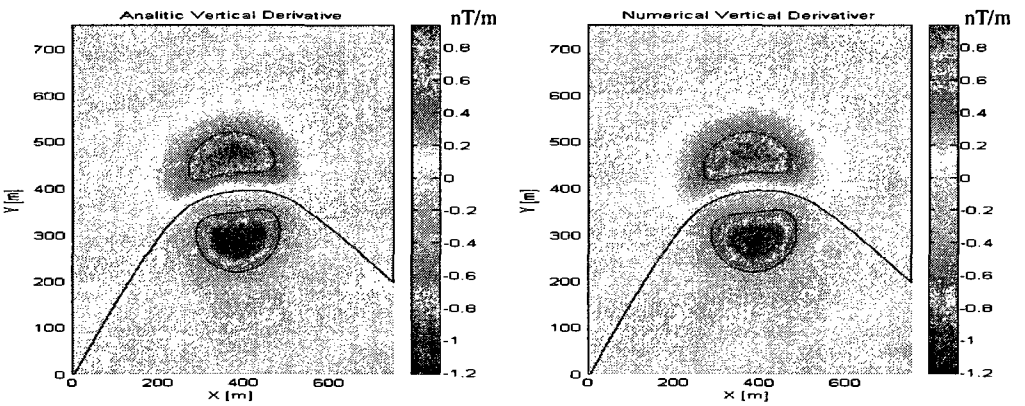

Fig.F.13 Contours of analytic vertical derivative and numerical vertical derivative of forth model, remanent inclination $=-10^{\circ}$

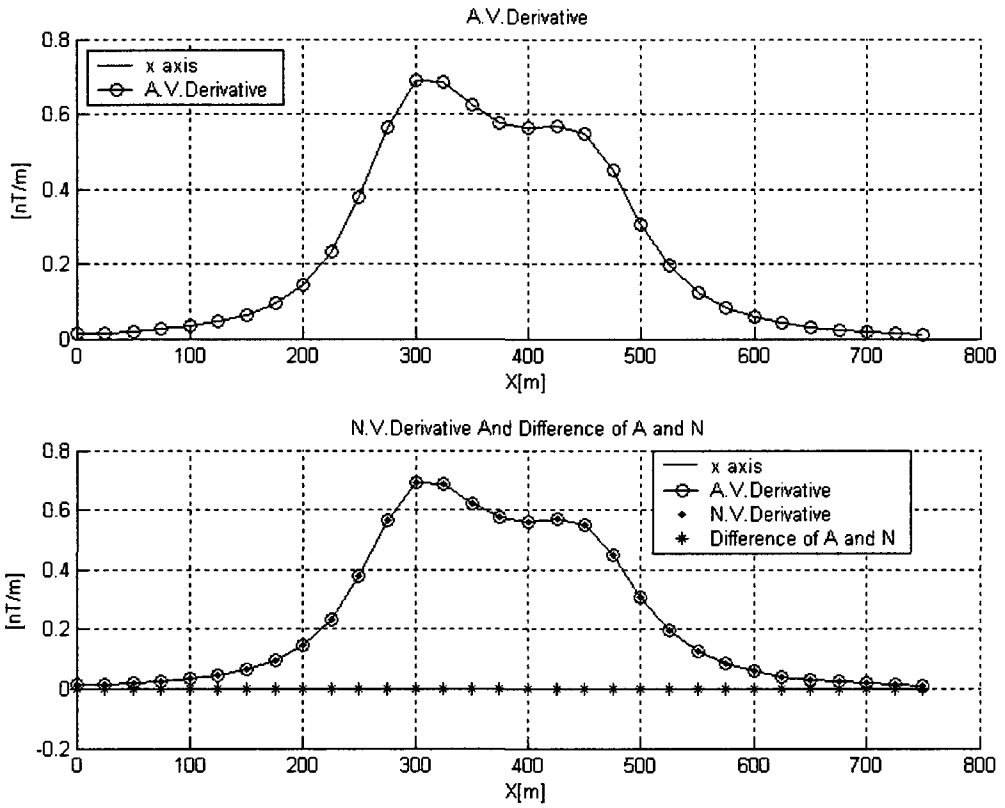

Fig.F.14 Profiles at y =425m of analytic vertical derivative and numerical vertical derivative of forth model, remanent inclination = -10°

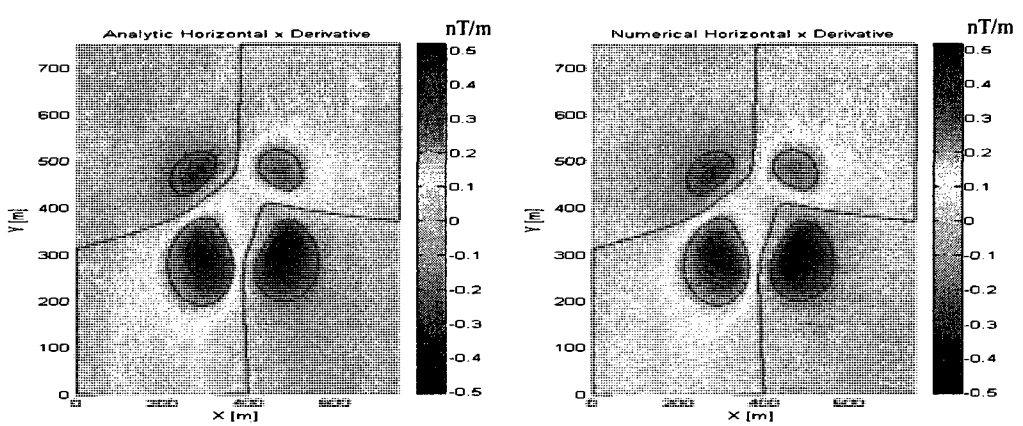

Fig.F.15 Contours of analytic x derivative and numerical x derivative of forth model, remanent inclination $=-10^{\circ}$

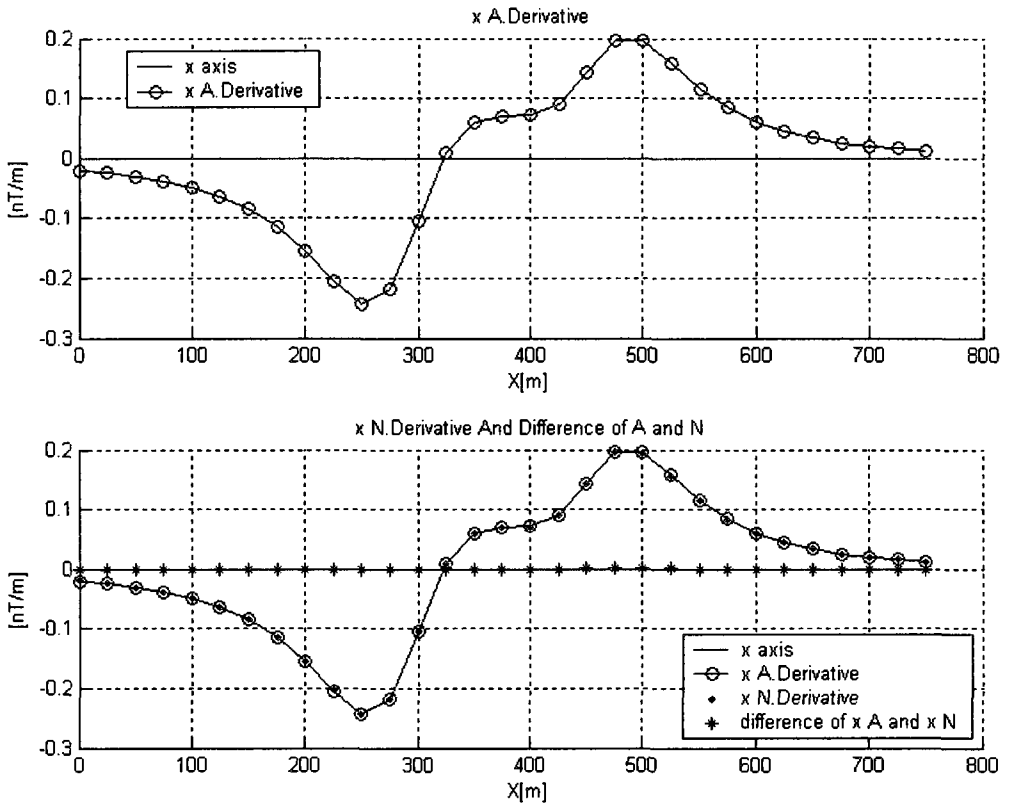

Fig.F.16 Profiles at y =425m of analytic x derivative and numerical x derivative of forth model, remanent inclination = -10°

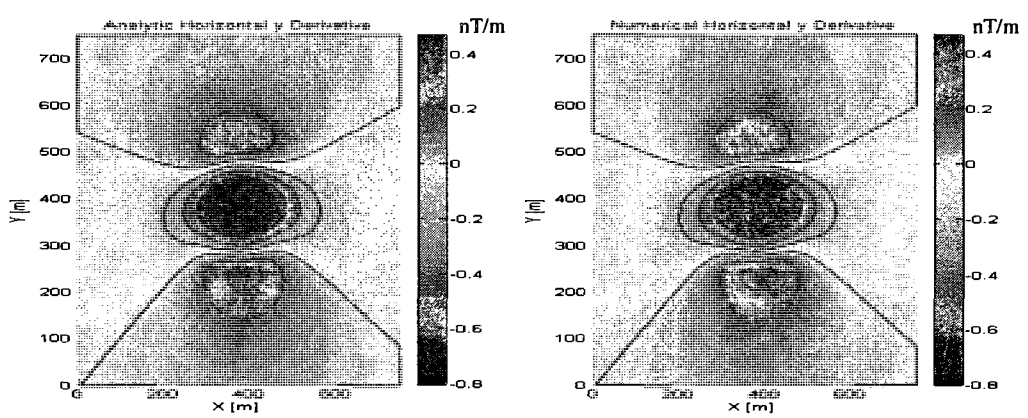

Fig.F.17 Contours of analytic y derivative and numerical y derivative of forth model, remanent inclination $=-10^{\circ}$

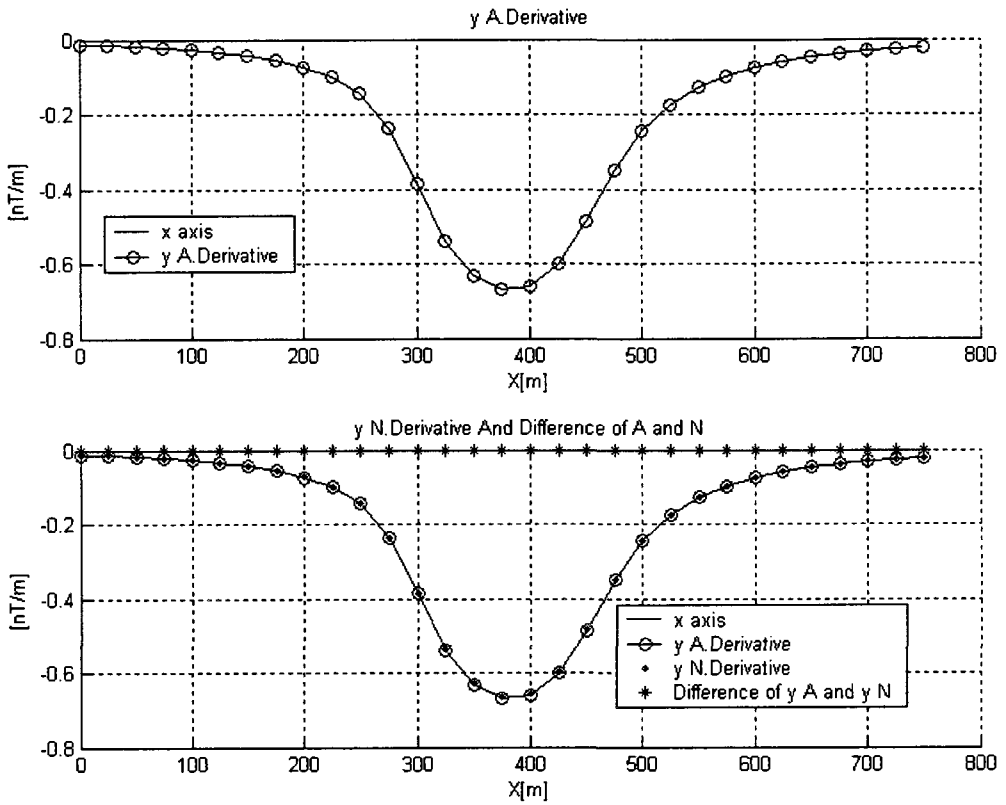

Fig.F.18 Profiles at y =425m of analytic y derivative and numerical y derivative of forth model, remanent inclination = -10°

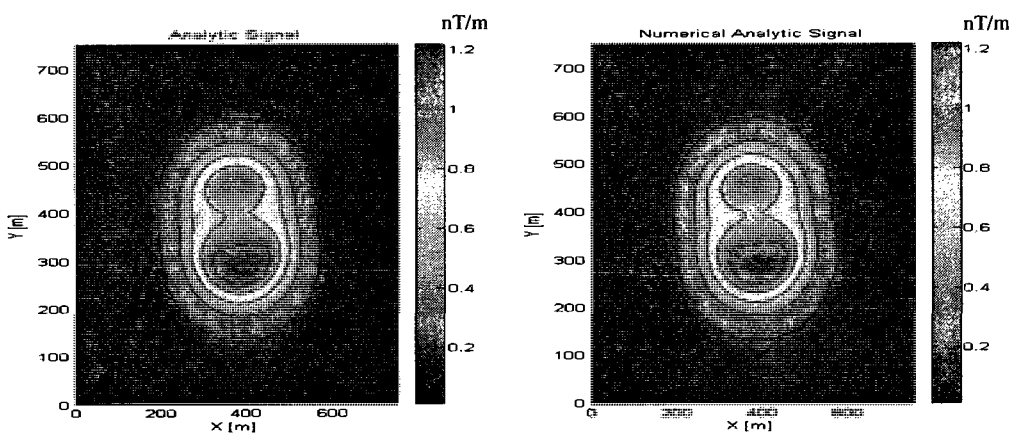

Fig.F.19 Contours of analytic signal and numerical analytic signal of forth model remanent inclination = -10°

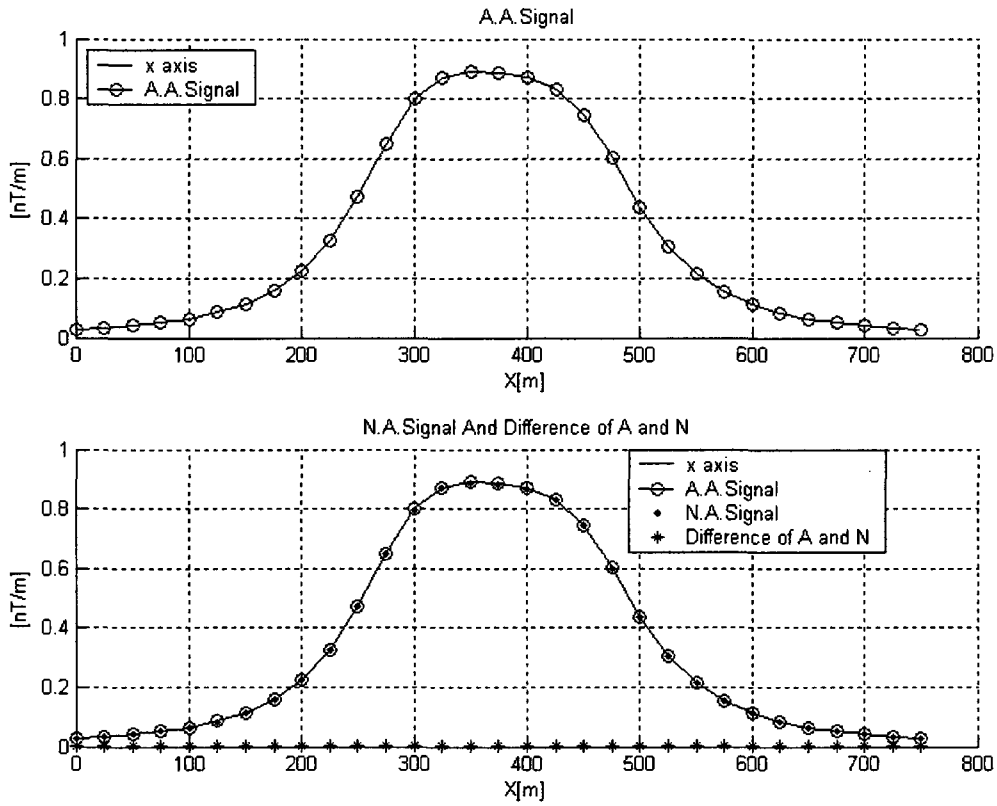

Fig.F.20 Profiles at y =425m of analytic signal and numerical analytic signal of forth model, remanent inclination = -10°

With the change of the remanent inclination, the vertical and y derivatives change, the x derivative shows little change. The values of the calculated analytic signal do not change much. In addition to that, I tested the sensibilities to Q (Jr/Ji) and to the declination. There is little sensibility to Q (Jr/Ji) and to declination.